Many-body physics with ultracold gases

Immanuel Bloch*

Institut für Physik, Johannes Gutenberg–Universität, D-55099 Mainz, Germany

Jean Dalibard[†]

Laboratoire Kastler Brossel, CNRS, Ecole Normale Supérieure,
24 rue Lhomond, F-75005 Paris, France

Wilhelm Zwerger[‡]

Physik-Department, Technische Universität München, D-85748 Garching, Germany

(Published 18 July 2008)

This paper reviews recent experimental and theoretical progress concerning many-body phenomena in dilute, ultracold gases. It focuses on effects beyond standard weak-coupling descriptions, such as the Mott-Hubbard transition in optical lattices, strongly interacting gases in one and two dimensions, or lowest-Landau-level physics in quasi-two-dimensional gases in fast rotation. Strong correlations in fermionic gases are discussed in optical lattices or near-Feshbach resonances in the BCS-BEC crossover.

CONTENTS

*bloch@uni-mainz.de
†jean.dalibard@lkb.ens.fr
‡zwerger@ph.tum.de

I. INTRODUCTION

The achievement of Bose-Einstein condensation (BEC) (Anderson *et al.*, 1995; Bradley *et al.*, 1995; Davis *et al.*, 1995), and of Fermi degeneracy (DeMarco and Jin, 1999; Schreck *et al.*, 2001; Truscott *et al.*, 2001), in ultracold, dilute gases has opened a new chapter in atomic and molecular physics, in which particle statistics and their interactions, rather than the study of single atoms or photons, are at center stage. For a number of years, a main focus in this field has been the exploration of the wealth of phenomena associated with the existence of coherent matter waves. Major examples include the observation of interference of two overlapping condensates (Andrews *et al.*, 1997), of long-range phase coherence (Bloch *et al.*, 2000), and of quantized vortices and vortex lattices (Matthews, 1999; Madison *et al.*, 2000; Abo-Shaeer *et al.*, 2001) and molecular condensates with bound pairs of fermions (Greiner *et al.*, 2003; Jochim *et*

al., 2003b; Zwierlein *et al.*, 2003b). Common to all of these phenomena is the existence of a coherent, macroscopic matter wave in an interacting many-body system, a concept familiar from the classic areas of superconductivity and superfluidity. It was the basic insight of Ginzburg and Landau (1950) that, quite independent of a detailed microscopic understanding, an effective description of the coherent many-body state is provided by a complex, macroscopic wave function $\psi(\mathbf{x}) = |\psi(\mathbf{x})| \times \exp i\phi(\mathbf{x})$. Its magnitude squared gives the superfluid density, while the phase $\phi(\mathbf{x})$ determines the superfluid velocity via $\mathbf{v}_s = (\hbar/M)\nabla\phi(\mathbf{x})$ (see the Appendix for a discussion of these concepts and their connection with the microscopic criterion for BEC). As emphasized by Cummings and Johnston (1966) and by Langer (1968), this picture is similar to the description of laser light as a coherent state (Glauber, 1963). It applies both to the standard condensates of bosonic atoms and to weakly bound fermion pairs, which are the building blocks of the BCS picture of superfluidity in Fermi systems. In contrast to conventional superfluids like ⁴He or superconductors, where the macroscopic wave function provides only a phenomenological description of the superfluid degrees of freedom, the situation in dilute gases is considerably simpler. In fact, as a result of the weak interactions, dilute BEC's are essentially pure condensates sufficiently below the transition. The macroscopic wave function is thus directly connected with the microscopic degrees of freedom, providing a complete and quantitative description of both static and time-dependent phenomena in terms of a reversible, nonlinear Schrödinger equation, the famous Gross-Pitaevskii equation (Gross, 1961; Pitaevskii, 1961). In dilute gases, therefore, the many-body aspect of a BEC is reduced to an effective single-particle description, where interactions give rise to an additional potential proportional to the local particle density. Adding small fluctuations around this zeroth-order picture leads to the well-known Bogoliubov theory of weakly interacting Bose gases. Like the closely related BCS superfluid of weakly interacting fermions, the many-body problem is then completely soluble in terms of a set of noninteracting quasiparticles. Dilute, ultracold gases provide a concrete realization of these basic models of many-body physics, and many of their characteristic properties have been verified quantitatively. Excellent reviews of this remarkably rich area of research have been given by Dalfovo *et al.* (1999) and by Leggett (2001) and, more recently, by Pethick and Smith (2002) and Pitaevskii and Stringari (2003).

In the past several years, two major new developments have considerably enlarged the range of physics that is accessible with ultracold gases. They are associated with (i) the ability to tune the interaction strength in cold gases by Feshbach resonances (Courteille *et al.*, 1998; Inouye *et al.*, 1998); and (ii) the possibility of changing the dimensionality with optical potentials and, in particular, of generating strong periodic potentials for cold atoms through optical lattices (Greiner *et al.*, 2002a). The two developments, either individually or in combination, allow one to enter a regime in which the

interactions even in extremely dilute gases can no longer be described by a picture based on noninteracting quasiparticles. The appearance of such phenomena is characteristic for the physics of strongly correlated systems. For a long time, this area of research was confined to the dense and strongly interacting quantum liquids of condensed matter or nuclear physics. By contrast, gases—almost by definition—were never thought to exhibit strong correlations.

The use of Feshbach resonances and optical potentials for exploring strong correlations in ultracold gases was crucially influenced by earlier ideas from theory. In particular, Stoof *et al.* (1996) suggested that Feshbach resonances in a degenerate gas of ⁶Li, which exhibits a tunable attractive interaction between two different hyperfine states, may be used to realize BCS pairing of fermions in ultracold gases. A remarkable idea in a rather unusual direction in the context of atomic physics was the proposal by Jaksch *et al.* (1998) to realize a quantum phase transition from a superfluid to a Mott-insulating state by loading a BEC into an optical lattice and increasing its depth. Further directions in the regime of strong correlations were opened with the suggestions by Olshanii (1998) and Petrov, Shlyapnikov, and Walraven (2000) to realize a Tonks-Girardeau gas with BEC's confined in one dimension and by Wilkin and Gunn (2000) to explore quantum Hall effect physics in fast-rotating gases.

Experimentally, the strong-coupling regime in dilute gases was first reached by Cornish *et al.* (2000) using Feshbach resonances for bosonic atoms. Unfortunately, in this case, increasing the scattering length a leads to a strong decrease in the condensate lifetime due to three-body losses, whose rate on average varies as a^4 (Fedichev, Reynold, and Shlyapnikov, 1996; Petrov, 2004). A quite different approach to the regime of strong correlations, which does not suffer from problems with the condensate lifetime, was taken by Greiner *et al.* (2002a). Loading BEC's into an optical lattice, they observed a quantum phase transition from a superfluid to a Mott-insulating phase even in the standard regime where the average interparticle spacing is much larger than the scattering length. Subsequently, the strong confinement available with optical lattices made possible the achievement of low-dimensional systems where new phases can emerge. The observation of a (Tonks-Girardeau) hard-core Bose gas in one dimension by Kinoshita *et al.* (2004) and Paredes *et al.* (2004) constituted a first example of a bosonic Luttinger liquid. In two dimensions, a Kosterlitz-Thouless crossover between a normal phase and one with quasi-long-range order was observed by Hadzibabic *et al.* (2006). The physics of strongly interacting bosons in the lowest Landau level is accessible with fast-rotating BEC's (Bretin *et al.*, 2004; Schweikhard *et al.*, 2004), where the vortex lattice is predicted to melt by quantum fluctuations. Using atoms like ⁵²Cr, which have a larger permanent magnetic moment, BEC's with strong dipolar interactions have been realized by Griesmaier *et al.* (2005). In combination with Feshbach resonances, this opens the way to tuning the

nature and range of the interaction (Lahaye *et al.*, 2007), which might, for instance, be used to reach many-body states that are not accessible in the context of the fractional quantum Hall effect.

In Fermi gases, the Pauli principle suppresses three-body losses, whose rate in fact decreases with increasing values of the scattering length (Petrov, Salomon, and Shlyapnikov, 2004). Feshbach resonances, therefore, allow one to enter the strong-coupling regime $k_F|a| \geqslant 1$ in ultracold Fermi gases (O'Hara *et al.*, 2002; Bourdel *et al.*, 2003). In particular, there exist stable molecular states of weakly bound fermion pairs in highly excited rovibrational states (Cubizolles *et al.*, 2003; Strecker *et al.*, 2003). The remarkable stability of fermions near Feshbach resonances allows one to explore the crossover from a molecular BEC to a BCS superfluid of weakly bound Cooper pairs (Bartenstein *et al.*, 2004a; Bourdel *et al.*, 2004; Regal *et al.*, 2004a; Zwierlein *et al.*, 2004). In particular, the presence of pairing due to many-body effects has been probed by rf spectroscopy (Chin *et al.*, 2004) or the measurement of the closed-channel fraction (Partridge *et al.*, 2005), while superfluidity has been verified by observation of quantized vortices (Zwierlein *et al.*, 2005). Recently, these studies have been extended to Fermi gases with unequal densities for the spin-up and spin-down components (Partridge *et al.*, 2006; Zwierlein *et al.*, 2006), where pairing is suppressed by the mismatch of the respective Fermi energies.

Repulsive fermions in an optical lattice allow one to realize an ideal and tunable version of the Hubbard model, a paradigm for the multitude of strong-correlation problems in condensed matter physics. Experimentally, some basic properties of degenerate fermions in periodic potentials, such as the existence of a Fermi surface and the appearance of a band insulator at unit filling, have been observed by Köhl *et al.* (2005a). While it is difficult to cool fermions to temperatures much below the bandwidth in a deep optical lattice, these experiments give hope that eventually magnetically ordered or unconventional superconducting phases of the fermionic Hubbard model will be accessible with cold gases. The perfect control and tunability of the interactions in these systems provide a novel approach for studying basic problems in many-body physics and, in particular, for entering regimes that have never been accessible in condensed matter or nuclear physics.

This review aims to give an overview of this rapidly evolving field, covering both theoretical concepts and their experimental realization. It provides an introduction to the strong-correlation aspects of cold gases, that is, phenomena that are not captured by weak-coupling descriptions like the Gross-Pitaevskii or Bogoliubov theory. The focus of this review is on examples that have already been realized experimentally. Even within this limitation, however, the rapid development of the field in recent years makes it impossible to give a complete survey. In particular, important subjects like spinor gases, Bose-Fermi mixtures, quantum spin systems in optical lattices, or dipolar gases will not be discussed [see, e.g., Lewenstein *et al.* (2007)]. Also, applications of cold atoms in optical lattices for quantum information are omitted completely; for an introduction, see Jaksch and Zoller (2005).

A. Scattering of ultracold atoms

For an understanding of the interactions between neutral atoms, first at the two-body level, it is instructive to use a toy model (Gribakin and Flambaum, 1993), in which the van der Waals attraction at large distances is cut off by a hard core at some distance r_c on the order of an atomic dimension. The resulting spherically symmetric potential,

$$V(r) = \begin{cases} -C_6/r^6 & \text{if } r > r_c \\ \infty & \text{if } r \leqslant r_c, \end{cases} \tag{1}$$

is, of course, not a realistic description of the short-range interaction of atoms; however, it captures the main features of scattering at low energies. The asymptotic behavior of the interaction potential is fixed by the van der Waals coefficient C_6. It defines a characteristic length

$$a_c = (2M_r C_6/\hbar^2)^{1/4} \tag{2}$$

at which the kinetic energy of the relative motion of two atoms with reduced mass M_r equals their interaction energy. For alkali-metal atoms, this length is typically on the order of several nanometers. It is much larger than the atomic scale r_c because alkali-metal atoms are strongly polarizable, resulting in a large C_6 coefficient. The attractive well of the van der Waals potential thus supports many bound states (of order 100 in ^{87}Rb). Their number N_b may be determined from the WKB phase

$$\Phi = \int_{r_c}^{\infty} dr \sqrt{2M_r|V(r)|}/\hbar = a_c^2/2r_c^2 \gg 1 \tag{3}$$

at zero energy, via $N_b = [\Phi/\pi + 1/8]$, where [ ] means taking the integer part.[1] The number of bound states in this model, therefore, depends crucially on the precise value of the short-range scale r_c. By contrast, the low-energy scattering properties are determined by the van der Waals length a_c, which is sensitive only to the asymptotic behavior of the potential. Consider the scattering in states with angular momentum $l=0,1,2,\ldots$ in the relative motion (for identical bosons or fermions, only even or odd values of l are possible, respectively). The effective potential for states with $l \neq 0$ contains a centrifugal barrier whose height is of order $E_c \simeq \hbar^2 l^3/M_r a_c^2$. Converting this energy into an equivalent temperature, one obtains for small l temperatures around 1 mK for typical atomic masses. At temperatures below that, the energy $\hbar^2 k^2/2M_r$ in the relative motion of two atoms is typically below the centrifugal barrier. Scattering in states with $l \neq 0$ is therefore frozen out, unless there exist so-called

---

[1]This result follows from Eq. (5) below by noting that a new bound state is pulled in from the continuum each time the scattering length diverges (Levinson's theorem).

shape resonances, i.e., bound states with $l \neq 0$ behind the centrifugal barrier, which may be in resonance with the incoming energy; see Boesten *et al.* (1997) and Dürr *et al.* (2005). For gases in the sub-millikelvin regime, therefore, usually the lowest-angular-momentum collisions dominate (*s*-wave for bosons, *p*-wave for fermions), which in fact *defines* the regime of ultracold atoms. In the *s*-wave case, the scattering amplitude is determined by the corresponding phase shift $\delta_0(k)$ via (Landau and Lifshitz, 1987)

$$f(k) = \frac{1}{k \cot \delta_0(k) - ik} \rightarrow \frac{1}{-1/a + r_e k^2/2 - ik}. \quad (4)$$

At low energies, it is characterized by the scattering length a and the effective range r_e as the only two parameters. For the truncated van der Waals potential (1), the scattering length can be calculated analytically as (Gribakin and Flambaum, 1993)

$$a = \bar{a}[1 - \tan(\Phi - 3\pi/8)], \quad (5)$$

where, Φ is the WKB phase (3) and $\bar{a} = 0.478 a_c$ is the so-called mean scattering length. Equation (5) shows that the characteristic magnitude of the scattering length is the van der Waals length. Its detailed value, however, depends on the short-range physics via the WKB phase Φ, which is sensitive to the hard-core scale r_c. Since the detailed behavior of the potential is typically not known precisely, in many cases neither the sign of the scattering length nor the number of bound states can be determined from *ab initio* calculations. The toy-model result, however, is useful beyond the identification of a_c as the characteristic scale for the scattering length. Indeed, if ignorance about the short-range physics is replaced by the (maximum likelihood) assumption of a uniform distribution of Φ in the relevant interval $[0, \pi]$, the probability for finding a positive scattering length, i.e., $\tan \Phi < 1$, is 3/4. A repulsive interaction at low energy, which is connected with a positive scattering length, is therefore three times more likely than an attractive one, where $a < 0$ (Pethick and Smith, 2002). Concerning the effective range r_e in Eq. (4), it turns out that r_e is also on the order of the van der Waals or the mean scattering length $\bar{a}$ rather than the short-range scale r_c, as might have been expected naively[2] (Flambaum *et al.*, 1999). Since $ka_c \ll 1$ in the regime of ultracold collisions, this implies that the k^2 contribution in the denominator of the scattering amplitude is negligible. In the low-energy limit, the two-body collision problem is thus completely specified by the scattering length a as the single parameter, and the corresponding scattering amplitude

$$f(k) = -a/(1 + ika). \quad (6)$$

As noted by Fermi in the context of scattering of slow neutrons and by Lee, Huang, and Yang for the low-temperature thermodynamics of weakly interacting quantum gases, Eq. (6) is the exact scattering amplitude at *arbitrary* values of k for the pseudopotential,[3]

$$V(\mathbf{x})(\cdots) = \frac{4\pi\hbar^2 a}{2M_r} \delta(\mathbf{x}) \frac{\partial}{\partial r}(r \cdots). \quad (7)$$

At temperatures such that $k_B T < E_c$, two-body interactions in ultracold gases may be described by a pseudopotential, with the scattering length usually taken as an experimentally determined parameter. This approximation is valid in a wide range of situations, provided no longer-range contributions come into play as, e.g., in the case of dipolar gases. The interaction is repulsive for positive and attractive for negative scattering lengths. Now, as shown above, the true interaction potential has many bound states, irrespective of the sign of a. For low-energy scattering of atoms, however, these bound states are irrelevant as long as no molecule formation occurs via three-body collisions. The scattering amplitude in the limit $k \rightarrow 0$ is sensitive only to bound (or virtual for $a < 0$) states near zero energy. In particular, within the pseudopotential approximation, the amplitude (6) has a single pole $k = i\kappa$, with $\kappa = 1/a > 0$ if the scattering length is positive. Quite generally, poles of the scattering amplitude in the upper complex k plane are connected with bound states with binding energy $\varepsilon_b = \hbar^2 \kappa^2 / 2M_r$ (Landau and Lifshitz, 1987). In the pseudopotential approximation, only a single pole is captured; the energy of the associated bound state is just below the continuum threshold. A repulsive pseudopotential thus describes a situation in which the full potential has a bound state with a binding energy $\varepsilon_b = \hbar^2 / 2M_r a^2$ on the order of or smaller than the characteristic energy E_c introduced above. The associated positive scattering length is then identical with the decay length of the wave function $\sim \exp(-r/a)$ of the highest bound state. In the attractive case $a < 0$, in turn, there is no bound state within a range E_c below the continuum threshold; however, there is a virtual state just above it.

B. Weak interactions

For a qualitative discussion of what defines the weak-interaction regime in dilute, ultracold gases, it is useful to start with the idealization of no interactions at all. Depending on the two fundamental possibilities for the statistics of indistinguishable particles, Bose or Fermi, the ground state of a gas of N noninteracting particles is either a perfect BEC or a Fermi sea. In the case of an ideal BEC, all particles occupy the lowest available single-particle level, consistent with a fully symmetric many-body wave function. For fermions, in turn, the

---

[2]This is a general result for deep potentials with a power-law decay at large distances, as long as the scattering energy is much smaller than the depth of the potential well.

[3]Because of the δ function, the last term involving the partial derivative with respect to $r = |\mathbf{x}|$ can be omitted when the potential acts on a function that is regular at $r = 0$.

particles fill the N lowest single-particle levels up to the Fermi energy $\epsilon_F(N)$, as required by the Pauli principle. At finite temperatures, the discontinuity in the Fermi-Dirac distribution at $T=0$ is smeared out, giving rise to a continuous evolution from the degenerate gas at $k_B T \ll \epsilon_F$ to a classical gas at high temperatures $k_B T \gtrsim \epsilon_F$. By contrast, bosons exhibit in three dimensions (3D) a phase transition at finite temperature, where the macroscopic occupancy of the ground state is lost. In the homogeneous gas, this transition occurs when the thermal de Broglie wavelength $\lambda_T = h/\sqrt{2\pi M k_B T}$ reaches the average interparticle distance $n^{-1/3}$. The surprising fact that a phase transition appears even in an ideal Bose gas is a consequence of the correlations imposed by the particle statistics alone, as noted already in Einstein's fundamental paper (Einstein, 1925). For trapped gases, with geometrical mean trap frequency $\bar{\omega}$, the transition to a BEC is in principle smooth.[4] Yet, for typical particle numbers in the range $N \approx 10^4 – 10^7$, there is a rather sharply defined temperature $k_B T_c^{(0)} = \hbar \bar{\omega} [N/\zeta(3)]^{1/3}$, above which the occupation of the oscillator ground state is no longer of order N. This temperature is again determined by the condition that the thermal de Broglie wavelength reaches the average interparticle distance at the center of the trap [see Eq. (95) and below].

As discussed above, interactions between ultracold atoms are described by a pseudopotential (7), whose strength $g = 4\pi\hbar^2 a/2M_r$ is fixed by the exact s-wave scattering length a. Now, for identical fermions, there is no s-wave scattering due to the Pauli principle. In the regime $ka_c \ll 1$, where all higher momenta $l \neq 0$ are frozen out, a single-component Fermi gas thus approaches an ideal, noninteracting quantum gas. To reach the necessary temperatures, however, requires thermalization by elastic collisions. For identical fermions, p-wave collisions dominate at low temperatures, whose cross section $\sigma_p \sim E^2$ leads to a vanishing of the scattering rates $\sim T^2$ (DeMarco et al., 1999). Evaporative cooling, therefore, does not work for a single-component Fermi gas in the degenerate regime. This problem may be circumvented by cooling in the presence of a different spin state that is then removed, or by sympathetic cooling with a another atomic species. In this manner, an ideal Fermi gas, which is one paradigm of statistical physics, has first been realized by DeMarco and Jin (1999), Schreck et al. (2001), and Truscott et al. (2001) (see Fig. 1).

In the case of fermion mixtures in different internal states, or for bosons, there is in general a finite scattering length $a \neq 0$, which is typically of the order of the van der Waals length Eq. (2). By a simple dimensional argument, interactions are expected to be weak when the scattering length is much smaller than the average interparticle spacing. Since ultracold alkali-metal gases have
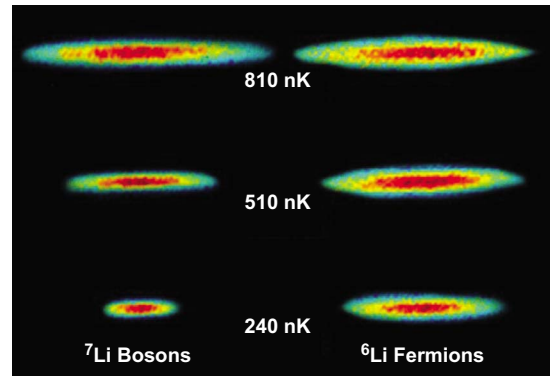

FIG. 1. (Color online) Simultaneous cooling of a bosonic and fermionic quantum gas of ^{17}Li and ^{6}Li to quantum degeneracy. In the case of the Fermi gas, the Fermi pressure prevents the atom cloud from shrinking further in space as quantum degeneracy is approached. From Truscott et al., 2001.

densities between 10^{12} and 10^{15} particles per cm^3, the average interparticle spacing $n^{-1/3}$ typically is in the range $0.1–1$ μm. As shown above, the scattering length, in turn, is usually only in the few-nanometer range. Interaction effects are thus expected to be very small, unless the scattering length happens to be large near a zero-energy resonance of Eq. (5). In the attractive case $a < 0$, however, even small interactions can lead to instabilities. In particular, attractive bosons are unstable toward collapse. However, in a trap, a metastable gaseous state arises for sufficiently small atom numbers (Pethick and Smith, 2002). For mixtures of fermions in different internal states, an arbitrary weak attraction leads to the BCS instability, where the ground state is essentially a BEC of Cooper pairs (see Sec. VIII). In the case of repulsive interactions, in turn, perturbation theory works in the limit $n^{1/3}a \ll 1$.[5] For fermions with two different internal states, an appropriate description is provided by the dilute gas version of Landau's theory of Fermi liquids. The associated ground-state chemical potential is given by (Lifshitz and Pitaevskii, 1980)

$$\mu_F = \frac{\hbar^2 k_F^2}{2M}\left(1 + \frac{4}{3\pi}k_F a + \frac{4(11 - 2\ln 2)}{15\pi^2}(k_F a)^2 + \cdots\right),$$

(8)

where the Fermi wave vector $k_F = (3\pi^2 n)^{1/3}$ is determined by the total density n in precisely the same manner as in the noninteracting case. Weakly interacting Bose gases, in turn, are described by the Bogoliubov theory, which has $\sqrt{na^3}$ as the relevant small parameter. For example, the chemical potential at zero temperature

---

[4] A Bose gas in a trap exhibits a sharp transition only in the limit $N \to \infty$, $\bar{\omega} \to 0$ with $N\bar{\omega}^3 = \text{const}$, i.e., when the critical temperature approaches a finite value in the thermodynamic limit.

[5] We neglect the possibility of a Kohn-Luttinger instability (Kohn and Luttinger, 1965) of repulsive fermious to a (typically) p-wave superfluid state, which usually only appears at temperatures very far below T_F; see Baranov et al. (1996).

for a homogeneous gas is given by (Lifshitz and Pitaevskii, 1980)

$$\mu_{\text{Bose}} = \frac{4\pi\hbar^2 a}{M} n \left[1 + \frac{32}{3}\left(\frac{na^3}{\pi}\right)^{1/2} + \cdots \right]. \tag{9}$$

Moreover, interactions lead to a depletion

$$n_0 = n[1 - \tfrac{8}{3}(na^3/\pi)^{1/2} + \cdots] \tag{10}$$

of the density n_0 of particles at zero momentum compared to the perfect condensate of an ideal Bose gas. The finite value of the chemical potential at zero temperature defines a characteristic length ξ by $\hbar^2/2M\xi^2 = \mu_{\text{Bose}}$. This is the so-called healing length (Pitaevskii and Stringari, 2003), which is the scale over which the macroscopic wave function $\psi(\mathbf{x})$ varies near a boundary (or a vortex core; see Sec. VII) where BEC is suppressed. To lowest order in $\sqrt{na^3}$, this length is given by $\xi = (8\pi na)^{-1/2}$. In the limit $na^3 \ll 1$, the healing length is therefore much larger than the average interparticle spacing $n^{-1/3}$. In practice, the dependence on the gas parameter na^3 is so weak that the ratio $\xi n^{1/3} \sim (na^3)^{-1/6}$ is never very large. On a microscopic level, ξ is the length associated with the ground-state energy per particle by the uncertainty principle. It can thus be identified with the scale over which bosons may be considered to be localized spatially. For weak-coupling BEC's, atoms are therefore smeared out over distances much larger than the average interparticle spacing.

Interactions also shift the critical temperature for BEC away from its value $T_c^{(0)}$ in the ideal Bose gas. To lowest order in the interactions, the shift is positive and linear in the scattering length (Baym et al., 1999),

$$T_c/T_c^{(0)} = 1 + cn^{1/3}a + \cdots \tag{11}$$

with a numerical constant $c \approx 1.32$ (Arnold and Moore, 2001; Kashurnikov et al., 2001). The unexpected increase of the BEC condensation temperature with interactions is due to a reduction of the critical density. While a quantitative derivation of Eq. (11) requires quite sophisticated techniques (Holzmann et al., 2004), the result can be recovered by a simple argument. To leading order, the interaction induced change in T_c depends only on the scattering length. Compared with the noninteracting case, the finite scattering length may be thought of as effectively increasing the quantum-mechanical uncertainty in the position of each atom due to thermal motion from λ_T to $\bar{\lambda}_T = \lambda_T + a$. To lowest order in a, the modified ideal gas criterion $n\bar{\lambda}_{T_c}^3 = \zeta(3/2)$ then gives rise to the linear and positive shift of the critical temperature in Eq. (11) with a coefficient $\bar{c} \approx 1.45$, which is not far from the numerically exact value.

In the standard situation of a gas confined in a harmonic trap with characteristic frequency $\bar{\omega}$, the influence of weak interactions is quantitatively different for temperatures near $T=0$ or near the critical temperature T_c. At zero temperature, the noninteracting Bose gas has a density distribution $n^{(0)}(\mathbf{x}) = N|\phi_0(\mathbf{x})|^2$, which reflects the

harmonic-oscillator ground state wave function $\phi_0(\mathbf{x})$. Its characteristic width is the oscillator length $\ell_0 = \sqrt{\hbar/M\bar{\omega}}$, which is on the order of 1 μm for typical confinement frequencies. Adding even small repulsive interactions changes the distribution quite strongly. Indeed, in the experimentally relevant limit $Na \gg \ell_0$, the density profile $n(\mathbf{x})$ in the presence of an external trap potential $U(\mathbf{x})$ can be obtained from the local-density approximation (LDA)

$$\mu[n(\mathbf{x})] + U(\mathbf{x}) = \mu[n(0)]. \tag{12}$$

For weakly interacting bosons in an isotropic harmonic trap, the linear dependence $\mu_{\text{Bose}} = gn$ of the chemical potential on the density in the homogeneous case then leads to a Thomas-Fermi profile $n(\mathbf{x}) = n(0)[1 - (r/R_{\text{TF}})^2]$. Using the condition $\int n(\mathbf{x}) = N$, the associated radius $R_{\text{TF}} = \zeta\ell_0$ exceeds considerably the oscillator length since the dimensionless parameter $\zeta = (15Na/\ell_0)^{1/5}$ is typically much larger than 1 (Giorgini et al., 1997).[6] This broadening leads to a significant decrease in the density $n(\mathbf{0})$ at the trap center by a factor ζ^{-3} compared with the noninteracting case. The strong effect of even weak interactions on the ground state in a trap may be understood from the fact that the chemical potential $\mu = \hbar\bar{\omega}\zeta^2/2$ is much larger than the oscillator ground-state energy. Interactions are thus able to mix in many single-particle levels beyond the harmonic trap ground state. Near the critical temperature, in turn, the ratio $\mu/k_BT_c \simeq [n(\mathbf{0})a^3]^{1/6}$ is small. Interaction corrections to the condensation temperature, which dominate finite-size corrections for particle numbers much larger than $N \simeq 10^4$, are therefore accessible perturbatively (Giorgini et al., 1997). In contrast to the homogeneous case, where the density is fixed and T_c is shifted upward, the dominant effect in a trap arises from the reduced density at the trap center. The corresponding shift may be expressed as $\Delta T_c/T_c = -\text{const} \times a/\lambda_{T_c}$ (Giorgini et al., 1997; Holzmann et al., 2004; Davis and Blakie, 2006). A precise measurement of this shift has been performed by Gerbier et al. (2004). Their results are in quantitative agreement with mean-field theory, with no observable contribution of critical fluctuations at their level of sensitivity. Quite recently, evidence for critical fluctuations has been inferred from measurements of the correlation length $\xi \sim (T-T_c)^{-\nu}$ very close to T_c. The observed value $\nu = 0.67 \pm 0.13$ (Donner et al., 2007) agrees well with the expected critical exponent of the 3D XY model.

In spite of the strong deviations in the density distribution compared to the noninteracting case, the one- and two-particle correlations of weakly interacting

---

[6]For fermions, the validity of the LDA, which is in fact just a semiclassical approximation [see, e.g., Brack and Bhaduri (1997)], does not require interactions. The leading term $\mu_{\text{Fermi}} \sim n^{2/3}$ of Eq. (8) leads to a density profile $n(\mathbf{x}) = n(0)[1 - (r/R_{\text{TF}})^2]^{3/2}$ with a radius $R_{\text{TF}} = \zeta\ell_0$. Here $\zeta = k_F(N)\ell_0 = (24N)^{1/6} \gg 1$ and the Fermi wave vector $k_F(N)$ in a trap is $\epsilon_F(N) = \hbar^2 k_F^2(N)/2M$.

bosons are well described by approximating the many-body ground state of N bosons by a product

$$\Psi_{GP}(\mathbf{x}_1, \mathbf{x}_2, \ldots, \mathbf{x}_N) = \prod_{i=1}^{N} \phi_1(\mathbf{x}_i) \tag{13}$$

in which all atoms are in the identical single-particle state $\phi_1(\mathbf{x})$. Taking Eq. (13) as a variational ansatz, the optimal macroscopic wave function $\phi_1(\mathbf{x})$ is found to obey the well-known Gross-Pitaevskii equation. More generally, it turns out that for trapped BEC's, the Gross-Pitaevskii theory can be derived mathematically by taking the limits $N \to \infty$ and $a \to 0$ in such a way that the ratio Na/ℓ_0 is fixed (Lieb *et al.*, 2000). A highly nontrivial aspect of these derivations is that they show explicitly that, in the dilute limit, interactions enter only via the scattering length. The Gross-Pitaevskii equation thus remains valid, e.g., for a dilute gas of hard spheres. Since the interaction energy is of kinetic origin in this case, the standard mean-field derivation of the Gross-Pitaevskii equation via the replacement of the field operators by a classical c number $\hat{\Psi}(\mathbf{x}) \to \sqrt{N}\phi_1(\mathbf{x})$ is thus incorrect in general. From a many-body point of view, the ansatz Eq. (13), where the ground state is written as a product of optimized single-particle wave functions, is the standard Hartree approximation. It is the simplest possible approximation to account for interactions; however, it contains no interaction-induced correlations between *different* atoms at all. A first step beyond that is the well-known Bogoliubov theory. This is usually introduced by considering small fluctuations around the Gross-Pitaevskii equation in a systematic expansion in the number of noncondensed particles (Castin and Dum, 1998). It is also instructive from a many-body point of view to formulate Bogoliubov theory such that the boson ground state is approximated by an optimized product (Lieb, 1963b)

$$\Psi_{Bog}(\mathbf{x}_1, \mathbf{x}_2, \ldots, \mathbf{x}_N) = \prod_{i<j} \phi_2(\mathbf{x}_i, \mathbf{x}_j) \tag{14}$$

of identical, symmetric two-particle wave functions ϕ_2. This allows one to include interaction effects beyond the Hartree potential of the Gross-Pitaevskii theory by suppressing configurations in which two particles are close together. The many-body state thus incorporates two-particle correlations that are important, e.g., to obtain the standard sound modes and the related coherent superposition of "particle" and "hole" excitations. This structure, which has been experimentally verified by Vogels *et al.* (2002), is expected to apply in a qualitative form even for strongly interacting BEC's, whose low-energy excitations are exhausted by harmonic phonons (see the Appendix).

Quantitatively, however, the Bogoliubov theory is restricted to the regime $\sqrt{na^3} \ll 1$, where interactions lead only to a small depletion (10) of the condensate at zero temperature. Going beyond that requires one to specify the detailed form of the interaction potential $V(r)$ and not only the associated scattering length a. The ground

state of a gas of hard-sphere bosons, for instance, loses BEC already for $na^3 \gtrsim 0.24$ by a first-order transition to a solid state (Kalos *et al.*, 1974). On a variational level, choosing the two-particle wave functions in Eq. (14) of the form $\phi_2(\mathbf{x}_i, \mathbf{x}_j) \sim \exp{-u(|\mathbf{x}_i - \mathbf{x}_j|)}$ with an effective two-body potential $u(r)$ describes so-called Jastrow wave functions. They allow taking into account strong short-range correlations; however, they still exhibit BEC even in a regime in which the associated one-particle density describes a periodic crystal rather than a uniform liquid, as shown by Chester (1970). Crystalline order may thus coexist with BEC. For a discussion of this issue in the context of a possible supersolid phase of ^{4}He, see Clark and Ceperley (2006).

For weakly interacting fermions at $k_F a \ll 1$, the variational ground state, which is analogous to Eq. (13), is a Slater determinant

$$\Psi_{HF}(\mathbf{x}_1, \mathbf{x}_2, \ldots, \mathbf{x}_N) = \det[\phi_{1,i}(\mathbf{x}_j)] \tag{15}$$

of optimized single-particle states $\phi_{1,i}(\mathbf{x}_j)$. In the translationally invariant case, they are plane waves $\phi_{1,i}(\mathbf{x}) = V^{-1/2} \exp(i\mathbf{k}_i \cdot \mathbf{x})$, where the momenta $\mathbf{k}_i$ are filled up to the Fermi momentum k_F. Although both the Bose and Fermi ground-state wave functions consist of symmetrized or antisymmetrized single-particle states, they describe fundamentally different physics. In the Bose case, the one-particle density matrix $g^{(1)}(\infty) = n_0/n$ approaches a finite constant at infinite separation, which is the basic criterion for BEC (see the Appendix). The many-body wave function is thus sensitive to changes of the phase at points separated by distances r that are large compared to the interparticle spacing. By contrast, the Hartree-Fock state (15) for fermions shows no long-range phase coherence, and indeed the one-particle density matrix decays exponentially $g^{(1)}(r) \sim \exp(-\gamma r)$ at any finite temperature (Ismail-Beigi and Arias, 1999). The presence of N *distinct* eigenstates in Eq. (15), which is a necessary consequence of the Pauli principle, leads to a many-body wave function that may be characterized as *nearsighted*. The notion of nearsightedness depends on the observable, however. As defined originally by Kohn (1996), it means that a localized external potential around some point $\mathbf{x}'$ is not felt at a point $\mathbf{x}$ at a distance much larger than the average interparticle spacing. This requires the density response function $\chi(\mathbf{x}, \mathbf{x}')$ to be short ranged in position space. In this respect, weakly interacting bosons, where $\chi(\mathbf{x}, \mathbf{x}') \sim [\exp(-|\mathbf{x} - \mathbf{x}'|/\xi)]/|\mathbf{x} - \mathbf{x}'|$ decays exponentially on the scale of the healing length ξ, are more nearsighted than fermions at zero temperature, where $\chi(\mathbf{x}, \mathbf{x}') \sim \sin(2k_F|\mathbf{x} - \mathbf{x}'|)/|\mathbf{x} - \mathbf{x}'|^3$ exhibits an algebraic decay with Friedel oscillations at twice the Fermi wave vector $2k_F$. The characterization of many-body wave functions in terms of the associated correlation functions draws attention to another basic point emphasized by Kohn (1999): in situations with a large number of particles, the many-body wave function itself is not a meaningful quantity because it cannot be calculated reliably for $N \gtrsim 100$. Moreover, physically accessible observables are sensitive only to the resulting

one-or two-particle correlations. Cold gases provide a concrete example for the latter statement: the standard time-of-flight technique of measuring the absorption image after a given free-expansion time t provides the one-particle density matrix in Fourier space, while the two-particle density matrix is revealed in the noise correlations of absorption images (see Sec. III).

C. Feshbach resonances

The most direct way of reaching the strong-interaction regime in dilute, ultracold gases is via Feshbach resonances, which allow the scattering length to be increased to values beyond the average interparticle spacing. In practice, this method works best for fermions because for them the lifetime due to three-body collisions becomes very large near a Feshbach resonance, in stark contrast to bosons, where it goes to zero. The concept was first introduced in the context of reactions forming a compound nucleus (Feshbach, 1958) and, independently, for a description of configuration interactions in multi-electron atoms (Fano, 1961). Quite generally, a Feshbach resonance in a two-particle collision appears whenever a bound state in a closed channel is coupled resonantly with the scattering continuum of an open channel. The two channels may correspond, for example, to different spin configurations for atoms. The scattered particles are then temporarily captured in the quasibound state, and the associated long time delay gives rise to a Breit-Wigner-type resonance in the scattering cross section. What makes Feshbach resonances in the scattering of cold atoms particularly useful is the ability to tune the scattering length simply by changing the magnetic field (Tiesinga *et al.*, 1993). This tunability relies on the difference in the magnetic moments of the closed and open channels, which allows the position of closed-channel bound states relative to the open-channel threshold to be changed by varying the external, uniform magnetic field. Note that Feshbach resonances can alternatively be induced optically via one- or two-photon transitions (Fedichev, Kagan, Shlyapnikov, *et al.*, 1996; Bohn and Julienne, 1999) as realized by Theis *et al.* (2004). The control parameter is then the detuning of the light from atomic resonance. Although more flexible in principle, this method suffers, however, from heating problems for typical atomic transitions, associated with the spontaneous-emission processes created by the light irradiation.

On a phenomenological level, Feshbach resonances are described by an effective pseudopotential between atoms in the open channel with scattering length

$$a(B) = a_{bg}[1 - \Delta B/(B - B_0)]. \tag{16}$$

Here a_{bg} is the off-resonant background scattering length in the absence of the coupling to the closed channel, while ΔB and B_0 describe the width and position of the resonance expressed in magnetic field units (see Fig. 2). In this section, we outline the basic physics of magnetically tunable Feshbach resonances, providing a connection of the parameters in Eq. (16) with the inter-
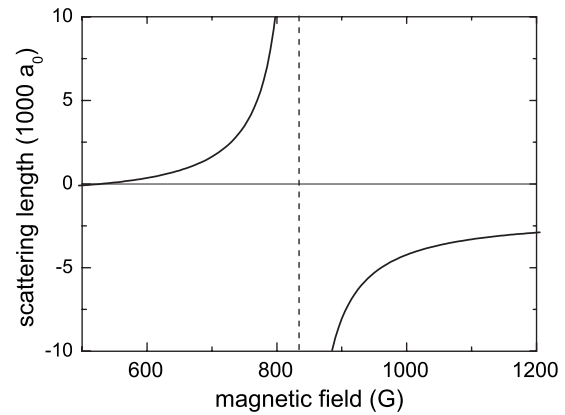

FIG. 2. Magnetic field dependence of the scattering length between the two lowest magnetic substates of ^{6}Li with a Feshbach resonance at $B_0 = 834$ G and a zero crossing at $B_0 + \Delta B = 534$ G. The background scattering length $a_{bg} = -1405 a_B$ is exceptionally large in this case (a_B the Bohr radius).

atomic potentials. Of course, our discussion covers only the basic background for understanding the origin of large and tunable scattering lengths. A more detailed presentation of Feshbach resonances can be found in the reviews by Timmermans *et al.* (2001); Duine and Stoof (2004); and Köhler *et al.* (2006).

Open and closed channels. We start with the specific example of fermionic ^{6}Li atoms, which have electronic spin $S = 1/2$ and nuclear spin $I = 1$. In the presence of a magnetic field **B** along the z direction, the hyperfine coupling and Zeeman energy lead for each atom to the Hamiltonian

$$\hat{H}' = a_{hf}\hat{\mathbf{S}} \cdot \hat{\mathbf{I}} + (2\mu_B \hat{S}_z - \mu_n \hat{I}_z)B. \tag{17}$$

Here $\mu_B > 0$ is the standard Bohr magneton and μ_n ($\ll \mu_B$) is the magnetic moment of the nucleus. This hyperfine Zeeman Hamiltonian actually holds for any alkali-metal atom, with a single valence electron with zero orbital angular momentum. If $B \to 0$, the eigenstates of this Hamiltonian are labeled by the quantum numbers f and m_f, giving the total spin angular momentum and its projection along the z axis, respectively. In the opposite Paschen-Back regime of large magnetic fields ($B \gg a_{hf}/\mu_B \simeq 30$ G in lithium), the eigenstates are labeled by the quantum numbers m_s and m_I, giving the projection on the z axis of the electron and nuclear spins, respectively. The projection $m_f = m_s + m_I$ of the total spin along the z axis remains a good quantum number for any value of the magnetic field.

Consider a collision between two lithium atoms, prepared in the two lowest eigenstates $|a\rangle$ and $|b\rangle$ of the Hamiltonian (17) in a large magnetic field. The lowest state $|a\rangle$ (with $m_{fa} = 1/2$) is $\approx |m_s = -1/2, m_I = 1\rangle$ with a small admixture of $|m_s = 1/2, m_I = 0\rangle$, whereas $|b\rangle$ (with $m_{fb} = -1/2$) is $\approx |m_s = -1/2, m_I = 0\rangle$ with a small admixture of $|m_s = 1/2, m_I = -1\rangle$. Two atoms in these two lowest

states thus predominantly scatter into their triplet state.[7] Quite generally, the interaction potential during the collision can be written as a sum

$$V(r) = \tfrac{1}{4}[3V_t(r) + V_s(r)] + \hat{\mathbf{S}}_1 \cdot \hat{\mathbf{S}}_2 [V_t(r) - V_s(r)] \quad (18)$$

of projections onto the singlet $V_s(r)$ and triplet $V_t(r)$ molecular potentials, where the $\hat{\mathbf{S}}_i$'s ($i=1,2$) are the spin operators for the valence electron of each atom. These potentials have the same van der Waals attractive behavior at long distances, but they differ considerably at short distances, with a much deeper attractive well for the singlet than for the triplet potential. Now, in a large but finite magnetic field, the initial state $|a,b\rangle$ is not a purely triplet state. Because of the tensorial nature of $V(r)$, this spin state will thus evolve during the collision. More precisely, since the second term in Eq. (18) is not diagonal in the basis $|a,b\rangle$, the spin state $|a,b\rangle$ may be coupled to other scattering channels $|c,d\rangle$, provided the z projection of the total spin is conserved ($m_{fc}+m_{fd} = m_{fa}+m_{fb}$). When the atoms are far apart, the Zeeman +hyperfine energy of $|c,d\rangle$ exceeds the initial kinetic energy of the pair of atoms prepared in $|a,b\rangle$ by an energy on the order of the hyperfine energy. Since the thermal energy is much smaller than that for ultracold collisions, the channel $|c,d\rangle$ is closed and the atoms always emerge from the collision in the open-channel state $|a,b\rangle$. However, due to the strong coupling of (a,b) to (c,d) via the second term in Eq. (18), which is typically on the order of eV, the effective scattering amplitude in the open channel can be strongly modified.

Two-channel model. We now present a simple two-channel model that captures the main features of a Feshbach resonance (see Fig. 3). Consider a collision between two atoms with reduced mass M_r, and model the system in the vicinity of the resonance by the Hamiltonian (Nygaard *et al.*, 2006)

$$\hat{H} = \begin{pmatrix} -\dfrac{\hbar^2}{2M_r}\nabla^2 + V_{op}(r) & W(r) \\ W(r) & -\dfrac{\hbar^2}{2M_r}\nabla^2 + V_{cl}(r) \end{pmatrix}. \quad (19)$$

Before collision, the atoms are prepared in the *open channel*, whose potential $V_{op}(r)$ gives rise to the background scattering length a_{bg}. Here the zero of energy is chosen such that $V_{op}(\infty)=0$. In the course of the collision, a coupling to the *closed channel* with potential $V_{cl}(r)$ [$V_{cl}(\infty)>0$] occurs via the matrix element $W(r)$, whose range is on the order of the atomic scale r_c. For simplicity, we consider here only a *single* closed channel, which is appropriate for an isolated resonance. We also assume that the value of a_{bg} is on the order of the van der Waals length (2). If a_{bg} is anomalously large, as occurs, e.g., for the ^{6}Li resonance shown in Fig. 2, an ad-
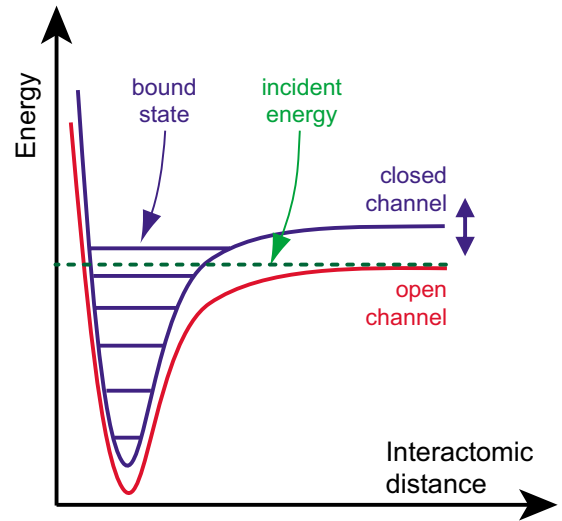

FIG. 3. (Color online) The two-channel model for a Feshbach resonance. Atoms prepared in the open channel, corresponding to the interaction potential $V_{op}(r)$, undergo a collision at low incident energy. In the course of the collision, the open channel is coupled to the closed channel $V_{cl}(r)$. When a bound state of the closed channel has an energy close to zero, a scattering resonance occurs. The position of the closed channel can be tuned with respect to the open one, e.g., by varying the magnetic field B.

ditional open-channel resonance has to be included in the model, as discussed by Marcelis *et al.* (2004).

We assume that the magnetic moments of the colliding states differ for the open and closed channels, and denote their difference by μ. Varying the magnetic field by δB, therefore, amounts to shifting the closed-channel energy by $\mu\delta B$ with respect to the open channel. In the following, we are interested in the magnetic field region close to B_{res} such that one (normalized) bound state $\phi_{res}(r)$ of the closed-channel potential $V_{cl}(r)$ has an energy $E_{res}(B)=\mu(B-B_{res})$ close to 0. It can thus be resonantly coupled to the collision state where two atoms in the open channel have a small positive kinetic energy. In the vicinity of the Feshbach resonance, the situation is now similar to the well-known Breit-Wigner problem [see, e.g., Landau and Lifshitz (1987), Sec. 134]. A particle undergoes a scattering process in a (single-channel) potential with a quasi- or true bound state at an energy ν, which is nearly resonant with the incoming energy $E(k)=\hbar^2k^2/2M_r$. According to Breit and Wigner, this leads to a resonant contribution

$$\delta_{res}(k) = -\arctan(\Gamma(k)/2[E(k)-\nu]) \quad (20)$$

to the scattering phase shift, where $\nu=\mu(B-B_0)$ is conventionally called the *detuning* in this context (for the difference between B_{res} and B_0, see below). The associated resonance width $\Gamma(k)$ vanishes near zero energy, with a threshold behavior linear in $k=\sqrt{2M_rE}/\hbar$ due to the free-particle density of states. It is convenient to define a characteristic length $r^\star>0$ by

---

[7]The fact that there is a nonvanishing *s*-wave scattering length for these states is connected with the different *nuclear* and not electronic spin in this case.

$$\Gamma(k \to 0)/2 = \hbar^2 k/2M_r r^\star. \tag{21}$$

The scattering length $a = -\lim_{k \to 0} \tan(\delta_{\mathrm{bg}} + \delta_{\mathrm{res}})/k$ then has the simple form

$$a = a_{\mathrm{bg}} - \hbar^2/2M_r r^\star \nu. \tag{22}$$

This agrees precisely with Eq. (16) provided the width parameter ΔB is identified with the combination $\mu \Delta B a_{\mathrm{bg}} = \hbar^2/2M_r r^\star$ of the two characteristic lengths a_{bg} and $r^\star$.

On a microscopic level, these parameters may be obtained from the two-channel Hamiltonian (19) by the standard Green's-function formalism. In the absence of coupling $W(r)$, the scattering properties of the open channel are characterized by $G_{\mathrm{op}}(E) = (E - H_{\mathrm{op}})^{-1}$, with $H_{\mathrm{op}} = P^2/2M_r + V_{\mathrm{op}}(r)$. We denote by $|\phi_0\rangle$ the eigenstate of H_{op} associated with the energy 0, which behaves as $\phi_0(r) \sim 1 - a_{\mathrm{bg}}/r$ for large r. In the vicinity of the resonance, the closed channel contributes through the state ϕ_{res}, and its Green's function reads

$$G_{\mathrm{cl}}(E, B) \simeq |\phi_{\mathrm{res}}\rangle\langle\phi_{\mathrm{res}}|/[E - E_{\mathrm{res}}(B)]. \tag{23}$$

With this approximation, one can project the eigenvalue equation for the Hamiltonian $\hat{H}$ onto the background and closed channels. One can then derive the scattering length $a(B)$ of the coupled-channel problem and write it in the form of Eq. (16). The position of the zero-energy resonance B_0 is shifted with respect to the "bare" resonance value B_{res} by

$$\mu(B_0 - B_{\mathrm{res}}) = -\langle\phi_{\mathrm{res}}|W G_{\mathrm{op}}(0)W|\phi_{\mathrm{res}}\rangle. \tag{24}$$

The physical origin of this resonance shift is that an infinite scattering length requires that the contributions to $k \cot \delta(k)$ in the total scattering amplitude from the open and closed channels precisely cancel. In a situation in which the background scattering length deviates considerably from its typical value $\bar{a}$ and where the off-diagonal coupling measured by ΔB is strong, this cancellation already appears when the bare closed-channel bound state is far away from the continuum threshold. A simple analytical estimate for this shift has been given by Julienne *et al.* (2004),

$$B_0 = B_{\mathrm{res}} + \Delta B x (1-x)/[1 + (1-x)^2], \tag{25}$$

where $x = a_{\mathrm{bg}}/\bar{a}$. The characteristic length r^* defined in Eq. (21) is determined by the off-diagonal coupling via

$$\langle\phi_{\mathrm{res}}|W|\phi_0\rangle = (\hbar^2/2M_r)\sqrt{4\pi/r^\star}. \tag{26}$$

Its inverse $1/r^*$ is therefore a measure of how strongly the open and closed channels are coupled. In the experimentally most relevant case of wide resonances, the length r^* is much smaller than the background scattering length. Specifically, this applies to the Feshbach resonances in fermionic ^{6}Li and ^{40}K at $B_0 = 834$ and 202 G, respectively, which have been used to study the BCS-BEC crossover with cold atoms (see Sec. VIII). They are characterized by the experimentally determined parameters $a_{\mathrm{bg}} = -1405 a_B$, $\Delta B = -300$ G, $\mu = 2\mu_B$ and $a_{\mathrm{bg}} = 174 a_B$, $\Delta B = 7.8$ G, $\mu = 1.68\mu_B$, respectively, where a_B

and μ_B are the Bohr radius and Bohr magneton. From these parameters, the characteristic length associated with the two resonances turns out to be $r^\star = 0.5 a_B$ and $r^\star = 28 a_B$, both obeying the wide-resonance condition $r^\star \ll |a_{\mathrm{bg}}|$.

Weakly bound states close to the resonance. In addition to the control of scattering properties, an important feature of Feshbach resonances concerns the possibility to form weakly bound dimers in the regime of small negative detuning $\nu = \mu(B - B_0) \to 0^-$, where the scattering length approaches $+\infty$. We briefly present below some key properties of these dimers, restricting for simplicity to the vicinity of the resonance $|B - B_0| \ll |\Delta B|$.

To determine the bound state for the two-channel Hamiltonian (19), one considers the Green's function $G(E) = (E - \hat{H})^{-1}$ and looks for the low-energy pole at $E = -\varepsilon_{\mathrm{b}} < 0$ of this function. The corresponding bound state can be written

$$\langle\mathbf{x}|\Psi^{(b)}\rangle = \begin{pmatrix} \sqrt{1-Z}\psi_{\mathrm{bg}}(r) \\ \sqrt{Z}\phi_{\mathrm{res}}(r) \end{pmatrix}, \tag{27}$$

where the coefficient Z characterizes the closed-channel admixture. The values of ε_{b} and Z can be calculated explicitly by projecting the eigenvalue equation for $\hat{H}$ on each channel. Close to resonance, where the scattering length is dominated by its resonant contribution, Eq. (22) and the standard relation $\varepsilon_b = \hbar^2/2M_r a^2$ for $a > 0$ show that the binding energy

$$\varepsilon_b = [\mu(B - B_0)]^2/\varepsilon^\star \tag{28}$$

of the weakly bound state vanishes quadratically, with characteristic energy $\varepsilon^\star = \hbar^2/2M_r(r^\star)^2$. In an experimental situation which starts from the atom continuum, it is precisely this weakly bound state which is reached upon varying the detuning by an adiabatic change in the magnetic field around B_0. The associated closed-channel admixture Z can be obtained from the binding energy as

$$Z = -\frac{\partial\varepsilon_b}{\partial\nu} \simeq 2\frac{|\nu|}{\epsilon^\star} = 2\frac{r^*}{|a_{\mathrm{bg}}|}\frac{|B - B_0|}{|\Delta B|}. \tag{29}$$

For a wide resonance, where $r^\star \ll |a_{\mathrm{bg}}|$, this admixture remains much smaller than 1 over the magnetic field range $|B - B_0| \lesssim |\Delta B|$.

The bound state $|\Psi^{(b)}\rangle$ just presented should not be confused with the bound state $|\Phi_{\mathrm{op}}^{(b)}\rangle$, that exists for $a_{\mathrm{bg}} > 0$ in the open channel, for a vanishing coupling $W(r)$. The bound state $|\Phi_{\mathrm{op}}^{(b)}\rangle$ has a binding energy of order $\hbar^2/(2M_r a_{\mathrm{bg}}^2)$, that is much larger than that of Eq. (28) when $|B - B_0| \ll |\Delta B|$. For $|B - B_0| \sim |\Delta B|$ the states $|\Psi^{(b)}\rangle$ and $|\Phi_{\mathrm{op}}^{(b)}\rangle$ have comparable energies and undergo an avoided crossing. The universal character of the above results is then lost and one has to turn to a specific study of the eigenvalue problem.

To conclude, Feshbach resonances provide a flexible tool to change the interaction strength between ultracold atoms over a wide range. To realize a proper many-body Hamiltonian with tunable two-body interactions,

however, an additional requirement is that the relaxation rate into deep bound states due to three-body collisions must be negligible. As discussed in Sec. VIII.A, this is possible for fermions, where the relaxation rate is small near Feshbach resonances (Petrov, Salomon, and Shlyapnikov, 2004, 2005).

II. OPTICAL LATTICES

In the following, we discuss how to confine cold atoms by laser light into configurations of a reduced dimensionality or in periodic lattices, thus generating situations in which the effects of interactions are enhanced.

A. Optical potentials

The physical origin of the confinement of cold atoms with laser light is the dipole force

$$\mathbf{F} = \frac{1}{2}\alpha(\omega_L)\,\boldsymbol{\nabla}\left[|\mathbf{E}(\mathbf{r})|^2\right] \tag{30}$$

due to a spatially varying ac Stark shift that atoms experience in an off-resonant light field (Grimm *et al.*, 2000). Since the time scale for the center-of-mass motion of atoms is much slower than the inverse laser frequency ω_L, only the time-averaged intensity $|\mathbf{E}(\mathbf{r})|^2$ enters. The direction of the force depends on the sign of the polarizability $\alpha(\omega_L)$. In the vicinity of an atomic resonance from the ground $|g\rangle$ to an excited state $|e\rangle$ at frequency ω_0, the polarizability has the form $\alpha(\omega_L) \approx |\langle e|\hat{d}_\mathbf{E}|g\rangle|^2/\hbar(\omega_0-\omega_L)$, with $\hat{d}_\mathbf{E}$ the dipole operator in the direction of the field. Atoms are thus attracted to the nodes or to the antinodes of the laser intensity for blue- ($\omega_L > \omega_0$) or red-detuned ($\omega_L < \omega_0$) laser light, respectively. A spatially dependent intensity profile $I(\mathbf{r})$, therefore, creates a trapping potential for neutral atoms. Within a two-level model, an explicit form of the dipole potential may be derived using the rotating-wave approximation, which is a reasonable approximation provided that the detuning $\Delta = \omega_L - \omega_0$ of the laser field is small compared to the transition frequency itself $|\Delta| \ll \omega_0$. With Γ as the decay rate of the excited state, one obtains for $|\Delta| \gg \Gamma$ (Grimm *et al.*, 2000)

$$V_{\mathrm{dip}}(\mathbf{r}) = \frac{3\pi c^2}{2\omega_0^3}\frac{\Gamma}{\Delta}I(\mathbf{r}), \tag{31}$$

which is attractive or repulsive for red ($\Delta < 0$) or blue ($\Delta > 0$) detuning, respectively. Atoms are thus attracted or repelled from an intensity maximum in space. It is important to note that, in contrast to the form suggested in Eq. (30), the light force is not fully conservative. Indeed, spontaneous emission gives rise to an imaginary part of the polarizability. Within a two-level approximation, the related scattering rate $\Gamma_{\mathrm{sc}}(\mathbf{r})$ leads to an absorptive contribution $\hbar\Gamma_{\mathrm{sc}}(\mathbf{r})$ to the conservative dipole potential (31), which can be estimated as (Grimm *et al.*, 2000)

$$\Gamma_{\mathrm{sc}}(\mathbf{r}) = \frac{3\pi c^2}{2\hbar\omega_0^3}\left(\frac{\Gamma}{\Delta}\right)^2 I(\mathbf{r}). \tag{32}$$

As Eqs. (31) and (32) show, the ratio of scattering rate to the optical potential depth vanishes in the limit $|\Delta| \gg \Gamma$. A strictly conservative potential can thus be reached in principle by increasing the detuning of the laser field. In practice, however, such an approach is limited by the maximum available laser power. For experiments with ultracold quantum gases of alkali-metal atoms, the detuning is typically chosen to be large compared to the excited-state hyperfine structure splitting and in most cases even large compared to the fine-structure splitting in order to sufficiently suppress spontaneous scattering events.

The intensity profile $I(r,z)$ of a Gaussian laser beam propagating along the z direction has the form

$$I(r,z) = [2P/\pi w^2(z)]e^{-2r^2/w^2(z)}. \tag{33}$$

Here P is the total power of the laser beam, r is the distance from the center, and $w(z) = w_0\sqrt{1+z^2/z_R^2}$ is the $1/e^2$ radius. This radius is characterized by a beam waist w_0 that is typically around $100\ \mu$m. Due to the finite beam divergence, the beam width increases linearly with z on a scale $z_R = \pi w_0^2/\lambda$, which is called the Rayleigh length. Typical values for z_R are in the millimeter to centimeter range. Around the intensity maximum, a potential depth minimum occurs for a red-detuned laser beam, leading to an approximately harmonic potential

$$V_{\mathrm{dip}}(r,z) \approx -V_{\mathrm{trap}}[1 - 2(r/w_0)^2 - (z/z_R)^2]. \tag{34}$$

The trap depth V_{trap} is linearly proportional to the laser power and typically ranges from a few kilohertz up to 1 MHz (from the nanokelvin to the microkelvin regime). The harmonic confinement is characterized by radial ω_r and axial ω_z trapping frequencies $\omega_r = (4V_{\mathrm{trap}}/Mw_0^2)^{1/2}$ and $\omega_z = 2V_{\mathrm{trap}}/Mz_R^2$. Optical traps for neutral atoms have a wide range of applications (Grimm *et al.*, 2000). In particular, they are inevitable in situations in which magnetic trapping does not work for the atomic states under consideration. This is often the case when interactions are manipulated via Feshbach resonances, involving high-field-seeking atomic states.

Optical lattices. A periodic potential is generated by overlapping two counterpropagating laser beams. Due to the interference between the two laser beams, an optical standing wave with period $\lambda/2$ is formed, in which atoms can be trapped. More generally, by choosing the two laser beams to interfere under an angle less than 180°, one can also realize periodic potentials with a larger period (Peil *et al.*, 2003; Hadzibabic *et al.*, 2004). The simplest possible periodic optical potential is formed by overlapping two counterpropagating beams. For a Gaussian profile, this results in a trapping potential of the form

$$V(r,z) \simeq -V_0 e^{-2r^2/w^2(z)}\sin^2(kz), \tag{35}$$

where $k = 2\pi/\lambda$ is the wave vector of the laser light and V_0 is the maximum depth of the lattice potential. Note
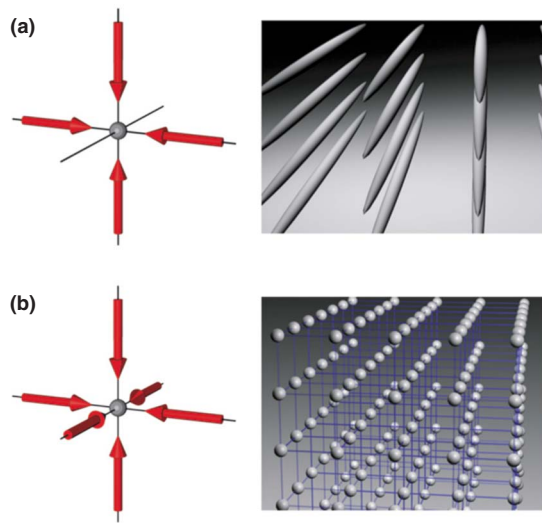
(a)

(b)

FIG. 4. (Color online) Optical lattices. (a) Two- and (b) three-dimensional optical lattice potentials formed by superimposing two or three orthogonal standing waves. For a two-dimensional optical lattice, the atoms are confined to an array of tightly confining one-dimensional potential tubes, whereas in the three-dimensional case the optical lattice can be approximated by a three-dimensional simple cubic array of tightly confining harmonic-oscillator potentials at each lattice site.

that due to the interference of the two laser beams, V_0 is four times larger than V_{trap} if the laser power and beam parameters of the two interfering lasers are equal.

Periodic potentials in two dimensions can be formed by overlapping two optical standing waves along different, usually orthogonal, directions. For orthogonal polarization vectors of the two laser fields, no interference terms appear. The resulting optical potential in the center of the trap is then a simple sum of a purely sinusoidal potential in both directions.

In such a two-dimensional optical lattice potential, atoms are confined to arrays of tightly confining one-dimensional tubes [see Fig. 4(a)]. For typical experimental parameters, the harmonic trapping frequencies along the tube are very weak (on the order of 10–200 Hz), while in the radial direction the trapping frequencies can become as high as up to 100 kHz. For sufficiently deep lattice depths, atoms can move only axially along the tube. In this manner, it is possible to realize quantum wires with neutral atoms, which allows one to study strongly correlated gases in one dimension, as discussed in Sec. V. Arrays of such quantum wires have been realized (Greiner *et al.*, 2001; Moritz *et al.*, 2003; Kinoshita *et al.*, 2004; Paredes *et al.*, 2004; Tolra *et al.*, 2004).

For the creation of a three-dimensional lattice potential, three orthogonal optical standing waves have to be overlapped. The simplest case of independent standing waves, with no cross interference between laser beams of different standing waves, can be realized by choosing orthogonal polarization vectors and by using slightly different wavelengths for the three standing waves. The

resulting optical potential is then given by the sum of three standing waves. In the center of the trap, for distances much smaller than the beam waist, the trapping potential can be approximated as the sum of a homogeneous periodic lattice potential

$$V_p(x,y,z) = V_0(\sin^2 kx + \sin^2 ky + \sin^2 kz) \qquad (36)$$

and an additional external harmonic confinement due to the Gaussian laser beam profiles. In addition to this, a confinement due to the magnetic trapping is often used.

For deep optical lattice potentials, the confinement on a single lattice site is approximately harmonic. Atoms are then tightly confined at a single lattice site, with trapping frequencies ω_0 of up to 100 kHz. The energy $\hbar\omega_0 = 2E_r(V_0/E_r)^{1/2}$ of local oscillations in the well is on the order of several recoil energies $E_r = \hbar^2 k^2/2m$, which is a natural measure of energy scales in optical lattice potentials. Typical values of E_r are in the range of several kilohertz for ^{87}Rb.

Spin-dependent optical lattice potentials. For large detunings of the laser light forming the optical lattices compared to the fine-structure splitting of a typical alkali-metal atom, the resulting optical lattice potentials are almost the same for all magnetic sublevels in the ground-state manifold of the atom. However, for more near-resonant light fields, situations can be created in which different magnetic sublevels can be exposed to vastly different optical potentials (Jessen and Deutsch, 1996). Such spin-dependent lattice potentials can, e.g., be created in a standing wave configuration formed by two counterpropagating laser beams with linear polarization vectors enclosing an angle θ (Jessen and Deutsch, 1996; Brennen *et al.*, 1999; Jaksch *et al.*, 1999; Mandel *et al.*, 2003a). The resulting standing wave light field can be decomposed into a superposition of a σ^+- and a σ^--polarized standing wave laser field, giving rise to lattice potentials $V_+(x,\theta) = V_0 \cos^2(kx + \theta/2)$ and $V_-(x,\theta) = V_0 \cos^2(kx - \theta/2)$. By changing the polarization angle θ, one can control the relative separation between the two potentials $\Delta x = (\theta/\pi)\lambda_x/2$. When θ is increased, both potentials shift in opposite directions and overlap again when $\theta = n\pi$, with n an integer. Such a configuration has been used to coherently move atoms across lattices and realize quantum gates between them (Jaksch *et al.*, 1999; Mandel *et al.*, 2003a, 2003b). Spin-dependent lattice potentials furthermore offer a convenient way to tune interactions between two atoms in different spin states. By shifting the spin-dependent lattices relative to each other, the overlap of the on-site spatial wave function can be tuned between zero and its maximum value, thus controlling the interspecies interaction strength within a restricted range. Recently, Sebby-Strabley *et al.* (2006) have also demonstrated a novel spin-dependent lattice geometry, in which 2D arrays of double-well potentials could be realized. Such "superlattice" structures allow for versatile intrawell and interwell manipulation possibilities (Fölling *et al.*, 2007; Lee *et al.*, 2007; Sebby-Strabley *et al.*, 2007). A variety of lattice structures can be obtained by interfering laser beams under different

angles; see, e.g., Jessen and Deutsch (1996) and Grynberg and Robillard (2001).

B. Band structure

We now consider single-particle eigenstates in an infinite periodic potential. Any additional potential from the intensity profile of the laser beams or from some magnetic confinement is neglected [for the single-particle spectrum in the presence of an additional harmonic confinement, see Hooley and Quintanilla (2004)]. In a simple cubic lattice, the potential is given by Eq. (36), with a tunable amplitude V_0 and lattice constant $d = \pi/k$. In the limit $V_0 \gg E_r$, each well supports a number of vibrational levels, separated by an energy $\hbar\omega_0 \gg E_r$. At low temperatures, atoms are restricted to the lowest vibrational level at each site. Their kinetic energy is then frozen, except for the small tunneling amplitude to neighboring sites. The associated single-particle eigenstates in the lowest band are Bloch waves with quasimomentum $\mathbf{q}$ and energy

$$\varepsilon_0(\mathbf{q}) = \tfrac{3}{2}\hbar\omega_0 - 2J(\cos q_x d + \cos q_y d + \cos q_z d) + \cdots. \tag{37}$$

The parameter $J > 0$ is the gain in kinetic energy due to nearest-neighbor tunneling. In the limit $V_0 \gg E_r$, it can be obtained from the width $W \to 4J$ of the lowest band in the 1D Mathieu equation

$$J \simeq \frac{4}{\sqrt{\pi}} E_r \left(\frac{V_0}{E_r}\right)^{3/4} \exp\left[-2\left(\frac{V_0}{E_r}\right)^{1/2}\right]. \tag{38}$$

For lattice depths larger than $V_0 > 15 E_r$, this approximation agrees with the exact values of J given in Table I to better than 10% accuracy. More generally, for any periodic potential $V_p(\mathbf{r}+\mathbf{R}) = V_p(\mathbf{r})$ which is not necessarily deep and separable, the exact eigenstates are Bloch functions $\psi_{n,\mathbf{q}}(\mathbf{r})$. They are characterized by a discrete band index n and a quasimomentum $\mathbf{q}$ within the first Brillouin zone of the reciprocal lattice (Ashcroft and Mermin, 1976). Since Bloch functions are multiplied by a pure phase factor $\exp(i\mathbf{q}\cdot\mathbf{R})$, upon translation by one of the lattice vectors $\mathbf{R}$, they are extended over the whole lattice. An alternative single-particle basis, which is useful for describing the hopping of particles among discrete lattice sites $\mathbf{R}$, is provided by Wannier functions $w_{n,\mathbf{R}}(\mathbf{r})$. They are connected with the Bloch functions by a Fourier transform

$$\psi_{n,\mathbf{q}}(\mathbf{r}) = \sum_{\mathbf{R}} w_{n,\mathbf{R}}(\mathbf{r}) e^{i\mathbf{q}\cdot\mathbf{R}} \tag{39}$$

on the lattice. The Wannier functions depend only on the relative distance $\mathbf{r}-\mathbf{R}$, and, at least for the lowest bands, they are centered around the lattice sites $\mathbf{R}$ (see below). By choosing a convenient normalization, they obey the orthonormality relation

TABLE I. Hopping matrix elements to nearest J and next-nearest neighbors $J(2d)$, bandwidth W, and overlap between the Wannier function and the local Gaussian ground state in 1D optical lattices. Table courtesy of M. Holthaus.

V_0/E_r	$4J/E_r$	W/E_r	$J(2d)/J$	$|\langle w | \phi \rangle|^2$
3	0.444 109	0.451 894	0.101 075	0.9719
5	0.263 069	0.264 211	0.051 641	0.9836
10	0.076 730	0.076 747	0.011 846	0.9938
15	0.026 075	0.026 076	0.003 459	0.9964
20	0.009 965	0.009 965	0.001 184	0.9975

$$\int d^3r \, w_n^*(\mathbf{r}-\mathbf{R}) w_{n'}(\mathbf{r}-\mathbf{R}') = \delta_{n,n'} \delta_{\mathbf{R},\mathbf{R}'} \tag{40}$$

for different bands n and sites $\mathbf{R}$. Since the Wannier functions for all bands n and sites $\mathbf{R}$ form a complete basis, the operator $\hat{\psi}(\mathbf{r})$, which destroys a particle at an arbitrary point $\mathbf{r}$, can be expanded in the form

$$\hat{\psi}(\mathbf{r}) = \sum_{\mathbf{R},n} w_n(\mathbf{r}-\mathbf{R}) \hat{a}_{\mathbf{R},n}. \tag{41}$$

Here $\hat{a}_{\mathbf{R},n}$ is the annihilation operator for particles in the corresponding Wannier states, which are not necessarily well localized at site $\mathbf{R}$. The Hamiltonian for free motion on a periodic lattice is then

$$\hat{H}_0 = \sum_{\mathbf{R},\mathbf{R}',n} J_n(\mathbf{R}-\mathbf{R}') \hat{a}_{\mathbf{R},n}^\dagger \hat{a}_{\mathbf{R}',n}. \tag{42}$$

It describes the hopping in a given band n with matrix elements $J_n(\mathbf{R})$, which in general connect lattice sites at arbitrary distance $\mathbf{R}$. The diagonalization of this Hamiltonian by Bloch states (39) shows that the hopping matrix elements $J_n(\mathbf{R})$ are uniquely determined by the Bloch band energies $\varepsilon_n(\mathbf{q})$ via

$$\sum_{\mathbf{R}} J_n(\mathbf{R}) \exp(i\mathbf{q}\cdot\mathbf{R}) = \varepsilon_n(\mathbf{q}). \tag{43}$$

In the case of separable periodic potentials $V_p(\mathbf{r}) = V(x) + V(y) + V(z)$, generated by three orthogonal optical lattices, the single-particle problem is one dimensional. A complete analysis of Wannier functions in this case has been given by Kohn (1959). Choosing appropriate phases for the Bloch functions, there is a unique Wannier function for each band, which is real and exponentially localized. The asymptotic decay $\sim \exp(-h_n|x|)$ is characterized by a decay constant h_n, which is a decreasing function of the band index n. For the lowest band $n=0$, where the Bloch function at $q=0$ is finite at the origin, the Wannier function $w(x)$ can be chosen to be symmetric around $x=0$ (and correspondingly it is antisymmetric for the first excited band). More precisely, the asymptotic behavior of the 1D Wannier functions and the hopping matrix elements is $|w_n(x)| \sim |x|^{-3/4} \exp(-h_n|x|)$ and $J_n(R) \sim |R|^{-3/2} \exp(-h_n|R|)$, respectively (He and Vanderbilt, 2001). In the particular
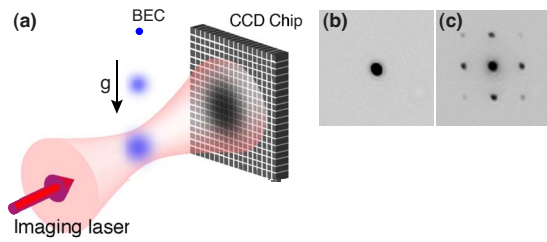
FIG. 5. (Color online) Absorption imaging. (a) Schematic setup for absorption imaging after a time-of-flight period. (b) Absorption image for a BEC released from a harmonic trap. (c) Absorption image for a BEC released from a shallow optical lattice ($V_0=6E_r$). Note the clearly visible interference peaks in the image.

case of a purely sinusoidal potential $V_0 \sin^2(kx)$ with lattice constant $d=\lambda/2$, the decay constant h_0 increases monotonically with V_0/E_r. In the deep-lattice limit $V_0 \gg E_r$, it approaches $h_0 d = \pi\sqrt{V_0/E_r}/2$. It is important to realize that, even in this limit, the Wannier function does not uniformly converge to the local harmonic-oscillator ground state ϕ of each well: $w_n(x)$ decays exponentially rather than in a Gaussian manner and always has nodes in order to guarantee the orthogonality relation (40). Yet, as shown in Table I, the overlap is near 1 even for shallow optical lattices.

C. Time-of-flight and adiabatic mapping

Sudden release. When releasing ultracold quantum gases from an optical lattice, two possible release methods can be chosen. If the lattice potential is turned off abruptly and interaction effects can be neglected, a given Bloch state with quasimomentum q will expand according to its momentum distribution as a superposition of plane waves with momenta $p_n=\hbar q \pm n2\hbar k$, with n an arbitrary integer. This is a direct consequence of the fact that Bloch waves can be expressed as a superposition of plane-wave states $\exp[i(\mathbf{q}+\mathbf{G})\cdot\mathbf{r}]$ with momenta $\mathbf{q}+\mathbf{G}$, which include arbitrary reciprocal-lattice vectors $\mathbf{G}$. In a simple cubic lattice with lattice spacing $d=\pi/k$, the vectors $\mathbf{G}$ are integer multiples of the fundamental reciprocal-lattice vector $2k$. After a certain

time of flight, this momentum distribution can be imaged using standard absorption imaging methods. If only a single Bloch state is populated, as is the case for a Bose-Einstein condensate with quasimomentum $q=0$, this results in a series of interference maxima that can be observed after a time-of-flight period t (see Fig. 5). As shown in Sec. III.A, the density distribution observed after a fixed time of flight at position $\mathbf{x}$ is the momentum distribution of the particles trapped in the lattice,

$$n(\mathbf{x}) = (M/\hbar t)^3 |\tilde{w}(\mathbf{k})|^2 \mathcal{G}(\mathbf{k}). \tag{44}$$

Here $\mathbf{k}$ is related to $\mathbf{x}$ by $\mathbf{k}=M\mathbf{x}/\hbar t$ due to the assumption of ballistic expansion, while $\tilde{w}(\mathbf{k})$ is the Fourier transform of the Wannier function. The coherence properties of the many-body state are characterized by the Fourier transform

$$\mathcal{G}(\mathbf{k}) = \sum_{\mathbf{R},\mathbf{R}'} e^{i\mathbf{k}\cdot(\mathbf{R}-\mathbf{R}')} G^{(1)}(\mathbf{R},\mathbf{R}') \tag{45}$$

of the one-particle density matrix $G^{(1)}(\mathbf{R},\mathbf{R}')=\langle \hat{a}_{\mathbf{R}}^\dagger \hat{a}_{\mathbf{R}'} \rangle$.

In a BEC, the long-range order in the amplitudes leads to a constant value of the first order coherence function $G^{(1)}(\mathbf{R},\mathbf{R}')$ at large separations $|\mathbf{R}-\mathbf{R}'|$ (see the Appendix). The resulting momentum distribution coincides with the standard multiple wave interference pattern obtained with light diffracting off a material grating [see Fig. 5(c) and Sec. IV.B]. The atomic density distribution observed after a fixed time-of-flight time thus yields information on the coherence properties of the many-body system. It should be noted, however, that the observed density distribution after time of flight can deviate from the in-trap momentum distribution if interaction effects during the expansion occur, or the expansion time is not so long that the initial size of the atom cloud can be neglected (far-field approximation) (Pedri *et al.*, 2001; Gerbier *et al.*, 2007).

Adiabatic mapping. One advantage of using optical lattice potentials is that the lattice depth can be dynamically controlled by simply tuning the laser power. This opens another possibility for releasing atoms from the lattice potential, e.g., by adiabatically converting a deep optical lattice into a shallow one and eventually completely turning off the lattice potential. Under adiabatic transformation of the lattice depth the quasimomentum
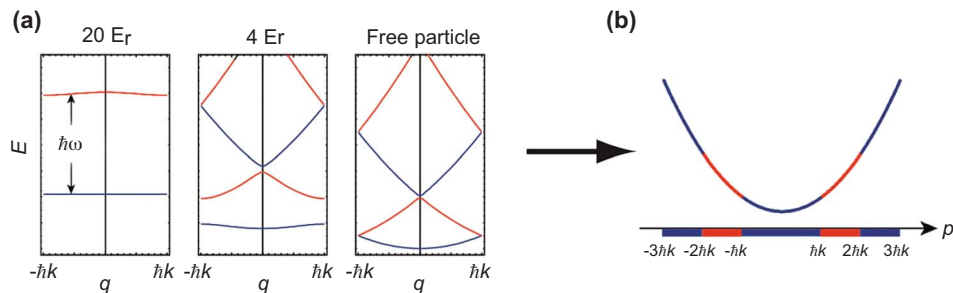

FIG. 6. (Color online) Adiabatic band mapping. (a) Bloch bands for different potential depths. During an adiabatic ramp down the quasimomentum is conserved and (b) a Bloch wave with quasimomentum q in the nth energy band is mapped onto a free particle with momentum p in the nth Brillouin zone of the lattice. From Greiner *et al.*, 2001.
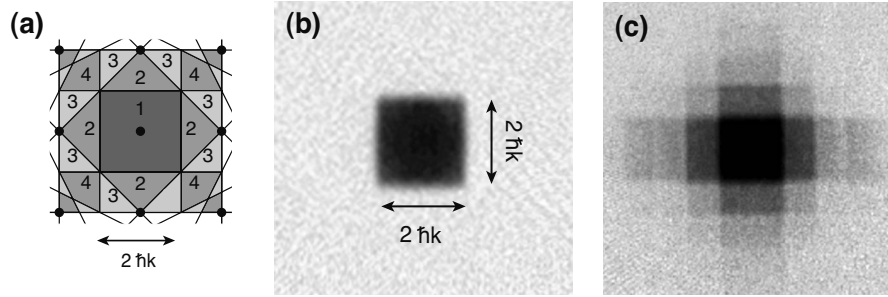
FIG. 7. Brillouin zones. (a) Brillouin zones of a 2D simple cubic optical lattice. (b) For a homogeneously filled lowest Bloch band, an adiabatic shutoff of the lattice potential leads to a homogeneously populated first Brillouin zone, which can be observed through absorption imaging after a time-of-flight expansion. (c) If in addition higher Bloch bands are populated, higher Brillouin zones become populated as well. From Greiner *et al.*, 2001.

q is preserved, and during the turn-off process a Bloch wave in the nth energy band is mapped onto a corresponding free-particle momentum **p** in the nth Brillouin-zone (see Fig. 6) (Kastberg *et al.*, 1995; Greiner *et al.*, 2001; Köhl *et al.*, 2005a).

The adiabatic mapping technique has been used with both bosonic (Greiner *et al.*, 2001) and fermionic (Köhl *et al.*, 2005a) atoms. For a homogeneously filled lowest-energy band, an adiabatic ramp down of the lattice potential leaves the central Brillouin zone—a square of width $2\hbar k$—fully occupied [see Fig. 7(b)]. If, on the other hand, higher-energy bands are populated, one also observes populations in higher Brillouin zones [see Fig. 7(c)]. As in this method each Bloch wave is mapped onto a specific free-particle momentum state, it can be used to efficiently probe the distribution of particles over Bloch states in different energy bands.

D. Interactions and two-particle effects

So far we have only discussed single-particle behavior of ultracold atoms in optical lattices. However, short-ranged s-wave interactions between particles give rise to an on-site interaction energy, when two or more atoms occupy a single lattice site. Within the pseudopotential approximation, the interaction between bosons has the form

$$\hat{H}' = (g/2) \int d^3r \, \hat{\psi}^\dagger(\mathbf{r}) \hat{\psi}^\dagger(\mathbf{r}) \hat{\psi}(\mathbf{r}) \hat{\psi}(\mathbf{r}). \qquad (46)$$

Inserting the expansion Eq. (41) leads to interactions involving Wannier states in both different bands and different lattice sites. The situation simplifies, however, for a deep optical lattice and with the assumption that only the lowest band is occupied. The overlap integrals are then dominated by the on-site term $U\hat{n}_\mathbf{R}(\hat{n}_\mathbf{R}-1)/2$, which is nonzero if two or more atoms are in the same Wannier state. At the two-particle level, the interaction between atoms in Wannier states localized around **R** and **R**′ is thus reduced to a local form $U\delta_{\mathbf{R},\mathbf{R}'}$ with

$$U = g \int d^3r |w(\mathbf{r})|^4 = \sqrt{8/\pi} \, ka E_r (V_0/E_r)^{3/4} \qquad (47)$$

(for simplicity, the band index $n=0$ is omitted for the lowest band). The explicit result for the on-site interaction U is obtained by taking $w(\mathbf{r})$ as the Gaussian ground state in the local oscillator potential. As mentioned above, this is not the exact Wannier wave function of the lowest band. In the deep-lattice limit $V_0 \gg E_r$, however, the result (47) provides the asymptotically correct behavior. Note that the strength $|U|$ of the on-site interaction increases with V_0, which is due to the squeezing of the Wannier wave function $w(\mathbf{r})$.

Repulsively bound pairs. Consider now an optical lattice at very low filling. An occasional pair of atoms at the same site has an energy U above or below the center of the lowest band. In the attractive case $U<0$, a two-particle bound state will form for sufficiently large values of $|U|$. In the repulsive case, in turn, the pair is expected to be unstable with respect to breakup into two separate atoms at different lattice sites to minimize the repulsive interaction. This process, however, is forbidden if the repulsion is above a critical value $U>U_c$. The physical origin for this result is that momentum and energy conservation do not allow the two particles to separate. There are simply no free states available if the energy lies more than zJ above the band center, which is the upper edge of the tight-binding band. Here z denotes the number of nearest neighbors on a lattice. Two bosons at the same lattice site will stay together if their interaction is sufficiently repulsive. In fact, the two-particle bound state above the band for a repulsive interaction is the precise analog of the standard bound state below the band for attractive interactions, and there is a perfect symmetry around the band center.

Such "repulsively bound pairs" have been observed in an experiment by Winkler *et al.* (2006). A dilute gas of $^{87}\text{Rb}_2$ Feshbach molecules was prepared in the vibrational ground state of an optical lattice. Ramping the magnetic field across a Feshbach resonance to negative a, these molecules can be adiabatically dissociated and then brought back again to positive a as repulsive pairs. Since the bound state above the lowest band is built
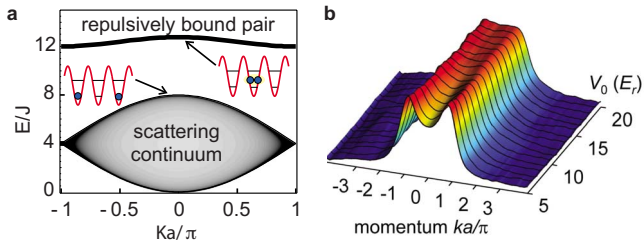
FIG. 8. (Color online) Repulsively bound atom pairs. (a) Spectrum of energy E of the 1D Bose-Hubbard Hamiltonian for $U/J=8$ as a function of the center-of-mass quasimomentum K. The Bloch band for respulsively bound pairs is located above the continuum of unbound states. (b) Experimentally measured quasimomentum distribution of repulsively bound pairs vs lattice depth V_0. From Winkler *et al.*, 2006.

from states in which the relative momentum of the two particles is near the edge of the Brillouin zone, the presence of repulsively bound pairs can be inferred from corresponding peaks in the quasimomentum distribution observed in a time-of-flight experiment (see Fig. 8) (Winkler *et al.*, 2006). The energy and dispersion relation of these pairs follows from solving $UG_K(E,0)=1$ for a bound state of two particles with center-of-mass momentum K. In close analogy to Eq. (79) below, $G_K(E,0)$ is the local Green's function for free motion on the lattice with hopping matrix element $2J$. Experimentally, the optical lattice was strongly anisotropic such that tunneling is possible only along one direction. The corresponding bound-state equation in one dimension can be solved explicitly, giving (Winkler *et al.*, 2006)

$$E(K,U_1) = 2J\sqrt{(2\cos Kd/2)^2 + (U_1/2J)^2} - 4J \qquad (48)$$

for the energy with respect to the upper band edge. Since $E(K=0, U_1) > 0$ for arbitrarily small values of $U_1 > 0$, there is always a bound state in one dimension. By contrast, in 3D there is a finite critical value, which is $U_c = 7.9136\,J$ for a simple cubic lattice. The relevant on-site interaction U_1 in one dimension is obtained from Eq. (78) for the associated pseudopotential. With ℓ_0 the oscillator length for motion along the direction of hopping, it is given by

$$U_1 = g_1 \int dx\, |w(x)|^4 = \sqrt{2/\pi}\,\hbar\omega_\perp a/\ell_0. \qquad (49)$$

Evidently, U_1 has the transverse confinement energy $\hbar\omega_\perp$ as the characteristic scale, rather than the recoil energy E_r of Eq. (47) in the 3D case.

Tightly confined atom pairs. The truncation to the lowest band requires that both the thermal and on-site interaction energy U are much smaller than $\hbar\omega_0$. In the deep-lattice limit $V_0 \gg E_r$, the condition $U \ll \hbar\omega_0$ leads to $ka(V_0/E_r)^{1/4} \ll 1$ using Eq. (47). This is equivalent to $a \ll \ell_0$, where $\ell_0 = \sqrt{\hbar/M\omega_0} = (E_r/V_0)^{1/4} d/\pi$ is the oscillator length associated with the local harmonic motion in the deep optical lattice wells. The assumption of staying in the lowest band in the presence of a repulsive interaction thus requires the scattering length to be much

smaller than ℓ_0, which is itself smaller than, but of the same order as, the lattice spacing d. For typical values $a \simeq 5$ nm and $d = 0.5\ \mu$m, this condition is well justified. In the vicinity of Feshbach resonances, however, the scattering lengths become comparable to the lattice spacing. A solution of the two-particle problem in the presence of an optical lattice for arbitrary values of the ratio a/ℓ_0 has been given by Fedichev *et al.* (2004). Neglecting interaction-induced couplings to higher bands, they have shown that the effective interaction at energies smaller than the bandwidth is described by a pseudopotential. For repulsive interactions $a > 0$, the associated effective scattering length reaches a bound $a_{\text{eff}} \approx d$ on the order of the lattice spacing even if $a \to \infty$ near a Feshbach resonance. In the case in which the free-space scattering length is negative, a_{eff} exhibits a geometric resonance that precisely describes the formation of a two-particle bound state at $|U| = 7.9136\,J$ as discussed above.

This analysis is based on the assumption that particles remain in a given band even in the presence of strong interactions. Near Feshbach resonances, however, this is usually not the case. In order to address the question of interaction-induced transitions between different bands, it is useful to consider two interacting particles in a harmonic well (Busch *et al.*, 1998). Provided the range of interaction is much smaller than the oscillator length ℓ_0, the interaction of two particles in a single well is described by a pseudopotential. The ratio of the scattering length a to ℓ_0, however, may be arbitrary. The corresponding energy levels $E = \hbar\omega_0(3/2 - \Omega)$ as a function of the ratio ℓ_0/a follow from the transcendental equation

$$\ell_0/a = \sqrt{2}\,\Gamma(\Omega/2)/\Gamma((\Omega-1)/2) = f_3(\Omega), \qquad (50)$$

where $\Gamma(z)$ is the standard gamma function. In fact, this is the analytical continuation to an arbitrary sign of the dimensionless binding energy Ω in Eq. (82) for $n=3$, since harmonic confinement is present in all three spatial directions.

As shown in Fig. 9, the discrete levels for the *relative*
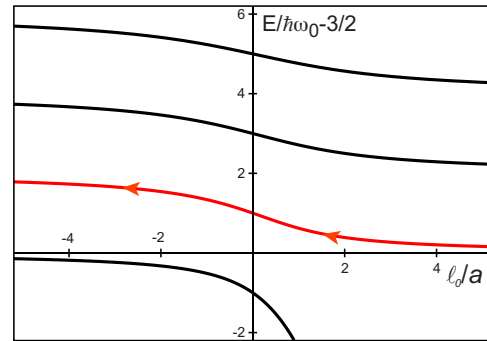

FIG. 9. (Color online) Energy spectrum of two interacting particles in a 3D harmonic-oscillator potential from Eq. (50). Arrows indicate the transfer of a pair in the ground state to the first excited level by sweeping across a Feshbach resonance. There is a single bound state below the lowest oscillator level, whose energy has been measured by Stöferle *et al.* (2006).
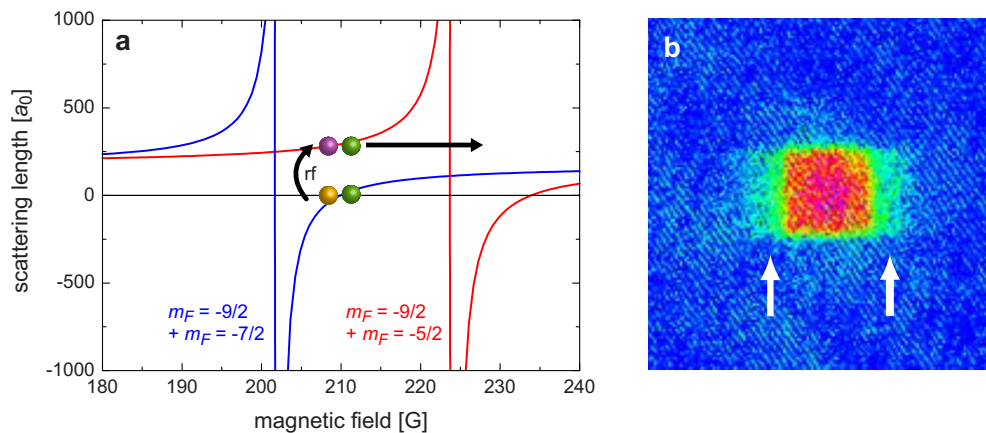
FIG. 10. (Color online) Experimentally observed interaction-induced transitions between Bloch bands. (a) Two Feshbach resonances between the $|F=9/2, m_F=-9/2\rangle$ and $|F=9/2, m_F=-7/2\rangle$ states (left) and the $|F=9/2, m_F=-9/2\rangle$ and $|F=9/2, m_F=-5/2\rangle$ states (right) are exploited to tune the interactions in the gas. (b) Quasimomentum distribution for a final magnetic field of B =233 G. Arrows indicate atoms in the higher bands. From Köhl $et\ al.$, 2005a.

motion of two particles form a sequence that, at infinite scattering length, is shifted upwards by precisely $\hbar\omega_0$ compared to the noninteracting levels at zero angular momentum $E^{(0)}(n_r)=\hbar\omega_0(2n_r+3/2)$. In particular, a change of the scattering length from small positive to small negative values, through a Feshbach resonance where a diverges, increases the energy by $2\hbar\omega_0$, while particles are transferred to the next higher level $n_r=1$. Feshbach resonances can thus be used to switch pairs of particles in individual wells of a deep optical lattice, where tunneling is negligible, to higher bands. Experimentally, this has been studied by Köhl $et\ al.$ (2005a). Starting from a two-component gas of fermionic ^{40}K at $a\approx0$ and unit filling, i.e., with two fermions at each lattice site in the center of the trap, atoms were transferred to a different hyperfine state and the magnetic field was then increased beyond the associated Feshbach resonance at $B_0=224$ G.[8] The resulting transfer of particles into higher bands is then revealed by observing the quasimomentum distribution in time-of-flight images after adiabatically turning off the optical lattice; see Fig. 10. Ho (2006) pointed out that such Feshbach sweeps open novel possibilities for creating fermionic Mott insulating states.

III. DETECTION OF CORRELATIONS

In order to probe interacting many-body quantum states with strong correlations, it is essential to use detection methods that are sensitive to higher-order correlations. This is possible using analogs of quantum optical detection techniques (Altman $et\ al.$, 2004; Duan, 2006; Gritsev $et\ al.$, 2006; Niu $et\ al.$, 2006; Polkovnikov $et\ al.$, 2006; Zhang $et\ al.$, 2007). Most of these techniques make use of the fact that quantum fluctuations in many ob-

servables, such as, e.g., the visibility of the interference pattern between two released quantum gases or fluctuations in the momentum distribution after release from the trap, contain information about the initial correlated quantum state. The noise-correlation techniques introduced below will yield information either on the first-order correlation function (see Secs. III.C and VI) or on the second- (or higher-) order correlation properties (see Sec. III.B). They can therefore probe various kinds of order in real space, such as, e.g., antiferromagnetically ordered states. Such correlation techniques for expanding atom clouds have been successfully employed in recent experiments, probing the momentum correlations between atomic fragments emerging from a dissociated molecule (Greiner $et\ al.$, 2005), revealing the quantum statistics of bosonic or fermionic atoms in an optical lattice (Fölling $et\ al.$, 2005; Rom $et\ al.$, 2006), or exploring the Kosterlitz-Thouless transition in two-dimensional Bose-Einstein condensates (Hadzibabic $et\ al.$, 2006). All correlation techniques for strongly correlated quantum gases can also benefit greatly from efficient single-atom detectors that have recently begun to be used in the context of cold quantum gases (Öttl $et\ al.$, 2005; Schellekens $et\ al.$, 2005; Jeltes $et\ al.$, 2007).

A. Time-of-flight versus noise correlations

We begin by considering a quantum gas released from a trapping potential. After a finite time of flight t, the resulting density distribution yields a three-dimensional density distribution $n_{3D}(\mathbf{x})$.[9] If interactions can be neglected during the time of flight, the average density distribution is related to the in-trap quantum state via

---

[8]Changing a from positive to negative values avoids creation of molecules in an adiabatic ramp.

[9]In this section, we denote in-trap spatial coordinates by $\mathbf{r}$ and spatial coordinates after time of flight by $\mathbf{x}$ for clarity.

$$\langle \hat{n}_{3D}(\mathbf{x})\rangle_{TOF} = \langle \hat{a}^\dagger_{TOF}(\mathbf{x})\hat{a}_{TOF}(\mathbf{x})\rangle_{TOF}$$

$$\approx \langle \hat{a}^\dagger(\mathbf{k})\hat{a}(\mathbf{k})\rangle_{trap} = \langle \hat{n}_{3D}(\mathbf{k})\rangle_{trap}, \qquad (51)$$

where $\mathbf{k}$ and $\mathbf{x}$ are related by the ballistic expansion condition $\mathbf{k}=M\mathbf{x}/\hbar t$ [a factor $(M/\hbar t)^3$ from the transformation of the volume elements $d^3x \to d^3k$ is omitted; see Eq. (44)]. Here we have used the fact that, for long times of flight, the initial size of the atom cloud in the trap can be neglected. It is important to realize that, in each experimental image, a single realization of the density is observed, not an average. Moreover, each pixel in the image records on average a substantial number N_σ of atoms. For each of those pixels, however, the number of atoms recorded in a *single realization* of an experiment will exhibit shot-noise fluctuations of relative order $1/\sqrt{N_\sigma}$, which will be discussed below. As shown in Eq. (51), the density distribution after time of flight represents a momentum distribution reflecting first-order coherence properties of the in-trap quantum state. This assumption is, however, correct only if during the expansion process interactions between atoms do not modify the initial momentum distribution, which we assume throughout. When interactions between atoms have been enhanced, e.g., by a Feshbach resonance, or a high-density sample is prepared, such an assumption is not always valid. Near Feshbach resonances, one therefore often ramps back to the zero crossing of the scattering length before expansion.

Density-density correlations in time-of-flight images. We now turn to the observation of density-density correlations in the expanding atom clouds (Altman *et al.*, 2004). These are characterized by the density-density correlation function after time-of-flight

$$\langle \hat{n}(\mathbf{x})\hat{n}(\mathbf{x}')\rangle = \langle \hat{n}(\mathbf{x})\rangle\langle \hat{n}(\mathbf{x}')\rangle g^{(2)}(\mathbf{x},\mathbf{x}') + \delta(\mathbf{x}-\mathbf{x}')\langle \hat{n}(\mathbf{x})\rangle,$$
$$(52)$$

which contains the normalized pair distribution $g^{(2)}(\mathbf{x},\mathbf{x}')$ and a self-correlation term. Relating the operators after time-of-flight expansion to the in-trap momentum operators, using Eq. (51), one obtains

$$\langle \hat{n}_{3D}(\mathbf{x})\hat{n}_{3D}(\mathbf{x}')\rangle_{TOF} \approx \langle \hat{a}^\dagger(\mathbf{k})\hat{a}(\mathbf{k})\hat{a}^\dagger(\mathbf{k}')\hat{a}(\mathbf{k}')\rangle_{trap}$$

$$= \langle \hat{a}^\dagger(\mathbf{k})\hat{a}^\dagger(\mathbf{k}')\hat{a}(\mathbf{k}')\hat{a}(\mathbf{k})\rangle_{trap}$$

$$+ \delta_{\mathbf{k}\mathbf{k}'}\langle \hat{a}^\dagger(\mathbf{k})\hat{a}(\mathbf{k})\rangle_{trap}. \qquad (53)$$

The last term on the right-hand side of the above equation is the autocorrelation term and will be dropped in the subsequent discussion, as it contributes to the signal only for $\mathbf{x}=\mathbf{x}'$ and contains no more information about the initial quantum state than the momentum distribution itself. The first term, however, shows that, for $\mathbf{x} \neq \mathbf{x}'$, subtle momentum-momentum correlations of the in-trap quantum states are present in the noise-correlation signal of the expanding atom clouds.

We now discuss the results obtained for two cases that have been analyzed in experiments: (i) ultracold atoms in a Mott-insulating state or a fermionic band-insulating

state released from a 3D optical lattice, and (ii) two interfering one-dimensional quantum gases separated by a distance $\mathbf{d}$.

B. Noise correlations in bosonic Mott and fermionic band insulators

Consider a bosonic Mott-insulating state or a fermionic band insulator in a three-dimensional simple cubic lattice. In both cases, each lattice site $\mathbf{R}$ is occupied by a fixed atom number $n_\mathbf{R}$. Such a quantum gas is released from the lattice potential and the resulting density distribution is detected after a time of flight t. In a deep optical lattice, the (in-trap) field operator $\hat{\psi}(\mathbf{r})$ can be expressed as a sum over destruction operators $\hat{a}_\mathbf{R}$ of localized Wannier states by using the expansion (41) and neglecting all but the lowest band. The field operator for destroying a particle with momentum $\mathbf{k}$ is therefore given by

$$\hat{a}(\mathbf{k}) = \int e^{-i\mathbf{k}\cdot\mathbf{r}}\hat{\psi}(\mathbf{r})d^3r \simeq \tilde{w}(\mathbf{k})\sum_\mathbf{R} e^{-i\mathbf{k}\cdot\mathbf{R}}\hat{a}_\mathbf{R}, \qquad (54)$$

where $\tilde{w}(\mathbf{k})$ denotes the Wannier function in momentum space.

For the two states considered here, the expectation value in Eq. (53) factorizes into one-particle density matrices $\langle \hat{a}^\dagger_\mathbf{R}\hat{a}_{\mathbf{R}'}\rangle = n_\mathbf{R}\delta_{\mathbf{R},\mathbf{R}'}$ with vanishing off-diagonal order. The density-density correlation function after a time of flight is then given by (omitting the autocorrelation term of order $1/N$)

$$\langle \hat{n}_{3D}(\mathbf{x})\hat{n}_{3D}(\mathbf{x}')\rangle = |\tilde{w}(M\mathbf{x}/\hbar t)|^2|\tilde{w}(M\mathbf{x}'/\hbar t)|^2 N^2$$

$$\times \left(1 \pm \frac{1}{N^2}\left|\sum_\mathbf{R} e^{i(\mathbf{x}-\mathbf{x}')\cdot\mathbf{R}(M/\hbar t)}n_\mathbf{R}\right|^2\right).$$
$$(55)$$

The plus sign in the above equation corresponds to the case of bosonic particles and the minus sign to the case of fermionic particles in a lattice. Both in a Mott state of bosons and in a filled band of fermions, the local occupation numbers $n_\mathbf{R}$ are fixed integers. The above equation then shows that correlations or anticorrelations in the density-density expectation value appear for bosons or fermions, whenever $\mathbf{k}-\mathbf{k}'$ is equal to a reciprocal-lattice vector $\mathbf{G}$ of the underlying lattice. In real space, where images are actually taken, this corresponds to spatial separations for which

$$|\mathbf{x}-\mathbf{x}'| = \ell = 2ht/\lambda M. \qquad (56)$$

Such spatial correlations or anticorrelations in the quantum noise of the density distribution of expanding atom clouds can in fact be traced back to the Hanbury Brown and Twiss (HBT) effect (Hanbury Brown and Twiss, 1956a, 1956b; Baym, 1998) and its analog for fermionic particles (Henny *et al.*, 1999; Oliver *et al.*, 1999; Kiesel *et al.*, 2002; Iannuzzi *et al.*, 2006; Rom *et al.*, 2006; Jeltes *et al.*, 2007). For the case of two atoms localized at two lattice sites, this can be understood in the following
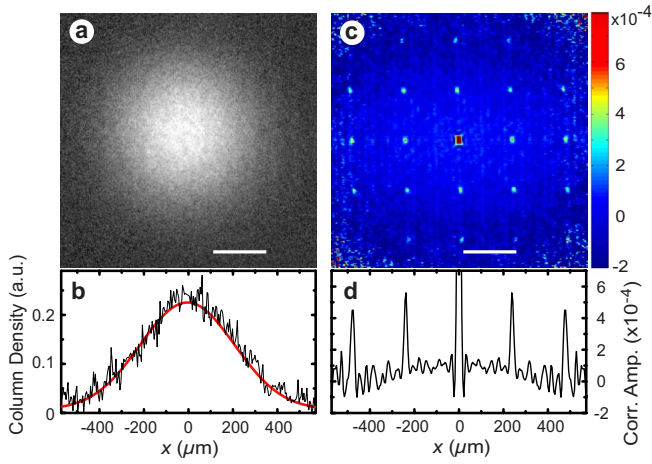
FIG. 11. (Color online) Noise correlations of a Mott insulator released from a 3D optical lattice. (a) Single-shot absorption image of a Mott insulator released from an optical lattice and associated cut through (b). A statistical correlation analysis over several independent images such as the one in (a) yields the correlation function (c). A cut through this two-dimensional correlation function reveals a Hanbury-Brown and Twiss type of bunching of the bosonic atoms (d). From Fölling *et al.*, 2005.

FIG. 12. (Color online) Noise correlations of a band-insulating Fermi gas. Instead of the correlation "bunching" peaks observed in Fig. 11, the fermionic quantum gas shows a HBT-type antibunching effect, with dips in the observed correlation function. From Rom *et al.*, 2006.

way: there are two possible ways for particles to reach two detectors at positions $\mathbf{x}$ and $\mathbf{x}'$, which differ by exchange. A constructive interference for bosons or a destructive interference for fermions then leads to correlated or anticorrelated quantum fluctuations that are registered in the density-density correlation function (Baym, 1998; Altman *et al.*, 2004).

Correlations for a bosonic Mott-insulating state and anticorrelations for a fermionic band-insulating state have been observed experimentally (Fölling *et al.*, 2005; Rom *et al.*, 2006; Spielman *et al.*, 2007). In these experiments, several single images of the desired quantum state are recorded after releasing atoms from the optical trapping potential and observing them after a finite time of flight [for one of these images, see, e.g., Fig. 11(a) or Fig. 12(a)]. These individually recorded images differ only in the atomic shot noise from one to the other. A set of such absorption images is then processed to yield the spatially averaged second-order correlation function $g_{\text{exp}}^{(2)}(\mathbf{b})$,

$$g_{\text{exp}}^{(2)}(\mathbf{b}) = \frac{\int \langle n(\mathbf{x}+\mathbf{b}/2) n(\mathbf{x}-\mathbf{b}/2)\rangle d^2\mathbf{x}}{\int \langle n(\mathbf{x}+\mathbf{b}/2)\rangle \langle n(\mathbf{x}-\mathbf{b}/2)\rangle d^2\mathbf{x}}. \tag{57}$$

As shown in Fig. 11, the Mott insulating state exhibits long-range order in the pair correlation function $g^{(2)}(\mathbf{b})$. This order is not connected with the trivial periodic modulation of the average density imposed by the optical lattice after time of flight, which is factored out in $g^{(2)}(\mathbf{x},\mathbf{x}')$ [see Eq. (52)]. Therefore, in the superfluid regime, one expects $g^{(2)}(\mathbf{x},\mathbf{x}') \equiv 1$ despite the periodic density modulation in the interference pattern after time of
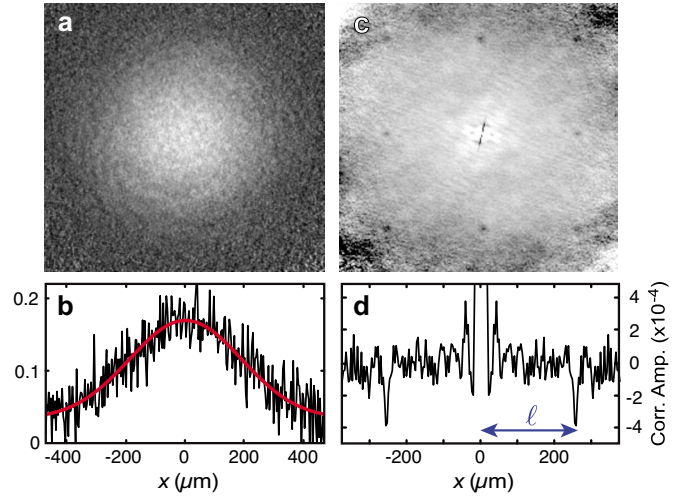
flight. It is interesting to note that correlations or anti-correlations can also be traced back to enhanced fluctuations in the population of Bloch waves with quasimomentum q for bosonic particles and the vanishing fluctuations in the population of Bloch waves with quasimomentum q for fermionic particles (Rom *et al.*, 2006).

Note that in general the signal amplitude obtained in experiments for the correlation function deviates significantly from the theoretically expected value of 1. In fact, one typically observes signal levels of 10^{-4}–10^{-3} (see Figs. 11 and 12). This can be explained by the finite optical resolution when the expanding atomic clouds are imaged, thus leading to a broadening of detected correlation peaks and thereby a decreased amplitude, as the signal weight in each correlation peak is preserved in the detection process. Using single-atom detectors with higher spatial and temporal resolution such as those used by Schellekens *et al.* (2005) and Jeltes *et al.* (2007), one can overcome such limitations and thereby also evaluate higher-order correlation functions.

C. Statistics of interference amplitudes for low-dimensional quantum gases

As a second example, we consider two bosonic one-dimensional quantum gases oriented along the z direction and separated by a distance d along the x direction. The density-density correlation function at positions $\mathbf{x} = (x, y=0, z)$ and $\mathbf{x}' = (x', y'=0, z')$ after time of flight is then given by

$$\langle \hat{n}_{3D}(\mathbf{x}) \hat{n}_{3D}(\mathbf{x}')\rangle = \langle \hat{a}_{\text{TOF}}^\dagger(\mathbf{x}) \hat{a}_{\text{TOF}}^\dagger(\mathbf{x}') \hat{a}_{\text{TOF}}(\mathbf{x}) \hat{a}_{\text{TOF}}(\mathbf{x}')\rangle$$
$$+ \delta_{\mathbf{x}\mathbf{x}'} n(\mathbf{x}) n(\mathbf{x}'). \tag{58}$$

The operators for the creation $\hat{a}_{\text{TOF}}^\dagger(\mathbf{x})$ and destruction $\hat{a}_{\text{TOF}}(\mathbf{x})$ of a particle after a time-of-flight period at position $\mathbf{x}$ can be related to the in-trap operators describing

the trapped quantum gases 1 and 2. Since the expansion mostly occurs along the initially strongly confined directions x and y, we can neglect for simplicity the expansion along the axial direction z and obtain for $y=0$

$$\hat{a}_{\text{TOF}}(\mathbf{x}) = \hat{a}_1(z)e^{ik_1x} + \hat{a}_2(z)e^{ik_2x}, \qquad (59)$$

with $k_{1,2}=M(x\pm d/2)/\hbar t$. The interference part,

$$\langle \hat{a}_2^\dagger(z)\hat{a}_1(z)\hat{a}_1^\dagger(z')\hat{a}_2(z')\rangle \times (e^{ik(x-x')} + \text{c.c.}), \qquad (60)$$

of the correlation function in Eq. (58) is an oscillatory function, with wave vector $k=Md/\hbar t$. In a standard absorption image, with the propagation direction of the imaging beam pointing along the z direction, one has to take into account additionally an integration along this direction over a length L from which a signal is recorded. We then obtain for the interfering part

$$\langle \hat{n}(x)\hat{n}(x')\rangle_{\text{int}} = \langle|\hat{A}_k|^2\rangle(e^{ik(x-x')} + \text{c.c.}), \qquad (61)$$

with the observable

$$\hat{A}_k = \int_{-L/2}^{L/2} dz\, \hat{a}_1^\dagger(z)\hat{a}_2(z). \qquad (62)$$

The above observable characterizes the phase and visibility of the interference pattern obtained in a single run of the experiment. Each run yields one of the eigenvalues of $\hat{A}_k$. Its typical magnitude is determined by the expectation value

$$\langle|\hat{A}_k|^2\rangle = \int dz \int dz' \langle \hat{a}_2^\dagger(z)\hat{a}_1(z)\hat{a}_1^\dagger(z')\hat{a}_2(z')\rangle, \qquad (63)$$

which can be obtained by statistical analysis of the visibility of the interference patterns obtained in several runs of the experiment. The basic example in this context is the observation of a pronounced interference pattern in a single realization of two overlapping but independent condensates with fixed particle numbers by Andrews et al. (1997). As discussed, e.g., by Javanainen and Yoo (1996) and by Castin and Dalibard (1997), the detection of particles at certain positions entails a nonvanishing interference amplitude in a single realization, whose typical visibility is determined by $\langle|\hat{A}_k|^2\rangle \neq 0$. Averaging over many realizations, in turn, completely eliminates the interference because $\langle \hat{A}_k \rangle = 0$ (Leggett, 2001).

For the case of identical (but still independent) homogeneous quantum gases, one can simplify Eq. (63) to yield

$$\langle|\hat{A}_k|^2\rangle \approx L \int_{-L/2}^{L/2} dz \langle \hat{a}^\dagger(z)\hat{a}(0)\rangle^2 = L \int |G^{(1)}(z)|^2 dz. \qquad (64)$$

Fluctuations in the interference pattern are directly linked to the coherence properties of the one-dimensional quantum systems. For the case of Luttinger liquids, the one-particle density matrix $G^{(1)}(z) \sim z^{-1/(2K)}$ at zero temperature decays algebraically with an expo-

nent determined by the Luttinger parameter K (see Sec. V.B). As a result, the interference amplitudes exhibit an anomalous scaling $\langle|\hat{A}_k|^2\rangle \propto L^{2-1/K}$ (Polkovnikov et al., 2006). By determining higher moments $\langle|\hat{A}_k|^{2n}\rangle$ of arbitrary order n of the visibility in an interference experiment, one can characterize the full distribution function of the normalized random variable $|\hat{A}_k|^2/\langle|\hat{A}_k|^2\rangle$. Full knowledge of the distribution function in fact amounts to a complete characterization of correlations in the many-body systems, as was shown by Gritsev et al. (2006) and allows one to infer the number statistics of the initial state (Polkovnikov, 2007). For the case of 1D Bose-Einstein condensates, this has recently been achieved by Hofferberth et al. (2008).

The above analysis for one-dimensional quantum systems can be extended to two-dimensional systems (Polkovnikov et al., 2006) and has been used to detect a Berezinskii-Kosterlitz-Thouless transition (Hadzibabic et al., 2006) with ultracold quantum gases (see Sec. VI). For lattice-based systems, it has been shown that noise correlations can be a powerful way to reveal, e.g., an antiferromagnetically ordered phase of two-component bosonic or fermionic quantum gases (Altman et al., 2004; Werner et al., 2005) to characterize Bose-Fermi mixtures (Ahufinger et al., 2005; Wang et al., 2005) and quantum phases with disorder (Rey et al., 2006), as well as to detect supersolid phases (Scarola et al., 2006).

IV. MANY-BODY EFFECTS IN OPTICAL LATTICES

As a first example illustrating how cold atoms in optical lattices can be used to study genuine many-body phenomena in dilute gases, we discuss the Mott-Hubbard transition for bosonic atoms. Following the proposal by Jaksch et al. (1998), this transition was first observed in 3D by Greiner et al. (2002a) and subsequently in 1D and 2D (Stöferle et al., 2004; Spielman et al., 2007, 2008). The theory of the underlying quantum phase transition is based on the Bose-Hubbard model, introduced by Fisher et al. (1989) to describe the destruction of superfluidity due to strong interactions and disorder.

A. Bose-Hubbard model

A conceptually simple model to describe cold atoms in an optical lattice at finite density is obtained by combining the kinetic energy (42) in the lowest band with the on-site repulsion arising from Eq. (46) in the limit of a sufficiently deep optical lattice. More precisely, the Bose-Hubbard model (BHM) is obtained from a general many-body Hamiltonian with a pseudopotential interaction under the following assumptions: (i) both the thermal and mean interaction energies at a single site are much smaller than the separation $\hbar\omega_0$ to the first excited band; and (ii) the Wannier functions decay essentially within a single lattice constant.

Under these assumptions, only the lowest band needs to be taken into account in Eq. (41). Moreover, the hopping matrix elements $J(\mathbf{R})$ are non-negligible only for

R = **0** or to nearest neighbors (NN) in Eq. (42), and the interaction constants are dominated by the on-site contribution (47). This leads to the BHM

$$\hat{H} = -J \sum_{\langle \mathbf{R}, \mathbf{R}' \rangle} \hat{a}_\mathbf{R}^\dagger \hat{a}_{\mathbf{R}'} + \frac{U}{2} \sum_\mathbf{R} \hat{n}_\mathbf{R}(\hat{n}_\mathbf{R} - 1) + \sum_\mathbf{R} \epsilon_\mathbf{R} \hat{n}_\mathbf{R}.$$
(65)

($\langle \mathbf{R}, \mathbf{R}' \rangle$ denotes a sum over all lattice sites **R** and its nearest neighbors at $\mathbf{R}' = \mathbf{R} + \mathbf{d}$, where **d** runs through the possible nearest-neighbor vectors.) The hopping matrix element $J(\mathbf{d}) = -J < 0$ to nearest neighbors is always negative in the lowest band, because the ground state must have zero momentum $\mathbf{q} = \mathbf{0}$ in a time-reversal invariant situation. For a separable lattice and in the limit $V_0 \gg E_r$, it is given by Eq. (38). More generally, the hopping matrix elements are determined by the exact band energy using Eq. (43). An alternative, but more indirect, expression is $J(\mathbf{R}) = \langle w(\mathbf{R}) | \hat{H}_0 | w(0) \rangle$ (Jaksch *et al.*, 1998).

Since the standard BHM includes next neighbor-hopping only, a convenient approximation for J in Eq. (65) is obtained by simply adjusting it to the given bandwidth. Concerning the on-site repulsion U, which disfavors configurations with more than one boson at a given site, its precise value as determined by Eq. (47) requires the exact Wannier function. In the low-filling $\bar{n} \sim 1$ regime, it follows from the single-particle Bloch states via Eq. (39). For higher fillings, the mean-field repulsion on each lattice site leads to an admixture of excited states in each well and eventually to a description where for $\bar{n} \gg 1$ one has a lattice of coupled Josephson junctions with a Josephson coupling $E_J = 2\bar{n}J$ and an effective charging energy U (Fisher *et al.*, 1989; Cataliotti *et al.*, 2001). For intermediate fillings, the Wannier functions entering both the effective hopping matrix element J and on-site repulsion U have to be adjusted to account for the mean-field interaction (Li *et al.*, 2006). The change in the on-site interaction energy with filling was observed experimentally by Campbell *et al.* (2006). In a more detailed description, the effects of interactions at higher filling can be accounted for by a multiorbital generalization of the Gross-Pitaevskii ansatz (Alon *et al.*, 2005). This leads to effective "dressed" Wannier states, which include higher bands and coupling between different sites. The last term with a variable on-site energy $\epsilon_\mathbf{R} = \tilde{V}(\mathbf{R})$ describes the effect of the smooth trapping potential $\tilde{V}(\mathbf{r})$. It includes the constant band center energy, arising from the $J(\mathbf{R} = 0)$ term of the hopping contribution (42), and acts like a spatially varying chemical potential.

The BHM describes the competition between the kinetic energy J, which is gained by delocalizing particles over lattice sites in an extended Bloch state, and the repulsive on-site interaction U, which disfavors having more than one particle at any given site. In an optical lattice loaded with cold atoms, the ratio U/J between these two energies can be changed by varying the dimensionless depth V_0/E_r of the optical lattice.

Indeed, from Eqs. (38) and (47), the ratio $U/J \sim (a/d) \exp(2\sqrt{V_0/E_r})$ increases exponentially with the lattice depth. Of course, to see strong interaction effects, the average site occupation $\langle \hat{n}_\mathbf{R} \rangle$ needs to be on the order of 1, otherwise the atoms never see each other. This was the situation for cold atoms in optical lattices in the 1990s, studied, e.g., by Westbrook *et al.* (1990), Grynberg *et al.* (1993), Hemmerich and Hänsch (1993), and Kastberg *et al.* (1995).

B. Superfluid–Mott-insulator transition

The BHM Eq. (65) is not an exactly soluble model, not even in one dimension, despite the fact that the corresponding continuum model in 1D, the Lieb-Liniger model, is exactly soluble. Nevertheless, the essential physics of the model and, in particular, the existence and properties of the quantum phase transition that the BHM exhibits as a function of U/J are rather well understood (Fisher *et al.*, 1989). In fact, for the 3D case and effectively unit filling, the existence of a quantum phase transition from a homogeneous BEC to a Mott insulator (MI) with a nonzero gap has been proven rigorously in a model of hard-core bosons in the presence of a staggered field by Aizenman *et al.* (2004). We first discuss the limiting cases, which describe the two possible phases in the ground state of the BHM.

Superfluid phase. In the trivial limit $U = 0$, the many-body ground state is simply an ideal BEC where all N atoms are in the $\mathbf{q} = \mathbf{0}$ Bloch state of the lowest band. Including the normalization factor in a lattice with N_L sites, this state can be written in the form

$$|\Psi_N\rangle (U = 0) = \frac{1}{\sqrt{N!}} \left(\frac{1}{\sqrt{N_L}} \sum_\mathbf{R} \hat{a}_\mathbf{R}^\dagger \right)^N |0\rangle.$$
(66)

In the limit $U/J \to 0$, therefore, the ground state of the BHM is a Gross-Pitaevskii-type state with a condensate fraction that is equal to 1. The critical temperature of the ideal Bose gas in an optical lattice at filling $\bar{n} = 1$ can be obtained from the condition $\int d\varepsilon \, g(\varepsilon) n_B(\beta_c \varepsilon) = 1$, where $g(\varepsilon)$ is the density of states in the lowest band and $n_B(x) = [\exp(x) - 1]^{-1}$ is the Bose-Einstein distribution. This gives $k_B T_c = 5.59 J$. In the presence of an optical lattice, therefore, the critical temperature for BEC is significantly reduced compared with the free-space situation, essentially due to the increased effective mass M^* of particles in the lattice. The relevant parameter, however, is not the temperature but the entropy, which is $S = 1.13 N k_B$ at T_c. Indeed, by starting with a deeply degenerate gas and adiabatically switching on the optical lattice, the entropy remains constant while the temperature is reduced by a factor M/M^* (Hofstetter *et al.*, 2002; Olshanii and Weiss, 2002; Blakie and Porto, 2004).

For a sufficiently large system $N, N_L \to \infty$ at fixed (not necessarily integer) density N/N_L [in the experiment (Greiner *et al.*, 2002a), the total number of occupied lattice sites was about 10^5], the perfect condensate Eq. (66)
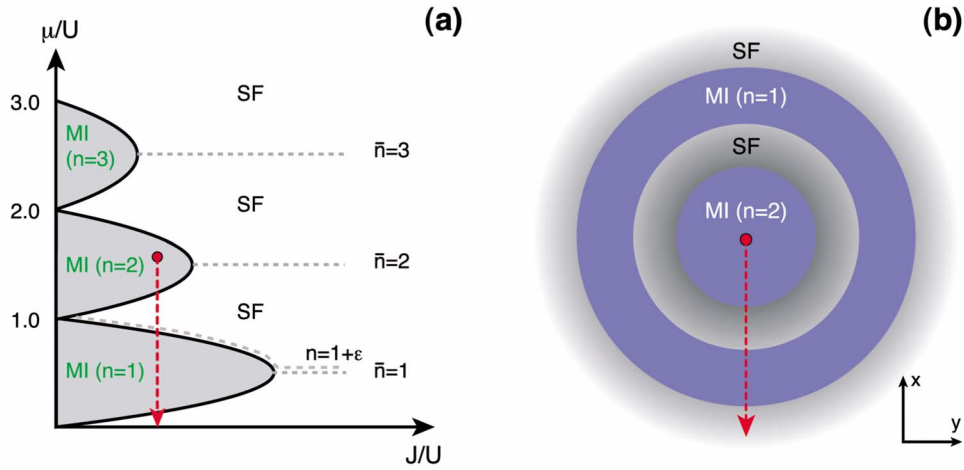
FIG. 13. (Color online) Schematic zero-temperature phase diagram of the Bose-Hubbard model. Dashed lines of constant-integer density $\langle \hat{n} \rangle = 1, 2, 3$ in the SF hit the corresponding MI phases at the tips of the lobes at a critical value of J/U, which decreases with increasing density $\bar{n}$. For $\langle \hat{n} \rangle = 1 + \varepsilon$ the line of constant density stays outside the $\bar{n} = 1$ MI because a fraction ε of the particles remains superfluid down to the lowest values of J. In an external trap with an $\bar{n} = 2$ MI phase in the center, a series of MI and SF regions appear on going toward the edge of the cloud, where the local chemical potential has dropped to zero.

becomes indistinguishable in practice from a coherent state

$$\exp(\sqrt{N}\hat{a}^{\dagger}_{q=0})|0\rangle = \prod_{\mathbf{R}} \left[\exp\left(\sqrt{\frac{N}{N_L}}\hat{a}^{\dagger}_{\mathbf{R}} \right)|0\rangle_{\mathbf{R}} \right]. \tag{67}$$

It factorizes into a product of *local* coherent states at every lattice site $\mathbf{R}$ with average $\bar{n} = \langle \hat{n} \rangle = N/N_L$, because boson operators at different sites commute. The probability distribution for the number of atoms at any given site for a perfect BEC in an optical lattice is therefore Poissonian with a standard deviation given by $\sigma(\bar{n}) = \sqrt{\bar{n}}$. Taking $N = N_L$, i.e., an average density such that there is one atom for each lattice site, there is a $1 - 2/e = 0.27$ probability that any given site is occupied by more than one atom. The kinetic energy minimization requirement that every atom wants to be at all lattice sites with equal amplitude thus necessarily leads to a substantial probability of finding more than one atom on a given site. At finite repulsion $U > 0$, such configurations are, of course, disfavored.

Mott-insulating phase. To understand the behavior in the opposite limit $U \gg J$, it is useful to consider the case of unit filling, i.e., the number N of atoms is precisely equal to the number N_L of lattice sites. In the limit $U \gg J$, hopping of atoms is negligible and the ground state

$$|\Psi_{N=N_L}\rangle(J=0) = \left(\prod_{\mathbf{R}} \hat{a}^{\dagger}_{\mathbf{R}} \right)|0\rangle \tag{68}$$

is a simple product of local Fock states with precisely one atom per site. With increasing J, atoms start to hop around, which involves double occupancy increasing the energy by U. Now as long as the gain J in kinetic energy due to hopping is smaller than U, atoms remain localized. For any $J \neq 0$, however, the ground state is no longer a simple product state as in Eq. (68). Once J becomes of the order of or larger than U, the gain in ki-

netic energy outweighs the repulsion due to double occupancies. Atoms then undergo a transition to a superfluid, in which they are delocalized over the whole lattice. This is a sharp quantum phase transition in the thermodynamic limit in two and three dimensions, because the state (66), in contrast to Eq. (68), exhibits off-diagonal long-range order, which cannot disappear in a continuous manner. By contrast, the evolution between these two states is completely smooth for, say, two particles in two wells, where a simple crossover occurs from a state with a well-defined relative phase at $J \gg U$ to one with a well-defined particle number in each well at $J \ll U$.

Phase diagram. The zero-temperature phase diagram of the homogeneous BHM is shown schematically in Fig. 13(a) as a function of J/U, with the density controlled by a chemical potential μ. At $U/J \to 0$, the kinetic energy dominates and the ground state is a delocalized superfluid, described by Eq. (67) to lowest order. At large values of U/J, interactions dominate and one obtains a series of MI phases with fixed integer filling $\bar{n} = 1, 2, \ldots$. These states are *incompressible*, implying that their density remains unchanged when the chemical potential is varied. In fact, it is the property $\partial n/\partial \mu = 0$ that is the defining property of a MI, and not the existence of local Fock states that exist only at $J = 0$. The transition between the superfluid (SF) and MI phases is associated with the loss of long-range order in the one-particle density matrix $g^{(1)}(\mathbf{x})$. In the 3D case, the order parameter of the SF-MI transition is therefore the condensate fraction n_0/n, which drops continuously from 1 at $U/J \ll 1$ to zero at $(U/J)_c$. The continuous nature of the SF-MI quantum phase transition in any dimension follows from the fact that the effective field theory for the complex order parameter ψ is that of a $(d+1)$-dimensional XY model (Fisher *et al.*, 1989; Sachdev, 1999). More precisely, this is valid for the special transition at integer density, which is

driven by phase fluctuations only. By contrast, if the SF-MI phase boundary is crossed by a change in the chemical potential, the associated change in the density gives rise to a different critical behavior (Fisher *et al.*, 1989). For instance, the excitation gap in the MI phase vanishes linearly with the distance from the boundary of the Mott lobe in this more generic case.

Within a mean-field approximation, the critical value for the transition from a MI to a SF is given by $(U/J)_c = 5.8z$ for $\bar{n} = 1$ and $(U/J)_c = 4\bar{n}z$ for $\bar{n} \gg 1$ (Fisher *et al.*, 1989; Sheshadri *et al.*, 1993; van Oosten *et al.*, 2001). Here z is the number of nearest neighbors and $2zJ$ is the total bandwidth of the lowest Bloch band, which is the relevant parameter that has to be compared with U. Recently, precise quantum Monte Carlo simulations by Capogrosso-Sansone *et al.* (2007) determined the critical value for the $\bar{n} = 1$ transition in a simple cubic lattice to be at $(U/J)_c = 29.36$, with an accuracy of about 0.1%. In one dimension, the SF-MI transition is of the Kosterlitz-Thouless type, with a finite jump of the superfluid density at the transition. Precise values for the critical coupling are available from density-matrix renormalization-group (DMRG) calculations, giving $(U_1/J)_c = 3.37$ (Kühner *et al.*, 2000; Kollath *et al.*, 2004), for the $\bar{n} = 1$ transition. For $\bar{n} \gg 1$, the BHM is equivalent to a chain of Josephson junctions with coupling energy $E_J = 2\bar{n}J$. The SF-MI transition is then desribed by the $(1+1)$-dimensional $O(2)$ model, which gives $(U_1/J)_c = 2.2\bar{n}$ (Hamer and Kogut, 1979; Roomany and Wyld, 1980).

From Eqs. (38) and (47), the critical value of the dimensionless lattice depth V_0/E_r for deep lattices is obtained from

$$(V_0/E_r)_c = \tfrac{1}{4} \ln^2[(\sqrt{2}d/\pi a)(U/J)_c]. \tag{69}$$

Using the experimental parameters $d = 426$ nm and $a = 5.7$ nm (Greiner *et al.*, 2002a), the precise result for $(U/J)_c$ in a simple cubic lattice gives a critical value $V_0/E_r|_c = 11.9$ for the SF-MI transition with $\bar{n} = 1$. Given that Eq. (38), on which the above estimate for the critical lattice depth is based, is not very precise in this regime, this result is in reasonable agreement with the lattice depth of $V_0 = 12 - 13E_r$, where the transition is observed experimentally (Greiner *et al.*, 2002a; Gerbier *et al.*, 2005b).

Consider now a filling with $\langle \hat{n} \rangle = 1 + \varepsilon$, which is slightly larger than 1. For large J/U, the ground state has all atoms delocalized over the whole lattice and the situation is hardly different from the case of unit filling. Upon lowering J/U, however, the line of constant density remains slightly above the $\bar{n} = 1$ "Mott lobe," and stays in the SF regime down to the lowest J/U (see Fig. 13). For any noninteger filling, therefore, the ground state remains SF as long as atoms can hop at all. This is a consequence of the fact that, even for $J \ll U$, there is a small fraction ε of atoms that remain SF on top of a frozen MI phase with $\bar{n} = 1$. Indeed, this fraction can still gain kinetic energy by delocalizing over the whole lattice without being blocked by the repulsive interaction U be-cause two of those particles will never be at the same place. The same argument applies to holes when ε is negative. As a result, in the homogeneous system, the quantum phase transition from a SF to a MI only appears if the density is equal to a commensurate, integer value.

In-trap density distribution. Fortunately, the situation is much less restrictive in the presence of a harmonic trap. Within the local-density approximation, the inhomogeneous situation in a harmonic trap is described by a spatially varying chemical potential $\mu_{\mathbf{R}} = \mu(0) - \epsilon_{\mathbf{R}}$ with $\epsilon_{\mathbf{R}} = 0$ at the trap center. Assuming, e.g., that the chemical potential $\mu(0)$ at the trap center falls into the $\bar{n} = 2$ Mott lobe, one obtains a series of MI domains separated by a SF by moving to the boundary of the trap where $\mu_{\mathbf{R}}$ vanishes [see Fig. 13(b)]. In this manner, all different phases that exist for given J/U below $\mu(0)$ are present simultaneously. The SF phase has a finite compressiblity $\kappa = \partial n / \partial \mu$ and a gapless excitation spectrum of the form $\omega(q) = cq$ because there is a finite superfluid density n_s (see the Appendix). By contrast, in the MI phase both n_s and κ vanish. As predicted by Jaksch *et al.* (1998), the incompressibility of the MI phase allows one to distinguish it from the SF by observing the local-density distribution in a trap. Since $\kappa = 0$ in the MI, the density stays constant in the Mott phases, even though the external trapping potential is rising. In the limit of $J \to 0$, the SF regions vanish and one obtains a "wedding-cake"-type density profile, with radii R_n of the different Mott insulating regions, given by $R_n = \sqrt{2[\mu(0) - nU]/M\omega^2}$ (De-Marco *et al.*, 2005).

The existence of such wedding-cake-like density profiles of a Mott insulator was supported by Monte Carlo (Batrouni *et al.*, 2002; Kashurnikov *et al.*, 2002; Wessel *et al.*, 2004; Rigol *et al.*, 2006) and DMRG (Kollath *et al.*, 2004) calculations in one, two, and three dimensions. Number-state-resolved, in-trap density profiles were detected experimentally by Campbell *et al.* (2006) and Fölling *et al.* (2006). In the latter case, it was possible to directly observe the wedding-cake density profiles and confirm the incompressibility of Mott-insulating regions of the atomic gas in the trapping potential. A sharp drop in the radii of the $n = 2$ occupied regions was observed when the transition point was crossed (Fölling *et al.*, 2006). It should be noted that in-trap density profiles can be used as a sensitive thermometer for the strongly interacting quantum gas. For typical experimental parameters, one finds that, for temperatures around $T^* \gtrsim 0.2U/k_B$, the wedding-cake profiles become completely washed out (Gerbier, 2007). Within the strongly interacting regime, the superfluid shells accommodate most entropy of the system and can already turn into a normal thermal gas at a lower temperature $T_c \sim zJ$ with the Mott-insulating shells still intact (Capogrosso-Sansone *et al.*, 2007; Gerbier, 2007; Ho and Zhou, 2007). In order to reach the lowest temperatures in this regime, it is advantageous to keep the external harmonic confinement as low as possible, or even decrease it during
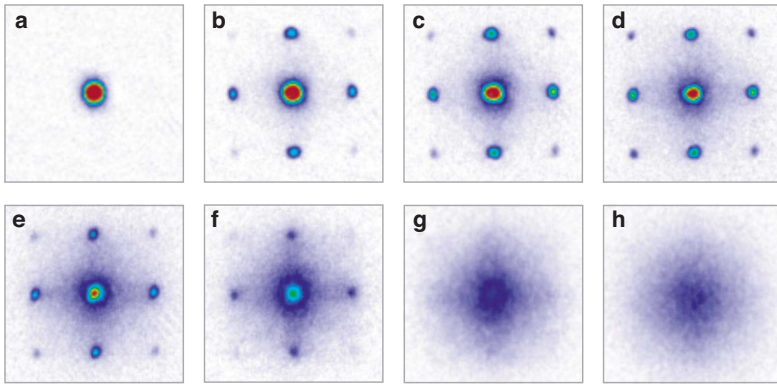
FIG. 14. (Color online) Absorption images of multiple matter-wave interference patterns after atoms were released from an optical lattice potential with a potential depth of (a) $0E_r$, (b) $3E_r$, (c) $7E_r$, (d) $10E_r$, (e) $13E_r$, (f) $14E_r$, (g) $16E_r$, and (h) $20E_r$. The ballistic expansion time was 15 ms. From Greiner *et al.*, 2002a.

an increase of the lattice depth (Gerbier, 2007; Ho and Zhou, 2007).

Phase coherence across the SF-MI transition. The disappearance of superfluidity (or better, of BEC) at the SF-MI transition was initially observed experimentally by a time-of-flight method (Greiner *et al.*, 2002a). The corresponding series of images is shown in Fig. 14 for different values of V_0, ranging between $V_0 = 0$ (a) and $20E_r$ (h). One observes a series of interference peaks around the characteristic "zero-momentum" peak of a condensate in the absence of an optical lattice. With increasing V_0, these peaks become more pronounced. Beyond a critical lattice depth around $V_0 \approx (12-13)E_r$ (e), which agrees well with the above estimate for the SF-MI transition for one boson per site, this trend is suddenly reversed, however, and the interference peaks eventually disappear completely. In order to understand why these pictures indeed provide direct evidence for the SF to MI transition predicted by the Bose-Hubbard model, it is useful to consider the idealized situation of a perfect periodic lattice in the absence of any trapping potential. From Eq. (44), the observed density at position $\mathbf{x}$ reflects the momentum distribution at $\mathbf{k} = M\mathbf{x}/\hbar t$. Factoring out the number of lattice sites, it is proportional to the lattice Fourier transform

$$n(\mathbf{k}) \sim |\tilde{w}(\mathbf{k})|^2 \sum_{\mathbf{R}} e^{i\mathbf{k}\cdot\mathbf{R}} G^{(1)}(\mathbf{R}) \qquad (70)$$

of the one-particle density matrix $G^{(1)}(\mathbf{R})$ at separation $\mathbf{R}$. For optical lattice depths below the critical value, the ground state in a 3D situation is a true BEC, where $G^{(1)}(|\mathbf{R}| \to \infty) = n_0$ approaches a finite value at large separation. For the MI phase, in turn, $G^{(1)}(\mathbf{R})$ decays to zero exponentially. The SF phase of cold atoms in a homogeneous optical lattice is thus characterized by a momentum distribution that exhibits sharp peaks at the reciprocal-lattice vectors $\mathbf{k} = \mathbf{G}$ [defined by $\mathbf{G}\cdot\mathbf{R} = 2\pi$ times an integer; see, e.g., Ashcroft and Mermin (1976)] plus a smooth background from short-range correlations. The fact that the peaks in the momentum distribution at $\mathbf{k} = \mathbf{G}$ initially grow with increasing depth of the lattice potential is a result of the strong decrease in spatial extent of the Wannier function $w(\mathbf{r})$, which entails a corresponding increase in its Fourier transform $\tilde{w}(\mathbf{k})$ at higher momenta. In the MI regime, where

$G^{(1)}(\mathbf{R})$ decays to zero, remnants of the interference peaks still remain [see, e.g., Fig. 14(f)] as long as $G^{(1)}(\mathbf{R})$ extends over several lattice spacings, because the series in Eq. (70) adds up constructively at $\mathbf{k} = \mathbf{G}$. A more detailed picture for the residual short-range coherence features beyond the SF-MI transition is obtained by considering perturbations deep in the Mott-insulating regime at $J = 0$. There $G^{(1)}(\mathbf{R})$ vanishes beyond $\mathbf{R} = 0$ and the momentum distribution is a structureless Gaussian, reflecting the Fourier transform of the Wannier wave function [see Fig. 14(h)]. With increasing tunneling J, the Mott state at $J/U \to 0$ is modified by a coherent admixture of particle-hole pairs. However, due the presence of a gapped excitation spectrum, such particle-hole pairs cannot spread out and are rather tightly bound to close distances. They do, however, give rise to a significant degree of short-range coherence. Using first-order perturbation theory with the tunneling operator as a perturbation on the dominating interaction term, one finds that the amplitude of the coherent particle-hole admixtures in a Mott-insulating state is proportional to J/U,

$$|\Psi\rangle_{U/J} \approx |\Psi\rangle_{U/J \to \infty} + \frac{J}{U} \sum_{\langle \mathbf{R}, \mathbf{R}' \rangle} \hat{a}_{\mathbf{R}}^\dagger \hat{a}_{\mathbf{R}'} |\Psi\rangle_{U/J \to \infty}. \qquad (71)$$

Close to the transition point, higher-order perturbation theory or a Green's-function analysis can account for coherence beyond nearest neighbors and the complete liberation of particle-hole pairs, which eventually leads to the formation of long-range coherence in the superfluid regime. The coherent particle-hole admixture and its consequences for the short-range coherence of the system have been investigated experimentally and theoretically by Gerbier *et al.* (2005a, 2005b) and Sengupta *et al.* (2005).

The SF-MI quantum phase transition, therefore, shows up directly in the interference pattern. For the homogeneous system, it reveals the existence or not of off-diagonal long-range order in the one-particle density matrix. The relevant order parameter is the condensate fraction. Of course the actual system is not homogeneous and numerical computation of the interference pattern is necessary for a quantitative comparison with experiment. This has been done, e.g., for the 3D case by Kashurnikov *et al.* (2002) and for the 1D case by Ba-

trouni *et al.* (2002) and Kollath *et al.* (2004). Due to the finite size and the fact that different MI phases are involved, the pattern evolves continuously from the SF to the MI regime. While critical values for J/U are different for the MI phases with $\bar{n}=1$ and 2, which are present in the experiment (Greiner *et al.*, 2002a), the transition seen in the time-of-flight images occurs rather rapidly with increasing lattice depth. Indeed, from Eq. (69), the experimental control parameter V_0/E_r depends only logarithmically on the relevant parameter U/J of the BHM. The small change from $V_0=13E_r$ in (e) to $V_0=14E_r$ in (f) thus covers a range in J/U wider than that which would be required to distinguish the $\bar{n}=1$ from the $\bar{n}=2$ transition. For a quantitative evaluation of interference patterns, one must also take into account the broadening mechanism during time-of-flight expansion, as discussed in Sec. II.C.

When approaching the SF-MI transition from the superfluid regime, the increasing interactions tend to increase the depletion of the condensate and thereby reduce the long-range phase-coherent component with increasing U/J (Orzel *et al.*, 2001; Hadzibabic *et al.*, 2004; Schori *et al.*, 2004; Xu *et al.*, 2006). For increasing lattice depth, the condensate density as a measure of the long-range coherent fraction then decreases continuously and vanishes at the transition point. The visibility of the interference pattern in general, however, evolves smoothly across the SF-MI transition, due to the presence of a strong short-range coherent fraction in the MI just across the transition point (see the discussion above). Above the transition point, the visibility of the interference pattern can also show kinks as the lattice depth is increased, which have been attributed to the beginning formation of shell structures in the MI state (Gerbier *et al.*, 2005a, 2005b; Sengupta *et al.*, 2005).

Excitation spectrum. A second signature of the SF-MI transition is the appearance of a finite excitation gap $\Delta \neq 0$ in the Mott insulator. Deep in the MI phase, this gap has size U, which is the increase in energy if an atom tunnels to an already occupied adjacent site (note that U is much smaller than the gap $\hbar\omega_0$ for excitation of the next vibrational state). The existence of a gap has been observed experimentally by applying a potential gradient in the MI (Greiner *et al.*, 2002a) or by using a modulation spectroscopy method (Stöferle *et al.*, 2004) and measuring the resulting excitations. Recent calculations indicate that such measurements simultaneously probe global (Iucci *et al.*, 2006; Huber *et al.*, 2007) and local properties of the system. In particular, for example, a peaked excitation spectrum can also appear in a strongly interacting superfluid regime, where $U>J$ (Kollath *et al.*, 2006). A way to probe global features of the many-body excitation spectrum, also close to the transition point, might be achieved by employing Bragg spectroscopy techniques as proposed by Rey *et al.* (2005), van Oosten *et al.* (2005), and Pupillo *et al.* (2006).

In the SF regime, there is no excitation gap. Instead, the homogeneous system exhibits a soundlike mode with frequency $\omega(q)=cq$. As shown in the Appendix, the associated sound velocity c is determined by $Mc^2=n_s/\kappa$ and thus gives information about the superfluid density n_s. The existence of a soundlike excitation even in the presence of an underlying lattice that explicitly breaks translation invariance is a consequence of long-range phase coherence in the SF. Its observation would therefore directly probe superfluidity, in contrast to the peaks in the interference pattern, which measure BEC.

Number statistics. Associated with the transition from a superfluid to a Mott-insulating state is a profound change in the atom number statistics per lattice site. As noted above, in the homogeneous system the ground state in the extreme MI limit ($J/U\rightarrow0$) is a product of Fock states with an integer number $\bar{n}$ of particles at each site. At finite hopping $J\neq0$, this simple picture breaks down because the atoms have a finite amplitude to be at different sites. The many-body ground state can then no longer be written as a simple product state. In the opposite limit $U\rightarrow0$, the ground state is a condensate of zero-quasimomentum Bloch states. In the limit $N,N_L\rightarrow\infty$ at fixed (not necessarily integer) density $\bar{n}=N/N_L$, the associated perfect condensate is a product of coherent states on each lattice site,

$$|\alpha\rangle = e^{-|\alpha|^2/2}\sum_n \frac{\alpha^n}{\sqrt{n!}}|n\rangle, \tag{72}$$

with α describing the amplitude and phase of the coherent matter wave-field. This corresponds to a Poissonian atom number distribution on each lattice site with average $|\alpha|^2=\bar{n}$.

A consequence of the representation (67) is that, at least for integer densities $\bar{n}=1,2,\ldots$, the many-body ground state may be factorized into a product over single sites,

$$|\Psi_{GW}\rangle = \prod_{\mathbf{R}} \left(\sum_{n=0}^{\infty} c_n |n\rangle_{\mathbf{R}} \right), \tag{73}$$

in both limits $J\rightarrow0$ and $U\rightarrow0$. The associated atom number probability distribution $p_n=|c_n|^2$ is either a pure Fock or a full Poissonian distribution. It is now plausible to use the factorized form in Eq. (73) as an *approximation* for arbitrary J/U, taking the coefficients c_n as variational parameters that are determined by minimizing the ground-state energy (Rokhsar and Kotliar, 1991; Sheshadri *et al.*, 1993). As pointed out by Rokhsar and Kotliar (1991), this is effectively a Gutzwiller ansatz for bosons. Beyond being simple computationally, this ansatz describes the SF to MI transition in a mean-field sense, becoming exact in infinite dimensions. In addition, it provides one with an intuitive picture of the transition to a MI state, which occurs precisely at the point, where the local number distribution becomes a pure Fock distribution. Indeed, within the Gutzwiller approximation, the expectation value

$$\langle \Psi_{GW}|\hat{a}_{\mathbf{R}}|\Psi_{GW}\rangle = \sum_{n=1}^{\infty} \sqrt{n}c_{n-1}^{*}c_{n} \qquad (74)$$

of the local matter-wave field vanishes if and only if the probability for finding different particle numbers at any given site is equal to zero. It is important, however, to emphasize that the Gutzwiller ansatz fails to account for nontrivial correlations between different sites present at any finite J. These correlations imply that the one-particle density matrix $G^{(1)}(\mathbf{R})$ is different from zero at finite distance $|\mathbf{R}| \neq 0$, becoming long ranged at the transition to a SF. By contrast, in the Gutzwiller approximation, the one-particle density matrix has no spatial dependence at all: it is zero at any $|\mathbf{R}| \neq 0$ in the MI and is completely independent of $\mathbf{R}$ in the SF. Moreover, in the Gutzwiller approximation, the phase transition is directly reflected in the local number fluctuations, with the variance of $n_{\mathbf{R}}$ vanishing throughout the MI phase. In reality, however, local variables such as the on-site number distribution will change in a smooth manner near the transition, and the variance of the local particle number will vanish only in the limit $J \to 0$.

Crossing the SF-MI transition, therefore, the number statistics evolves rather smoothly from a Poissonian distribution to Fock states on each lattice site. Recent experimental progress has allowed measurements of the number distribution in the optical lattice via microwave spectroscopy exploiting collisional frequency shifts (Campbell *et al.*, 2006) or spin-changing collisions (Gerbier *et al.*, 2006). When crossing the SF-MI transition, Campbell *et al.* (2006) were able to observe the emergence of a discrete excitation spectrum with hertz resolution. In a second experiment, the change in atom number statistics from Poissonian to Fock states was revealed (Gerbier *et al.*, 2006). Another possibility for observing the number squeezing of the initially Poissonian atom number distribution in the weakly interacting regime due to increasing interatomic interactions has been to use a matter-wave beam splitter and observe the time scale of the collapse in the ensuing phase diffusion dynamics (Greiner *et al.*, 2002a; Jo *et al.*, 2007; Sebby-Strabley *et al.*, 2007). This is discussed in the following section.

C. Dynamics near quantum phase transitions

One major advantage of cold atoms in studying many-body phenomena is the possibility of changing the parameters characterizing the relative strength of the kinetic and interaction energy dynamically. This opens the possibility of studying the real-time dynamics of strongly correlated systems in a controlled manner. As a simple example, we discuss the quench of the system from the superfluid into the Mott-insulating regime. This issue was investigated in an experiment observing collapses and revivals of the matter wave due to the coherent superposition of states with different atom numbers in the SF (Greiner *et al.*, 2002b). In the weakly interacting regime of a BEC in an optical lattice potential, the ground

state (67) is a product of coherent states on each lattice site with a Poissonian atom number distribution. If the lattice depth is now suddenly increased to a parameter regime where the ground state of the system is a Mott-insulating state, the initial atom number fluctuations of the coherent state will be frozen out, as the system is not given enough time to redistribute toward the novel many-body ground state. The evolution with time of such a coherent state can be evaluated by taking into account the time evolution of the different Fock states forming the coherent state,

$$|\alpha\rangle(t) = e^{-|\alpha|^2/2}\sum_{n} \frac{\alpha^n}{\sqrt{n!}}e^{-iUn(n-1)t/2\hbar}|n\rangle. \qquad (75)$$

The coherent matter-wave field ψ on each lattice site can then be evaluated through $\psi = \langle \alpha(t)|\hat{a}|\alpha(t)\rangle$, which exhibits an intriguing dynamical evolution (Yurke and Stoler, 1986; Sols, 1994; Wright *et al.*, 1996; Castin and Dalibard, 1997; Imamoglu *et al.*, 1997). At first, the different phase evolutions of the atom number states lead to a collapse of ψ. However, at integer multiples in time of h/U, all phase factors in the above equation rephase modulo 2π and thus lead to a revival of the initial coherent state. In fact, precise revivals appear as long as the initial state can be written in the factorized form of Eq. (73). Since the time-evolution operator $\exp(-i\hat{H}t/\hbar)$ factorizes into a product of on-site terms $\exp[-in(n-1)Ut/2\hbar]$, the time dependence is perfectly periodic with period $t_{\text{rev}} = h/U_f$, where U_f is the value of the on-site repulsion after the quench. Clearly the period is independent of the initial number distribution $|c_n|^2$. The collapse time $t_c \approx t_{\text{rev}}/\sigma_n$ depends in turn on the variance $\sigma_n^2 = \langle \hat{n}^2 \rangle - \langle \hat{n} \rangle^2$ of the local number distribution. Its measurement thus provides information about how the coherent superposition of different particle numbers in the SF state is eventually destroyed on approaching the MI regime (Greiner *et al.*, 2002b).

The collapse and revival of the coherent matter-wave field of a BEC is reminiscent of the collapse and revival of Rabi oscillations in the interaction of a single atom with a single-mode electromagnetic field in cavity quantum electrodynamics (Brune *et al.*, 1996; Rempe *et al.*, 1987). There the nonlinear atom-field interaction induces the collapse and revival of Rabi oscillations, whereas here the nonlinearity due to interactions between the atoms themselves leads to the series of collapses and revivals of the matter-wave field. It should be pointed out that such behavior has also been theoretically predicted to occur for a coherent light field propagating in a nonlinear medium (Yurke and Stoler, 1986), but to our knowledge it has never been observed experimentally. Such dynamical evolution of the atomic quantum state due to the nonlinear interactions between the particles is also known as quantum phase diffusion and was detected by Greiner *et al.* (2002b) for low atom numbers on each site. For larger atom numbers, the initial time evolution of the quantum phase diffusion was recently observed by Jo *et al.* (2007) in a double-well scenario.

The simple single-site description is valid only in the limits $U_i \ll J$ of a nearly perfect SF in the initial state and $U_f \gg J$ of negligible tunneling after the quench. To determine the dynamics in a more general situation is a complicated nonequilibrium many-body problem. Numerical results for arbitrary values of U_i and U_f have been obtained for the 1D BHM by Kollath *et al.* (2007) using the time-dependent density-matrix renormalization group (Schollwöck, 2005).

In a related scenario, it was proposed that on jumping from an initial Mott-insulating state into the superfluid regime one should observe oscillations of the superfluid order parameter (Altman and Auerbach, 2002; Polkovnikov *et al.*, 2002). For large filling factors, oscillating coherence was observed after a quench from a deep to a shallow lattice by Tuchman *et al.* (2006). The formation of a superfluid from an initial Mott-insulating phase poses a general problem in the context of the dynamics of strongly correlated quantum systems. Both experiments (Greiner *et al.*, 2002a) and theory (Clark and Jaksch, 2004) have confirmed that the emergence of coherence in the system can occur rather rapidly on time scales of a few tunneling times $\hbar/J$. It is an open question, however, whether off-diagonal long-range order in the one-particle density matrix sets in within such a short time, and what length scales over which order has been established are relevant in order to observe coherence in a time-of-flight picture.

D. Bose-Hubbard model with finite current

The SF-MI transition discussed in Sec. IV.B is a continuous phase transition in the ground state of a many-body Hamiltonian. Observation from the time-of-flight images—that long-range phase coherence is lost beyond a critical value of U/J—provides a signature for the disappearance of BEC. The expected simultaneous loss of *superfluidity* across this transition may be studied by considering the phase boundary, where stationary states with a finite current lose their stability. Such stationary out-of-equilibrium states may be created experimentally by boosting the condensate to a finite-momentum state (Fallani *et al.*, 2004), or by inducing a center-of-mass oscillation in the trap (Fertig *et al.*, 2005). The question of what happens to the equilibrium SF-MI transition in a situation with a finite current was addressed by Polkovnikov *et al.* (2005). For a given number $\bar{n}$ of bosons per site, the kinetic energy term in the BHM (65) gives rise to a Josephson coupling energy $E_J = 2\bar{n}J$ due to next-neighbor tunneling, which favors a vanishing relative phase between adjacent lattice sites. In the limit $E_J \gg U$, there is a nonvanishing matter-wave field $\psi_{\mathbf{R}} = \langle \hat{a}_{\mathbf{R}} \rangle$. In the ground state, all bosons have zero momentum and $\psi_{\mathbf{R}}$ is uniform. States with a finite current, in turn, are BEC's in which single-particle states with nonzero momentum $\mathbf{q}$ are macroscopically occupied. To zeroth order in U/E_J, their energy is the Bloch band energy Eq. (37). The associated current per particle $\mathcal{J} = (2J/\hbar)\sin q_x d$ for motion along the x direction has a
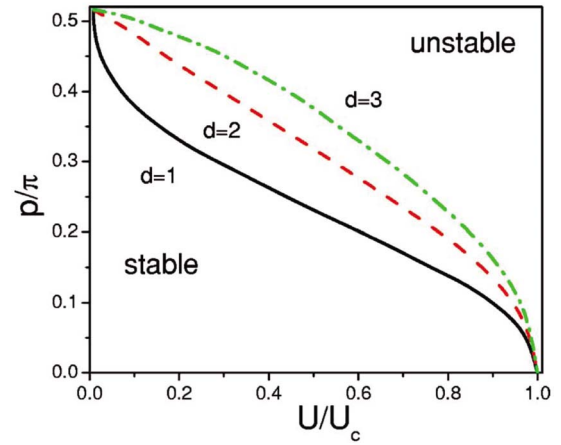

FIG. 15. (Color online) Mean-field phase diagram separating stable and unstable motion of condensate regions. The vertical axis denotes the condensate momentum in inverse lattice units and the horizontal axis denotes the normalized interaction. From Polkovnikov *et al.*, 2005.

maximum at $p = q_x d = \pi/2$. States with a larger momentum are unstable in a linear stability analysis (Polkovnikov *et al.*, 2005). This instability was observed experimentally by Fallani *et al.* (2004) and also by Cristiani *et al.* (2004). A moving optical lattice is created by two counterpropagating beams at frequencies that differ by a small detuning $\delta\nu$. Averaged over the optical frequencies, this gives rise to an interference pattern that is a standing wave moving at velocity $v = \lambda \delta\nu/2$. Adiabatically switching on such a lattice in an existing BEC then leads to a condensate in a state with quasimomentum $q = Mv/\hbar$. Its lifetime shows a rapid decrease for momenta near the critical value q_c.

In the strongly interacting regime near the SF-MI transition, such a single-particle picture is no longer valid. At the mean-field level, the problem may be solved using the field-theoretical description of the SF-MI transition. The SF phase is then characterized by a nonzero complex order parameter ψ, whose equilibrium value $|\psi| \sim \xi^{-1}$ vanishes as the inverse of the correlation length ξ (this relation holds in the mean-field approximation, which is appropriate for the transition at integer densities in 3D). The stationary solutions of the dimensionless order parameter equation $\nabla^2 \psi + \xi^{-2}\psi = |\psi|^2 \psi$ with *finite* momentum are of the form $\psi(x) = \sqrt{\xi^{-2} - p^2}\exp(ipx)$. Evidently, such solutions exist only if $|p| < 1/\xi$. The critical value of the dimensionless momentum p, where current-carrying states become unstable, thus approaches zero continuously at the SF-MI transition (Polkovnikov *et al.*, 2005). In fact, the same argument can be used to discuss the vanishing of the critical current in superconducting wires near T_c; see Tinkham (1996). The complete mean-field phase diagram, shown in Fig. 15, interpolates smoothly between the classical instability at $p_c = \pi/2$ and $p_c \to 0$ in the limits $U \to 0$ and $U \to U_c$, respectively. In contrast to the equilibrium transition at $p = 0$, which is continuous, the dynamical transi-
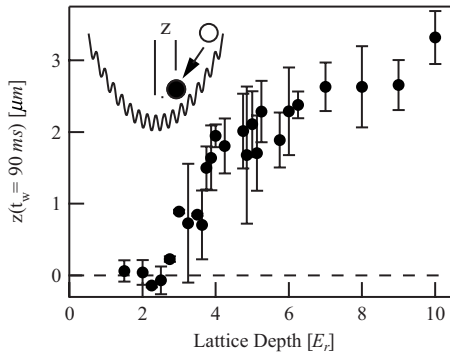
FIG. 16. Inhibition of transport in a one-dimensional bosonic quantum system with an axial optical lattice. For lattice depths above approximately $2E_r$, an atom cloud displaced to the side of the potential minimum (see inset) is stuck at this position and does not relax back to the minimum. From Fertig *et al.*, 2005.

tion is of *first order*. Crossing the phase boundary at any nonzero current is therefore connected with an irreversible decay of the current to zero. Experimentally, the decrease of the critical momentum near the SF-MI transition has been observed by Mun *et al.* (2007). Their results are in good agreement with the phase diagram shown in Fig. 15.

In the mean-field picture, states of a SF with nonzero momentum have an infinite lifetime. More precisely, however, such states can only be metastable because the ground state of any time-reversal-invariant Hamiltonian necessarily has zero current. The crucial requirement for SF in practice, therefore, is that current-carrying states have lifetimes that far exceed experimentally relevant scales. This requires these states to be separated from the state with vanishing current by energy barriers, which are much larger than the thermal or relevant zero-point energy.[10] The rate for phase slips near the critical line in Fig. 15 was calculated by Polkovnikov *et al.* (2005). It turns out that the mean-field transition survives fluctuations in 3D, so in principle it is possible to locate the equilibrium SF-MI transition by extrapolating the dynamical transition line to zero momentum. In the experiments of Fertig *et al.* (2005), the system showed sharp interference peaks even in the "overdamped" regime where the condensate motion was locked by the optical lattice (see Fig. 16). This may be due to localized atoms at the sample edges, which block the dipole oscillation even though atoms in the center of the trap are still in the SF regime. A theoretical study of the damped oscillations of 1D bosons was given by Gea-Banacloche *et al.* (2006).

A different method of driving a SF-MI transition dynamically was suggested by Eckardt *et al.* (2005). Instead of a uniformly moving optical lattice, it employs an os-

cillating linear potential $K\cos(\omega t)\hat{x}$ along one of the lattice directions (in a 1D BHM, $\hat{x}=\Sigma_j j\hat{n}_j$ is the dimensionless position operator). For modulation frequencies such that $\hbar\omega$ is much larger than the characteristic scales J and U of the unperturbed BHM, the driven system behaves like the undriven one, but with a renormalized tunneling matrix element $J_{\mathrm{eff}}=J\mathcal{J}_0(K/\hbar\omega)$, where $\mathcal{J}_0(x)$ is the standard Bessel function. Since U is unchanged in this limit, the external perturbation completely suppresses the tunneling at the zeros of the Bessel function. Moreover, it allows one to invert the sign of J_{eff} to negative values, where, for example, the superfluid phase corresponds to a condensate at finite momentum $q=\pi/d$. In recent experiments by Lignier *et al.* (2007), the dynamical suppression of tunneling with increasing driving K was observed through measurement of the expansion velocity along the direction of the optical lattice after switching off the axial confinement.

E. Fermions in optical lattices

In this section, we focus on fermions in 3D optical lattice potentials and experimental results that have been obtained in these systems. Interacting fermions in a periodic potential can be described by the Hubbard Hamiltonian. For now we restrict the discussion to the case of atoms confined to the lowest-energy band and to two possible spin states $|\uparrow\rangle$, $|\downarrow\rangle$ for the fermionic particles. The single-band Hubbard Hamiltonian thus reads

$$H = -J \sum_{\langle\mathbf{R},\mathbf{R}'\rangle,\sigma} (\hat{c}^\dagger_{\mathbf{R},\sigma}\hat{c}_{\mathbf{R}',\sigma} + \mathrm{H.c.}) + U\sum_{\mathbf{R}} \hat{n}_{\mathbf{R}\uparrow}\hat{n}_{\mathbf{R}\downarrow}$$
$$+ \frac{1}{2}M\omega^2 \sum_{\mathbf{R},\sigma} \mathbf{R}^2\hat{n}_{\mathbf{R},\sigma}. \tag{76}$$

As in the case of bosonic particles, the zero temperature phase diagram depends strongly on the filling and the ratio between the interaction and kinetic energies. An important difference between the bosonic and fermionic Hubbard Hamiltonian can also be seen in the form of the interaction term, where only two particles of different spin states are allowed to occupy the same lattice site, giving rise to an interaction energy U between atoms.

Filling factor and Fermi surfaces. A crucial parameter in the fermionic Hubbard model is the filling factor of atoms in the lattice. Due to the overall harmonic confinement of atoms [last term in Eq. (76)], this filling fraction changes over the cloud of trapped atoms. One can, however, specify an average characteristic filling factor,

$$\rho_c = N_F d^3/\zeta^3, \tag{77}$$

with $\zeta=\sqrt{2J/M\omega^2}$ describing the typical delocalization length of the single-particle wave functions in the combined periodic lattice and external harmonic trapping potential (Rigol and Muramatsu, 2004; Köhl *et al.*, 2005a). The characteristic filling factor can be controlled experimentally either by increasing the total number of fermionic atoms N_F or by reducing J via an increase of

---

[10]This is different from the well-known Landau criterion of superfluid flow below a finite critical velocity (Pitaevskii and Stringari, 2003). Indeed, the existence of phase slips implies that the critical velocity is always zero in a strict sense.
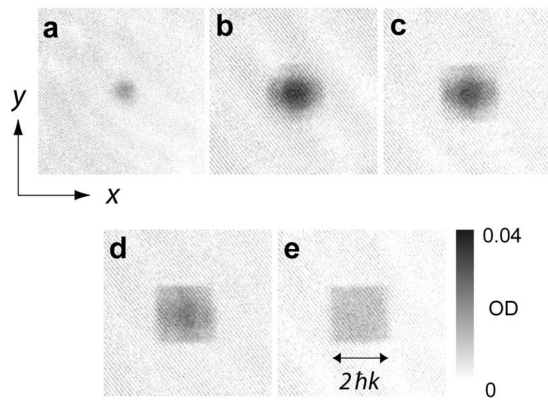
FIG. 17. Fermi surfaces vs band filling for ultracold fermionic ^{40}K atoms in a three-dimensional simple cubic lattice potential. From (a) to (e), the filling factor has been continuously increased, bringing the system from a conducting to a band-insulating state. From Köhl *et al.*, 2005a.

the lattice depth or via an increase of the overall harmonic confinement. The latter case, however, has the disadvantage that a strong harmonic confinement will lead to a decoupling of the lattice sites, as the tunnel coupling J will not be large enough to overcome the potential energy offset due to the overall harmonic confinement. One is then left with an array of uncoupled, independent harmonic oscillators. The characteristic filling factor of the system can be revealed experimentally by observing the population of the different Bloch states via adiabatic band mapping, introduced in Sec. II.C. By changing the atom number or the lattice depth, Köhl *et al.* (2005a) observed a change from a low-filling to a band-insulating state, where the single-species particles are completely localized to individual lattice sites (see Fig. 17).

Thermometry and pair correlations. An important question regarding fermionic quantum gases in optical lattices is the temperature of the many-body system. It has been shown by Köhl (2006) that for noninteracting 50:50 spin mixtures of fermions, the number of doubly occupied spin states can be used to determine the temperature of the system. For zero temperature and deep optical lattices, one would expect all lattice sites to be occupied by spin-up and spin-down atoms equally. For finite temperatures, however, atoms could be thermally excited to higher-lying lattice sites at the border of the system, thus reducing the number of doubly occupied lattice sites. By converting doubly occupied sites into fermionic molecules, it was possible to determine the number of doubly vs singly occupied sites and obtain an estimate for the temperature of the spin mixture (Stöferle *et al.*, 2006). Another possibility for determining the temperature of the system even for a single-species fermionic quantum gas in the lattice has been provided by the use of quantum noise correlations, as introduced in Sec. III. For higher temperatures of the quantum gas, atoms tend to spread out in the harmonic confinement and thus increase the spatial size of the

trapped atom cloud. As the shape of each noise-correlation peak essentially represents the Fourier transform of the in-trap density distribution, but with fixed amplitude of 1 [see Eq. (55)], an increase in the size of the fermionic atom cloud by temperature will lead to a decrease in the observed correlation signal, as was detected by Rom *et al.* (2006).

When increasing a red-detuned optical lattice on top of a fermionic atom cloud, this usually also leads to an increased overall harmonic confinement of the system. It was shown that, for such a case, the density of states of the system can be significantly modified, thus leading to an adiabatic heating of the fermionic system by up to a factor of 2 for a strong overall harmonic confinement (Köhl, 2006). In order to reach low temperatures for the fermionic system, it would thus be advantageous to keep the harmonic confinement as low as possible, or even decrease it, as the optical lattice depth is increased. Such a configuration is possible, e.g., with a blue-detuned optical lattice in conjunction with a red-detuned optical dipole trap.

V. COLD GASES IN ONE DIMENSION

The confinement of cold atoms in a quantum wire geometry that can be achieved via strong optical lattices (Kinoshita *et al.*, 2004; Paredes *et al.*, 2004) provides a means of reaching the strong-interaction regime in dilute gases. This opens the possibility to realize both bosonic and fermionic Luttinger liquids and a number of exactly soluble models in many-body physics.

A. Scattering and bound states

Here we consider cold atoms subject to a strong 2D optical lattice in the y, z plane, which confines the motion to the (axial) x direction. We also derive results for a planar geometry, where atoms move freely in the x-y plane while being strongly confined in the z axis, that will be useful in Sec. VI. In the regime where the excitation energy $\hbar\omega_\perp$ for motion in the radial y, z directions is much larger than the chemical potential, only the lowest transverse eigenmode is accessible. In terms of the oscillator length $\ell_\perp = \sqrt{\hbar/M\omega_\perp}$ for the transverse motion, this requires the 1D density $n_1 = n\pi\ell_\perp^2$ to obey $n_1 a \ll 1$. The effective interaction of atoms confined in such a geometry was first discussed by Olshanii (1998). In the realistic case where $\ell_\perp$ is much larger than the effective range r_e of the atom-atom interaction,[11] the two-particle scattering problem at low energies can be described by a (3D) pseudopotential. However, the asymptotic scattering states are of the form $\phi_0(y, z)\exp(\pm ikx)$, where $\phi_0(y, z)$ is the Gaussian ground-state wave function for the transverse motion and k is the wave vector for motion along the axial direction. Now, away from Feshbach

---

[11]For a typical frequency $\omega_\perp = 2\pi \cdot 100$ kHz, the transverse oscillator length is equal to 34 nm for ^{87}Rb.

resonances, the 3D scattering length is much smaller than the transverse oscillator length. In this weak-confinement limit $|a| \ll \ell_\perp$, the effective 1D interaction is obtained by integrating the 3D pseudopotential $g \int d^3x |\phi_0(y,z)|^2 \delta(\mathbf{x})$ over the ground-state density of the transverse motion. The resulting effective 1D interaction is then of the form $V(x) = g_1 \delta(x)$ with

$$g_1(|a| \ll \ell_\perp) = g|\phi_0(0,0)|^2 = 2\hbar\omega_\perp a. \qquad (78)$$

Trivially, an attractive or repulsive pseudopotential leads to a corresponding sign of the 1D interaction. In order to discuss what happens near Feshbach resonances, where the weak-confinement assumption breaks down, we consider bound states of two particles in a strong transverse confinement. Starting with an attractive 3D pseudopotential $a < 0$, the effective 1D potential (78) has a bound state with binding energy $\varepsilon_b = M_r g_1^2 / 2\hbar^2$. With increasing magnitude of a, this binding energy increases, finally diverging at a Feshbach resonance. In turn, upon crossing the resonance to the side where $a > 0$, the effective potential (78) becomes repulsive. The bound state, therefore, has disappeared even though there is one in the 3D pseudopotential for $a > 0$. Obviously, this cannot be correct. As pointed out above, the result (78) applies only in the weak-confinement limit $|a| \ll \ell_\perp$. In the following, we present the scattering properties of confined particles for arbitrary values of the ratio $|a|/\ell_\perp$. To this end, we first consider the issue of two-particle bound states with a pseudopotential interaction in quite general terms by mapping the problem to a random-walk process. Subsequently, we derive the low-energy scattering amplitudes by analytic continuation.

Confinement-induced bound states. Quite generally, two-particle bound states may be determined from the condition $V\hat{G} = 1$ of a pole in the exact T matrix. In the case of a pseudopotential with scattering length a, the matrix elements $\langle \mathbf{x}| \cdots |0\rangle$ of this equation lead to

$$\frac{1}{4\pi a} = \frac{\partial}{\partial r}[rG(E,\mathbf{x})]_{r=0} = \lim_{r\to 0}\left(G(E,\mathbf{x}) + \frac{1}{4\pi r}\right), \qquad (79)$$

in units where $\hbar = 2M_r = 1$. Here $G(E,\mathbf{x}) = \langle \mathbf{x}|(E - \hat{H}_0)^{-1}|0\rangle$ is the Green's function of the free Schrödinger equation, and $\hat{H}_0$ includes both the kinetic energy and the harmonic confining potential. As $r \to 0$, the Green's function diverges as $-(4\pi r)^{-1}$, thus providing the regularization for the pseudopotential through the second term of Eq. (79). For energies E below the bottom of the spectrum of $\hat{H}_0$, the resolvent $(E - \hat{H}_0)^{-1} = -\int_0^\infty dt \exp(E - \hat{H}_0)t$ can be written as a time integral. Moreover, by the Feynman-Kac formulation of quantum mechanics, the (imaginary-time) propagator $P(\mathbf{x},t) = \langle \mathbf{x}|\exp(-\hat{H}_0 t)|0\rangle$ can be interpreted as the sum over Brownian motion trajectories from $\mathbf{x} = 0$ to $\mathbf{x}$ at time t weighted with $\exp(-\int_0^t U[\mathbf{x}(t')])$, where $U(\mathbf{x})$ is the external potential in the free Hamiltonian $\hat{H}_0$. Similarly, the contribution $(4\pi r)^{-1} = \int_0^\infty dt P^{(0)}(\mathbf{x},t)$ can be written in terms of probability density of free Brownian motion with the

diffusion constant $D = 1$ in units where $\hbar = 2M_r = 1$. Taking the limit $r \to 0$, Eq. (79) finally leads to the exact equation

$$1/4\pi a = \int_0^\infty dt\,[P^{(0)}(t) - e^{Et}P(t)] \qquad (80)$$

for the bound-state energies E of two particles with a pseudopotential interaction and scattering length a. Here $P^{(0)}(t) = (4\pi t)^{-3/2}$ is the probability density at the origin of a free random walk after time t, starting and ending at $\mathbf{x} = \mathbf{0}$, while $P(t)$ is the same quantity in the presence of an additional confining potential. Note that, in the formulation of Eq. (80), the regularization of the $1/r$ singularity in $G(E,\mathbf{x})$ is accounted for by cancellation of the short-time divergence due to $P(t \to 0) = (4\pi t)^{-3/2}$, because the random walk does not feel the confinement as $t \to 0$. For two particles in free space, where $P(t) = P^{(0)}(t)$ at all times, Eq. (80) gives the standard result that a bound state at $E = -\varepsilon_b$ below the continuum at $E = 0$ exists only for $a > 0$, with $\varepsilon_b = \hbar^2/2M_r a^2$. In the presence of an additional confinement, however, there is a bound state for an arbitrary sign of the scattering length. The quasibound state in the continuum at $a < 0$ thus becomes a true bound state, i.e., it is shifted upward by less than the continuum threshold E_c. The physics behind this is the fact that the average time $\sim \int dt\,P(t)\exp(E_c t)$ spent near the origin is infinite for the *confined* random walk. This provides an intuitive understanding of why an infinitesimally small (regularized) δ potential is able to bind a state.

For harmonic confinement, the probability density $P(t) = [(4\pi)^3 \det\hat{J}(t)]^{-1/2}$ can be calculated from the determinant $\det\hat{J}(t)$ for small fluctuations around the trivial Brownian path $\mathbf{x}(t') \equiv \mathbf{0}$. Here $\hat{J}(t)$ obeys the simple 3×3 matrix equation (Schulman, 1981)

$$(-\partial_t^2 + \hat{\omega}^2)\hat{J}(t) = 0 \quad \text{with} \quad \hat{J}(0) = 0, \quad \partial_t\hat{J}(t)|_{t=0} = 1, \qquad (81)$$

where $\hat{\omega}^2$ is the (diagonal) matrix of the trap frequencies. The fluctuation determinant is thus equal to $\det\hat{J}(t) = t[\sinh(\omega_\perp t)/\omega_\perp]^2$ for two confining directions and equal to $\det\hat{J}(t) = t^2 \sinh(\omega_z t)/\omega_z$ for a pancake geometry. Since the continua start at $\hbar\omega_\perp$ and $\hbar\omega_z/2$, respectively, we write the bound-state energies as $E = \hbar\omega_\perp - \varepsilon_b$ or $E = \hbar\omega_z/2 - \varepsilon_b$. The dimensionless binding energy $\Omega = \varepsilon_b/\hbar\omega_{\perp,z}$ in the presence of confinement then follows from the transcendental equation

$$\frac{\ell_{\perp,z}}{a} = \int_0^\infty \frac{du}{\sqrt{4\pi u^3}}\left(1 - \frac{e^{-\Omega u}}{\{[1 - \exp(-2u)]/2u\}^{n/2}}\right)$$
$$= f_n(\Omega), \qquad (82)$$

where $n = 1,2$ is the number of confined directions.

The functions $f_{1,2}$ are shown in Fig. 18. For small binding energies $\Omega \ll 1$, their asymptotic behavior is $f_1(\Omega) = \ln(\pi\Omega/B)/\sqrt{2\pi}$ and $f_2(\Omega) = -1/\sqrt{\Omega} + A$ with numerical
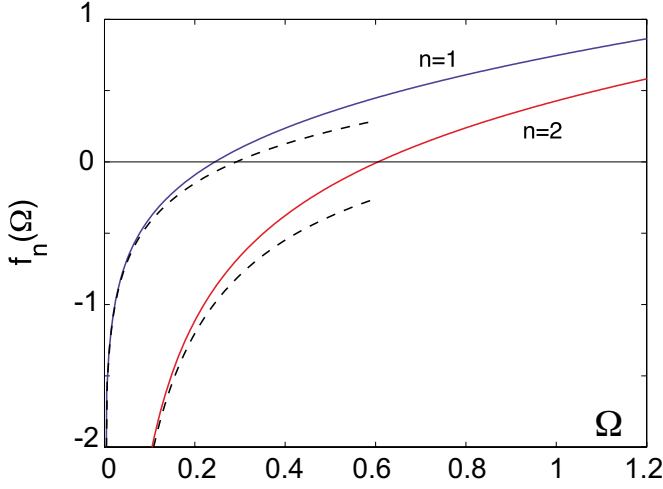
FIG. 18. (Color online) The functions $f_n(\Omega)$ defined in Eq. (82) for $n=1,2$. The limiting dependence $f_1(\Omega)=\ln(\pi\Omega/B)/\sqrt{2\pi}$ and $f_2(\Omega)=-1/\sqrt{\Omega}+A$ on the dimensionless binding energy Ω for $\Omega\ll 1$ is indicated by dashed lines.

constants $A=1.036$ and $B=0.905$. In the range $\Omega\lesssim 0.1$, where these expansions are quantitatively valid, the resulting bound-state energies are

$$\varepsilon_b = \hbar\omega_z(B/\pi)\exp(-\sqrt{2\pi}\ell_z/|a|) \tag{83}$$

in a 2D pancake geometry or

$$\varepsilon_b = \hbar\omega_\perp/(\ell_\perp/|a|+A)^2 \tag{84}$$

in a 1D waveguide. These results were obtained using different methods by Petrov and Shlyapnikov (2001) and by Bergeman *et al.* (2003), respectively. With increasing values of $|a|$, the binding energy increases, reaching finite, universal values $\varepsilon_b=0.244\hbar\omega_z$ or $0.606\hbar\omega_\perp$ precisely at the Feshbach resonance for one or two confined directions. Going beyond the Feshbach resonance, where $a>0$, the binding energy increases further, finally reaching the standard 3D result in the weak-confinement limit $a\ll\ell_\perp$. Here the binding is unaffected by the nature of confinement and $f_n(\Omega\gg 1)=\sqrt{\Omega}=f_0(\Omega)$.

Experimentally, confinement-induced bound states have been observed by rf spectroscopy in an array of 1D quantum wires using a mixture of fermionic ^{40}K atoms in their two lowest hyperfine states $m_F=-9/2$ and $-7/2$ (Moritz *et al.*, 2005). The different states allow for a finite *s*-wave scattering length that may be tuned using a Feshbach resonance at $B_0=202$ G [see Fig. 10(a)]. In the absence of the optical lattice, a finite binding energy appears only for magnetic fields below B_0, where $a>0$. In the situation with a strong transverse confinement, however, there is a nonzero binding energy both below and above B_0. Using Eq. (16) for the magnetic field dependence of the scattering length, the value of ε_b is in perfect agreement with the result obtained from Eq. (82). In particular, the prediction $\varepsilon_b=0.606\hbar\omega_\perp$ for the binding energy right at the Feshbach resonance has been verified by changing the confinement frequency $\omega_\perp$.

Scattering amplitudes for confined particles. Con-

sider now two-particle scattering in the continuum, i.e., for energies $E=\hbar\omega_\perp+\hbar^2 k^2/2M_r$ above the transverse ground-state energy. Quite generally, the effective 1D scattering problem is described by a unitary S matrix with reflection and transmission amplitudes r and t. They are related to the even and odd scattering phase shifts $\delta_{e,o}(k)$ by the eigenvalues $\exp[2i\delta_{e,o}(k)]=t\pm r$ of the S matrix. In analogy to the 3D case, the corresponding scattering amplitudes are defined as $f_{e,o}(k)=\{\exp[2i\delta_{e,o}(k)]-1\}/2$. For the particular case of a δ-function interaction, the odd scattering amplitude and phase shift vanish identically. The relevant dimensionless scattering amplitude $f_e(k)=r(k)=t(k)-1$ is thus simply the standard reflection amplitude. In the low-energy limit, a representation analogous to Eq. (4) allows one to define a 1D scattering length a_1 by[12]

$$f(k) = -1/[1+i\cot\delta(k)] \rightarrow -1/(1+ika_1) \tag{85}$$

with corrections of order k^3 because $\cot\delta(k)$ is odd in k. The universal limit $f(k=0)=-1$ reflects the fact that finite 1D potentials become impenetrable at zero energy. For a δ-function potential $V(x)=g_1\delta(x)$, the low-energy form of Eq. (85) holds for arbitrary k, with a scattering length $a_1\equiv-\hbar^2/M_r g_1$, which approaches $a_1\rightarrow-\ell_\perp^2/a$ in the weak-confinement limit. More generally, the exact value of a_1 for an arbitrary ratio $a/\ell_\perp$ may be determined by using the connection $\varepsilon_b=\hbar^2\kappa^2/2M_r$ between the bound-state energy and a pole at $k=i\kappa=i/a_1$ of the 1D scattering amplitude (85) in the upper complex k plane. Using Eq. (84) for the bound-state energy in the regime $a<0$ and the fact that a_1 must be positive for a bound state, one finds $a_1(a)=-\ell_\perp^2/a+A\ell_\perp$. Since the effective 1D pseudopotential is determined by the scattering length a_1, two-particle scattering is described by an interaction of the form

$$V_{1D}(x) = g_1\delta(x) \quad \text{with } g_1(a) = 2\hbar\omega_\perp a/(1-Aa/\ell_\perp). \tag{86}$$

From its derivation, this result appears to be valid only for g_1 small and negative, such that the resulting dimensionless binding energy $\Omega\lesssim 0.1$ is within the range of validity of Eq. (84). Remarkably, however, the result (86) is exact, as far as scattering of two particles above the continuum is concerned, at *arbitrary* values of $a/\ell_\perp$. This is a consequence of the fact that Eq. (86) is the *unique* pseudopotential consistent with the behavior of $f(k)$ up to order k^3. The exact scattering length is thus fixed by the binding energy (84) at small values of Ω. Moreover, the result uniquely extends into the regime where a_1 becomes negative, i.e., the pseudopotential ceases to support a bound state. The associated change of sign in g_1 at $a=\ell_\perp/A$ is called a confinement-induced resonance (Olshanii, 1998). It allows one to change the sign of the interaction between atoms by purely geometrical means.

---

[12]As in the 3D case, the scattering length is finite only for potentials decaying faster than $1/x^3$. Dipolar interactions are therefore marginal even in one dimension.

As shown by Bergeman *et al.* (2003), it can be understood as a Feshbach resonance where a bound state in the closed channel drops below the continuum of the ground state. Now, in a 1D waveguide, the separation between energy levels of successive transverse eigenstates with zero angular momentum is exactly $2\hbar\omega_\perp$, independent of the value of a (Bergeman *et al.*, 2003). The confinement-induced resonance thus appears precisely when the exact bound-state energy ε_b—which *cannot* be determined from the pseudopotential (86) unless $\Omega < 0.1$—reaches $2\hbar\omega_\perp$. An analogous confinement-induced resonance appears in a 2D pancake geometry; see Petrov, Holzmann, and Shlyapnikov (2000).

B. Bosonic Luttinger liquids; Tonks-Girardeau gas

To describe the many-body problem of bosons confined to an effectively 1D situation, the basic microscopic starting point is a model due to Lieb and Liniger (1963),

$$H = -\frac{\hbar^2}{2M}\sum_{i=1}^N \frac{\partial^2}{\partial x_i^2} + g_1\sum_{i<j}\delta(x_i - x_j). \qquad (87)$$

It is based on pairwise interactions with a pseudopotential $\sim g_1\delta(x)$, as given in Eq. (86). This is a valid description of the actual interatomic potential provided that the two-body scattering amplitude has the low-energy form of Eq. (85) for all relevant momenta k. In the limit $\mu \ll \hbar\omega_\perp$ of a single transverse mode, they obey $k\ell_\perp \ll 1$. Remarkably, in this regime, the pseudopotential approximation is always applicable. Indeed, it follows from the leading correction $\sim\Omega$ in the low-binding-energy expansion $f_2(\Omega) = -1/\sqrt{\Omega} + A + b\Omega + \cdots$ of the function defined in Eq. (82) that the denominator of the 1D scattering amplitude (85) has the form $1 + ika_1 - ib(k\ell_\perp)^3 + \cdots$ at low energies with a numerical coefficient $b = 0.462$. Since $a_1 \approx -\ell_\perp^2/a$ in typical situations where $a \ll \ell_\perp$, the condition $k^2 < 1/a\ell_\perp$ for a negligible cubic term in the scattering amplitude is always obeyed in the regime $k\ell_\perp \ll 1$ of a single transverse mode. In this limit, the interaction between cold atoms in a 1D tube is therefore generically described by the integrable Hamiltonian (87). In the homogeneous case, stability requires g_1 to be positive,[13] i.e., the 3D scattering length obeys $\ell_\perp > Aa > 0$. At a given 1D density $n_1 = N/L$, the strength of the interactions in Eq. (87) is characterized by a single dimensionless parameter

$$\gamma = \frac{g_1 n_1}{\hbar^2 n_1^2/M} = \frac{2}{n_1|a_1|} \approx \frac{2a}{n_1\ell_\perp^2} \quad \text{if } \ell_\perp \gg a. \qquad (88)$$

In marked contrast to the 3D situation, the dimensionless interaction strength γ scales inversely with the 1D density n_1 (Petrov, Shlyapnikov, and Walraven, 2000). In one dimension, therefore, it is the low-density limit

where interactions dominate. This rather counterintuitive result can be understood physically by noting that the scattering amplitude Eq. (85) approaches -1 as $k \to 0$. Since, at a given interaction strength g_1, the low-energy limit is reached at low densities, atoms in this regime are perfectly reflected by the repulsive potential of surrounding particles. For $\gamma \gg 1$, therefore, the system approaches a gas of impenetrable bosons where all energy is kinetic.[14] In particular, as shown by Girardeau (1960), at $\gamma = \infty$, the hard-core condition of a vanishing wave function whenever two particle coordinates coincide is satisfied by a wave function

$$\Psi_B(x_1, \ldots, x_N) = \prod_{i<j}|\sin[\pi(x_j - x_i)/L]|, \qquad (89)$$

which coincides with the absolute value of the wave function of a noninteracting spinless Fermi gas. Strongly interacting bosons in 1D thus acquire a fermionic character, a fact well known from the exact solution of a hard-core Bose or spin-1/2 system on a 1D lattice in terms of noninteracting fermions by the Jordan-Wigner transformation; see, e.g., Wen (2004).

Crossover diagram in a harmonic trap. In the presence of an additional harmonic confinement $V(x) = M\omega_0^2 x^2/2$ along the axial direction, the relative interaction strength depends, in addition to the parameter γ introduced above, also on the ratio $\alpha = \ell_0/|a_1| \approx 2a\ell_0/\ell_\perp^2$ between the oscillator length $\ell_0 = \sqrt{\hbar/M\omega_0}$ and the magnitude of the 1D scattering length. For tight radial confinement $\ell_\perp \approx 40$ nm and typical values $\ell_0 \approx 2$ μm for the axial oscillator length, one obtains $\alpha \approx 12$ for ^{87}Rb. This is in fact the interesting regime, since for $\alpha \ll 1$ the typical relative momenta $k \approx 1/\ell_0$ of two particles are so large that the strong-interaction limit $k|a_1| \ll 1$ cannot be reached at all. The conditions for realizing the Tonks-Girardeau (TG) limit in a trap have been discussed by Petrov, Shlyapnikov, and Walraven (2000) using a quantum hydrodynamic description [see also Ho and Ma (1999) and the review by Petrov, Gangardt, and Shlyapnikov (2004) on trapped gases in low dimensions]. Using Eq. (A8) in the Appendix, the phase fluctuations in a 1D Bose gas behave like $\delta\phi^2(x) = [\ln(|x|/\xi)]/K$ at zero temperature. From the Lieb-Liniger solution discussed below, both the characteristic healing length $\xi \approx K(\gamma)/n_1$ and the dimensionless so-called Luttinger parameter K are monotonically decreasing functions of the interaction strength. In particular, $K(\gamma) \to \pi/\sqrt{\gamma}$ is much larger than 1 in the limit $\gamma \ll 1$. In this limit, the 1D Bose gas loses its phase coherence on a scale $\ell_\phi(T=0) = \xi \exp K$ [defined by $\delta\phi^2(x = \ell_\phi) \approx 1$], which exceeds the healing length by an exponentially large factor. The gas behaves like a true condensate as long as its size R is smaller than ℓ_ϕ. Applying the Gross-Pitaevskii equation plus the

---

[13]For a possible extension to a metastable "super-Tonks" regime at $g_1 < 0$, see Astrakharchik *et al.* (2005a).

[14]In fact, it follows from the Lieb-Liniger solution that the ratio of the interaction and kinetic energy per particle diverges as $1/\sqrt{\gamma}$ for $\gamma \ll 1$ and decreases monotonically to zero as $1/\gamma$ for $\gamma \gg 1$.

local-density approximation, the radius of the associated Thomas-Fermi profile $n_1(x)$ is $R_{TF} \simeq (N\alpha)^{1/3}\ell_0$ (Petrov, Shlyapnikov, and Walraven, 2000). The condition $R_{TF} \gg \ell_0$ for the validity of the Thomas-Fermi approximation is thus always obeyed if $\alpha \gtrsim 1$. In contrast to the analogous situation in 3D, however, the weak-coupling regime requires *high* densities. The local value $n_1(0)\xi \approx K[\gamma(0)]$ of the Luttinger parameter at the trap center must thus be large compared to 1. This requires $\gamma(0) \ll 1$ or, equivalently, $n_1(0)\ell_0 \approx N\ell_0/R_{TF} \gg \alpha$. As a result, the Thomas-Fermi profile becomes invalid if $N < N_\star = \alpha^2 \gg 1$. For particle numbers below $N_\star$, the trapped gas reaches the TG regime. The density distribution is eventually that of a free Fermi gas, with a chemical potential $\mu = N\hbar\omega_0$ and a cloud size $R_{TG} = \sqrt{2N}\ell_0$. The continuous evolution of the density profile and cloud size between the weak-coupling and the TG limit was discussed by Dunjko *et al.* (2001).

At finite temperatures, the dominant phase fluctuations give rise to a linear increase $\delta\phi^2(x) = |x|/\ell_\phi(T)$ with distance on a scale $\ell_\phi(T) = \hbar^2 n_s/Mk_BT$, which depends only on the 1D superfluid density n_s.[15] In a trap of size R, these fluctuations are negligible if $\ell_\phi > R$. Using $n_s \approx N/R$ and the zero-temperature result for the Thomas-Fermi radius at $N > N_\star$, this translates to $k_BT \lesssim \hbar\omega_0(N/N_\star)^{1/3}$. In this range, the trapped gas is effectively a true BEC with a Thomas-Fermi density profile and phase coherence extending over the full cloud size. With increasing temperature, phase fluctuations are non-negligible; however, density fluctuations become relevant only if T exceeds the degeneracy temperature $T_d = N\hbar\omega_0$ (Petrov, Shlyapnikov, and Walraven, 2000). Defining a characteristic temperature $T_\phi = T_d/(N\alpha)^{2/3} \ll T_d$ below which phase fluctuations are irrelevant over the system size, there is a wide range $T_\phi < T < T_d$ in which the density profile is still that of a BEC; however, phase coherence is lost. The system can be thought of as a collection of independently fluctuating local BEC's and is called a *quasicondensate* (Petrov, Shlyapnikov, and Walraven, 2000). At higher temperatures $k_BT \gtrsim N\hbar\omega_0$, the gas eventually evolves into the nondegenerate regime of a Boltzmann gas. The complete crossover diagram is shown in Fig. 19.

Experimentally, the presence of strong phase fluctuations in a 1D situation already shows up in very elongated 3D condensates that still have a Thomas-Fermi density profile in the radial direction (i.e., $\mu \gg \hbar\omega_\perp$ such that many transverse modes are involved). In a trap, the strong interaction prevents local velocity fields due to phase fluctuations from showing up in the density profile. When the trap is switched off, however, the interaction becomes negligible after a certain expansion time, and then phase fluctuations are indeed converted into density fluctuations. These have been seen as stripes in absorption images of highly elongated BEC's by Dett-
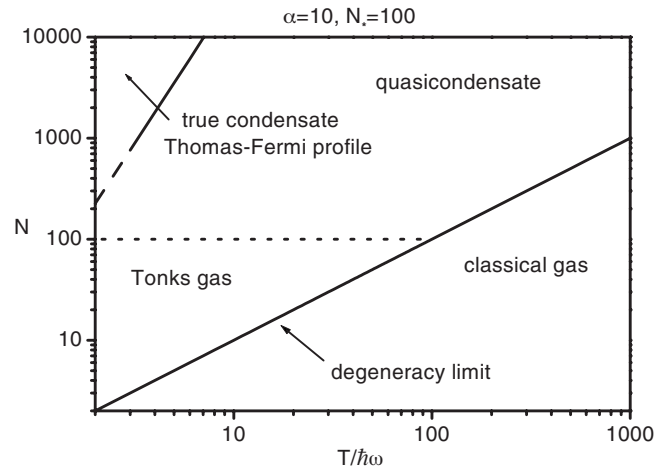

FIG. 19. Phase diagram for a 1D Bose gas in a harmonic trap with $\alpha = 10$. The Tonks-Girardeau regime is reached for small particle numbers $N < N_\star = \alpha^2$ and temperatures below the degeneracy limit $N\hbar\omega_0$. From Petrov, Shlyapnikov, and Walraven, 2000.

mer *et al.* (2001). The linear increase of phase fluctuations $\delta\phi^2(x)$ at finite temperature leads to an exponential decay of the first-order coherence function. The resulting Lorentzian momentum distribution was observed experimentally by Hellweg *et al.* (2003) and Richard *et al.* (2003) using Bragg spectroscopy. This enabled a quantitative measurement of $\ell_\phi(T)$. Moreover, at very low temperatures, no significant density fluctuations were present, thus confirming the quasi-BEC picture in which $\langle n(\mathbf{x})^2\rangle \approx \langle n(\mathbf{x})\rangle^2$.

Lieb-Liniger solution. As shown by Lieb and Liniger (1963), the model Eq. (87) can be solved by the Bethe ansatz. The essential physical property that lies behind the possibility of this exact solution is the fact that, in one dimension, interactions give rise only to scattering but not to diffraction. All eigenstates of the many-body problem in the domain $0 \le x_1 \le x_2 \le \cdots \le x_N \le L$ can thus be written as a sum

$$\Psi_B(x_1, \ldots, x_N) = \sum_P a(P)\exp\left(i\sum_{l=1}^{N} k_{P(l)}x_l\right) \qquad (90)$$

of plane waves with N distinct wave vectors k_l. They are combined with the coordinates x_l in all $N!$ possible permutations $k_{P(l)}$ of the k_l. The associated amplitude $a(P) = \Pi_{(ij)}e^{i\theta_{ij}}$ factorizes into two-particle scattering phase shifts $\theta_{ij} = \pi + 2\arctan(k_i - k_j)a_1/2$, with a_1 the 1D scattering length associated with the pseudopotential $g_1\delta(x)$. Here the product (ij) runs over all permutations of two wave numbers that are needed to generate a given permutation P of the k_l from the identity. Because $a_1 \sim -1/g_1$, the two-particle phase shifts $\theta_{ij} \sim g_1/(k_i - k_j)$ are singular as a function of the momenta in the limit $g_1 \to 0$ of an eventually ideal Bose gas. In the limit $\gamma \gg 1$, the phase shifts approach $\theta_{ij} = \pi$ for all momenta. Thus $a(P)_{\gamma=\infty} = (-1)^{|P|}$ is the parity of the permutation P, and the Bethe ansatz wave function Eq. (90) is reduced

---

[15]To simplify the notation, the dimensionality is not indicated in the superfluid or quasicondensate densities n_s and $\tilde{n}_0$.
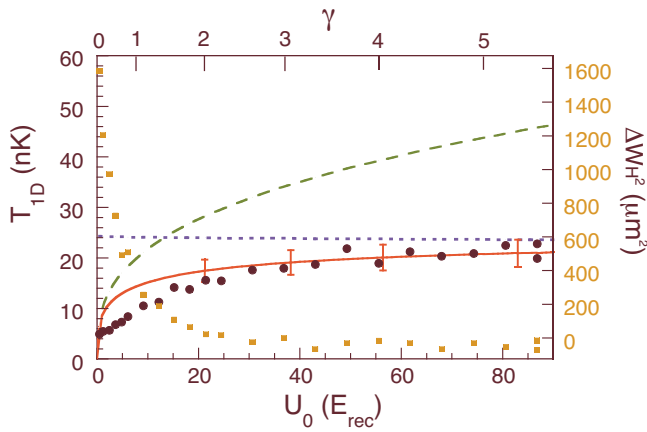
FIG. 20. (Color online) Average axial energy per particle and equivalent temperature T_{1D} as a function of the transverse confinement U_0. With increasing values of U_0, the energy crosses over from a weakly interacting Bose gas (long-dashed line) to a Tonks-Girardeau gas (short-dashed line), where T_{1D} is independent of U_0. From Kinoshita *et al.*, 2004.

to the free-fermion-type wave function Eq. (89) of a Tonks-Girardeau gas. For arbitrary coupling, both the ground-state energy per particle $E_0/N=(n_1^2\hbar^2/2M)e(\gamma)$ and the chemical potential $\mu=\partial E_0/\partial N$ are monotonically increasing functions of γ at fixed density n_1. For weak interactions $\gamma\ll1$, the chemical potential $\mu=g_1n_1$ follows the behavior expected from a mean-field approach, which is valid here for high densities $n_1|a_1|\gg1$. In the low-density regime $\gamma\gg1$, in turn, $\mu=\hbar^2(\pi n_1)^2/2M$ approaches a coupling-independent value that is just the Fermi energy associated with $k_F=\pi n_1$. The energy per particle in this regime is of completely kinetic origin, independent of the interaction strength γ. This remarkable property of the Tonks-Girardeau gas was observed experimentally by Kinoshita *et al.* (2004) (see Fig. 20). They measured the axial expansion energy of an array of 1D Bose gases as a function of the strength U_0 of the transverse confinement. Since $\omega_\perp\sim\sqrt{U_0}$, the dimensionless coupling γ is monotonically increasing with U_0 at fixed density n_1. In the weak-confinement limit, the expansion energy scales linearly with $\sqrt{U_0}$, reflecting the mean-field behavior $e(\gamma)=\gamma(1-4\sqrt{\gamma}/3\pi+\cdots)$ of the average energy per particle. By contrast, for large values of $\sqrt{U_0}$, where $|a_1|$ becomes shorter than the average interparticle spacing, the energy $e(\gamma)=\pi^2(1-4/\gamma+\cdots)/3$ saturates at a value that is fixed by the density.

The low-lying excitations of the Lieb-Liniger model have been obtained exactly by Lieb (1963a). Surprisingly, it turned out that there are two types of excitations, both with a linear spectrum $\omega=cq$ at low momenta. One of them has a Bogoliubov-like dispersion, linear at $q\xi\ll1$ and quadratic at $q\xi\gg1$. The crossover from collective to single-particle behavior occurs at a characteristic length ξ, which is related to the chemical potential in the ground state via $\mu=\hbar^2/2M\xi^2$. In the limit $\gamma\ll1$, the crossover length can be expressed as ξn_1

$=\gamma^{-1/2}\gg1$. Similar to the situation in three dimensions, the weak-coupling regime can therefore be characterized by the fact that the healing length is much larger than the average interparticle spacing n_1^{-1}. By contrast, for strong coupling $\gamma\gg1$, where the chemical potential approaches the Fermi energy of a spinless, noninteracting Fermi gas at density n_1, the healing length ξ is essentially identical with the average interparticle distance. The sound velocity c turns out to coincide with the simple thermodynamic formula $Mc^2=\partial\mu/\partial n$, which is obtained from the quantum hydrodynamic Hamiltonian Eq. (A6) under the assumption that the superfluid density at $T=0$ coincides with the full density. The ground state of the Lieb-Liniger gas is in fact fully superfluid at arbitrary values of γ in the sense of Eq. (A4), despite the fact that phase fluctuations destroy a plain BEC even at zero temperature. The sound velocity increases monotonically with γ, approaching the finite value $c(\infty)=v_F=\hbar\pi n_1/M$ of an ideal Fermi gas in the Tonks-Girardeau limit. The second type of excitation found by Lieb (1963a) also has a linear dispersion at small q with the same velocity. However, in contrast to the Bogoliubov-like spectrum discussed before, it is restricted to a finite range $|q|\lesssim\pi n_1$ and terminates with a vanishing group velocity. It turns out that these excitations are precisely the solitons of the nonlinear Schrödinger equation (Ishikawa and Takayama, 1980); for a discussion in the cold gas context, see Jackson and Kavoulakis (2002).

Momentum distribution in the Luttinger liquid regime. To obtain the momentum distribution of a strongly correlated 1D Bose gas, it is convenient to start from a quantum hydrodynamic description of the one-particle density matrix. At zero temperature, the logarithmic increase $\delta\phi^2(x)=(\ln|x|/\xi)/K$ of the phase fluctuations with distance [see Eq. (A8)] leads to an algebraic decay of $g^{(1)}(x)$ at scales beyond the healing length ξ. The associated exponent $1/(2K)$ is rather small in the weak-coupling regime and approaches its limiting value $1/2$ in the TG limit. The resulting momentum distribution thus exhibits a power-law divergence $\tilde{n}(k)\sim k^{-[1-(1/2K)]}$ for $k\xi\ll1$. At any finite temperature, however, this divergence is cut off due to thermal phase fluctuations. Indeed, these fluctuations increase linearly with distance $\delta\phi^2(x)=|x|/\ell_\phi(T)$ on a scale $\ell_\phi(T)$, implying an exponential decay of the one-particle density matrix for $|x|>\ell_\phi$. This leads to a rounding of the momentum distribution at small $k\simeq1/\ell_\phi$.

Experimentally, the momentum distribution of a Tonks-Girardeau gas was observed for ultracold atoms in a 2D optical lattice by Paredes *et al.* (2004). There a weak optical lattice was applied along the axial direction in order to tune the system into the strongly interacting regime, where K is close to 1. Indeed, for the low filling factors $f\ll1$ used in the experiment, there is no Mott-insulating phase. Instead, the 1D Bose-Hubbard model at $f\ll1$ describes a bosonic Luttinger liquid with $K\approx1+4\pi f/\gamma_L$ (Cazalilla, 2004b), where $\gamma_L=U/J$ is the effective coupling parameter on a lattice. When the axial lattice depth is increased, this ratio becomes very large,
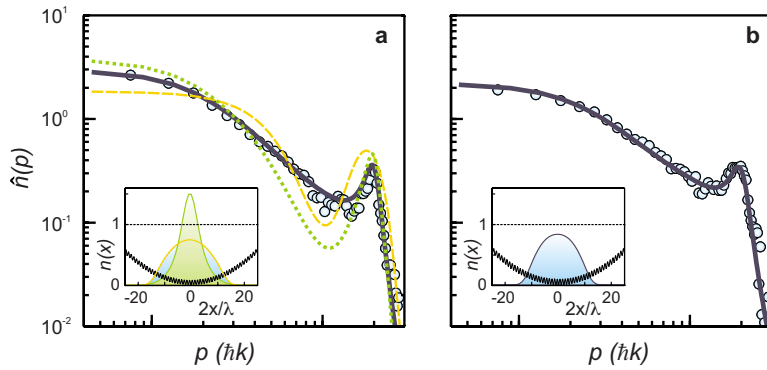
FIG. 21. (Color online) Axial momentum distribution of a lattice-based one-dimensional bosonic quantum gas for (a) $\gamma_L \approx 14$ and (b) $\gamma_L \approx 24$. The solid curve is the theoretical momentum distribution based on fermionization, and short- and long-dashed curves in (a) denote the expected values for a noninteracting Bose gas and a noninteracting Fermi gas, respectively. The insets show the corresponding in-trap density distributions. From Paredes *et al.*, 2004.

of order $\gamma_L = 5$–200. As shown in Fig. 21, the observed momentum distributions exhibit a power-law decay over a wide momentum range. They are in good agreement with a fermionization-based calculation of a hard-core Bose gas in a harmonic confinement. The momentum distributions at finite values of U have been studied by quantum Monte Carlo calculations. Although the final hard-core limit is only reached for large values of $\gamma_L \rightarrow \infty$ (Pollet *et al.*, 2004), deviations in the momentum distribution compared to fermionized bosons are less than a few percent already for $\gamma_L > 5$ (Wessel *et al.*, 2005). In the experiment, a significant deviation from the limiting value of $1 - 1/(2K) \rightarrow 1/2$ of the exponent in the momentum distribution at small values of k is found. In fact, the low-k divergence of the momentum distribution is masked by finite-temperature effects and finite-size cutoffs. For larger momenta, the momentum distribution of the quantum gas is determined by short-range correlations between particles, which can increase the coefficient of the power-law decay in the momentum distribution above $1/2$ in experiments. In fact, it was shown by Olshanii and Dunjko (2003) that the momentum distribution of a homogeneous 1D Bose gas at large momenta $k\xi \gg 1$ should behave like $1/k^4$ as long as $kr_e \ll 1$.

The parameter $K = \pi\hbar\kappa c$ determines the asymptotic behavior not only of the one-particle density matrix but in fact of all correlation functions. This may be understood from Haldane's description of 1D quantum liquids[16] in terms of their long-wavelength density oscillations (Haldane, 1981). In its most elementary form, this is the 1D version of the quantum hydrodynamic Hamiltonian equation (A6). On introducing a field $\hat{\theta}(x)$ that is related to small fluctuations around the average density by $\delta\hat{n}_1(x) = \partial_x\hat{\theta}(x)/\pi$, the effective Hamiltonian describing the low-lying excitations is of the form

$$\hat{H} = \frac{\hbar c}{2\pi} \int dx \left(K(\partial_x\hat{\phi})^2 + \frac{1}{K}(\partial_x\hat{\theta})^2 \right) \qquad (91)$$

with sound velocity c. The low-energy physics of a 1D Bose liquid is determined by the velocity c and the di-

mensionless parameter K. In the translation-invariant case, $K = \pi\hbar n_1/Mc$ is fixed by c and the average density. Moreover, for interactions that may be described by a 1D pseudopotential, K may be expressed in terms of the microscopic coupling constant γ using the Lieb-Liniger solution. The resulting value of $K = v_F/c$ decreases monotonically from $K(\gamma) = \pi/\sqrt{\gamma} \gg 1$ in the weak-interaction, high-density limit to $K(\gamma) = 1 + 4/\gamma + \cdots$ in the Tonks-Girardeau limit [see Cazalilla (2004a)]. The property $K > 1$ for repulsive bosons is valid for interactions that decay faster than $1/x^3$ such that the 1D scattering length a_1 is finite. The algebraic decay of $g^{(1)}(x)$ in a 1D gas at zero temperature is formally similar to the situation in 2D at finite temperatures, where $g^{(1)}(r)$ exhibits a power-law decay with exponent η [see Eq. (100)]. Apart from the different nature of phase fluctuations (quantum versus thermal), there is, however, an important difference between the two situations. In the 2D case, superfluidity is lost via the BKT transition once $\eta > 1/4$ [see Eq. (101)]. By contrast, in one dimension, there is no such restriction on the exponent and superfluidity still persists if $K < 2$. The origin of this difference is related to the fact that phase slips in one dimension require a nonzero modulation of the potential, e.g., by a weak optical lattice (Büchler *et al.*, 2003). Formally, it is related to a Berry-phase term beyond Eq. (91), which confines vortex-antivortex pairs in this case; see Wen (2004).

Two- and three-particle correlations. An intuitive understanding of the evolution from a weakly interacting quasicondensate to a Tonks-Girardeau gas with increasing values of γ is provided by considering the pair distribution function $g^{(2)}(x)$. It is defined by the density correlation function $\langle\hat{n}(x)\hat{n}(0)\rangle = n_1\delta(x) + n_1^2 g^{(2)}(x)$ and is a measure of the probability of finding two particles separated by a distance x. For an ideal BEC in three dimensions, the pair distribution function is $g^{(2)}(\mathbf{x}) \equiv 1$ at arbitrary distances. Above T_c, it drops monotonically from $g^{(2)}(0) = 2$ to the trivial limit $g^{(2)}(\infty) = 1$ of any homogeneous system on the scale of the thermal wavelength λ_T. For cold atoms in 3D, these basic results on bosonic two-particle correlations were verified experimentally by Schellekens *et al.* (2005). For the Lieb-Liniger gas, the local value of the pair correlation $g^{(2)}(0) = de(\gamma)/d\gamma$ can be obtained from the derivative of the dimensionless ground-state energy (Gangardt and Shlyapnikov, 2003).

---

[16]In the context of cold gases, the notion of a quantum *liquid* is purely conventional. These systems are stable only in the gaseous phase, yet may be strongly interacting.
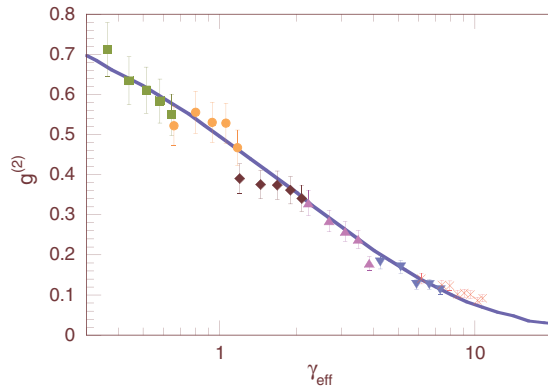
FIG. 22. (Color online) Local pair correlation function from photoassociation measurements as a function of the interaction parameter γ_{eff} averaged over an ensemble of 1D Bose gases. The theoretical prediction is shown as a solid line. From Kinoshita *et al.*, 2005.

The exact result for $e(\gamma)$ then gives $g^{(2)}(0)=1-2\sqrt{\gamma}/\pi+\cdots$ and $g^{(2)}(0)=(2\pi/\sqrt{3}\gamma)^2\to 0$ in the limits $\gamma\ll 1$ and $\gamma\gg 1$, respectively. For weak coupling, therefore, there is only a small repulsive correlation hole around each particle. By contrast, in the strong-coupling limit, the probability of finding two bosons at the same point vanishes as $1/\gamma^2$. In the Tonks-Girardeau limit, the equivalence of density correlations to those of a free Fermi gas allows one to determine the full pair distribution function exactly as $g^{(2)}(x)=1-[\sin(\pi n_1 x)/\pi n_1 x]^2$. For low densities, therefore, the zero-range repulsion strongly suppresses configurations in which two bosons come closer than their mean interparticle distance. Note that the pair correlation exhibits appreciable oscillations with wave vector $2k_F=2\pi n_1$ even though the momentum distribution is completely continuous at k_F. Experimentally, the local value $g^{(2)}(0)$ of the pair correlation function was determined by Kinoshita *et al.* (2005) using photoassociation. As suggested by Gangardt and Shlyapnikov (2003), the rate $K_1=K_3 g^{(2)}(0)$ for stimulated transitions in which two atoms in a continuum state are transferred to a bound molecule is reduced by a factor $g^{(2)}(0)$ from the corresponding value in 3D, provided the transfer occurs locally on a length scale much less than the transverse oscillator length. The photoassociation rate in a one-dimensional situation is strongly reduced at $\gamma\gg 1$ due to the much smaller probability for two atoms to be at the same point. From measurements of the atom loss after a variable time of photoassociation in an array of several thousand 1D traps with particle numbers in the range $40<N<240$, Kinoshita *et al.* (2005) extracted the value of $g^{(2)}(0)$. As shown in Fig. 22, the results are in good agreement with theory over a wide range of interaction constants up to $\gamma\approx 10$.

The local value of three-body correlation function $g^{(3)}(0)$ was also calculated by Gangardt and Shlyapnikov (2003). It behaves as $g^{(3)}(0)=1-6\sqrt{\gamma}/\pi+\cdots$ and $g^{(3)}(0)\sim(\pi/\gamma)^6$ for small and large γ, respectively. The predicted suppression of three-body recombination losses

was observed by Tolra *et al.* (2004) using the strong confinement in a 2D optical lattice.

In situ measurements of density fluctuations were performed by Esteve *et al.* (2006). They observed a crossover from an effectively high-temperature regime at low densities $n_1\ll(|a_1|/\lambda_T^4)^{1/3}$, where the number fluctuations exceed the shot-noise level due to bunching in an essentially ideal Bose gas. At high densities, a quasicondensate regime is reached with $n_1 a\simeq 0.7$, close to the limit of a single transverse mode. There the number fluctuations are strongly suppressed and may be described by a 1D Bogoliubov description of quasicondensates (Mora and Castin, 2003).

Weak optical lattices and coupled 1D gases. The problem of a 1D Bose gas in a weak optical lattice was discussed by Büchler *et al.* (2003). Using the extension in 1D of the phase-density representation (A7) of the field operator in a quantum hydrodynamic description, which accounts for the discrete nature of the particles (Haldane, 1981), a periodic potential commensurate with the average particle density gives rise to an additional nonlinear term $\cos 2\theta(x)$ in Eq. (91). This is the well-known sine-Gordon model (Giamarchi, 2004), which exhibits a transition at a critical value $K_c=2$. For $K>2$, the ground state of the Lieb-Liniger gas remains superfluid in a weak optical lattice. For $(1<)K<2$, in turn, atoms are locked in an incompressible Mott state even in an arbitrary weak periodic lattice. From the exact Lieb-Liniger result for $K(\gamma)$, the critical value $K_c=2$ is reached at $\gamma_c\approx 3.5$.

In a configuration using 2D optical lattices, a whole array of typically several thousand parallel 1D gases is generated. For a very large amplitude of the optical lattice $V_\perp\gtrsim 30 E_r$, hopping between different 1D gases is negligible and the system decouples into independent 1D tubes. By continuously lowering $V_\perp$, however, it is possible to study the crossover from a 1D to a 3D situation. The equilibrium phase diagram of an array of 1D tubes with an adjustable transverse hopping $J_\perp$ was studied by Ho *et al.* (2004). It exhibits a fully phase-coherent BEC for sufficiently large values of $J_\perp$ and the 1D Luttinger parameter K. For a detailed discussion of weakly coupled 1D gases, see Cazalilla *et al.* (2006).

C. Repulsive and attractive fermions

As mentioned in Sec. V.A, ultracold Fermi gases in a truly 1D regime $\varepsilon_F\ll\hbar\omega_\perp$ have been realized using strong optical lattices. In the presence of an additional axial confinement with frequency ω_0, the Fermi energy is $\varepsilon_F=N\hbar\omega_0$. The requirement that only the lowest transverse mode is populated, therefore, requires small particle numbers $N\ll\omega_\perp/\omega_0$. Typical temperatures in these gases are around $k_B T\approx 0.2\varepsilon_F$ (Moritz *et al.*, 2005). In the following, we briefly discuss some of the basic phenomena that may be studied with ultracold fermions in one dimension.

In a spin-polarized 1D Fermi gas, only p-wave interactions are possible. As shown by Granger and Blume

(2004), the corresponding Feshbach resonances are shifted due to the confinement in a similar way as in Eq. (86) above. This was confirmed experimentally by Günter *et al.* (2005). In the case of two different states, *s*-wave scattering dominates in the ultracold limit. For repulsive interactions, one obtains a fermionic Luttinger liquid, which is a two-component version of the quantum hydrodynamic Hamiltonian (91). It has a twofold linear excitation spectrum for fluctuations of the total density and the density difference ("spin density"), respectively. Generically, the velocities of "charge" and spin excitations are different. This is the most elementary form of "spin-charge separation," which has been verified experimentally in semiconductor quantum wires (Auslaender *et al.*, 2005). In the context of ultracold Fermi gases in a harmonic trap, spin-charge separation effects show up in collective excitation frequencies (Recati *et al.*, 2003) or in the propagation of wave packets (Kollath *et al.*, 2005). A genuine observation of spin-charge separation, however, requires one to study single-particle correlations and cannot be inferred from collective excitations only.

For *attractive* interactions, a spin-1/2 Fermi gas in one dimension is a so-called Luther-Emery liquid. Its fluctuations in the total density have a linear spectrum $\omega(q) = cq$; however, there is a finite gap for spin excitations (Giamarchi, 2004). The origin of this gap is the appearance of bound pairs of fermions with opposite spin. The spectrum $\omega_s(q) = \sqrt{(\Delta_s/2\hbar)^2 + (v_s q)^2}$ for small oscillations of the spin density is similar to that of quasiparticles in the BCS theory. In analogy to Eq. (88) for the bosonic problem, the dimensionless coupling constant $\gamma = -2/n_1 a_1 < 0$ is inversely proportional both to the 1D scattering length $a_1 = -\ell_\perp^2/a + A\ell_\perp$ (now for fermions in different states; note that attractive interactions $a < 0$ imply a *positive* 1D scattering length a_1) and to the total 1D density $n_1 = n_{1\uparrow} + n_{1\downarrow}$. As shown by Gaudin (1967) and Yang (1967), the model is exactly soluble by the Bethe ansatz. For weak coupling, $|\gamma| \lesssim 1$, the spin gap $\Delta_s \equiv 2\Delta_{\mathrm{BCS}}$,

$$\Delta_s(\gamma) = (16\varepsilon_F/\pi)\sqrt{|\gamma|/\pi}e^{-\pi^2/2|\gamma|}, \qquad (92)$$

has a form similar to that in BCS theory, except for an interaction-dependent prefactor $\sim \sqrt{|\gamma|}$. Note, however, that the weak-coupling regime is reached at high densities $n_1|a_1| \gg 1$, in contrast to the situation in 3D, where $k_F|a| \ll 1$ in the BCS limit. At low densities, where $1/\gamma \to 0^-$, the spin gap approaches the two-body bound-state energy $\Delta_s \to \varepsilon_b$, which was measured by rf spectroscopy (Moritz *et al.*, 2005), as discussed above. In this regime, tightly bound fermion pairs behave like a hard-core Bose gas. The strong-coupling BEC limit of attractive fermions in 1D thus appears to be a Tonks-Girardeau gas, very different from the nearly ideal Bose gas expected in a 3D situation (see Sec. VIII). However, in the presence of a harmonic waveguide, the associated transverse oscillator length $\ell_\perp \equiv \sqrt{\hbar/M\omega_\perp}$ defines an additional length not present in a strictly 1D description. As shown in Sec. V.A, the exact solution of the scattering

problem for two particles in such a waveguide always exhibits a two-body bound state, whatever the sign and magnitude of the scattering length *a*. Its binding energy right at the confinement-induced resonance is $\varepsilon_b = 2\hbar\omega_\perp$. Since $\hbar\omega_\perp \gg \varepsilon_F$ in the limit of a singly occupied transverse channel, the two-particle bound-state energy ε_b is the largest energy scale in the problem beyond this point. In the regime after the confinement-induced resonance, where γ becomes positive, the appropriate degrees of freedom are therefore no longer single atoms, but instead are strongly bound fermion pairs. An exact solution of the four-body problem in a quasi-1D geometry with tight harmonic confinement shows that these dimers have a *repulsive* interaction (Mora *et al.*, 2005). Attractive fermions in 1D therefore continuously evolve from a Luther-Emery liquid to a gas of repulsive bosons. As realized by Fuchs *et al.* (2004) and Tokatly (2004), the 1D BCS-BEC crossover problem can be solved exactly by the Bethe ansatz, connecting the Gaudin-Yang model on the fermionic side with the Lieb-Liniger model on the bosonic side.

The problem of attractive Fermi gases in one dimension at different densities $n_\uparrow \neq n_\downarrow$ of the two components was solved by Hu, Liu, and Drummond (2007) and Orso (2007). The superfluid ground state with equal densities becomes unstable above a critical chemical potential difference $\mu_\uparrow - \mu_\downarrow = \Delta_s$. This is the analog of the Clogston-Chandrasekhar limit (Chandrasekhar, 1962; Clogston, 1962), where the paired ground state is destroyed by the paramagnetic, or Pauli, mechanism. In 3D, this has been observed by Zwierlein *et al.* (2006). In contrast to the 3D case, however, the transition is continuous in 1D and the result $\Delta\mu_c = \Delta_s$ holds for arbitrary coupling strengths. Moreover, since the gap becomes large at low densities, the SF phase with zero-density imbalance appears at the trap edge. The phase in the trap center, in turn, is a partially polarized phase that still has superfluid correlations. As argued by Yang *et al.* (2001) using bosonization, this phase exhibits an oscillating superfluid order parameter similar to that predicted by Fulde and Ferrell (1964) and Larkin and Ovchinnikov (1965) in a narrow range above the Clogston-Chandrasekhar limit. In contrast to the 3D situation, nonconventional superfluid order is thus expected in a rather wide range of parameters.

VI. TWO-DIMENSIONAL BOSE GASES

The two-dimensional Bose gas is a system that presents many interesting features from a many-body physics perspective. The first question that arises concerns the possibility of reaching Bose-Einstein condensation in a uniform system. The answer to this question is negative, for both the ideal and the interacting gas. Indeed, as in one dimension long-range order is destroyed by thermal fluctuations at any finite temperature. However, in an interacting 2D gas the destruction of order is only marginal and superfluidity can still occur below a finite critical temperature T_c. Above T_c, quasi-long-range or-

der is destroyed via the mechanism that was elucidated by Berezinskii (1971) and Kosterlitz and Thouless (1973) and that consists in the breaking of pairs of vortices with opposite circulations. As shown by Nelson and Kosterlitz (1977), this scenario implies a jump in the superfluid density[17] from a finite and universal value $n_s(T_c)/k_B T_c = 2M/\pi\hbar^2$ to zero, right at T_c. Equivalently, the thermal wavelength λ_T obeys $n_s(T_c)\lambda_T^2 = 4$. This prediction has been experimentally tested using helium films (Bishop and Reppy, 1978, 1980).

Quantum atomic gases provide a system where this concept of a quasi-long-range order can be experimentally tested. However, the addition of a harmonic potential to confine the gas in the plane changes the problem significantly. For example, conventional Bose-Einstein condensation of an ideal gas is possible in a 2D harmonic potential. For an interacting gas, the situation is more involved; a true BEC is still expected at extremely low temperature. At slightly higher temperature, phase fluctuations may destabilize it and turn it into a quasi-condensate phase, which is turned into a normal gas above the degeneracy temperature. We review the main features of atomic 2D gases, and discuss the experimental results obtained so far.

We start with an ideal gas of N bosons at temperature T, confined in a square box of size L^2. Using the Bose-Einstein distribution and assuming a smooth variation of the population of the various energy states, we take the thermodynamic limit $N, L \to \infty$ in such a way that the density $n = N/L^2$ stays constant. We then find a relation between the density n, the thermal wavelength $\lambda_T = h/(2\pi M k_B T)^{1/2}$, and the chemical potential μ,

$$n\lambda_T^2 = -\ln(1 - e^{\mu/k_B T}). \tag{93}$$

This relation allows one to derive the value of μ for any degeneracy parameter $n\lambda_T^2$ value. It indicates that no condensation takes place in 2D, in contrast to the 3D case. In the latter case, the relation between $n_{3D}\lambda_T^3$ and μ ceases to admit a solution above the critical value $n_{3D}\lambda_T^3 = 2.612$, which is the signature for BEC.

Consider now N bosons confined by the potential $V(r) = M\omega^2 r^2/2$ in the x, y plane. The presence of a trap modifies the density of states, and BEC is predicted to occur for an ideal gas when the temperature is below the critical temperature T_0 (Bagnato and Kleppner, 1991),

$$N = (\pi^2/6)(k_B T_0/\hbar\omega)^2. \tag{94}$$

However, it should be pointed out that the condensation remains a fragile phenomenon in a 2D harmonic potential. To show this point, we calculate the spatial density $n(\mathbf{x})$ using the local-density and semiclassical approximations, which amounts to replacing μ by $\mu - V(\mathbf{x})$ in Eq. (93),

---

[17]Note that, unless indicated, all densities in this section are *areal* and not volume densities.

$$n(\mathbf{x})\lambda_T^2 = -\ln(1 - e^{[\mu - V(\mathbf{x})]/k_B T}). \tag{95}$$

Taking $\mu \to 0$ to reach the condensation threshold and integrating over $\mathbf{x}$, we recover the result (94). But we also note that $n_{max}(0) = \infty$, which means that the condensation in a 2D harmonic potential occurs only when the 2D spatial density at the center of the trap is infinite. This should be contrasted with the result for a 3D harmonically trapped Bose gas, where condensation occurs at a central density $n_{3D,max}(0) = \zeta(3/2)/\lambda_T^3$, which is equal (in the semiclassical approximation) to the threshold density in a homogeneous system [see, e.g., Pitaevskii and Stringari (2003)].

A. The uniform Bose gas in two dimensions

We now turn to the more realistic case of a system with repulsive interactions, and consider the case of a uniform gas. We restrict ourselves here to well-established results, since the main goal is to prepare the discussion of the trapped gas case, which will be addressed next. The first task is to model the atom interaction in a convenient way. As done for a 1D system, it is tempting to use a contact term $g_2\delta(\mathbf{x})$, which leads to a chemical potential $\mu = g_2 n$ in the mean-field approximation. However, two-dimensional scattering has peculiar properties, and we explain that in general it is not possible to describe interactions in 2D by a coupling constant g_2, and that one has to turn to an energy-dependent coefficient. We then discuss the many-body state expected at low temperature, and present the Berezinskii-Kosterlitz-Thouless transition.

We start by some considerations concerning quantum scattering in two dimensions. Consider two particles of mass M moving in the x, y plane, and we restrict ourselves here to low-energy motion where the scattering is isotropic. The scattering state can be written (Adhikari, 1986)

$$\psi_k(\mathbf{x}) \sim e^{i\mathbf{k}\cdot\mathbf{x}} - \sqrt{i/8\pi}f(k)e^{ikr}/\sqrt{kr}, \tag{96}$$

where $\mathbf{k}$ is the incident wave vector and $f(k)$ is the dimensionless scattering amplitude for the relative energy $E = \hbar^2 k^2/M$. At low energy, one gets for the scattering amplitude the following variation:

$$f(k) = 4/[-\cot\delta_0(k) + i] \to 4\pi/[2\ln(1/ka_2) + i\pi], \tag{97}$$

which defines the 2D scattering length a_2. Taking, for instance, a square-well interaction potential of depth V_0 and diameter b, it is equal to $a_2 = bF(k_0 b)$, with $F(x) = \exp[J_0(x)/xJ_1(x)]$ and $k_0 = \sqrt{2MV_0}/\hbar$. Note that, in contrast to the situation in 3D, where $\lim_{k\to 0} f(k) = -a$, in 2D $f(k)$ tends to 0 when $k \to 0$. The total cross section $\lambda = |f(k)|^2/4k$ (dimension of a length), however, tends to infinity.

Since the coupling coefficient g_2 is directly related to the scattering amplitude, it appears that 2D systems are peculiar in the sense that the coupling coefficient is intrinsically energy dependent, in contrast to 1D and 3D

systems. In addition to the scattering amplitude $f(k)$, one may need the off-shell T matrix when addressing many-body problems. It was calculated for 2D hard disks by Morgan *et al.* (2002). The extension of a zero-range interaction potential to the two-dimensional case is discussed by Olshanii and Pricoupenko (2002).

We now turn to a macroscopic assembly of bosonic particles, and address the $T=0$ situation. The case of a gas of hard disks of diameter b and surface density n was studied by Schick (1971). The conclusion is that Bose-Einstein condensation is reached with a large condensate fraction, provided $[\ln(1/nb^2)]^{-1} \ll 1$. This constitutes the small parameter of the problem, to be compared with $\sqrt{na^3}$ in 3D. The chemical potential is then $\mu \simeq 4\pi\hbar^2 n/M \ln(1/nb^2)$, indicating that the proper choice for g_2 is (within logarithmic accuracy) $g_2 = \hbar^2 \tilde{g}_2/M$, where the dimensionless number $\tilde{g}_2$ is equal to the scattering amplitude $f(k)$ for energy $E = 2\mu$. Corrections to the result of Schick (1971) for more realistic densities have been calculated by Andersen (2002), Pricoupenko (2004), and Pilati *et al.* (2005).

In the finite-temperature case, the impossibility of a 2D BEC already mentioned for an ideal gas remains valid for an interacting gas with repulsive interactions. This was anticipated by Peierls (1935) in the general context of long-range order in low-dimensional systems. It was shown for interacting bosons by Hohenberg (1967), based on arguments by Bogoliubov (1960). A completely equivalent argument was given for lattice spin systems by Mermin and Wagner (1966). To prove this result, one can make a *reductio ad absurdum*. Suppose that the temperature is small but finite ($T \neq 0$) and that a condensate is present in the mode $\mathbf{k}=\mathbf{0}$, with a density n_0. By the Bogoliubov inequality, the number of particles $\tilde{n}_k$ in state $\mathbf{k} \neq \mathbf{0}$ satisfies

$$\tilde{n}_k + \frac{1}{2} \geq \frac{k_B T}{\hbar^2 k^2/M} \frac{n_0}{n}. \tag{98}$$

In the thermodynamic limit, the number of particles N' in the excited states is

$$N' = \sum_k \tilde{n}_k = \frac{L^2}{4\pi^2} \int \tilde{n}_k d^2k. \tag{99}$$

When k tends to zero, the dominant term in the lower bound given above varies as $1/k^2$. In 2D, this leads to a logarithmically diverging contribution of the integral originating from low momenta. This means that the starting hypothesis (the existence of a condensate in $\mathbf{k}=\mathbf{0}$) is wrong in 2D.

Even though there is no BEC for a homogeneous, infinite 2D Bose gas, the system at low temperature can be viewed as a quasicondensate, i.e., a condensate with a fluctuating phase (Kagan *et al.*, 1987; Popov, 1987). The state of the system is well described by a wave function $\psi(\mathbf{x}) = \sqrt{\tilde{n}_0(\mathbf{x})}e^{i\phi(\mathbf{x})}$, and the two-dimensional character is revealed by the specific statistical behavior of spatial correlation functions of the phase $\phi(\mathbf{x})$ and the quasi-condensate density $\tilde{n}_0(\mathbf{x})$. Actually, repulsive interac-
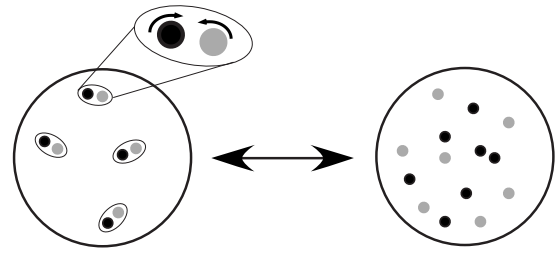

FIG. 23. Microscopic mechanism at the origin of the superfluid transition in the uniform 2D Bose gas. Below the transition temperature, vortices exist only in the form of bound pairs formed by two vortices with opposite circulation. Above the transition, temperature-free vortices proliferate, causing an exponential decay of the one-body correlation function $g_1(r)$.

tions tend to reduce the density fluctuations and one can in first approximation focus on phase fluctuations only. The energy arising from these phase fluctuations has two contributions. The first one originates from phonon-type excitations, where the phase varies smoothly in space. The second one is due to quantized vortices, i.e., points at which the density is zero and around which the phase varies by a multiple of 2π. For our purpose, it is sufficient to consider only singly charged vortices, where the phase varies by $\pm 2\pi$ around the vortex core.

Berezinskii (1971) and Kosterlitz and Thouless (1973) have identified how a phase transition can occur in this system when the temperature is varied (Fig. 23). At low temperature, the gas has a finite superfluid density n_s. The one-body correlation function decays algebraically at large distance,

$$ng^{(1)}(r) = \langle \hat{\psi}(\mathbf{x})\hat{\psi}(0) \rangle \propto r^{-\eta} \quad \text{for } T < T_c, \tag{100}$$

with $\eta = (n_s \lambda_T^2)^{-1}$. The fact that there is an exact relation between the coherence properties of the system and the superfluid density is explained in the Appendix. Free vortices are absent in this low-temperature phase, and vortices exist only in the form of bound pairs, formed by two vortices with opposite circulations. At very low temperatures, the contribution of these vortex pairs to the correlation function $g^{(1)}$ is negligible, and the algebraic decay of $g^{(1)}$ is dominated by phonons. When T increases, bound vortex pairs lead to a renormalization of n_s, which remains finite as long as T is lower than the critical temperature T_c defined by

$$n_s \lambda_T^2 = 4 \quad \text{for } T = T_c. \tag{101}$$

Above T_c, the decay of $g^{(1)}(r)$ is exponential or even Gaussian, once the temperature is large enough that the gas is close to an ideal system. With increasing temperature, therefore, the superfluid density undergoes a jump at the critical point from $4/\lambda_T^2(T_c)$ to 0 (Nelson and Kosterlitz, 1977). Note that Eq. (101) is actually an implicit equation for the temperature since the relation between the superfluid density $n_s(T)$ and the total density n remains to be determined. The physical phenomenon at the origin of the Berezinskii-Kosterlitz-Thouless phase transition is related to the breaking of the pairs of vor-

tices with opposite circulation. For T slightly above T_c, free vortices proliferate and form a disordered gas of phase defects, which are responsible for the exponential decay of $g^{(1)}$. For higher temperatures, the gas eventually exhibits strong density fluctuations and the notion of vortices becomes irrelevant.

The value given above for the transition temperature can be recovered by evaluating the likelihood of having a free vortex appearing in a superfluid occupying a disk of radius R (Kosterlitz and Thouless, 1973). One needs to calculate the free energy $F = E - TS$ of this state. The energy E corresponds to the kinetic energy of the superfluid; assuming that the vortex is at the center of the disk, the velocity field is $v = \hbar/Mr$, hence $E = \pi M n_s \int v^2(r) r \, dr = (\pi \hbar^2 n_s/M) \ln(R/\xi)$, where we set the lower bound of the integral equal to the healing length ξ, since it gives approximately the size of the vortex core. The entropy associated with positioning the vortex core of area $\pi \xi^2$ in the superfluid disk of area πR^2 is $k_B \ln(R^2/\xi^2)$; hence the free energy is

$$F/k_B T = \tfrac{1}{2}(n_s \lambda_T^2 - 4)\ln(R/\xi). \qquad (102)$$

For $n_s \lambda_T^2 > 4$, the free energy is large and positive for a large system ($R \gg \xi$), indicating that the appearance of a free vortex is very unlikely. On the contrary, for $n_s \lambda_T^2 < 4$, the large and negative free energy signals the proliferation of free vortices. The critical temperature estimated above from a single-vortex picture turns out to coincide with the temperature where pairs of vortices with opposite circulation dissociate. Such pairs have a finite energy even in an infinite system (Kosterlitz and Thouless, 1973).

The question remains of how to relate the various spatial densities appearing in this description, such as the total density n and the superfluid density n_s. In the Coulomb gas analogy where positive and negative charges correspond to clockwise and counterclockwise vortices [see, e.g., Minnhagen (1987)], these two quantities are related by $n_s/n = 1/\varepsilon(T)$, where $\varepsilon(T)$ is the dielectric constant of the 2D Coulomb gas. For an extremely dilute Bose gas, the relation between n and n_s was addressed by Fisher and Hohenberg (1988). Their treatment is valid in the limit of ultraweak interactions $\epsilon = 1/\ln(\ln[1/(na_2^2)]) \ll 1$, where a_2 is the 2D scattering length. They obtained the result $n_s/n \sim \epsilon$ on the low-temperature side of the transition point. Using Monte Carlo calculations, Prokof'ev et al. (2001) studied the case of weak but more realistic interactions. Denoting by $\hbar^2 \tilde{g}_2/m$ the effective long-wavelength interaction constant [see Eq. (105)], they obtained the following result for the total density at the critical point: $n\lambda_T^2 = \ln(C/\tilde{g}_2)$, where the dimensionless number $C = 380 \pm 3$. A typical value for $\tilde{g}_2$ in cold atom experiments is in the range 0.01-0.2, which leads to a total phase-space density at the critical point $n\lambda_T^2$ in the range 7.5-10.5. Prokof'ev et al. (2001) also evaluated the reduction of density fluctuations with respect to the expected result $\langle n^2 \rangle = 2\langle n \rangle^2$ for an ideal gas. They observed that these fluctuations are strongly reduced at the transition point for the domain of coupling parameters relevant for atomic gases. These high-precision Monte Carlo methods also allow one to study the fluctuation region around the transition point (Prokof'ev and Svistunov, 2005).

The BKT mechanism has been the subject of several studies and has been confirmed in various branches of condensed-matter physics [for a review, see Minnhagen (1987)]. In the context of Bose fluids, Bishop and Reppy (1978) performed an experiment with helium films adsorbed on an oscillating substrate. The change in the moment of inertia of the system gave access to the superfluid fraction and provided evidence for the BKT transition. In an experiment performed with atomic hydrogen adsorbed on superfluid helium, Safonov et al. (1998) observed a rapid variation of the recombination rate of the 2D hydrogen gas when the phase-space density was approaching the critical value Eq. (101). However, it is still a matter of debate whether one can reach a quantitative agreement between these experimental observations and the theoretical models (Stoof, 1994; Kagan et al., 2000; Andersen et al., 2002).

B. The trapped Bose gas in 2D

Recent progress concerning the manipulation, cooling, and trapping of neutral atomic gases with electromagnetic fields has opened the way to the study of planar Bose gases. In order to prepare 2D atomic gases, one freezes the motion along the z direction using either light-induced forces or magnetic forces. This confining potential $V(z)$ has to be strong enough so that all relevant energies for the gas (chemical potential, temperature) are well below the excitation energy from the ground state to the first excited state in $V(z)$. The two other directions x and y are much more weakly confined. The potential in the x,y plane is harmonic in all experiments so far. Here we first review the main experimental schemes that have been implemented. We then discuss the new features that appear because of the harmonic confinement in the x,y plane, and present the current status of experimental investigations concerning the coherence properties of these trapped 2D gases.

Experimental realizations of a 2D gas. The conceptually simplest scheme to produce a 2D gas is to use a sheet of light with a red detuning with respect to the atomic resonance. The dipole potential then attracts atoms toward the locations of high light intensity, and ensures a strong confinement in the direction perpendicular to the light sheet. This technique was implemented at MIT by Görlitz et al. (2001) for sodium atoms. A 1064 nm laser was focused using cylindrical lenses, and provided a trapping frequency $\omega_z/2\pi$ around 1000 Hz along the z direction. The red-detuned light sheet also ensured harmonic trapping in the x,y plane, with much smaller frequencies (30 and 10 Hz along the x and y directions, respectively). An adjustable number of atoms, varying between 2×10^4 and 2×10^6, was loaded in the dipole trap, starting with a 3D condensate. The mea-

surements were essentially devoted to the size of the atom cloud after free ballistic expansion. For small numbers of atoms (below 10^5) it was observed that the z motion was indeed frozen, with a release energy essentially equal to the kinetic energy of the ground state, $\hbar\omega_z/4$. For larger atom numbers, the interaction energy exceeded $\hbar\omega_z$ and the gas was approaching the 3D Thomas-Fermi limit.

Another way of implementing a 2D trap consists in using an evanescent wave propagating at the surface of a glass prism. In 2004, Grimm and co-workers in Innsbruck loaded such a trap with a condensate of cesium atoms (Rychtarik *et al.*, 2004). The light was blue detuned from resonance, so that atoms levitated above the light sheet, at a distance $\sim 4~\mu$m from the horizontal glass surface ($\omega_z/2\pi \sim 500$ Hz). The confinement in the horizontal x,y plane was provided by an additional hollow laser beam, which was blue detuned from the atomic resonance and propagating vertically. This provided an isotropic trapping with a frequency $\omega_\perp/2\pi \sim 10$ Hz. As in the MIT experiment, a time-of-flight technique revealed that, for small atom numbers, the vertical expansion energy was approximately equal to $\hbar\omega_z/4$, meaning that the z motion was frozen. The number of atoms was decreased together with temperature, and a rapid increase of the spatial density, causing an increase of losses due to three-body recombination, was observed when the gas approached quantum degeneracy. These data were consistent with the formation of a condensate or a quasicondensate at the bottom of the trap.

A hybrid trap was investigated in Oxford, where a blue-detuned, single-node, Hermite Gaussian laser beam trapped Rb atoms along the z direction, whereas the confinement in the x,y plane was provided by a magnetic trap (Smith *et al.*, 2005). This allowed a very large anisotropy factor (~ 700) between the z axis and the transverse plane to be achieved. Here the 2D regime was also reached for a degenerate gas with $\sim 10^5$ atoms.

Trapping potentials that are not based on light beams have also been investigated. One possibility discussed by Hinds *et al.* (1998) consists in trapping paramagnetic atoms just above the surface of a magnetized material, producing an exponentially decaying field. The advantage of this technique lies in the very large achievable frequency ω_z, typically in the megahertz range. One drawback is that the optical access in the vicinity of the magnetic material is not as good as with optically generated trapping potentials. Another technique to produce a single 2D sheet of atoms uses the so-called radio-frequency dressed-state potentials (Zobay and Garraway, 2001). Atoms are placed in an inhomogeneous static magnetic field, with a radio-frequency field superimposed, whose frequency is on the order of the energy splitting between two consecutive Zeeman sublevels. The dressed states are the eigenstates of the atomic magnetic moment coupled to the static and radio-frequency fields. Since the magnetic field is not homogeneous, the exact resonance occurs on a 2D surface. There one dressed state (or possibly several, depending

on the atom spin) has an energy minimum, and atoms prepared in this dressed state can form a 2D gas. This method was implemented experimentally for a thermal gas by Colombe *et al.* (2004), but no experiment has yet been performed in the degenerate regime.

Finally, a 1D optical lattice setup, formed by the superposition of two running laser waves, is a convenient way to prepare stacks of 2D gases (Orzel *et al.*, 2001; Burger *et al.*, 2002; Köhl *et al.*, 2005b; Morsch and Oberthaler, 2006; Spielman *et al.*, 2007). The 1D lattice provides a periodic potential along z with an oscillation frequency ω_z that can easily exceed the typical scale for chemical potential and temperature (a few kilohertz). The simplest lattice geometry is formed by two counterpropagating laser waves, and it provides the largest ω_z for a given laser intensity. One drawback of this geometry is that it provides a small lattice period ($\lambda/2$ where λ is the laser wavelength), so that many planes are simultaneously populated. Therefore, practical measurements provide only averaged quantities. Such a setup has been successfully used to explore the transition between a superfluid and a Mott insulator in a 2D geometry (Köhl *et al.*, 2005b; Spielman *et al.*, 2007). Another geometry consists in forming a lattice with two beams crossing at an angle θ smaller than $180°$ (Hadzibabic *et al.*, 2004). In this case, the distance $\lambda/[2\sin(\theta/2)]$ between adjacent planes is adjustable, and each plane can be individually addressable if this distance is large enough (Schrader *et al.*, 2004; Stock *et al.*, 2005). Furthermore, the tunneling matrix element between planes can be made completely negligible, which is important if one wants to achieve a true 2D geometry and not a modulated 3D situation.

From 3D to 2D scattering. In Sec. VI.A, we discussed the properties of a 2D gas consisting of hard disks. Cold atomic gases, however, interact through van der Waals forces, and one has to understand how to switch from the 3D coupling constant to the 2D case. The confining potential along z is $V(z)=M\omega_z^2 z^2/2$, and we assume that $\mu, k_B T \ll \hbar\omega_z$ such that the single-atom motion along the z direction is frozen into the Gaussian ground state.

The scattering amplitude in this regime was calculated by Petrov, Holzmann, and Shlyapnikov (2000) and Petrov and Shlyapnikov (2001). Quite generally, low-energy scattering in 2D is described by a scattering amplitude of the form Eq. (97). Since $f(k)$ has a pole at $k = i/a_2$, the relation between a_2 and the basic scattering length a of the 3D pseudopotential may be determined from the bound-state energy $\varepsilon_b = \hbar^2/(2M_r a_2^2)$ in a 2D confined geometry. This has been calculated in Sec. V.A for arbitrary values of the ratio between the 3D scattering length a and the confinement length ℓ_z. Using Eq. (83) in the limit of small binding energies, the 2D scattering length is related to its 3D counterpart and the confinement scale $\ell_z = (\hbar/M\omega_z)^{1/2}$ by

$$a_2(a) = \ell_z \sqrt{\frac{\pi}{B}} \exp\left(-\sqrt{\frac{\pi}{2}}\frac{\ell_z}{a}\right) \tag{103}$$

with $B=0.905$ (Petrov and Shlyapnikov, 2001). As in 1D, the scattering length for particles in the continuum is

determined uniquely by the two-particle binding energy in the limit $\varepsilon_b \ll \hbar\omega_z$. The fact that $a_2(a)$ is positive, independent of the sign of a, shows that for a 3D interaction described by a pseudopotential, a two-particle bound state exists for an arbitrary sign and strength of the ratio a/ℓ_z as discussed in Sec. V.A. Note that, for realistic parameters $\ell_z \sim 100$ nm and a of the order of a few nanometers, the 2D scattering length is incredibly small. This is compensated for by the logarithmic dependence of the scattering amplitude on $a_2(a)$. Indeed, from Eqs. (97) and (103), the effective low-energy scattering amplitude of a strongly confined 2D gas is given by

$$f(k) = 4\pi/[\sqrt{2\pi}\ell_z/a + \ln(B/\pi k^2 \ell_z^2) + i\pi]. \qquad (104)$$

When the binding along z is not very strong, ℓ_z is much larger than a so that the logarithm and the imaginary term in Eq. (104) are negligible. This weak-confinement limit corresponds to the relevant regime for experiments to date. The resulting scattering amplitude

$$f(k) \simeq \sqrt{8\pi}a/\ell_z \equiv \tilde{g}_2 \ll 1 \qquad (105)$$

is independent of energy, and the dimensionless coupling parameter $\tilde{g}_2 = Mg_2/\hbar^2$ is much smaller than 1. This implies that the gas is weakly interacting in the sense that, in the degenerate regime where $n\lambda_T^2 \simeq 1$, the chemical potential $\mu \simeq g_2 n$ is much smaller than the temperature ($\mu/k_B T = \tilde{g}_2/2\pi$). An important feature of the two-dimensional gas is that the criterion for distinguishing the weakly and strongly interacting regimes does not depend on density. Indeed the analog of the ratio γ given in Eq. (88) is equal to $\tilde{g}_2$. In analogy to Eq. (78) in the 1D case, the result (105) can be recovered by integrating the 3D pseudopotential over the z oscillator ground state. One often refers to a gas in this collisional regime as a quasi-2D system in the sense that it can be considered as a 2D system from the statistical physics point of view, but the dynamics of binary collision remains governed by 3D properties; in particular, the 3D scattering length a remains a relevant parameter.

More generally, since the relevant energy for relative motion is twice the chemical potential, the momentum $k = \sqrt{2M\mu}/\hbar$ in Eq. (104) is the inverse healing length ξ. At very low energies therefore, the effective interaction in 2D is always repulsive, independent of the sign of the 3D scattering length (Petrov and Shlyapnikov, 2001). This result, however, is restricted to a regime where $\ln(\xi/\ell_z) \gg \ell_z/a$. The logarithmic correction in Eq. (104) is therefore significant in the case of a strongly confining potential, when ℓ_z and a are comparable. One then recovers a variation for $f(k)$ that is formally similar to that of a pure 2D square well (97) with scattering length $a_2 \simeq \ell_z$. This regime could be relevant in a situation in which the 3D scattering length a is enhanced by a Feshbach resonance (Wouters *et al.*, 2003; Rajagopal *et al.*, 2004; Kestner and Duan, 2006). If the 3D scattering length a is positive, the logarithmic correction in Eq. (104) is a reduction of the scattering amplitude. On the other hand, for negative a, this correction can lead to a strong increase of the amplitude for a particular value of ℓ_z (Petrov, Holzman, and Shlyapnikov, 2000), leading to a confinement-induced resonance similar to those encountered in the 1D case.

Is there a true condensation in a trapped 2D Bose gas? This question has been debated over the past decade as two opposing lines of reasoning can be proposed. On the one hand, we recall that for an ideal gas the presence of a trap modifies the density of states so that Bose-Einstein condensation becomes possible in 2D. One could thus expect that this remains valid in the presence of weak interactions. On the other hand, in the presence of repulsive interactions, the extension of the (quasi) condensate in the trap must increase with the number of atoms N. When N is large, the local-density approximation entails that the correlation function $g^{(1)}(r)$ decays algebraically as in Eq. (100) over a domain where the density is approximately uniform. This prevents us from obtaining long-range order except for extremely low temperatures. A related reasoning uses the fact that, for the ideal gas, condensation is reached when the spatial density calculated semiclassically becomes infinite [see Eq. (95)], which cannot occur in the presence of repulsive interactions. The fragility of the condensation of the ideal Bose gas in 2D is further illustrated by the existence at any temperature of a noncondensed Hartree-Fock solution, for arbitrarily small repulsive interactions (Bhaduri *et al.*, 2000). However, for very low temperature, this solution is not the absolute minimizer of the free energy, as shown using the Hartree-Fock-Bogoliubov method by Fernández and Mullin (2002), Gies and Hutchinson (2004), and Gies *et al.* (2004).

Currently, the converging answer, though not yet fully tested experimentally, is the following. At ultralow temperature, one expects a true BEC, i.e., a system that is phase coherent over its full extension. The ground-state energy and density of a 2D Bose gas in the limit $T=0$ can be obtained using the Gross-Pitaevskii equation, as shown by Lieb *et al.* (2001) [see also Kim *et al.* (2000), Cherny and Shanenko (2001), Lee *et al.* (2002), and Posazhennikova (2006)]. The crossover from a three- to a two-dimensional gas at $T=0$ has been addressed by Tanatar *et al.* (2002) and Hechenblaikner *et al.* (2005).

When the temperature increases, one encounters the quasicondensate superfluid regime, where phase fluctuations due to phonons dominate. The scenario is then reminiscent of the uniform case, and has been analyzed by Petrov, Gangardt, and Shlyapnikov (2004). The function $g^{(1)}(r)$ decays algebraically and vortices are found only in the form of bound pairs. Finally, at larger temperature these vortex pairs break and the system becomes normal. A BKT transition is still expected in the thermodynamic limit $N \to \infty$, $\omega \to 0$, $N\omega^2$ constant, but the jump in the total superfluid fraction is suppressed because of the inhomogeneous atomic density profile (Holzmann *et al.*, 2007). Indeed, the energy for breaking a vortex pair depends on the local density, and superfluidity will probably be lost gradually from the edges of the quasicondensate to the center as the temperature increases. Assuming that the atomic distribution is well

approximated by the Hartree-Fock solution at the transition point, Holzmann *et al.* (2007) predicted that the BKT transition temperature for a trapped gas is slightly lower than the ideal BEC transition temperature (94), by an amount related to the (small) dimensionless coupling parameter $\tilde{g}_2 = Mg_2/\hbar^2$.

We focus for a moment on the quasicondensate regime. It is described by a macroscopic wave function $\psi(\mathbf{x}) = \sqrt{\tilde{n}_0(\mathbf{x})} \exp i\phi(\mathbf{x})$, and the density and phase fluctuations can be analyzed using a Bogoliubov analysis. We refer the reader to the work of Mora and Castin (2003) and Castin (2004) for a discussion on extension of Bogoliubov theory to quasicondensates. As for the uniform gas (Prokof'ev *et al.*, 2001), repulsive interactions reduce the density fluctuations for $k_B T \lesssim \mu$ and $n\lambda_T^2 \gg 1$, so that $\langle \tilde{n}_0^2(\mathbf{x}) \rangle \simeq [\langle \tilde{n}_0(\mathbf{x}) \rangle]^2$. For large atom numbers ($N\tilde{g}_2 \gg 1$), the equilibrium shape of the gas can be derived using a Thomas-Fermi approximation, as for a true condensate. The kinetic energy plays a negligible role, and the density profile results from the balance between the trapping potential and the repulsive interatomic potential. It varies as an inverted parabola

$$\tilde{n}_0(\mathbf{x}) = \tilde{n}_0(0)(1 - r^2/R^2), \quad (\hbar^2/M)\tilde{g}_2\tilde{n}_0(0) = \mu, \quad (106)$$

where the chemical potential μ and the radius of the clouds R are

$$\mu = \hbar\omega(N\tilde{g}_2/\pi)^{1/2}, \quad R = \sqrt{2}a_\perp(N\tilde{g}_2/\pi)^{1/4}, \quad (107)$$

with $a_\perp = \sqrt{\hbar/M\omega}$.

The parabolic Thomas-Fermi profile appears on the top of a broader background formed by atoms out of the (quasi)condensate. Such a profile was experimentally observed first by Görlitz *et al.* (2001) and Rychtarik *et al.* (2004). A precise measurement of the onset at which a pure thermal distribution turns into a bimodal (Thomas-Fermi + thermal) profile was performed by Krüger *et al.* (2007). The experiment was performed with a rubidium gas confined in a 1D optical lattice, such that $\tilde{g}_2 = 0.13$. The phase-space density at which bimodality arises was found to be in good agreement with the prediction of Prokof'ev *et al.* (2001) for the BKT threshold $n(0)\lambda_T^2 = \ln(C/\tilde{g}_2) \simeq 8.0$, which is relevant here if the local-density approximation is valid at the center of the trap. At the critical point, the total number of atoms in each plane significantly exceeded the result (94) expected in the ideal case. In this experiment, two to three planar gases were produced simultaneously, and they could interfere with each other when overlapping during time of flight, provided their spatial coherence was large enough. It was observed that the onset of bimodality coincides (within experimental accuracy) with the onset of clearly visible interferences.

It is important to note that, since the expected Thomas-Fermi profile is identical for a true and a quasicondensate, its observation cannot be used to discriminate between the two situations. The phase fluctuations have been calculated by Petrov and Shlyapnikov (2001)
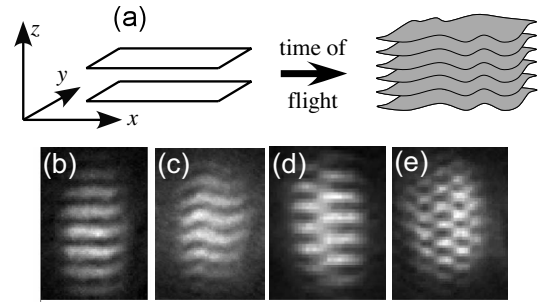

FIG. 24. Matter-wave heterodyning of 2D gases. (a) Principle of the method: two planar Bose gases are released from the trap, expand, and overlap, giving rise to an interference pattern that is probed by absorption imaging. (b)–(e) Examples of experimental interference patterns obtained well below (b) and in the vicinity (c) of the degeneracy temperature. Some patterns show one (d) or several (e) dislocations, revealing the presence of vortices in one of the gases. From Hadzibabic *et al.*, 2006.

and Petrov, Gangardt, and Shlyapnikov (2004) in the regime $\mu \lesssim k_B T$ and $n\lambda_T^2 \gg 1$ [see Eq. (A8) in the Appendix],

$$\delta\phi^2(\mathbf{x}) = \langle [\phi(0) - \phi(\mathbf{x})]^2 \rangle \simeq [2/\tilde{n}_0(0)\lambda_T^2]\ln(r/\xi). \quad (108)$$

This expression, which is reminiscent of the uniform result (100), is valid for points $\mathbf{x}$ inside the quasicondensate. The healing length $\xi = \hbar/\sqrt{2M\mu}$ satisfies $\xi R = a_\perp^2$. Therefore, it is only at a temperature much below the degeneracy temperature, such that $\Delta\phi(R) \lesssim \pi$, that one recovers a quasiuniform phase over the whole sample, and hence a true condensate.

Experimental investigations of phase fluctuations. A convenient way to access experimentally the phase coherence of quasi-2D gases is the matter-wave heterodyning technique. It consists in studying the statistical properties of the matter-wave interference pattern that forms when two independent, parallel 2D Bose gases are released from the trap and overlap [Fig. 24(a)]. A detailed analysis of these patterns was given by Polkovnikov *et al.* (2006) (see Sec. III.C for the 1D case). Assume that the two gases have the same uniform amplitude ψ_0 and fluctuating phases $\varphi_a(x,y)$ and $\varphi_b(x,y)$. The interference signal $S(x,z)$ is recorded by sending an imaging beam along the y direction, which integrates the atomic density over a length L_y,

$$S(x,z) \propto 2\psi_0^2 + e^{2i\pi z/D}c(x) + e^{-2i\pi z/D}c^*(x), \quad (109)$$

with

$$c(x) = \frac{\psi_0^2}{L_y}\int_{-L_y/2}^{L_y/2} e^{i[\varphi_a(x,y)-\varphi_b(x,y)]}dy. \quad (110)$$

The period D of the interference pattern is $D = 2\pi\hbar t/Md$, where d is the initial distance between the two planes and t is the expansion time. We now integrate the coefficient $c(x)$ appearing in Eq. (109) over a variable length L_x,

$$C(L_x) = \frac{1}{L_x} \int_{-L_x/2}^{L_x/2} c(x)dx, \tag{111}$$

and average $|C(L_x)|^2$ over many images recorded in the same conditions. Using the fact that the phases φ_a and φ_b are uncorrelated, we obtain, for $L_x \gg L_y$,

$$\langle |C(L_x)|^2 \rangle = \frac{1}{L_x^2} \int \int \langle c(x)c^*(x') \rangle dx \, dx'$$
$$= \frac{1}{L_x} \int_{-L_x/2}^{L_x/2} |g^{(1)}(x,0)|^2 dx \propto \left(\frac{1}{L_x}\right)^{2\alpha}, \tag{112}$$

where we have assumed that the two gases have the same statistical properties. The long-range physics is then captured in a single parameter, the exponent α. It is straightforward to understand the expected values of α in some simple cases. In a system with true long-range order, $g^{(1)}$ would be constant and the interference fringes would be perfectly straight. In this case $\alpha=0$, corresponding to no decay of the contrast upon integration. In the low-temperature regime, where $g^{(1)}$ decays algebraically [see Eq. (100)], the exponent α coincides with the exponent $\eta(T)$, which describes the quasi-long-range order in $g^{(1)}$. In the high-temperature case, where $g^{(1)}$ decays exponentially on a length scale much shorter than L_x, the integral in Eq. (112) is independent of L_x. In this case $\alpha=0.5$, corresponding to adding up local interference fringes with random phases. The BKT mechanism corresponds to a transition from a power law with exponent $1/n_s\lambda_T^2 \le 0.25$ to an exponential decay of $g^{(1)}$. It should thus manifest itself as a sudden jump of α from 0.25 to 0.5 when the temperature varies around T_c.

This method has been implemented at ENS with two rubidium planar gases, forming two parallel, elongated strips ($L_x=120$ μm, $L_y=10$ μm) (Hadzibabic et al., 2006) [Figs. 24(b)–24(e)]. The experimental results confirm the expected behavior, at least qualitatively. At relatively large temperature, the fitted exponent α is close to 0.5. When the temperature decreases, a rapid transition occurs and α drops to $\sim$0.25. At the transition, the estimated phase-space density of the quasicondensate is $\tilde{n}_0(0)\lambda_T^2 \sim 6$. Note that, for a quantitative comparison between experiments and theory, one should account for density fluctuations that are likely to play an important point near the transition, in contrast to the situation in superfluid liquid helium. Also the geometry effects in these elongated samples ($R_x \sim 12R_y$) may be significant.

In addition to the rapid variation of the exponent η characterizing the decay of $g^{(1)}$, these experiments gave evidence for isolated vortices (Stock et al., 2005; Hadzibabic et al., 2006) [Figs. 24(d) and 24(e)]. A vortex appears as a dislocation of the fringes in the interference pattern (Chevy et al., 2001b; Inouye et al., 2001), and these dislocations indeed proliferate on the high-temperature side of the transition. Using a theoretical analysis based on a classical field method, Simula and Blakie (2006) obtained phase patterns of quasicondensates close to the critical temperature that indeed exhibit

an isolated, free vortex, in good agreement with experimental observation. The probability for observing a vortex pair in a similar configuration was calculated by Simula et al. (2005).

The Berezinskii-Kosterlitz-Thouless mechanism was also investigated recently using a two-dimensional periodic array of $\sim$200 Josephson coupled Bose-Einstein condensates (Schweikhard et al., 2007). Each tubelike condensate contains a few thousand atoms, and has a length $\sim$35 μm along the z direction. The condensates are localized at the sites of a 2D hexagonal optical lattice of period 4.7 μm in the x,y plane, and the coupling J between adjacent sites can be tuned by varying the optical lattice intensity. The phase properties of the ensemble are probed by ramping down the lattice and recording the density profile in the x,y plane when wave functions from the various sites overlap. Vortices appear as holes in the atomic density distribution, and the vortex surface density is measured as a function of the Josephson coupling J and the temperature T. A universal vortex activation curve is obtained as a function of the parameter J/T, showing vortex proliferation for $J/T \lesssim 1$, in good agreement with the predictions of the BKT mechanism.

Breathing mode of a 2D gas. In the preceding section, we were mostly interested in the static properties of 2D Bose gases. Here we point out a remarkable dynamical property of these systems in an isotropic harmonic potential, when the interaction potential between particles is such that $V(\lambda r) = V(r)/\lambda^2$. Pitaevskii and Rosch (1997) showed that, when the gas is prepared in an arbitrary out-of-equilibrium state, the quantity $\langle r^2 \rangle$ oscillates at the frequency 2ω without any damping, irrespective of the strength of the interaction. They also proved that this property originates from the presence of a hidden symmetry, described by the two-dimensional Lorentz group SO(2,1). In fact, precisely the same symmetry occurs in the case of a unitary gas in 3D, as discussed in Sec. VIII.B.

The Dirac distribution in 2D $\delta^{(2)}(r)$ belongs to the class of functions satisfying $V(\lambda r) = V(r)/\lambda^2$. It makes this SO(2,1) symmetry relevant for trapped neutral atoms at low energies, when the range of interaction is small compared to all other scales. However, a true contact interaction is singular in 2D, and leads to logarithmic ultraviolet divergences that are cut off by the finite range of the real interatomic potential. Therefore, one cannot hope to observe a fully undamped breathing mode in atomic systems, but rather a very weakly damped dynamics. It was pointed out by Fedichev et al. (2003) that vortex pair nucleation could play a role in the residual expected damping of this breathing mode. Note that the difficulties with the contact interaction do not arise at the level of the Gross-Pitaevskii equation, where the same property has been predicted (Kagan et al., 1996; Pitaevskii, 1996)

A precursor of this long-lived breathing mode was observed in a 3D, quasicylindrical geometry by Chevy et al. (2001a). The transverse breathing mode of the cylinder

was found to oscillate at a frequency very close to 2ω with an extremely small damping (quality factor of the mode >2000). The damping and shift of the oscillation frequency was calculated theoretically with a good precision by Jackson and Zaremba (2002) [see also Guilleumas and Pitaevskii (2003)]. In this case, part of the damping is due to the nucleation of pairs of phonons propagating along $\pm z$ (Kagan and Maksimov, 2003), a mechanism that is of course absent in a pure 2D geometry. This breathing mode has also been observed in a fast rotating gas by Stock *et al.* (2004). Its frequency was also $\sim 2\omega$, with a small correction due to the nonharmonicity of the trapping potential that was necessary to stabilize the center-of-mass motion of the atom cloud in the fast rotating regime (see Sec. VII.B).

VII. BOSE GASES IN FAST ROTATION

The investigation of rotating gases or liquids is a central issue in the study of superfluidity (Donnelly, 1991). It is relevant for the study of liquid helium, rotating nuclei, neutron stars, and pulsars, and for the behavior of superconductors in a magnetic field. During recent years, several experiments using rotating Bose-Einstein condensates have provided a spectacular illustration of the notion of quantized vortices (Matthews *et al.*, 1999; Madison *et al.*, 2000; Abo-Shaeer *et al.*, 2001; Hodby *et al.*, 2001). Depending on the rotation frequency Ω of the gas, a single vortex or several vortices can be observed experimentally. When the number of vortices is large compared to 1, they form an Abrikosov lattice, i.e., a triangular array with a surface density $n_v = M\Omega/\pi\hbar$. Since the circulation of the velocity around a single charged vortex is h/M, this ensures that the velocity field of the condensate, when calculated after coarse graining over adjacent vortices, is equal to the orthoradial, rigid-body velocity field $v = \Omega r$ (Feynman, 1955).

For a gas confined in a harmonic potential, the fast-rotation regime corresponds to stirring frequencies Ω of the order of the trapping frequency ω in the plane perpendicular to the rotation axis (hereafter denoted z). From a classical point of view, the transverse trapping and centrifugal forces then compensate each other, and the motion of the particles in the x,y plane is only driven by Coriolis and interatomic forces. This situation is similar to that of an electron gas in a magnetic field, since Lorentz and Coriolis forces have the same mathematical structure. The single-particle energy levels are macroscopically degenerate, as the celebrated Landau levels obtained for the quantum motion of a single charge in a magnetic field. When interactions between atoms are taken into account, the fast-rotation regime presents a strong analogy with quantum Hall physics. One can distinguish two limiting cases in this fast-rotation regime. First, when the number of vortices inside the fluid N_v remains small compared to the number of atoms N, the ground state of the system is still a Bose-Einstein condensate described by a macroscopic wave function $\psi(\mathbf{x})$. This situation has been referred to as the

mean-field quantum Hall regime (Ho, 2001; Fischer and Baym, 2003). Second, when Ω tends to ω, the number of vortices reaches values comparable to the total number of atoms N. The description by a single macroscopic wave function breaks down, and one expects a strongly correlated ground state, such as that of an electron gas in the fractional quantum Hall regime (Cooper *et al.*, 2001).

In this section, we start by setting the lowest Landau level (LLL) framework for the discussion of the fast-rotation regime, and discuss the main properties of a fast rotating condensate when the mean-field description remains valid. We then present recent experimental results where the LLL regime has indeed been reached. Finally, we review some theoretical proposals to reach beyond mean-field physics that present a close analogy with the physics of the fractional quantum Hall effect. We do not discuss here the physics of a slowly rotating system, where one or a few vortices are involved. We refer the reader to the review article of Fetter and Svidzinsky (2001) and to Aftalion (2006). Note that a rigorous derivation of the Gross-Pitaevskii energy functional in the slowly rotating case was given by Lieb and Seiringer (2006).

A. The lowest-Landau-level formalism

The Landau levels. We consider first a single particle confined in a two-dimensional isotropic harmonic potential of frequency ω in the x,y plane. We are interested here in the energy level structure in the frame rotating at angular frequency Ω (>0) around the z axis, perpendicular to the x,y plane. The Hamiltonian of the particle is

$$H^{(1)} = \frac{p^2}{2M} + \frac{M\omega^2 r^2}{2} - \Omega L_z$$
$$= \frac{(\mathbf{p} - \mathbf{A})^2}{2M} + \frac{1}{2}M(\omega^2 - \Omega^2)r^2 \quad (113)$$

with $r^2 = x^2 + y^2$, $\mathbf{A} = M\mathbf{\Omega} \wedge \mathbf{x}$; L_z is the z component of the angular momentum. Equation (113) is formally identical to the Hamiltonian of a particle of unit charge placed in a uniform magnetic field $2m\Omega\hat{\mathbf{z}}$, and confined in a potential with a spring constant $M(\omega^2 - \Omega^2)$. A common eigenbasis of L_z and H is the set of (not normalized) Hermite functions

$$\phi_{j,k}(\mathbf{x}) = e^{r^2/2a_\perp^2}(\partial_x + i\partial_y)^j(\partial_x - i\partial_y)^k(e^{-r^2/a_\perp^2}), \quad (114)$$

where j and k are non-negative integers and $a_\perp = \sqrt{\hbar/M\omega}$. The eigenvalues are $\hbar(j-k)$ for L_z and

$$E_{j,k} = \hbar\omega + \hbar(\omega - \Omega)j + \hbar(\omega + \Omega)k \quad (115)$$

for H. For $\Omega = \omega$, these energy levels group in series of states with a given k, corresponding to the well-known, infinitely degenerate, Landau levels. For Ω slightly smaller than ω, this structure in terms of Landau levels labeled by the index k remains relevant, as shown in Fig. 25. Two adjacent Landau levels are separated by $\sim 2\hbar\omega$,
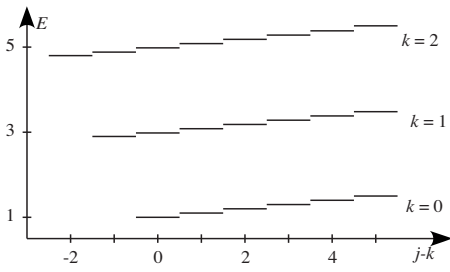
FIG. 25. Single-particle energy spectrum for $\Omega = 0.9\omega$. The index k labels the Landau levels. The energy is expressed in units of $\hbar\omega$. For $\Omega = \omega$, the Landau levels are infinitely degenerate.

whereas the distance between two adjacent states in a given Landau level is $\hbar(\omega - \Omega) \ll \hbar\omega$. It is clear from these considerations that the rotation frequency Ω must be chosen smaller than the trapping frequency in the x,y plane. Otherwise, the single-particle spectrum (115) is not bounded from below. Physically, this corresponds to the requirement that the expelling centrifugal force $M\Omega^2 r$ must not exceed the trapping force in the x,y plane, $-M\omega^2 r$.

We now consider an assembly of cold identical bosons rotating at a frequency Ω close to ω. Since the effective trapping potential in Eq. (113) becomes weaker as Ω increases, we expect that, as $\Omega \to \omega$, the equilibrium size of the atom cloud increases indefinitely, and the interaction energy and the chemical potential μ tend to zero. We define the lowest Landau level regime as the situation in which $\mu, k_B T \ll \hbar\omega$, so that the state of the system can be accurately described in terms of Hermite functions $\phi_{j,k}$ with $k=0$ only. Each basis function $\phi_{j,0}(\mathbf{x})$ is proportional to $(x+iy)^j e^{-r^2/(2a_\perp^2)}$ and takes significant values on a ring centered on 0 with an average radius $\sqrt{j}a_\perp$ and a width $\sim a_\perp$. Any function $\psi(\mathbf{x})$ of the LLL is a linear combination of the $\phi_{j,0}$'s and can be cast in the form

$$\psi(\mathbf{x}) = e^{-r^2/2a_\perp^2} P(u), \tag{116}$$

where $u = x + iy$ and $P(u)$ is a polynomial (or an analytic function) of u. When $P(u)$ is a polynomial of degree n, an alternative form of $\psi(\mathbf{x})$ is

$$\psi(\mathbf{x}) = e^{-r^2/(2a_\perp^2)} \prod_{j=1}^{n} (u - \zeta_j), \tag{117}$$

where ζ_j $(j=1,\dots,n)$ are the n complex zeros of $P(u)$. Each ζ_j is the position of a single-charged, positive vortex, since the phase of $\psi(\mathbf{x})$ changes by $+2\pi$ along a closed contour encircling ζ_j. Therefore, in the LLL, there is a one-to-one correspondence between atom and vortex distributions, contrary to what happens for slower rotation frequencies. This has interesting consequences for the hydrodynamics of the gas, which cannot be described by conventional Bernoulli and continuity equations (Bourne *et al.*, 2006).

Equilibrium shape of a fast rotating BEC. We now

address the question of the distribution of particles and vortices in the case of fast rotation, assuming that a mean-field description is valid. We suppose that the motion along the rotation axis z is frozen in a way similar to the preceding section devoted to static 2D gases.

Consider first the case of an ideal gas. At zero temperature, all atoms accumulate in the $j=k=0$ ground state. At low but finite temperature ($k_B T \ll 2\hbar\omega$), the occupied states belong to the LLL. The gas can be described at any time by a Hartree wave function of the type (116), where the coefficients c_m of the polynomial $P(u) = \Sigma c_m u^m$ are random independent variables. This fast-rotating ideal gas can be viewed as a physical realization of a random polynomial (Castin *et al.*, 2006). A measurement of the density distribution of the gas will reveal the presence of the vortices, i.e., the roots of $P(u)$. Although the gas is ideal, one can show that the positions of the vortices are correlated and exhibit a strong antibunching phenomenon [see Castin *et al.* (2006), and references therein].

The case of a fast-rotating condensate with repulsive interactions has been analyzed by Ho (2001), Cooper *et al.* (2004), Watanabe *et al.* (2004), and Aftalion *et al.* (2005), and we review the main results. In this section, we assume that the pairwise interaction between atoms i and j can be described by the contact term $g_2 \delta(\mathbf{x}_i - \mathbf{x}_j)$. We furthermore assume that the 3D scattering length a is much smaller than the extension ℓ_z of the ground state of the motion along z, so that $g_2 \simeq \hbar^2 \tilde{g}_2/M$, with $\tilde{g}_2 = \sqrt{8\pi}a/\ell_z \ll 1$ [see Eq. (105)]. Note that the restriction of the contact interaction to the LLL subspace is a regular operator: it does not lead to the same mathematical difficulties as the ones encountered by considering the contact interaction in the whole Hilbert space of 2D wave functions. In fact, quite generally, interactions in the LLL are described by the Haldane pseudopotentials V_m (Haldane, 1983). For a pseudopotential with scattering length a, the resulting 2D contact interaction has $V_m = \sqrt{2/\pi}\hbar\omega a/\ell_z$ for $m=0$ and zero otherwise. In the fermionic case, where only odd values of m are allowed, the analog of this interaction is a hard-core model, where $V_m \neq 0$ only for $m=1$. The fact that the Laughlin states, discussed in Sec. VII.C, are exact eigenstates for such pseudopotentials was realized by Trugman and Kivelson (1985).

We start with a gas rotating exactly at the trap frequency ($\Omega = \omega$), with an infinite number of particles but a finite spatial density. In this case, the numerical minimization of the Gross-Pitaevskii energy functional indicates that vortices form an infinite regular triangular lattice. We turn now to a gas with a finite number of particles, rotating at a frequency Ω slightly below ω. The initial treatment of Ho (2001) assumed an infinite, regular triangular vortex lattice also in this case. The total energy of the system was minimized by varying the spacing of the vortex lattice. When substituted into Eq. (117), this led to the prediction of a Gaussian atom distribution after coarse graining over the vortex lattice spacing. A more detailed analysis has been performed,
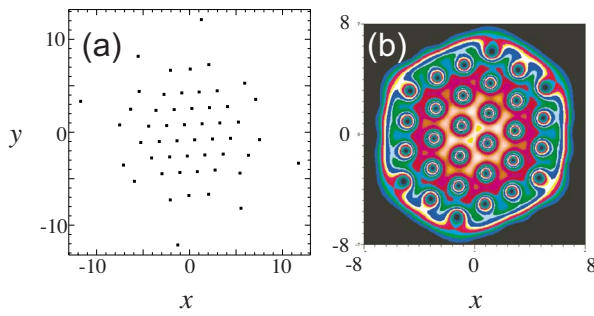
FIG. 26. (Color online) Calculated structure of the ground state of a rotating Bose-Einstein condensate described by a LLL wave function, showing (a) vortex locations and (b) atomic density profile. The parameters of the calculation correspond to 1000 rubidium atoms confined in a trap with frequency $\omega/(2\pi)=150$ Hz and rotating at a frequency $\Omega=0.99\omega$. The unit for the positions x and y is $[\hbar/(m\omega)]^{1/2}$. From Aftalion *et al.*, 2005.

where the position ζ_j of each vortex is taken as a variational parameter (Cooper *et al.*, 2004; Watanabe *et al.*, 2004; Aftalion *et al.*, 2005) [see also Anglin (2002) and Sheehy and Radzihovsky (2004a, 2004b) for the case of a slower rotation]. One spans in this way the whole LLL subspace. These studies have shown that the vortex distribution that minimizes the total energy is nearly regular with the density $M\Omega/\pi\hbar$ close to the center of the condensate, but is strongly deformed on the edges, with a rarefaction of vortices (see Fig. 26). For large atom numbers, the predicted coarse-grained density distribution is not Gaussian as for a uniform vortex lattice, but approaches a Thomas-Fermi distribution $n_2(\mathbf{x}) \propto R^2 - r^2$ similar to Eq. (106), for the effective trapping potential $M(\omega^2 - \Omega^2)r^2/2$. This Thomas-Fermi prediction is in good agreement with results obtained in the experiments described later in this section. The cloud radius is

$$R \simeq a_\perp \left(\frac{2b}{\pi} \frac{N\tilde{g}_2}{1 - \Omega/\omega} \right)^{1/4} \quad (118)$$

and diverges for $\Omega \rightarrow \omega$, as expected from the compensation of the trapping force by the centrifugal one. The dimensionless coefficient b is the Abrikosov parameter $b=1.1596$ (Kleiner *et al.*, 1964) for a triangular lattice. It expresses the fact that, due to the restriction to the LLL and to the presence of vortices, the energy and size of the condensate are actually slightly larger than one expects for a static trap with spring constant $m(\omega^2 - \Omega^2)$ and a smooth equilibrium distribution. The chemical potential is

$$\mu \simeq \hbar\omega[(2b/\pi)N\tilde{g}_2(1 - \Omega/\omega)]^{1/2},$$

so that the condition $\mu \ll \hbar\omega$ for the validity of the LLL approach reads $1 - \Omega/\omega \ll 1/N\tilde{g}_2$. It is also instructive to calculate the number N_v of "visible" vortices, i.e., those that exist in the disk of area πR^2. Using $\Omega \simeq \omega$ so that $n_v \simeq m\omega/\pi\hbar$, we get

$$N_v/N \simeq (\tilde{g}_2/N(1 - \Omega/\omega))^{1/2}.$$

As we see further on, the mean-field approach is valid only if $N_v \ll N$ so that the validity domain of the mean-field LLL approach corresponds to the interval

$$\tilde{g}_2/N \ll 1 - \Omega/\omega \ll 1/N\tilde{g}_2 \quad \text{for mean-field LLL.}$$

$$(119)$$

Note that the total number of vortices, including those outside the Thomas-Fermi radius, can be shown to be infinite for the wave function that minimizes the energy in the LLL subspace (Aftalion *et al.*, 2006).

It is interesting to compare the behavior of a fast-rotating BEC with that of a fast-rotating bucket of superfluid liquid helium, or a type-II superconductor in a large magnetic field (Fischer and Baym, 2003). In the latter cases, the size of the sample is constant and the vortex density increases as the rotation frequency (or the magnetic field) increases. Since the size of a vortex core ℓ_c depends only on the spatial density of the fluid ($\ell_c \sim \xi$ the healing length), it stays constant as Ω increases and one eventually reaches a point where the cores of adjacent vortices overlap. This corresponds to a loss of superfluidity or superconductivity. For superfluid liquid helium, the rotation frequency Ω_{c2} where this phenomenon should occur is beyond the reach of realistic experiments. For superconductors, on the contrary, the critical field H_{c2} where the superconductivity is lost is a relevant experimental parameter. For fast-rotating, harmonically trapped gases, the scenario is very different: (i) the vortex density saturates to a constant value $n_v = M\omega/\pi\hbar = 1/\pi a_\perp^2$ when Ω approaches ω; and (ii) the size ℓ_c of the vortex core for a wave function of the type (117) is no longer dictated by interactions that would lead to $\ell_c \sim \xi$ as for an incompressible fluid, but it is on the order of the vortex spacing $a_\perp$. Therefore, the fractional area $\tilde{n}_0\ell_c^2$ occupied by vortices tends to a finite value, as the trapped BEC rotates faster and faster. The crossover between the standard to the LLL regime has been studied by Baym and Pethick (2003) and Cozzini *et al.* (2006).

B. Experiments with fast-rotating gases

The most intuitive way to rotate a trapped atomic gas is to superpose a rotating anisotropic potential onto the axisymmetric trapping potential $V(r) = M\omega^2 r^2/2$. The stirring anisotropy can be written $\delta V(\mathbf{x},t) = \epsilon M\omega^2(X^2 - Y^2)/2$, where the coordinates (X,Y) are deduced from the static ones (x,y) by a rotation of angle Ωt. The dimensionless parameter ϵ characterizes the strength of the stirring potential with respect to the trapping one. In practice, because of experimental limitations, ϵ has to be on the order of at least a few percent. Indeed, it must overcome by a significant factor the residual static anisotropy of the trapping potential, which is typically in the $10^{-3}-10^{-2}$ range (Guéry-Odelin, 2000).

The stirring potential can be created by a modulated laser beam (Madison *et al.*, 2000; Abo-Shaeer *et al.*,

2001) or by a rotating magnetic field (Haljan *et al.*, 2001; Hodby *et al.*, 2001). The stirring method has been successfully used to nucleate single vortices as well as large vortex arrays in rotating BEC's. However, it is not fully appropriate for approaching the fast-rotating regime of a harmonically trapped gas. Indeed the center-of-mass motion of the atom cloud is dynamically unstable when the rotation frequency Ω is set in the interval $[\omega\sqrt{1-\epsilon}, \omega\sqrt{1+\epsilon}]$ (Rosenbusch *et al.*, 2002). A precise description of the rotating system at the edge of the instability region $\Omega = \omega\sqrt{1-\epsilon}$ has been given by Sinha and Shlyapnikov (2005) [see also Fetter (2007)], who showed that the gas forms in this case a novel elongated quantum fluid, with a roton-maxon excitation spectrum. Excitation modes with zero energy appear above a critical interaction strength, leading to the creation of rows of vortices.

A possible way to circumvent the center-of-mass expulsion occurring at $\Omega \sim \omega$ consists in adding an extra trapping potential that provides a stronger than quadratic confinement. This method was explored experimentally by Bretin *et al.* (2004). In this experiment, the dipole potential created by a strongly focused laser beam provided quartic confinement, in addition to the usual quadratic one. It was then possible to explore the critical region $\Omega \sim \omega$ and to approach the LLL regime $\mu \sim 2\hbar\omega$. A striking observation was a strong decrease of the visibility of the vortex pattern in this region. Its origin is not fully understood yet, but it may be related to the fact that the rotating gas was not in the 2D regime. The shape of the rotating cloud was close to spherical, and the vortex lines may have undergone a strong bending with respect to the trap axis, which made them hardly visible in the imaging process. This explanation is favored in the theoretical study by Aftalion and Danaila (2004): when looking for the ground state of the system using imaginary-time evolution of the Gross-Pitaevskii equation, it was found that much longer times were required for $\Omega \simeq \omega$ to reach a well-ordered vortex lattice.

Note that the addition of a quartic potential brings some interesting and novel aspects to the vortex dynamics in the trap, with the possibility of nucleating "giant" vortices. This was initially explored by Fetter (2001), Kasamatsu *et al.* (2002), and Lundh (2002). The mean-field description of the dynamics of a BEC in nonharmonic potentials was the subject of important theoretical activity, and we refer the reader to the work of Cozzini *et al.* (2006), and references therein.

Another successful method to reach the fast-rotation regime is the evaporative spin-up technique developed by Engels *et al.* (2002). The cloud is first set in rotation at a frequency Ω well below ω using a magnetic stirrer, which is subsequently switched off. Then a nearly one-dimensional radio-frequency evaporation along the axis of rotation cools the cloud. Simultaneously, the rotation speed of the gas increases since evaporated atoms carry less angular momentum than average. With this tool, Schweikhard *et al.* (2004) has succeeded in producing a gas rotating at $\Omega > 0.99\omega$ with a purely harmonic con-
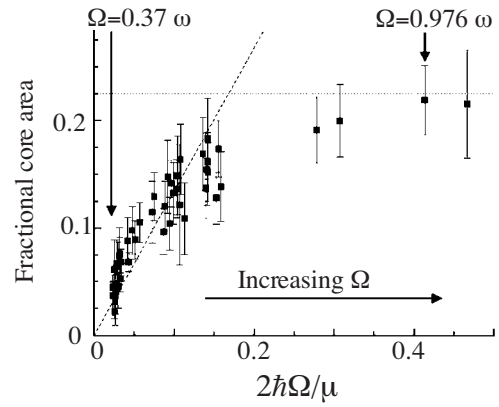

FIG. 27. Fraction of the condensate surface area occupied by the vortex cores as a function of $2\hbar\Omega/\mu$. The vortex radius r_v is defined as the rms radius of the Gaussian function giving the best fit to the density dip at the vortex location. Dashed line is the predicted 3D bulk value $r_v = 1.94\xi$, where ξ is the healing length. For fast rotation, the vortex core area deviates from this prediction and it saturates at a value close to the prediction by Baym (2003) (continuous line). From Schweikhard *et al.* (2004).

finement. Thanks to the centrifugal deformation, the radius of the gas in the xy plane increases, whereas the thickness along z shrinks to the size of the ground state $\sqrt{\hbar/m\omega_z}$, setting the gas well inside the 2D regime. As the total volume of the gas increases, interactions are reduced: the chemical potential $\mu \sim 10$ Hz drops below the splitting between two Landau levels $2\hbar\omega$ (17 Hz), and the LLL regime is reached (Schweikhard *et al.*, 2004). With this setup, it was possible to test the prediction that the fractional core area of the vortices saturates to a value on the order of 0.2 (Coddington *et al.*, 2004; Schweikhard *et al.*, 2004), as predicted theoretically (Baym, 2003) (Fig. 27). In addition, the expected distortion of the vortex lattice with respect to an ideal triangular array could be detected experimentally on the edge of the rotating condensate (Coddington *et al.*, 2004). Following Anglin and Crescimanno (2002), another interesting investigation performed on this system dealt with the Tkachenko oscillations (Tkachenko, 1966) [for a review, see Sonin (1987)], i.e., the long-wavelength transverse excitations of the vortex lattice (Coddington *et al.*, 2003). The Tkachenko waves could be directly imaged and their frequency could be measured with good precision. Theoretical analysis of these oscillations was performed within the mean-field approximation [Baym (2003, 2004); Choi *et al.* (2003); Baksmaty *et al.* (2004); Cozzini *et al.* (2004); Gifford and Baym (2004); Mizushima *et al.* (2004); Woo *et al.* (2004); Sonin (2005a, 2005b); and Chevy (2006)].

Fast rotation of a BEC can also be achieved by stirring the gas with a potential that is more elaborate than a quadratic one. One can use in particular a rotating optical lattice that creates a rotating, spatially periodic pattern on the gas. This was explored by Tung *et al.* (2006), who superimposed on a rotating BEC a set of

columnar pinning sites created by a two-dimensional, corotating optical lattice. For a sufficiently large laser intensity, the optical lattice can impose its structure to the vortex lattice; Tung *et al.* (2006) studied, in particular, the transition from the usual triangular Abrikosov lattice to a square configuration imposed by light. Theoretical investigations of this problem were carried out by Reijnders and Duine (2004, 2005) and Pu *et al.* (2005) who found that a rich variety of structural phases can emerge in this geometry, from the competition between vortex–vortex and vortex–optical lattice interactions.

C. Beyond the mean-field regime

In the mean-field description of a fast-rotating gas, the macroscopic wave function $\psi(\mathbf{x})$ is a solution of the nonlinear Gross-Pitaesvkii equation and corresponds to a vortex lattice. The radius of the atom cloud, given in Eq. (118), is a measure of the number j_{max} of single-particle LLL states $\phi_{j,0}$ that have a significant population. Recalling that $\phi_{j,0}$ is maximum for a radius $\sqrt{j}a_\perp$, we find

$$j_{max} \simeq (R/a_\perp)^2 \simeq [N\tilde{g}_2/(1-\Omega/\omega)]^{1/2}. \qquad (120)$$

The filling factor $\nu=N/j_{max}$ gives the average number of particles in each occupied single-particle state. When $\nu \geqslant 1$, one expects the mean-field treatment to be valid, and j_{max} is equal to the number N_v of visible vortices existing in the atom disk. On the contrary, when Ω tends to ω, ν becomes of the order of unity or below, the number of vortices N_v exceeds the number of atoms, N, and one has to turn to a full many-body treatment of the problem. This breakdown of the mean-field approximation occurs when

$$1 - \Omega/\omega \lesssim \tilde{g}_2/N \quad \text{(non-mean-field)}. \qquad (121)$$

Analysis of this ultrafast-rotating regime presents strong analogies with the fractional quantum Hall effect (FQH). In the latter case, one is interested in the correlated state of a 2D electron gas with Coulomb interaction when it is placed in a strong magnetic field. In both cases, the states of interest are restricted to the LLL and one looks for specific filling factors where ground states with specific properties can emerge. Note that, for bosons, the filling factor can be arbitrarily large within the LLL, while for fermions it is restricted to $\nu<1$. One remarkable feature is incompressibility, meaning that the ground state is separated from all excited states by a "macroscopic" energy gap scaling as g_2. Moreover, it leads to the appearance of edge states near the boundary of the system, similar to the wedding-cake structure of the Mott-insulating state of the Bose-Hubbard model (see Sec. IV.B). These edge states are crucial for understanding the quantization of the Hall conductance; see MacDonald (1994) and—on a more mathematical level—Fröhlich and Studer (1993).

Numerical studies. So far the ultra fast-rotation regime has not been reached experimentally. Even for the fastest rotations realized in the laboratory, the filling factor ν is $\sim 10^3$ ($N \sim 10^5$, $N_v \sim 10^2$), well inside the mean-field regime. Therefore, results obtained so far originate from an exact numerical diagonalization of the many-body Hamiltonian and from the connection with known features of the fermionic FQH.

Most studies are performed by considering states with a given total angular momentum L_z, so that the problem essentially consists in finding the eigenstates of the interaction energy

$$V_{int} = \frac{\hbar^2 \tilde{g}_2}{M} \sum_{i<j} \delta(\mathbf{x}_i - \mathbf{x}_j). \qquad (122)$$

All states considered hereafter belong to the LLL subspace, so their functional form in the xy plane is

$$\Psi(\mathbf{x}_1, \ldots, \mathbf{x}_N) = P(u_1, \ldots, u_N)\exp\left(-\sum_{j=1}^N r_j^2/2a_\perp^2\right), \qquad (123)$$

where $u_j=x_j+iy_j$, $r_j^2=x_j^2+y_j^2$ and $P(u_1, \ldots, u_N)$ is a symmetric polynomial. The z motion is expected to be "frozen" to its ground state, and it is not explicitly written in what follows. If one is interested only in the bulk properties of the vortex liquid state, it is convenient to replace the inhomogeneous disk geometry of a real experimental setup by a compact, homogeneous geometry. Both torus (Cooper *et al.*, 2001) and spherical (Nakajima and Ueda, 2003; Regnault and Jolicoeur, 2003), manifolds have been considered. The LLL is then a space of finite dimension d_{LLL}, proportional to the area $\mathcal{A}$ of the torus or the sphere: $d_{LLL}=\mathcal{A}/\pi a_\perp^2$. This allows one to define in a nonambiguous way the filling factor ν ($\nu=N/d_{LLL}$) even for values on the order of 1 or below, where the notion of visible vortices becomes dubious.

Melting of the vortex lattice. When increasing the rotation speed of the gas, the first expected deviation from the mean-field regime is the quantum melting of the vortex lattice. This has been observed by Cooper *et al.* (2001) in exact numerical calculations for filling factors $\nu=N/N_v \sim 6$–10. This value can be recovered by calculating the quantum fluctuations Δ of vortex positions and applying the Lindemann criterion $\Delta_{melt} \sim \ell/10$, where ℓ is the vortex spacing (Sinova *et al.*, 2002). For ν smaller than the melting threshold, one meets for the ground state of the many-body system a series of strongly correlated ground states that we now discuss.

The Laughlin state and its daughter states. Since increasing the angular momentum spreads out the atoms in space, one expects the interaction energy $E(L_z)$ of the ground state for a given L_z to decrease as L_z increases [see, e.g., Jackson and Kavoulakis (2000)]. This decrease stops when one reaches the celebrated Laughlin wave function, adapted here for bosonic particles,

$$P_{Lau}(u_1,u_2, \ldots, u_N) = \prod_{i<j} (u_i - u_j)^2. \qquad (124)$$

Indeed, since the probability to get two particles at the same point vanishes, this state has the remarkable property of being an eigenstate of the contact interaction potential with eigenvalue 0 (Trugman and Kivelson,

1985). Increasing L_z beyond this point cannot reduce further $E(L_z)$. The total angular momentum $L_z/\hbar$ of this state is equal to the degree $N(N-1)$ of each term of the polynomial P_{Lau}, and this state expands over all LLL single-particle wave functions $\phi_{j,0}$ from $j=0$ to $j_{\max} = 2(N-1)$, i.e., a filling factor $\nu = 1/2$. The Laughlin state is incompressible and the gap to the first excited state is $\sim 0.1 \tilde{g}_2 \hbar \omega$ (Regnault and Jolicoeur, 2003, 2004). The Laughlin state is characterized by a quasiuniform density of particles over the circle of radius $a_\perp \sqrt{2N}$. The two-body correlation function for this state shows a strong antibunching $g^{(2)}(r \rightarrow 0) \sim r^2$. This correlation function has been calculated numerically for a number of bosons N up to 8 by Barberán et al. (2006).

For $L_z/\hbar > N(N-1)$, any state $P(u_1, \ldots, u_N) = P_{\mathrm{Lau}}(u_1, \ldots, u_N) Q(u_1, \ldots, u_N)$, where Q is an arbitrary symmetric polynomial, is a ground state of the system with interaction energy 0. Depending on the total degree d_Q of Q, the physical interpretation of the state can be (i) for $d_Q \sim 1$, edge excitations of the Laughlin state (Cazalilla, 2003; Cazalilla et al., 2005); (ii) for $d_Q = N$, quasiholes at a given point U_0 are obtained by taking $Q = \Pi_j(u_j - U_0)$ (Paredes et al., 2001, 2002); and (iii) for $d_Q \sim N^2$, Laughlin-type wave functions with smaller filling factors, by replacing the exponent 2 by 4,6,… in Eq. (124).

The composite fermion sequence. For filling factors between the melting point $\nu \sim 10$ and the Laughlin state $\nu = 1/2$, it is not possible to give an exact analytical expression of the ground state at any given ν. One finds, however, strong overlap between numerically determined ground states and some relevant states for the physics of the electronic fractional quantum Hall effect. An example is the composite fermion sequence, which presents strong analogies with the Jain principal sequence for fermions (Jain, 1989). The first evidence for this sequence was found by Cooper and Wilkin (1999), and was studied by Regnault and Jolicoeur (2003, 2004). The physics at the origin of the states of this sequence is reminiscent of that explored in the section on 1D gases, where the problem of bosonic particles with repulsive interaction is mapped onto the properties of an assembly of noninteracting fermionic particles. Here one considers that the gas is formed with fermionic composite entities, each resulting from the attachment of a fermionic particle with a vortex carrying one unit of statistical flux. These composite fermions can be viewed as independent particles that occupy various Landau levels. When they occupy exactly n Landau levels, they form an incompressible state. This occurs when the filling fraction in the initial state is $\nu = n/(n+1)$. From a more quantitative point of view, the composite fermion ansatz corresponds to a wave function of the type

$$P(u_1, \ldots, u_N) = \mathcal{P}_{\mathrm{LLL}}\left[Q_n(u_1, \ldots, u_N) \prod_{i<j} (u_i - u_j)\right].$$
(125)

$\mathcal{P}_{\mathrm{LLL}}$ describe the projector onto the LLL subspace [for its precise definition, see, e.g., Chang et al. (2004)]. The

first term in the brackets, $Q_n(u_1, \ldots, u_N)$, is a Slater determinant giving the state of N fictitious fermions filling exactly n Landau levels. The second term involving products of $u_i - u_j$ (Jastrow factor) corresponds to the attachment of a vortex to each fermion. Since both terms in the brackets are antisymmetric in the exchange of two particles, their product is a symmetric wave function, suitable for the description of our N identical bosons. Numerical evidence for such states was obtained for $\nu = 2/3$ and $3/4$ by Regnault and Jolicoeur (2003, 2004) and Chang et al. (2004). The surface waves of vortex liquids whose wave functions can be described by the composite fermion ansatz have been studied by Cazalilla (2003), Regnault and Jolicoeur (2004), and Cazalilla et al. (2005).

The Read-Moore state and the Read-Rezayi series. For the filling factor $\nu = 1$, yet another type of approximate ground state has been identified (Cooper et al., 2001), namely, the Moore-Read state, or Pfaffian. Assuming that N is even, the expression of this state is

$$P(u_1, \ldots, u_N) = \mathcal{S}\left[\prod_{i<j \leqslant N/2} (u_i - u_j)^2 \prod_{N/2 < l < n} (u_l - u_n)^2\right],$$
(126)

where $\mathcal{S}$ indicates symmetrization over all indices. The total degree of each term of this polynomial is $N(N-2)/2$ and the state expands over single-particle LLL wave functions from $k=0$ up to $k_{\max} = N-2$, corresponding to a filling factor $\nu = 1$. For $\nu = 1/2$, the ground state is incompressible with a gap $\sim 0.05 \tilde{g}_2 \hbar \omega$ (Chang et al., 2004). It is noteworthy that for this state the probability is zero to have three particles at the same location in space.

For even larger filling factors (ν between 1 and 10), an analysis performed in a torus geometry suggested that the system has incompressible ground states belonging to a family containing clusters of k particles (Cooper et al., 2001) and corresponding to integer or half-integer filling factors. This so-called Read-Rezayi series (Read and Rezayi, 1999) is constructed by taking symmetrized products of k Laughlin states of the type $\Pi_{i<j \leqslant N/k}(u_i - u_j)^2$ (assuming that N is a multiple of k). The Laughlin and Moore-Read states correspond to $k=1$ and 2, respectively. The filling factor associated with these states is $k/2$ and the total angular momentum is $L_z/\hbar \sim N^2/k$. Further calculations performed in the spherical geometry could not draw any conclusion concerning the survival of the incompressibility of such states at the thermodynamic limit (Regnault and Jolicoeur, 2004).

Possible detection schemes for fractional quantum Hall effects. We now review some possible ways to observe effects related to fractional quantum Hall physics experimentally. Note that it is unlikely that condensed-matter-type techniques, based on transport properties with specific conductance plateaus, can be implemented with rotating atomic gases, at least in the near future. We also point out that the condition (121) giving the threshold for the observation of mean-field effects imposes *de facto* the requirement to work with very

small atomic samples. Consider, for example, a purely harmonic trap. Due to residual trap imperfections, it seems unlikely that one can achieve rotation frequencies Ω larger than 0.999ω [rotation frequencies $\sim 0.99\omega$ have been achieved by Schweikhard *et al.* (2004)]. Taking $\tilde{g}_2 \sim 0.1$, this sets an upper bound of ~ 100 on the atom number. Working with such small atom numbers is not intractable, but it immediately makes this type of experiment challenging from a technical point of view.

A first possible experimental signature of the Laughlin and Read-Moore states could lie in the fact that three particles can never be at the same location in space for these wave functions. As three-body recombination is often the main source of atom losses, one can expect that the achievement of these states could be revealed by a strong increase of the lifetime of the gas, similar to what has been observed in one dimension by Tolra *et al.* (2004), where $g^{(3)}(0)$ is suppressed.

We now turn to more quantitative studies of these incompressible states. A "simple" experimental evidence for a state such as the Laughlin wave function could come from its specific density profile, which is uniform over a disk of radius $a_\perp \sqrt{2N}$, and zero elsewhere. This flat profile with density $1/(2\pi a_\perp^2)$ is notably different from the parabolic density profile expected in the mean-field regime, and its observation would constitute a clear signature of a beyond mean-field effect. Usually one does not measure directly the in-trap density profile, because the relevant distances are on the order of a few micrometers only, which is too small to be detected with good accuracy by optical means. The standard procedure to circumvent this problem is to use a time-of-flight technique, where the potential confining the atoms is suddenly switched off so that atoms fly away ballistically during an adjustable time before being detected. For an arbitrary initial state, the functional form of the density distribution is modified during the time of flight. For an LLL wave function, this modification is scaling, at least when interactions between atoms are negligible during the time of flight (Read and Cooper, 2003). In particular, the disk-shaped structure associated with the Laughlin state should remain invariant in ballistic expansion.

If the number of atoms is larger than that required to form a Laughlin wave function at the particular frequency Ω that is used, one expects a wedding-cake structure for the atomic density (Cooper *et al.*, 2005). This result is obtained within a local-density approximation and is reminiscent of the structure appearing in an atomic Mott insulator confined in a harmonic trap. At the center of the trap where the density is the largest, atoms may form an incompressible fluid corresponding, for example, to the filling factor 2/3, which is one of the composite fermion states identified above. The atomic density is then expected to be constant and equal to $2/3\pi a_\perp^2$ over a central disk of radius R_1. For $r = R_1$, the gas switches abruptly (over a distance $\sim a_\perp$) to the Laughlin state with filling factor 1/2 and the density drops to the value $1/(2\pi a_\perp^2)$. It then stays constant over a ring of outer radius R_2 ($R_2 > R_1$), and for $r > R_2$ the density drops to zero. The values of R_1 and R_2 can be obtained from a simple energy minimization (Cooper *et al.*, 2005). For larger atom numbers, several plateaus, with decreasing densities corresponding to the various filling factors of the incompressible states, are expected.

The possibility of adding an optical lattice along the z direction adds an interesting degree of freedom to the problem, and brings hope to experimentalists of working with a notably larger atom number. In this configuration, one deals with a stack of N_d parallel disks, all rotating at the same frequency Ω along the z axis. Each disk is coupled to its neighbors by tunneling across the lattice barrier, with a strength that can be adjusted. For large coupling, the situation is similar to a bulk 3D problem; when the coupling is reduced, the system evolves to the quasi-2D regime. This raises interesting questions even at the level of a single-vortex motion, as pointed out by Martikainen and Stoof (2003). The melting of the vortex lattice in a stack of N_d layers was investigated by Cooper *et al.* (2005) and Snoek and Stoof (2006a, 2006b). For smaller filling factors, both the density profiles along z and in the xy plane should show the wedding-cake structure characteristic of incompressible states (Cooper *et al.*, 2005).

More elaborate techniques have been proposed to test the anyonic nature of the excitations of incompressible states. Paredes *et al.* (2001) investigated the possibility of creating anyons in a Laughlin state by digging a hole in the atomic gas with a tightly focused laser. If the hole is moved adiabatically inside the cloud, it should accumulate a phase that could be measured by an interference experiment. The accumulated phase should then reveal the anyonic structure of the hole-type excitation [see also Paredes *et al.* (2002)].

D. Artificial gauge fields for atomic gases

As shown in Eq. (113), rotating a neutral particle system is equivalent to giving these particles a unit charge and placing them in a magnetic field proportional to the rotation vector Ω [see Eq. (113)]. Other possibilities have been suggested for applying an artificial gauge field on a neutral gas. The common idea in these proposals is to exploit the Berry's phase (Berry, 1984) that arises when the atomic ground level is split (e.g., by an electromagnetic field) into several space-dependent sublevels, and the atoms follow one of them adiabatically. We consider the one-body problem, and label $\{|n_{\mathbf{x}}\rangle\}$ the local energy basis of the atomic ground level, with the associated energies $E_n(\mathbf{x})$. The most general state of the atom is a spinor $\Sigma_n \psi_n(\mathbf{x})|n_{\mathbf{x}}\rangle$, which evolves under the Hamiltonian $p^2/(2m) + \Sigma_n E_n(\mathbf{x}) |n_{\mathbf{x}}\rangle\langle n_{\mathbf{x}}|$. Suppose now that the atom is prepared in a given sublevel n, and that the motion of the atomic center of mass is slow enough to neglect transitions to other internal sublevels n'. This is the case in particular in a magnetic trap where the index n simply labels the various Zeeman substates. One can then write a Schrödinger equation for the component $\psi_n(\mathbf{x})$, and the corresponding Hamil-

tonian reads $H=[\mathbf{p}-\mathbf{A}_n(\mathbf{x})]^2/(2m)+V_n(\mathbf{x})$. The vector potential $\mathbf{A}_n$ is related to the spatial variation of the sublevel $|n\rangle$,

$$\mathbf{A}_n(\mathbf{x}) = i\hbar\langle n_\mathbf{x}|\boldsymbol{\nabla} n_\mathbf{x}\rangle, \tag{127}$$

and the scalar potential V_n is

$$V_n(\mathbf{x}) = E_n(\mathbf{x}) + (\hbar^2/2m)(\langle\boldsymbol{\nabla} n_\mathbf{x}|\boldsymbol{\nabla} n_\mathbf{x}\rangle - |\langle n_\mathbf{x}|\boldsymbol{\nabla} n_\mathbf{x}\rangle|^2). \tag{128}$$

If the spatial variation of the sublevels $|n_\mathbf{x}\rangle$ is such that $\boldsymbol{\nabla}\wedge\mathbf{A}_n\neq\mathbf{0}$, this gauge field can in principle have the same effect as rotating the atomic gas.

The simplest occurrence of an artificial gauge field happens in a Ioffe-Pritchard magnetic trap (Ho and Shenoy, 1996). The sublevels $|n_\mathbf{x}\rangle$ are the various Zeeman substates, which are space dependent because the direction of the trapping magnetic field is not constant over the trap volume. However, the gauge field $\mathbf{A}_n$ that is generated in this configuration is too small to initiate the formation of vortices. The addition of a strong electric field could increase the magnitude of the artificial gauge field, as shown by Kailasvuori et al. (2002). An alternative and promising line of research considers the concept of *dark states*, where two sublevels of the atomic ground state are coupled by two laser waves to the same excited state. If the laser frequencies are properly chosen, there exists a linear combination of the two sublevels that is not coupled to the light, and the spatial evolution of atoms prepared in this dark state involves the vector and scalar potentials given above (Dum and Olshanii, 1996; Visser and Nienhuis, 1998; Dutta et al., 1999). Possible spatial profiles of laser waves optimizing the resulting artificial rotation field have been discussed by Juzeliunas and Öhberg (2004), Juzeliunas et al. (2005, 2006), and Zhang et al. (2005). These proposals have not yet been implemented experimentally.

Similar effects have also been predicted in a lattice geometry by Jaksch and Zoller (2003), where atoms with two distinct internal ground-state sublevels are trapped in different columns of the lattice. Using a two-photon transition between the sublevels, one can induce a non-vanishing phase of particles moving along a closed path on the lattice. Jaksch and Zoller (2003) showed that one can reach a "high-magnetic-field" regime that is not experimentally accessible for electrons in metals, characterized by a fractal band structure (the Hofstadter butterfly). The connection between the quantum Hall effect and the lattice geometry in the presence of an artificial gauge potential has been analyzed by Mueller (2004) and Sørensen et al. (2005). One can also generalize the Berry's phase approach to the case in which several energy states are degenerate (Wilczek and Zee, 1984). Non-Abelian gauge fields emerge in this case, and possible implementations on cold-atom systems have been investigated theoretically by Osterloh et al. (2005) and Ruseckas et al. (2005).

VIII. BCS-BEC CROSSOVER

One of the basic many-body problems that has been brought into focus by the study of ultracold atoms is that of a two-component attractive Fermi gas near a resonance of the s-wave scattering length. The ability to tune the interaction through a Feshbach resonance allows one to explore the crossover from a BCS superfluid, when the attraction is weak and pairing shows up only in momentum space, to a Bose-Einstein condensate of tightly bound pairs in real space. Here we discuss the problem in the spin-balanced case, which—in contrast to the situation at finite imbalance—is now well understood.

A. Molecular condensates and collisional stability

The experimental study of the BCS-BEC crossover problem with ultracold atoms started with the realization of Fermi gases in the regime of resonant interactions $k_F|a|\geqslant1$ by O'Hara et al. (2002). They observed an anisotropic expansion, characteristic of hydrodynamic behavior. Typically, this is associated with superfluidity because ultracold gases above the condensation temperature are in the collisionless regime. Near a Feshbach resonance, however, a hydrodynamic expansion is observed both above and below the transition temperature. It is only through the observation of stable vortices that superfluid- and collision-dominated hydrodynamics can be distinguished. The BEC side of the crossover was first reached by creating ultracold molecules. This may be done by direct evaporative cooling on the positive a side (Jochim et al., 2003a), where the weakly bound molecules are formed by inelastic three-body collisions. Alternatively, molecules can be generated in a reversible manner by using a slow ramp of the magnetic field through a Feshbach resonance (Cubizolles et al., 2003; Regal et al., 2003). This allows a quasibound state of two fermions at $a<0$ to be converted into a true bound state at $a>0$ [for a review of this technique, see Köhler et al. (2006)]. Subsequently, a BEC of those molecules was realized both by direct evaporative cooling (Jochim et al., 2003b; Zwierlein et al., 2003b) for $a>0$, or by converting a sufficiently cold attractive Fermi gas at $a<0$ to a molecular condensate, using an adiabatic ramp across the Feshbach resonance (Greiner et al., 2003). Experiments are done with an equal mixture of the two lowest hyperfine states of ^{6}Li or of ^{40}K confined optically in a dipole trap. This allows the scattering length to be changed by a magnetically tunable Feshbach resonance at $B_0=835$ or 202 G, respectively. On the BEC side, the fact that molecules are condensed can be verified experimentally by observing a bimodal distribution in a time-of-flight experiment. Probing superfluidity in Fermi gases on the BCS side of the crossover, however, is more difficult. In particular, a time-of-flight analysis of the expanding cloud does not work here. Indeed, due to the factor $\exp[-\pi/(2k_F|a|)]$ in the critical temperature [see Eq. (136) below], superfluidity is lost upon expansion at constant phase-space density in contrast to the situation in

BEC's.[18] As discussed below, this problem may be circumvented by a rapid ramp back into the BEC regime before the expansion. A major surprise in the study of strongly interacting Fermi gases was the long lifetime of molecules near a Feshbach resonance (Cubizolles *et al.* 2003; Jochim *et al.*, 2003a; Strecker *et al.*, 2003), in stark contrast to the situation encountered with bosonic atoms (Herbig *et al.*, 2003; Dürr *et al.*, 2004). The physics behind this was clarified by Petrov, Salomon, and Shlyapnikov (2004), who solved the problem of scattering and relaxation into deeply bound states of two fermions in the regime where the scattering length is much larger than the characteristic range of the interaction, r_e. As shown in Sec. I.A, this range is essentially the van der Waals length Eq. (2), which is much smaller than a in the vicinity of a Feshbach resonance. The basic physics that underlies the stability of fermionic dimers in contrast to their bosonic counterparts is the fact that relaxation into deep bound states is strongly suppressed by the Pauli principle. Indeed, the size of the weakly bound dimer states is the scattering length a, while that of the deep bound states is $r_e \ll a$. By energy and momentum conservation, a relaxation into a deep bound state requires that at least three fermions are at a distance of order r_e. Since two of them are necessarily in the same internal state and their typical momenta are of order $k \approx 1/a$, the probability of a close three- (or four-) body encounter is suppressed by a factor $(kr_e)^2 \sim (r_e/a)^2$ due to the antisymmetrization of the corresponding wave function. From a detailed calculation (Petrov *et al.*, 2005), the relaxation into deeply bound states has a rate constant (in units of cm^3/s)

$$\alpha_{\text{rel}} = C(\hbar r_e/M)(r_e/a)^s, \tag{129}$$

which vanishes near a Feshbach resonance with a nontrivial power law. The exponent $s = 2.55$ or 3.33 and the dimensionless prefactor C depend on whether the relaxation proceeds via dimer-dimer or dimer-atom collisions. From experimental data, the coefficient of the dominant dimer-dimer relaxation is $C \approx 20$ (Bourdel *et al.*, 2004; Regal *et al.*, 2004b). Its value depends on short-range physics on the scale r_e and thus cannot be calculated within a pseudopotential approximation. At a finite density, the power-law dependence a^{-s} holds only as long as the scattering length is smaller than the average interparticle distance. The actual relaxation rate $n\alpha_{\text{rel}}$, in fact, stays finite near a Feshbach resonance and is essentially given by replacing the factor r_e/a in Eq. (129) by $k_F r_e \ll 1$ (Petrov, Salomon, and Shlyapnikov, 2004). In practice, the measured lifetimes are on the order of 0.1 s for ^{40}K and up to about 30 s for ^{6}Li. This long lifetime of fermionic atoms near a Feshbach resonance is essential

for a study of the BCS-BEC crossover, because it allows one to reduce the physics near the resonance to an idealized, conservative many-body problem in which relaxational processes are negligible.

The issue of dimer-dimer collisions has an additional aspect, which is important for the stability of the strongly attractive Fermi gas. Indeed, molecules consisting of two bound fermions also undergo purely elastic scattering. It is obvious that a molecular condensate will be stable only if the interaction of these effectively bosonic dimers is repulsive. From an exact solution of the four-particle Schrödinger equation with pseudopotential interactions, Petrov, Salomon, and Shlyapnikov (2004) have shown that in the limit where the distance R (denoted by $R/\sqrt{2}$ in their paper) between the centers of mass of two dimers is much larger than the dimer size a and at collision energies much smaller than their respective binding energies $\hbar^2/2M_r a^2$, the wave function has the asymptotic form

$$\Psi(\mathbf{x}_1, \mathbf{x}_2, \mathbf{R}) = \varphi_0(r_1)\varphi_0(r_2)(1 - a_{\text{dd}}/R), \tag{130}$$

with $a_{\text{dd}} \simeq 0.60a$. Here $\varphi_0(r) \sim \exp(-r/a)$ is the bound-state wave function of an individual dimer and $\mathbf{x}_{1,2}$ are the interparticle distances between the two distinguishable fermions of which they are composed. It follows from Eq. (130) that the effective dimer-dimer interaction at low energies is characterized by a positive scattering length, which is proportional to the scattering length between its fermionic constituents. This guarantees the stability of molecular condensates and also implies that there are no four-particle bound states for zero-range interactions.[19] Experimentally, the dimer-dimer scattering length can be inferred from the radius $R = \ell_0(15Na_{\text{dd}}/\ell_0)^{1/5}$ of a molecular condensate with N dimers in a trap. The value found in fact agrees well with the prediction $a_{\text{dd}} = 0.60a$ (Bartenstein *et al.*, 2004a; Bourdel *et al.*, 2004). Physically, the repulsion between dimers can be understood as a statistical interaction due to the Pauli principle of its constituents. Within a phenomenological Ginzburg-Landau description of the molecular condensate by a complex order parameter $\psi(\mathbf{x})$, it is related to a positive coefficient of the $|\psi|^4$ term. In fact, the repulsive interaction between dimers was first derived from a coherent-state functional integral representation of the crossover problem (Drechsler and Zwerger, 1992; Sá de Melo *et al.*, 1993). These results, however, were restricted to a Born approximation of the scattering problem, where $a_{\text{dd}}^{(B)} = 2a$ (Sá de Melo *et al.*, 1993). A derivation of the exact result $a_{\text{dd}} = 0.60a$ from diagrammatic many-body theory has been given by Brodsky *et al.* (2006) and Levinsen and Gurarie (2006). It is important to note that the stability of attractive fermions along the BCS-BEC crossover relies crucially on the fact that the range of the attractive interaction is much smaller than the interparticle spacing. For more general

---

[18]In this respect, the situation in two dimensions, where pair binding appears for arbitrary values of the scattering length a, is much more favorable because the two-particle binding energy (83) is density-independent. Since $T_c \sim \sqrt{\varepsilon_b \varepsilon_F} \sim n^{1/2}$, the superfluid transition can be reached by an adiabatic expansion at constant T/T_F; see Petrov *et al.* (2003).

[19]Such states are discussed in nuclear physics, where α particles in a nucleus may appear due to pairing correlations; see, e.g., Röpke *et al.* (1998).

interactions, where this is not the case, instabilities may arise, as discussed by Fregoso and Baym (2006).

B. Crossover theory and universality

For a description of the many-body physics of the BCS-BEC crossover, a natural starting point is a two-channel picture in which fermions in an open channel couple resonantly to a closed-channel bound state. The resulting Hamiltonian

$$\hat{H}_{BF} = \int d^3x \left[\sum_\sigma \hat{\psi}_\sigma^\dagger \left(-\frac{\hbar^2}{2M}\nabla^2 \right)\hat{\psi}_\sigma + \hat{\psi}_B^\dagger \left(-\frac{\hbar^2}{4M}\nabla^2 + \nu \right)\hat{\psi}_B \right.$$
$$\left. + \tilde{g}(\hat{\psi}_B^\dagger \hat{\psi}_\uparrow \hat{\psi}_\downarrow + \text{H.c.}) \right] \tag{131}$$

defines the Bose-Fermi resonance model. It was introduced in this context by Holland *et al.* (2001) and by Timmermans *et al.* (2001) and was used subsequently, by Ohashi and Griffin (2002) and Drummond and Kheruntsyan (2004), among others. Here $\hat{\psi}_\sigma(\mathbf{x})$ are fermionic field operators describing atoms in the open channel. The two different hyperfine states are labeled by a formal spin variable $\sigma = \uparrow, \downarrow$. The bound state in the closed channel is denoted by the bosonic field operator $\hat{\psi}_B$. Its energy is detuned by ν with respect to the open-channel continuum, and $\tilde{g}$ is the coupling constant for the conversion of two atoms into a closed-channel state and vice versa. It is caused by the off-diagonal potential $W(r)$ in Eq. (19) whose range is on the order of the atomic dimension r_c. As a result, the conversion is point-like on scales beyond r_e where a pseudopotential description applies. The magnitude of $\tilde{g} = \langle \phi_{\text{res}} | W | \phi_0 \rangle$ is determined by the matrix element of the off-diagonal potential between the closed- and open-channel states. Using Eq. (26), its value is directly connected with the characteristic scale $r^\star$ introduced in Eq. (21), such that $(2M_r\tilde{g}/\hbar^2)^2 = 4\pi/r^\star$ (Bruun and Pethick, 2004). For simplicity, the background scattering between fermions is neglected, i.e., there is no direct term quartic in the fermionic fields. This is justified close enough to resonance $|B - B_0| \ll |\Delta B|$, where the scattering length is dominated by its resonant contribution.

Broad and narrow Feshbach resonances. As discussed in Sec. I.C, the weakly bound state that appears at negative detuning always has a vanishing closed-channel admixture near resonance. For the experimentally relevant case $|a_{\text{bg}}| \gg r^\star$, the virtual or real bound states within the range $|\nu| < \mu|\Delta B|$ of the detuning may therefore be effectively described as a *single-channel* zero-energy resonance. This criterion is based on two-body parameters only. In order to justify a single-channel model for describing the physics of the crossover at a *finite* density $n = k_F^3/3\pi^2$ of fermions, it is necessary that the potential resonance description be valid in the relevant regime $k_F|a| \gtrsim 1$ of the many-body problem. Now the range in the detuning where $k_F|a| \gtrsim 1$ is given by $|\nu| \lesssim \sqrt{\varepsilon_F\varepsilon^\star}$. Since the closed-channel contribution is negligible as long as

$\nu \ll \varepsilon^\star$, a single-channel description applies if $\varepsilon_F \ll \varepsilon^\star$ or $k_F r^\star \ll 1$ (Bruun and Pethick, 2004; Diener and Ho, 2004). This is the condition for a "broad" Feshbach resonance, which involves only the *many-body* parameter $k_F r^\star$. In quantitative terms, the Fermi wavelength $\lambda_F = 2\pi/k_F$ of dilute gases is on the order of micrometers, while $r^\star$ is typically on the order of or even smaller than the effective range r_e of the interaction. The condition $k_F r^\star \ll 1$ is, therefore, satisfied unless one is dealing with exceptionally narrow Feshbach resonances. Physically, the assumption of a broad resonance implies that the bosonic field in Eq. (131), which gives rise to the resonant scattering, is so strongly coupled to the open channel that the relative phase between the two fields is perfectly locked, i.e., closed-channel molecules condense simultaneously with particles in the open channel. In contrast to the two-particle problem, therefore, there is a finite Z factor precisely on resonance, as verified experimentally by Partridge *et al.* (2005). An important point to realize is that this situation is opposite to that encountered in conventional superconductors, where the role of $\varepsilon^\star$ is played by the Debye energy $\hbar\omega_D$. The ratio $\hbar\omega_D/\varepsilon_F$ is very small in this case, on the order of the sound velocity divided by the Fermi velocity. Effectively, this corresponds to the case of *narrow* resonances, where $k_F r^\star \gg 1$. The effective Fermi-Fermi interaction is then retarded and the Bose field in Eq. (131) is basically unaffected by the condensation of fermions. On a formal level, this case can be treated by replacing the closed-channel field by a c number, giving rise to a reduced BCS model with a mean-field gap parameter $\Delta = \tilde{g}\langle \hat{\psi}_B \rangle$ (DePalo *et al.*, 2005; Sheehy and Radzihovsky, 2006).

There is an essential simplification in describing the crossover problem in the limit $k_F r^\star \ll 1$. This is related to the fact that the parameter $r^\star$ can be understood as an effective range for interactions induced by a Feshbach resonance. Indeed, consider the resonant phase shift for two-body scattering as given in Eq. (20). At zero detuning $\nu = 0$ and small k, the associated scattering amplitude can be shown to be precisely of the form (4) with an effective range $r_e = -2r^\star$. Therefore, in the limit $k_F r^\star \ll 1$, the two-body interaction near resonance is described by the scattering amplitude Eq. (6) of an ideal pseudopotential even at $k = k_F$. As a result, the Fermi energy is the only energy scale in the problem right at unitarity. As pointed out by Ho (2004), the thermodynamics of the unitary Fermi gas is then universal, depending only on the dimensionless temperature $\theta = T/T_F$. In fact, as found by Nikolic and Sachdev (2007), the universality is much more general and is tied to the existence of an unstable fixed point describing the unitary balanced gas at zero density. As a result, by a proper rescaling, the complete thermodynamics and phase diagram of low-density Fermi gases with short-range attractive interactions can be expressed in terms of universal functions of temperature T, detuning ν, chemical potential μ, and the external field h conjugate to a possible density imbalance.

Universality. The universality provides considerable insight into the problem even without a specific solution of the relevant microscopic Hamiltonian. For simplicity, we focus on the so-called unitary Fermi gas right at the Feshbach resonance and the spin-balanced case of an equal mixture of both hyperfine states that undergo pairing. This problem was in fact first discussed in nuclear physics as a parameter-free model of low-density neutron matter (Baker, 1999; Heiselberg, 2001). By dimensional arguments, at $a=\infty$, the particle density n and the temperature T are the only variables on which the thermodynamics depends. The free energy per particle, which has n and T as its natural variables, thus acquires a universal form

$$F(T,V,N) = N\varepsilon_F f(\theta) \tag{132}$$

with $\varepsilon_F \sim n^{2/3}$ the bare Fermi energy and $\theta = T/T_F$ the dimensionless temperature. The function $f(\theta)$ is monotonically decreasing, because $s = -f'(\theta)$ is the entropy per particle. As shown below, the fact that the ground state is superfluid implies that $f(0) - f(\theta)$ vanishes like θ^4 as the temperature approaches zero, in contrast to a Fermi gas (or liquid), where the behavior is $\sim \theta^2$. Physically, this is due to the fact that the low-lying excitations are sound modes and not fermionic quasiparticles. By standard thermodynamic relations, the function f determines both the dimensionless chemical potential according to

$$\mu/\varepsilon_F = [5f(\theta) - 2\theta f'(\theta)]/3 =: \xi(\theta) \tag{133}$$

and the pressure via $p/n\varepsilon_F = \mu/\varepsilon_F - f(\theta)$, consistent with the Gibbs-Duhem relation $\mu N = F + pV$ for a homogeneous system. Moreover, the fact that $-f'(\theta)$ is the entropy per particle implies that $3pV = 2(F+TS)$. The internal energy u per volume is therefore connected with pressure and density by $p = 2u/3$, valid at all temperatures (Ho, 2004). Naively, this appears like the connection between pressure and energy density in a noninteracting quantum gas. In the present case, however, the internal energy has a nonvanishing contribution $\langle \hat{H}' \rangle$ from interactions. A proper way of understanding the relation $p = 2u/3$ is obtained by considering the quantum virial theorem $2\langle \hat{H}_0 \rangle - k\langle \hat{H}' \rangle = 3pV$ for a two-body interaction $V(\mathbf{x}_i - \mathbf{x}_j) \sim |\mathbf{x}_i - \mathbf{x}_j|^k$, which is a homogeneous function of the interparticle distance. It implies that $p = 2u/3$ is valid for an interacting system if $k = -2$. The pressure of fermions at unitarity is thus related to the energy density as if the particles had a purely inverse square interaction. An important consequence of this is the virial theorem (Thomas *et al.*, 2005)

$$\langle \hat{H}_{\text{tot}} \rangle = 2\langle \hat{H}_{\text{trap}} \rangle = 2\int d^3x\, U_{\text{trap}}(\mathbf{x}) n(\mathbf{x}) \tag{134}$$

for a harmonically trapped unitary gas, which allows the thermodynamics of the unitary gas to be determined from its equilibrium density profile $n(\mathbf{x})$. Equation (134) follows quite generally from the quantum virial theorem

with $k = -2$ and the fact that the contribution $3pV$ of the external forces to the virial in the case of a box with volume V is replaced by $2\langle \hat{H}_{\text{trap}} \rangle$ in the presence of an external harmonic potential. It is therefore valid for finite temperature and arbitrary trap anisotropy. An alternative derivation of Eq. (134) was given by Werner and Castin (2006). They noted that the unitary Fermi gas in 3D exhibits a scale invariance that is related to a hidden SO(2,1) symmetry. In fact, since the interaction potential at unitarity effectively obeys $V(\lambda r) = V(r)/\lambda^2$, the situation is analogous to that discussed in Sec. VI for the 2D Bose gas with a pseudopotential interaction. In particular, scale invariance implies a simple evolution of arbitrary initial states in a time-dependent trap and the existence of undamped breathing modes with frequency 2ω (Werner and Castin, 2006).

At zero temperature, the ground-state properties of the unitary gas are characterized by a *single* universal number $\xi(0) = 5f(0)/3$, which is sometimes called the Bertsch parameter [most experimental papers use $\beta = -1 + \xi(0)$ instead]. It is smaller than 1 (i.e., $\beta < 0$), because the attractive interaction leads to a reduction of the chemical potential at unitarity from its noninteracting value $\mu^{(0)} = \varepsilon_F$ to $\mu = \xi(0)\varepsilon_F$.[20] Experimentally, the most direct way of measuring the universal number $\xi(0)$ is obtained from *in situ*, absorption imaging of the density distribution $n(\mathbf{x})$ in a trap. Indeed, within the local-density approximation Eq. (12), free fermions in an isotropic trap exhibit a density profile $n(\mathbf{x}) = n(0)(1 - r^2/R_{\text{TF}}^2)^{3/2}$ with a Thomas-Fermi radius $R_{\text{TF}}^{(0)} = (24N)^{1/6}\ell_0$. Since $\mu \sim n^{2/3}$ at unitarity has the same dependence on density as noninteracting fermions, with a prefactor reduced just by $\xi(0) < 1$, the profile at unitarity is that of a free Fermi gas with a rescaled size. For a given total particle number N and mean trap frequency $\bar{\omega}$, the resulting Thomas-Fermi radius at zero temperature, is therefore reduced by a factor $\xi^{1/4}(0)$. Ideally, the value $R_{\text{TF}}^{(0)}$ would be measured by sweeping the magnetic field to the zero crossing of the scattering length at $B = B_0 + \Delta B$, where an ideal Fermi gas is realized. In practice, e.g., for ^{6}Li, there is appreciable molecule formation and subsequent decay processes at this field, and it is more convenient to ramp the field to values far on the BCS side, where the thermodynamics is again essentially that of an ideal Fermi gas. Results for the universal parameter $\xi(0)$ at the lowest attainable temperatures of around $\theta \approx 0.04$ have been obtained from *in situ* measurements of the density profile by Bartenstein *et al.* (2004a), with the result $\xi(0) = 0.32 \pm 0.1$. More recent measurements by Partridge *et al.* (2006) find a larger value, $\xi(0) = 0.46 \pm 0.05$. Alternatively, the parameter ξ may be determined by measuring the release energy of an expanding cloud (Bourdel *et al.*, 2004; Stewart *et al.*,

---

[20]In a trap, the chemical potential $\mu_{\text{trap}} \sim R^2$ is reduced by a factor $\sqrt{\xi(0)}$ and not $\xi(0)$ as in the homogeneous case, because the density in the trap center is increased by the attractive interaction.

2006). In the latter case, however, an appreciable temperature dependence is found, which makes extrapolations to $T=0$ difficult. In particular, at finite temperature, the relation between the density distributions at $a=0$ and ∞ involves the complete function $\xi(\theta)$ because the Fermi temperature continuously decreases as one moves away from the trap center.

On the theoretical side, the ground-state properties of a resonantly interacting Fermi gas have been obtained numerically by fixed-node Green's function Monte Carlo calculations. They provide quantitative results for the equation of state (Carlson *et al.*, 2003; Astrakharchik *et al.*, 2004) at arbitrary values of a, and in particular at unitarity. The resulting values for $\xi(0)$ are 0.43 (Carlson *et al.*, 2003) or 0.41 (Astrakharchik *et al.*, 2004). Recently, the chemical potential and the gap of the unitary Fermi gas at zero temperature were calculated analytically from an effective field theory using an $\epsilon=4-d$ expansion (Nishida and Son, 2006). The possibility of such an expansion is based on an observation made by Nussinov and Nussinov (2006) that a unitary Fermi gas in four dimensions is in fact an ideal Bose gas. Indeed, in $d=4$, a two-particle bound state in a zero-range potential appears only at infinitely strong attraction. Thus, already at $\varepsilon_b=0^+$, the resulting dimer size vanishes. At finite density, therefore, one ends up with a noninteracting BEC, similar to the situation as $a\to 0^+$ in three dimensions. The expansion about the upper critical dimension $d=4$ may be complemented by an expansion around the lower critical dimension, which is 2 for the present problem (Nishida and Son, 2007). Indeed, for $d\leq 2$ a bound state at zero binding energy appears for an arbitrary weak attractive interaction, as shown in Sec. V.A. A unitary Fermi gas in $d\leq 2$ thus coincides with the noninteracting gas and $\xi(0)\equiv 1$ for all $d\leq 2$ (Nussinov and Nussinov, 2006). The $d-2$ expansion, however, only captures nonsuperfluid properties like the equation of state, while all effects associated with superfluidity are nonperturbative. Using a Borel-Padé method for the three-loop expansion in $\epsilon=4-d$, the most precise field-theoretical result for the Bertsch parameter is $\xi(0)=0.367\pm0.009$ (Arnold *et al.*, 2007).

Critical temperature and pseudogap. Within a single-channel description, a zero-range interaction $V(\mathbf{x}-\mathbf{x}')=g_0\delta(\mathbf{x}-\mathbf{x}')$ between fermions of opposite spin σ gives rise to an interaction Hamiltonian in momentum space,

$$\hat{H} = \frac{g_0}{2V}\sum_{\sigma}\sum_{k,k',Q} c^{\dagger}_{k+Q,\sigma}c^{\dagger}_{-k,-\sigma}c_{-k',-\sigma}c_{k'+Q,\sigma}. \tag{135}$$

Here $c^{\dagger}_{k,\sigma}$ are fermion creation operators with momentum $\mathbf{k}$ and spin σ and V is the volume of the system. Moreover, $\mathbf{k}-\mathbf{k}'$ is the momentum transfer due to the interaction and $\mathbf{Q}$ is the conserved total momentum in the two-particle scattering process. The bare coupling strength g_0 is determined by the s-wave scattering length a after a regularization in which the δ potential is replaced by the proper pseudopotential with finite

strength g (see below). For attractive interactions $g<0$,[21] the Hamiltonian (135) was first discussed by Gor'kov and Melik-Barkhudarov (1961). In the weak-coupling regime $k_F|a|\ll 1$, where the magnitude of the scattering length is much less than the average interparticle spacing, they showed that a BCS instability to a state with bound pairs appears at the temperature

$$T_c = [8e^C/(4e)^{1/3}\pi e^2]T_F\exp[-\pi/(2k_F|a|)] \tag{136}$$

($C=0.577$ is Euler's constant). As expected for a weak-coupling BCS instability, the critical temperature vanishes with an essential singularity. The absence of an energy cutoff in the interaction leaves the Fermi temperature as the characteristic scale. For typical densities and off-resonant scattering lengths in cold gases, the parameter $k_F|a|\approx 0.02$ is very small, so Eq. (136) is applicable in principle. In practice, however, fermionic superfluidity in dilute gases, where T_F is only of the order of microkelvins, is unobservable unless $k_F|a|$ becomes of order 1. In fact, the range of accessible coupling strengths on the BCS side of the crossover is limited by the finite level spacing in the trap or, alternatively, by the trap size R, which must be larger than the size $\xi_b\approx\hbar v_F/k_B T_c$ of a Cooper pair (Tinkham, 1996). Using the local-density approximation, the condition $k_B T_c\gtrsim\hbar\omega$ on the BCS side is equivalent to $\xi_b\lesssim R$ and implies particle numbers $N\gtrsim N_\star=\exp[3\pi/(2k_F|a|)]$. Since $N_\star=10^5$ at $k_F|a|=0.4$, this shows that with typical values for the particle numbers in a trap, the regime $k_F|a|\ll 1$ is no longer described by the theory of a locally homogeneous system. Instead, for $N<N_\star$ one reaches a regime that is similar to that of pairing in nuclei, where the resulting energy gap obeys $\Delta_0\ll\hbar\omega$; see, e.g., Heiselberg and Mottelson (2002).

In the strong-coupling regime $k_F|a|\gtrsim 1$ near the unitarity limit, where the critical temperature lies in an accessible range of order T_F itself, no analytical solution of the problem is available. In particular, the singular nature of the two-particle scattering amplitude $f(k)=i/k$ right at unitarity rules out any perturbative approach. It is only far on the BEC side of the problem that $k_F a\ll 1$ again provides a small parameter. In this regime, the binding energy ε_b is much larger than the Fermi energy ε_F. At temperatures $k_B T\ll\varepsilon_b$, therefore, a purely bosonic description applies for a dilute gas of strongly bound pairs[22] with density $n/2$ and a repulsive interaction described by the dimer-dimer scattering length of

---

[21]Note that the model (135) does not make sense in the regime $g>0$, where it describes repulsive fermions. However, with a proper pseudopotential, the two-particle interaction has a bound state for positive scattering length. The Hamiltonian (135) then describes fermions along this branch and not in their continuum states, where the interaction would be repulsive

[22]Note that the pseudopotential bound state is strongly bound in the BEC limit of the crossover only as far as the scales relevant for the BCS-BEC crossover are concerned, while it is a very weakly bound state on the scale of the actual interatomic potential; see Sec. I.A.
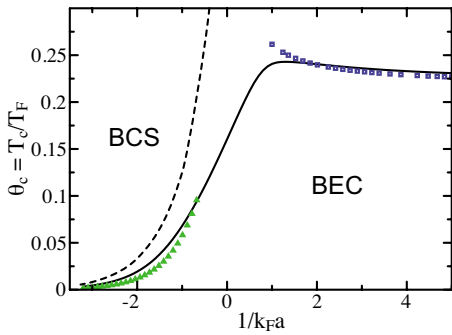
FIG. 28. (Color online) Critical temperature of the homogeneous gas as a function of the coupling strength. The full line is the result obtained by Haussmann *et al.* (2007) and gives T_c $=0.16T_F$ at unitarity. The exact asymptotic results Eqs. (136) and (11) in the BCS and BEC limits are indicated by triangles (green) and squares (blue), respectively. The dashed line gives the schematic evolution of T^*. From Haussmann *et al.*, 2007.

Eq. (130). Its dimensionless coupling constant $(n/2)^{1/3}a_{dd}=0.16k_F a$ is much smaller than 1 in the regime $1/k_F a \gtrsim 2$. Since the dimers eventually approach an ideal Bose gas, with density $n/2$ and mass $2M$, the critical temperature in the BEC limit is obtained by converting the associated ideal BEC condensation temperature into the original Fermi energy. In the homogeneous case this gives $T_c(a\rightarrow 0)=0.218T_F$, while in a trap the numerical factor is 0.518. The fact that T_c is completely independent of the coupling constant in the BEC limit is simple to understand, On the BCS side, superfluidity is destroyed by fermionic excitations, namely, the breakup of pairs. The critical temperature is therefore of the same order as the pairing gap at zero temperature, consistent with the well-known BCS relation $2\Delta_0/k_B T_c=3.52$. A relation of this type is characteristic for a situation in which the transition to superfluidity is driven by the gain in *potential* energy associated with pair formation. In particular, the formation and condensation of fermion pairs occur at the same temperature. By contrast, on the BEC side, the superfluid transition is driven by a gain in *kinetic* energy, associated with the condensation of preformed pairs. The critical temperature is then on the order of the degeneracy temperature of the gas, which is completely unrelated to the pair binding energy.

To lowest order in $k_F a$ in this regime, the shift Eq. (11) in the critical temperature due to the repulsive interaction between dimers is positive and linear in $k_F a$. The critical temperature in the homogeneous case, therefore, has a maximum as a function of the dimensionless inverse coupling constant $v=1/k_F a$, as found in the earliest calculation of T_c along the BCS-BEC crossover by Nozières and Schmitt-Rink (1985). A more recent calculation of the universal curve $\theta_c(v)$, which accounts for fluctuations of the order parameter beyond the Gaussian level due to interactions between noncondensed pairs, has been given by Haussmann *et al.* (2007). The resulting critical temperature exhibits a maximum around $v\approx 1$, which is rather small, however (see Fig. 28). The associated universal ratio $T_c/T_F=0.16$ at the unitarity point v

$=0$ agrees well with the value 0.152(7) obtained from precise quantum Monte Carlo calculations for the negative-U Hubbard model at low filling by Burovski *et al.* (2006). Considerably larger values 0.23 and 0.25 for the ratio T_c/T_F at unitarity have been found by Bulgac *et al.* (2006) from auxiliary field quantum Monte Carlo calculations and by Akkineni *et al.* (2007) from restricted path-integral Monte Carlo methods, the latter working directly with the continuum model. In the presence of a trap, the critical temperature has been calculated by Perali *et al.* (2004). In this case, no maximum is found as a function of $1/k_F a$ because the repulsive interaction between dimers on the BEC side leads to a density reduction in the trap center, which eliminates the T_c maximum at fixed density.

The increasing separation between the pair formation and the pair condensation temperature as $v=1/k_F a$ varies between the BCS and the BEC limit implies that, in the regime $-2\lesssim v\lesssim +2$ near unitarity, there is a substantial range of temperatures above T_c where preformed pairs exist but do not form a superfluid. From recent path-integral Monte Carlo calculations, the characteristic temperature T^* below which strong pair correlations appear has been found to be of order $T^*\approx 0.7T_F$ at unitarity (Akkineni *et al.*, 2007), which is at least three times the condensation temperature T_c at this point. It has been shown by Randeria *et al.* (1992) and Trivedi and Randeria (1995) that the existence of preformed pairs in the regime $T_c < T \lesssim T^*$ leads to a normal state very different from a conventional Fermi liquid. For instance, the spin susceptibility is strongly suppressed due to singlet formation above the superfluid transition temperature.[23] This is caused by strong attractive interactions near unitarity, which leads to pairs in the superfluid, whose size is of the same order as the interparticle spacing. The temperature range between T_c and T^* is a regime of strong superconducting fluctuations. Such a regime is present also in high-temperature superconductors, where it is called the Nernst region of the pseudogap phase (Lee *et al.*, 2006). Its characteristic temperature T^* approaches T_c in the regime of weak coupling (see Fig. 28). Similarly, the Nernst region in underdoped cuprates disappears where T_c vanishes. By contrast, the temperature below which the spin susceptibility is suppressed, *increases* at small doping (Lee *et al.*, 2006). Apart from the different nature of the pairing in both cases (*s*- versus *d*-wave), the nature of the pseudogap in the cuprates, which appears in the proximity of a Mott insulator with antiferromagnetic order, is thus a rather complex set of phenomena, which still lack a proper microscopic understanding (Lee *et al.*, 2006). For a discussion of the similarities and differences between the pseudogap phase in the BCS-BEC crossover and that in high-T_c cuprates, see, e.g., the reviews by Randeria (1998) and Chen *et al.* (2005).

---

[23]For a proposal to measure the spin susceptibility in trapped Fermi gases, see Recati *et al.* (2006).

Extended BCS description of the crossover. A simple approximation, which covers the complete range of coupling strengths analytically, is obtained by assuming that, at least for the ground state, only zero-momentum pairs are relevant. In the subspace of states with only zero-momentum pairs, all contributions in Eq. (135) with $\mathbf{Q} \neq \mathbf{0}$ vanish. The resulting Hamiltonian

$$\hat{H}'_{\text{BCS}} = \frac{g_0}{2V} \sum_{\sigma} \sum_{k,k'} c^\dagger_{k,\sigma} c^\dagger_{-k,-\sigma} c_{-k',-\sigma} c_{k',\sigma} \qquad (137)$$

thus involves only two momentum sums. Equation (137) is in fact the reduced BCS Hamiltonian, which is a standard model Hamiltonian to describe the phenomenon of superconductivity. It is usually solved by a variational ansatz

$$\Psi_{\text{BCS}}(1,2,\ldots,N) = \hat{\mathcal{A}}[\phi(1,2)\phi(3,4)\cdots\phi(N-1,N)] \qquad (138)$$

in which an identical two-particle state $\phi(1,2)$ is assumed for each pair. Here the arguments $1 = (\mathbf{x}_1, \sigma_1)$, etc., denote position and spin, $\hat{\mathcal{A}}$ is the operator that antisymmetrizes the many-body wave function, and we have assumed an even number of fermions for simplicity. The wave function (138) is a simple example of a so-called Pfaffian state (see Sec. VII.C) with $(N-1)!!$ terms, which is the square root of the determinant of the completely antisymmetric $N \times N$ matrix $\phi(i,j)$. In second quantization, it can be written in the form $|\Psi_{\text{BCS}}(1,2,\ldots,N)\rangle = (\hat{b}_0^\dagger)^{N/2}|0\rangle$ of a Gross-Pitaevskii-like state. The operator $\hat{b}_0^\dagger = \Sigma_k \phi_k c^\dagger_{k,\uparrow} c^\dagger_{-k,\downarrow}$ creates a pair with zero total momentum, with $\phi_k = V^{-1/2} \int \phi(\mathbf{x}) \exp(-i\mathbf{k}\cdot x)$ the Fourier transform of the spatial part of the two-particle wave function $\phi(1,2)$ in Eq. (138). It is important to note, however, that $\hat{b}_0^\dagger$ is not a Bose operator. It develops this character only in the limit where the two-particle wave function $\phi(1,2)$ has a size much smaller than the interparticle spacing (see below). To avoid the difficult task of working with a fixed particle number, it is standard practice to use a coherent state

$$|\text{BCS}\rangle = C_{\text{BCS}} \exp(\alpha \hat{b}_0^\dagger)|0\rangle = \prod_k (u_k + v_k c^\dagger_{k,\uparrow} c^\dagger_{-k,\downarrow})|0\rangle. \qquad (139)$$

Since $\langle \hat{b}_0^\dagger \hat{b}_0 \rangle = |\Sigma_k \phi_k u_k v_k|^2 = |\alpha|^2 = N/2$ by the number equation (see below), this state is characterized by a macroscopic occupation of a single state, which is a bound fermion pair with zero total momentum. The amplitudes u_k, v_k are connected to the two-particle wave function via $v_k/u_k = \alpha \phi_k$. Since u_k^2 or v_k^2 are the probabilities of a pair $\mathbf{k}\uparrow, -\mathbf{k}\downarrow$ being empty or occupied, they obey the normalization $u_k^2 + v_k^2 = 1$. The overall normalization constant $C_{\text{BCS}} = \exp[-\frac{1}{2}\Sigma_k \ln(1+|\alpha\phi_k|^2)] \rightarrow \exp(-|\alpha|^2/2)$ approaches the standard result of a coherent state of bosons in the strong-coupling limit, where $|\alpha\phi_k|^2 \approx v_k^2 \ll 1$ for all k. In this limit, $\hat{b}_0^\dagger$ is indeed a Bose operator and the wave function Eq. (138) is that of

an ideal BEC of dimers. In fact, antisymmetrization becomes irrelevant in the limit where the occupation v_k^2 of all fermion states is much less than 1.[24] The BCS wave function has the gap Δ as a single variational parameter, which appears in the fermion momentum distribution

$$v_k^2 = \tfrac{1}{2}[1 - (\varepsilon_k - \mu)/\sqrt{(\varepsilon_k - \mu)^2 + \Delta^2}]. \qquad (140)$$

With increasing strength of the attractive interaction, this evolves continuously from a slightly smeared Fermi distribution to a rather broad distribution $v_k^2 \rightarrow \Delta^2/4(\varepsilon_k - \mu)^2 \sim [1 + (k\xi_b)^2]^{-2}$ in the BEC limit, where the chemical potential is large and negative (see below). Its width ξ_b^{-1} increases as the pair size $\xi_b = \hbar/\sqrt{2M|\mu|}$ approaches zero. Experimentally the fermionic momentum distribution near the Feshbach resonance has been determined from time-of-flight measurements by Regal *et al.* (2005). Accounting for the additional smearing due to the trap, the results are in good agreement with Monte Carlo calculations of the momentum distribution for the model (135) (Astrakharchik *et al.*, 2005b). Analysis of the distribution at finite temperature allows determination of the decrease of the average fermionic excitation gap with temperature (Chen *et al.*, 2006b).

Within the extended BCS description, the magnitude of Δ is determined by the standard gap equation

$$-\frac{1}{g_0} = \frac{1}{2V} \sum_k \frac{1}{\sqrt{(\varepsilon_k - \mu)^2 + \Delta^2}}, \qquad (141)$$

where $E_k = \sqrt{(\varepsilon_k - \mu)^2 + \Delta^2}$ is the BCS quasiparticle energy. In conventional superconductors, the momentum sum in Eq. (141) is restricted to a thin shell around the Fermi energy and the solution $\Delta \sim \exp[-1/|g_0|N(0)]$ for $g_0 < 0$ depends only on the density of states per spin $N(0)$ in the normal state right at the Fermi energy. In cold gases, however, there is no such cutoff as long as $\varepsilon_F \ll \varepsilon^\star$. Moreover, the true dimensionless coupling constant $N(0)|g| = 2k_F|a|/\pi$ is far from small, approaching infinity at the Feshbach resonance. The pairing interaction thus affects fermions deep in the Fermi sea and eventually completely melts the Fermi sphere. Within the pseudopotential approximation, the apparent divergence in Eq. (141) can be regularized by the replacement $1/g_0 \rightarrow 1/g - (1/2V)\Sigma_k(1/\varepsilon_k)$. Physically, this amounts to integrating out the high-energy contributions in Eq. (141), where the spectrum is unaffected by the pairing. A general procedure for doing this, including the case of strong pairing in nonzero-angular-momentum states, has been given by Randeria *et al.* (1990). Converting the sum over k to an integral over the free-particle density of states, the renormalized gap equation at zero temperature can then be written in the form

---

[24]Note that the wave function (138) still contains $(N-1)!!$ terms even in the BEC limit. In practice, however, only a single term is relevant, unless one is probing correlations between fermions in different pairs.

$$1/k_F a = (\tilde{\mu}^2 + \tilde{\Delta}^2)^{1/4} P_{1/2}(x). \tag{142}$$

Here $\tilde{\mu} = \mu/\varepsilon_F$ and $\tilde{\Delta} = \Delta/\varepsilon_F$ are the dimensionless chemical potential and gap, respectively, while $P_{1/2}(x)$ is a Legendre function of the first kind. The parameter $x = -\mu/(\mu^2 + \Delta^2)^{1/2}$ varies between -1 in the BCS and $+1$ in the BEC limit because the fermion chemical potential continously drops from $\mu = \varepsilon_F$ in weak coupling to $\mu \rightarrow -\varepsilon_b/2$ for strongly bound pairs and $|\mu| \gg \Delta$ in both limits. Physically the behavior of the chemical potential in the BEC limit can be understood by noting that the energy gained by adding two fermions is the molecular binding energy. The detailed evolution of μ as a function of the dimensionless coupling strength $1/k_F a$ follows from $N = 2\Sigma_k v_k^2$ for the average particle number. In dimensionless form this gives

$$4/\pi = \tilde{\mu}(\tilde{\mu}^2 + \tilde{\Delta}^2)^{1/4} P_{1/2}(x) + (\tilde{\mu}^2 + \tilde{\Delta}^2)^{3/4} P_{-1/2}(x). \tag{143}$$

Equations (142) and (143), originally discussed by Eagles (1969) and Leggett (1980), determine the gap, the chemical potential, and related quantities such as the condensate fraction (Ortiz and Dukelsky, 2005)

$$\lambda_{BCS} = \left. \frac{n_0}{n} \right|_{BCS} = \frac{3\pi}{16} \frac{\tilde{\Delta}^2}{\mathrm{Im}(\tilde{\mu} + i\tilde{\Delta})^{1/2}} \tag{144}$$

for arbitrary coupling (see Fig. 29).

They provide a simple approximation for the crossover between weak coupling $1/k_F a \rightarrow -\infty$ and the BEC limit $1/k_F a \rightarrow \infty$ within the variational ansatz Eq. (139) for the ground-state wave function. In fact, as realized long ago by Richardson and Gaudin, the results are *exact* for the reduced BCS Hamiltonian Eq. (137) and not just of a *variational* nature, as usually presented.[25] Both the gap and the condensate fraction increase continuously with coupling strength, while the chemical potential becomes negative for $1/k_F a > 0.55$. The values $\xi_{BCS}(0) = 0.59$, $\tilde{\Delta}_{BCS} = 0.69$, and $\lambda_{BCS} = 0.70$ for the chemical potential, the gap, and the condensate fraction at unitarity differ, however, considerably from the corresponding results $\xi(0) \approx 0.4$, $\tilde{\Delta} \approx 0.5$, and $\lambda \approx 0.6$ obtained by both numerical and field-theoretic methods for the physically relevant model (135). For strong coupling, the gap increases as $\tilde{\Delta} = 4(3\pi k_F a)^{-1/2}$. Apparently, this is much smaller than the two-particle binding energy. To explain why 2Δ differs from the energy ε_b of a strongly bound dimer even in the BEC limit, it is necessary to determine the minimum value of the energy $E_k = \sqrt{(\varepsilon_k - \mu)^2 + \Delta^2}$ for single-fermion excitations. For negative chemical potentials, this minimum is not at Δ as in

---

[25]For a review, see Dukelsky *et al.* (2004). It is interesting to note that, although the BCS wave function (139) gives the exact thermodynamics of the model, its number-projected form does not seem to be exact beyond the trivial weak-coupling or BEC limit; see Ortiz and Dukelsky (2005).
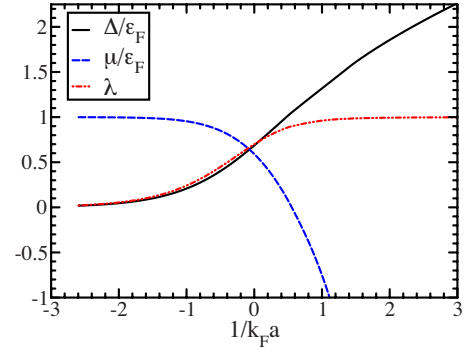
FIG. 29. (Color online) Solution of the gap and number equations (142) and (143) for the reduced BCS Hamiltonian Eq. (137). The dimensionless gap parameter, chemical potential, and condensate fraction (144) of the ground state are shown as functions of the dimensionless interaction parameter $1/k_F a$.

the usual situation $\mu > 0$, but at $\sqrt{\Delta^2 + \mu^2}$ (see Fig. 30). Since $|\mu| \gg \Delta$ in the BEC limit, the minimum energy for a single-fermionic excitation is therefore $|\mu| = \varepsilon_b/2$ and not Δ (Randeria *et al.* 1990). Note that the spectrum E_k near $k = 0$ changes from negative to positive curvature as μ goes through zero.

The size of the pairs ξ_b shrinks continuously from an exponentially large value $k_F \xi_b \simeq \varepsilon_F/\Delta$ in the BCS limit to essentially zero $\xi_b \simeq a$ in the BEC limit of tightly bound pairs. For weak coupling, the size of the pair coincides with the coherence length ξ. This is no longer the case on the BEC side of the crossover, however. Indeed, as shown by Pistolesi and Strinati (1996) and Engelbrecht *et al.* (1997), the coherence length reaches a minimum value on the order of the interparticle spacing around the unitary limit and then increases slowly to approach the value $\xi = (4\pi n a_{dd})^{-1/2}$ of a weakly interacting Bose gas of dimers with density $n/2$. This minimum is closely related to a maximum in the critical velocity around the unitary point. Indeed, as discussed in Sec. IV.D, the critical momentum for superfluid flow within a mean-field description is $k_c \approx 1/\xi$. More precisely, the critical velocity v_c on the BEC side of the crossover coincides with the sound velocity according to the Landau criterion. Near unitarity, this velocity reaches $c = v_F \sqrt{\xi(0)/3} \approx 0.36 v_F$ (see below). On the BCS side, the destruction of superfluidity does not involve the excitation of phonons but is due to pair breaking. As shown by Combescot *et al.* (2006) and Sensarma *et al.* (2006), the resulting critical velocity exhibits a maximum $v_c^{max} \approx 0.36 v_F$ around the unitarity point that is close to the value of the local sound velocity there. Using a moving optical lattice near the trap center, this prediction was verified by Miller *et al.* (2007).

Failure of extended BCS theory. In the regime of weak coupling, the gap $\tilde{\Delta}_{BCS} = (8/e^2)\exp(-\pi/2k_F|a|)$ is exponentially small. Using Eq. (136) for the critical temperature, however, the ratio $2\Delta/k_B T_c$ differs from the well-known BCS value $2\pi/e^C = 3.52$ by a factor of $(4e)^{1/3}$. The reason for this discrepancy is subtle and important from
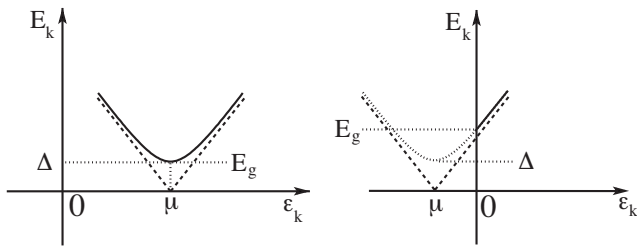
FIG. 30. Change in the fermionic excitation spectrum of the extended BCS description as the chemical potential changes from positive to negative values.

a basic point of view. It has to do with the fact that the reduced BCS model contains only zero-momentum pairs and thus no density fluctuations are possible. By contrast, the original model (135) includes such fluctuations, which are present in any neutral system. The innocent looking BCS assumption of pairs with zero momentum eliminates an important part of the physics. To understand why the reduced BCS model fails to account for the correct low-energy excitations, it is useful to rewrite the interaction Eq. (137) in real space, where

$$\hat{H}'_{\mathrm{BCS}} = \frac{g_0}{2V} \sum_\sigma \int_x \int_{x'} \hat{\psi}_\sigma^\dagger(\mathbf{x}) \hat{\psi}_{-\sigma}^\dagger(\mathbf{x}) \hat{\psi}_{-\sigma}(\mathbf{x}') \hat{\psi}_\sigma(\mathbf{x}'). \quad (145)$$

The associated nonstandard (note the order of $\mathbf{x}$ and $\mathbf{x}'$) "interaction" $V_{\mathrm{BCS}}(\mathbf{x}-\mathbf{x}')=g_0/V$ has *infinite* range, but is scaled with $1/V$ to give a proper thermodynamic limit. It is well known that models of this type are exactly soluble and that their phase transitions are described by mean-field theory. Moreover, while Eq. (145) is invariant under a *global* gauge transformation $\psi_\sigma(\mathbf{x}) \to e^{i\phi} \psi_\sigma(\mathbf{x})$ (particle number is conserved), this is no longer the case if $\phi(\mathbf{x})$ varies spatially. In the exactly soluble reduced BCS model, therefore, the change in energy associated with a slowly varying phase does not vanish like $[\nabla \phi(\mathbf{x})]^2$, as it should for a superfluid (see the Appendix). Omission of pairs with finite momentum thus eliminates the well-known Bogoliubov-Anderson mode $\omega(q)=cq$ of a neutral superfluid (Anderson, 1958b). A proper description of the crossover problem in a neutral system like a cold gas requires one to account for both the bosonic and fermionic excitations. By contrast, for charged superconductors, the Bogoliubov-Anderson mode is pushed up to a high-frequency plasmon mode, which is irrelevant for the description of superconductivity. A reduced BCS model, in which they are omitted anyway, is thus appropriate.

The absence of the collective Bogoliubov-Anderson mode implies that already the leading corrections to the ground state in powers of $k_F|a|$ are incorrect in a reduced BCS description. For weak interactions, one misses the Gorkov–Melik-Barkhudarov reduction of the gap. Indeed, as shown by Heiselberg *et al.* (2000), density fluctuations give rise to a screening of the attractive interaction at finite density, changing the dimensionless coupling constant of the two-particle problem to $g_{\mathrm{eff}}=g$

$+g^2 N(0)(1+2\ln 2)/3+\cdots$. Since the additional contribution to the two-body scattering amplitude $g<0$ is positive, the bare attraction between two fermions is weakened. Due to the nonanalytic dependence of the weak-coupling gap or transition temperature on the coupling constant $k_F a$, the renormalization $g \to g_{\mathrm{eff}}$ gives rise to a reduction of both the gap and the critical temperature by a finite factor $(4e)^{-1/3} \approx 0.45$. The universal ratio $2\Delta/k_B T_c=3.52$, valid in weak coupling, is thus unaffected. It is interesting to note that a naive extrapolation of the Gorkov–Melik-Barkhudarov result $\Delta/\varepsilon_F = (2/e)^{7/3} \exp(-\pi/2k_F|a|)$ for the zero-temperature gap to infinite coupling $k_F a=\infty$ gives a value $\Delta(v=0) = 0.49\varepsilon_F$ that is close to the one obtained from quantum Monte Carlo calculations at unitarity (Carlson *et al.*, 2003). In the BEC limit, the condensate fraction Eq. (144) reaches the trivial limit 1 of the ideal Bose gas as $\lambda_{\mathrm{BCS}}=1-2\pi na^3+\cdots$. The correct behavior, however, is described by the Bogoliubov result Eq. (10) with density $n/2$ and scattering length $a \to a_{\mathrm{dd}}$, i.e., it involves the square root of the gas parameter na^3. As pointed out by Lamacraft (2006), the presence of pairs with nonzero momentum is also important for measurements of noise correlations in time-of-flight pictures near the BCS-BEC crossover. As discussed in Sec. III.B, such measurements provide information about the second-order correlation function in momentum space

$$G_{\uparrow\downarrow}(\mathbf{k}_1,\mathbf{k}_2) = \langle \hat{n}_\uparrow(\mathbf{k}_1)\hat{n}_\downarrow(\mathbf{k}_2) \rangle - \langle \hat{n}_\uparrow(\mathbf{k}_1) \rangle \langle \hat{n}_\downarrow(\mathbf{k}_2) \rangle. \quad (146)$$

The momenta $\mathbf{k}_{1,2}=M\mathbf{x}_{1,2}/\hbar t$ are related to the positions $\mathbf{x}_{1,2}$ at which the correlations are determined after a free-flight expansion for time t. While the formation of bound states shows up as a peak at $\mathbf{k}_1=-\mathbf{k}_2$ as observed by Greiner *et al.* (2005) in a molecular gas above condensation, the presence of pairs with nonzero momenta gives rise to an additional contribution proportional to $1/|\mathbf{k}_1+\mathbf{k}_2|$. This reflects the depletion of the condensate due to bosons at finite momentum as found in the Bogoliubov theory of an interacting Bose gas.

Crossover thermodynamics. As pointed out above, a complete description of the BCS-BEC crossover involves both bosonic and fermionic degrees of freedom. Since the fermionic spectrum has a gap, only the bosonic Bogoliubov-Anderson mode is relevant at low temperatures (Liu, 2006). Similar to the situation in superfluid ^{4}He, these sound modes determine the low-temperature thermodynamics along the full BCS-BEC crossover. They give rise to an entropy

$$S(T) = V(2\pi^2/45)k_B(k_B T/\hbar c)^3 + \cdots, \quad (147)$$

which vanishes like T^3 for arbitrary coupling strength. The associated sound velocity c at zero temperature follows from the ground-state pressure or the chemical potential via the thermodynamic relation $Mc^2=\partial p/\partial n = n\partial\mu/\partial n$. It was shown by Engelbrecht *et al.* (1997) that the sound velocity decreases monotonically from $c=v_F/\sqrt{3}$ to zero on the BEC side. There, to lowest order in $k_F a$, it is given by the Gross-Pitaevskii result $(c/v_F)^2=k_F a_{\mathrm{dd}}/6\pi$ for the sound velocity of a dilute gas

of dimers with a repulsive interaction obtained from Eq. (130). At unitarity, $c = v_F \sqrt{\xi(0)/3} \approx 0.36 v_F$ is related to the Fermi velocity by the universal constant $\xi(0)$. This has been used in recent measurements of the sound velocity along the axial z direction of an anisotropic trap by Joseph *et al.* (2007). The velocity $c_0 = c(z=0)$ measured near the trap center is given by $c_0^2 = \sqrt{\xi(0)}(v_F^{(0)})^2/5$. Here $v_F^{(0)}$ is the Fermi velocity of a noninteracting gas, which is fixed by the associated Fermi energy in the trap by $\varepsilon_F(N) = M(v_F^{(0)})^2/2$. A factor $3/5$ arises from averaging over the transverse density profile (Capuzzi *et al.*, 2006). An additional factor $1/\sqrt{\xi(0)}$ is due to the fact that, at unitarity, attractive interactions increase the local density $n(0)$ in the trap center compared to that of a noninteracting Fermi gas by a factor $\xi(0)^{-3/4}$. The local Fermi velocity $v_F[n(0)]$ is thus enhanced by $\xi(0)^{-1/4}$ compared to $v_F^{(0)}$. Precise measurements of the ratio $c_0/v_F^{(0)} = 0.362 \pm 0.006$ (Joseph *et al.*, 2007) at the lowest available temperatures thus give $\xi(0) = 0.43 \pm 0.03$, in good agreement with the quantum Monte Carlo results. In addition, the lack of dependence of this ratio on the density has been tested over a wide range, thus confirming the universality at the unitary point.

Numerical results on the crossover problem at finite temperatures have been obtained by Bulgac *et al.* (2006), Burovski *et al.* (2006), and Akkineni *et al.* (2007) at the unitarity point. More recently, they have been complemented by analytical methods, using expansions around the upper and lower critical dimensions (Nishida, 2007) or in the inverse number $1/N$ of an attractive Fermi gas with $2N$ components (Nikolic and Sachdev, 2007). A rather complete picture of the crossover thermodynamics for arbitrary couplings and temperatures in the spin-balanced case was given by Haussmann *et al.* (2007) on the basis of a variational approach to the many-body problem developed by Luttinger and Ward (1960) and by De Dominicis and Martin (1964a, 1964b). The theory does not capture correctly the critical behavior near the superfluid transition, which is a continuous transition of the 3D XY type for arbitrary coupling. Since the approximations involved are conserving, however, the results obey standard thermodynamic relations and the specific relation $p = 2u/3$ at unitarity at the level of a few percent. In addition, the resulting value $T_c/T_F \approx 0.16$ for the critical temperature at unitarity agrees well with the presently most precise numerical results by Burovski *et al.* (2006). As an example, a 3D plot of the entropy per particle is shown in Fig. 31. Apparently, the freezing out of fermionic excitations with increasing coupling v leads to a strong suppression of the low-temperature entropy. An adiabatic ramp across the Feshbach resonance from the BEC to the BCS side is associated with a lowering of the temperature, as emphasized by Carr *et al.* (2004). In particular, it is evident from this picture that a molecular condensate can be reached by going isentropically from negative to positive scattering lengths even if the initial state on the fermionic side is above the transition to superfluidity, as was the case in the experiments by Greiner *et al.* (2003). The plot provides a quantitative
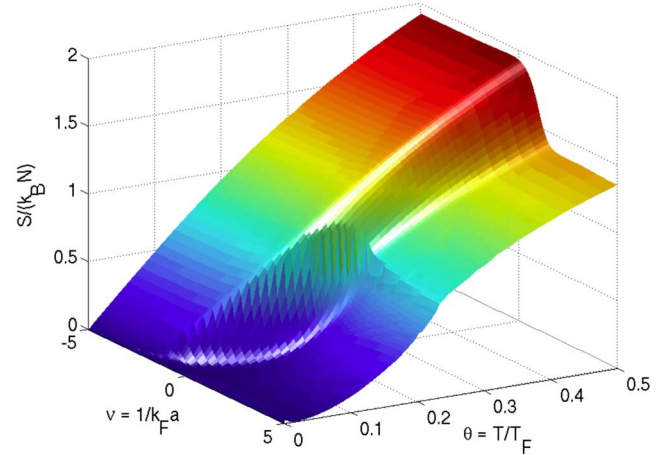

FIG. 31. (Color online) Entropy per particle in units of k_B as a function of the dimensionless coupling $1/k_F a$ and temperature $\theta = T/T_F$. The crossover from a Fermi gas with a tiny superfluid regime as $T \to 0$ to a Bose gas that is superfluid below $T \approx 0.2 T_F$ occurs in a narrow range of coupling strengths. An isentropic ramp, starting in the normal phase on the negative a side at sufficiently low T, leads to a molecular condensate. From Haussmann *et al.*, 2007.

picture of how an attractive gas of fermions gradually evolves into a repulsive gas of bosons. Apparently, most of the quantitative change happens in the range $-2 \lesssim v \lesssim +2$, which is precisely the regime accessible experimentally with cold atoms. Note that the exact entropy and its first derivative are continuous near the critical temperature. Indeed, the singular contribution to $S(T)$ is proportional to $|T - T_c|^{(1-\alpha)}$ and $\alpha < 0$ for the 3D XY transition. Moreover, the value $S(T_c)/N \approx 0.7 k_B$ of the entropy per particle at T_c at the unitarity point (Haussmann *et al.*, 2007) provides a limit on the entropy of any initial state, which is required to reach the superfluid regime $T < T_c$ near unitarity by an adiabatic process. In a harmonic trap, the fact that the local ratio T/T_F increases upon approaching the trap edge, gives rise to a considerably larger entropy $S(T_c) \simeq 1.6 N k_B$ (Haussmann and Zwerger, 2008).

C. Experiments near the unitarity limit

Thermodynamic properties. The thermodynamics of a strongly interacting Fermi gas near unitarity was studied experimentally by Kinast *et al.* (2005). It was found that the spatial profiles of both the trapped and released gas are rather close to a Thomas-Fermi profile with a size parameter determined from hydrodynamic scaling. This is consistent with the fact that the equation of state of the unitary gas is identical with that of a noninteracting gas up to a scale factor. Strictly speaking, however, this is true only at zero temperature. At finite temperature, the function $\xi(\theta)$ defined in Eq. (133) is different from that of an ideal Fermi gas. Assuming a Thomas-Fermi profile, the effective temperature of a near-unitary gas can be inferred from fitting the observed cloud profiles. The

temperature-dependent internal energy $E(T)$ and specific heat of the gas could then be determined by adding a well-defined energy to the gas through a process by which the cloud is released abruptly and recaptured after a varying expansion time (Kinast *et al.*, 2005). The resulting $E(T)$ curve essentially follows that of a noninteracting gas above a characteristic temperature $\tilde{T}_c$ $\approx 0.27 T_F^{(0)}$. The data below $\tilde{T}_c$ follow a power law $E(T)$ $- E_0 \sim T^a$ with $a \simeq 3.73$, which is not far from the exact low-T result $E(T) - E_0 = V(\pi^2/30) k_B T (k_B T/\hbar c)^3$ of a uniform superfluid in the phonon-dominated regime $k_B T$ $\ll Mc^2$. Quantitatively, the data are well described by a finite-temperature generalization of the extended BCS description of the crossover (Chen *et al.*, 2005). The characteristic temperature $\tilde{T}_c$ is, however, considerably larger than the transition temperature $T_c^{\text{trap}} \simeq 0.21 T_F^{(0)}$ to the superfluid state. Indeed, within the local-density approximation (LDA), the superfluid transition in a trap occurs when the local Fermi temperature $T_F[n(0)]$ in the trap center reaches the critical value T_c of the homogeneous gas at density $n(0)$. At the unitarity point, the latter is obtained from the universal ratio $T_c/T_F \approx 0.16$. As noted above, attractive interactions increase the local density in the trap center compared to the noninteracting gas with (bare) Fermi energy $\varepsilon_F(N) = \hbar \bar{\omega}(3N)^{1/3}$ $= k_B T_F^{(0)}$. Using LDA, the resulting superfluid transition temperature is $T_c^{\text{trap}} \simeq 0.21 T_F^{(0)}$ (Haussmann and Zwerger, 2008). Recently, precise results for the critical temperature of the unitary gas have been obtained by Shin *et al.* (2008). They rely on using gases with a finite imbalance $n_\uparrow \neq n_\downarrow$, which have always a fully polarized outer shell in a trap. Since a single species Fermi gas is noninteracting in the ultracold limit, the temperature can be reliably determined from cloud profiles. Extrapolating to zero imbalance, the measured critical temperature at unitarity in units of the local T_F at the center of the trap appears to be close to the value $T_c/T_F \simeq 0.15$ predicted by theory (Shin *et al.*, 2008).

Experimental results on thermodynamic properties that do not rely on the difficult issue of a proper temperature calibration are possible using the virial theorem Eq. (134). It allows the energy of the strongly interacting gas to be measured directly from its density profile. Within the LDA, the contributions to $\langle \hat{H}_{\text{trap}} \rangle$ from the three spatial directions are identical, even in an anisotropic trap. The total energy per particle thus follows directly from the average mean-square radius E/N $= 3M\omega_z^2 \langle z^2 \rangle$ along (say) the axial direction. The predicted linear increase of $\langle z^2 \rangle$ at unitarity with the energy input was verified experimentally by Thomas *et al.* (2005). More generally, since the internal energy per particle is $f(\theta) - \theta f'(\theta)$ in units of the bare Fermi energy, the universal function $f(\theta)$ is accessible in principle by measuring the density profile. A possible way to do thermometry for such measurements was developed by Luo *et al.* (2007). They measured entropy as a function of energy by determining the energy from the mean-square radii and the entropy by adiabatically ramping the magnetic
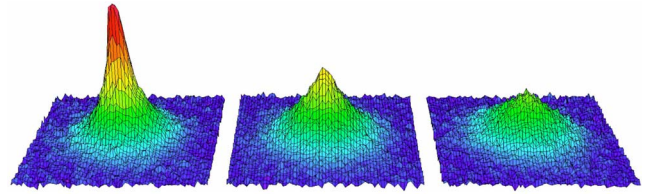

FIG. 32. (Color online) Time-of-flight images showing a fermionic condensate after projection onto a molecular gas. The images show condensates at different detunings $\Delta B = 0.12$, 0.25, and 0.55. G (left to right) from the Feshbach resonance (BCS side), starting with initial temperatures $T/T_F = 0.07$. From Regal *et al.*, 2004a.

field far into the BCS regime. There the gas is essentially an ideal Fermi gas in a trap, and its entropy may be inferred again from $\langle z^2 \rangle$. The experimental results for $S(E)$ are in fair agreement with theories for the thermodynamics of the unitary gas which are based on an extension (Hu *et al.*, 2007) of the approach by Nozières and Schmitt-Rink (1985) or on finite temperature Monte Carlo calculations (Bulgac *et al.*, 2007). The measured value $(E_0/N\varepsilon_F)_{\text{trap}} = 0.48 \pm 0.03$ implies $\xi(0) = 0.40 \pm 0.03$, because the total energy in the trap is twice the result $E_0/N\varepsilon_F = f(0) = 3\xi(0)/5$ obtained in a uniform system. The fact that the entropy is a perfectly smooth function of energy, with $dS/dE = 1/T$, makes it difficult, however, to infer a reliable value for T_c from these measurements.

Condensate fraction. The standard signature of BEC in ultracold gases is the appearance of a bimodal density distribution below the condensation temperature. Fitting the density profile from the absorption image to a superposition of a Thomas-Fermi profile and a Gaussian background from the thermal atoms allows a rather precise measurement of the condensate fraction n_0/n. In the case of fermionic superfluidity, this does not work because pairs break in time-of-flight. This problem is avoided by the rapid transfer technique (Regal *et al.*, 2004a; Zwierlein *et al.*, 2004), in which fragile pairs on the BCS side of the crossover are preserved by sweeping the magnetic field fast toward the BEC side of the resonance, transforming them to stable molecules. In an adiabatic situation, each fermionic pair is thereby transformed into a tightly bound dimer, and a time-of-flight picture then indeed reflects the momentum distribution of the original pairs on the BCS side of the crossover. The resulting absorption images are shown in Fig. 32.

In practice, the process is nonadiabatic and essentially projects the initial many-body state onto that of a molecular condensate. A theoretical analysis of the condensate fraction extracted using the rapid transfer technique was given by Altman and Vishwanath (2005) and Perali *et al.* (2005). The fraction of molecules depends on the sweep rate and, in a strongly nonadiabatic situation, provides information about pair correlations in the initial state even in the absence of a condensate (Altman and Vishwanath, 2005). Experimentally, the observed condensate fractions in ^{40}K were at most around 0.14 (Regal *et al.*, 2004a), much smaller than the expected equilib-
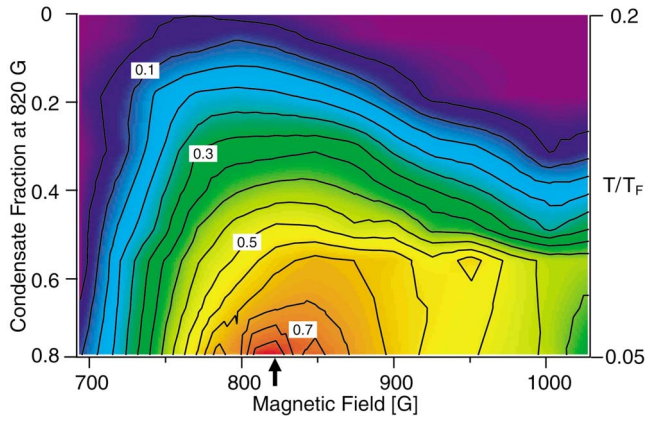
FIG. 33. (Color online) Condensate fraction as a function of magnetic field and temperature. The highest condensate fractions and onset temperatures are obtained on the BEC side, close to the resonance at $B_0=834$ G. As a measure of temperature, the condensate fraction at 820 G (see arrow) is used as the vertical axis. From Zwierlein *et al.*, 2004.

rium values $n_0/n \approx 0.5$ at unitarity. Apart from uncertainties inherent in the rapid transfer technique, a possible origin of this discrepancy may be the rather short lifetime of ^{40}K dimers near resonance, on the order of 100 ms. Yet the qualitative features of the phase diagram agree with an analysis based on an equilibrium theory (Chen *et al.*, 2006a). For ^{6}Li, in turn, the condensate fractions determined via the rapid transfer technique turned out to be much larger, with a maximum value 0.8 at $B \approx 820$ G, on the BEC side of the resonance (Zwierlein *et al.*, 2004) (see Fig. 33). The observation (Zwierlein *et al.*, 2004) that the condensate fraction decreases to zero on the BEC side (see Fig. 33) instead of approaching 1 is probably caused by fast vibrational relaxation into deeply bound states further away from the resonance.

Collective modes. Collective modes in a harmonic trap have been a major tool for studying cold gases in the BEC regime, where the dynamics is determined by superfluid hydrodynamics. For a mixture of fermions with an adjustable attractive interaction, the corresponding eigenfrequencies have been worked out by Heiselberg (2004) and by Stringari (2004). For a highly elongated trap, where the axial trap frequency ω_z is much smaller than the radial confinement frequency $\omega_\perp$, two important eigenmodes are the axial and radial compression modes, with respective frequencies (Heiselberg, 2004; Stringari, 2004)

$$\omega_B = \omega_z \sqrt{3 - 1/(\gamma+1)} \quad \text{and} \quad \omega_r = \omega_\perp \sqrt{2(\gamma+1)}.$$
$$(148)$$

They are determined by the effective polytropic index $\gamma = d \ln p / d \ln n - 1$ and thus give information about the equation of state $p(n)$ through the crossover. Since $\gamma = 2/3$ exactly for the unitary Fermi gas, one obtains universal numbers for these frequencies precisely at the Feshbach resonance, as pointed out by Stringari (2004).
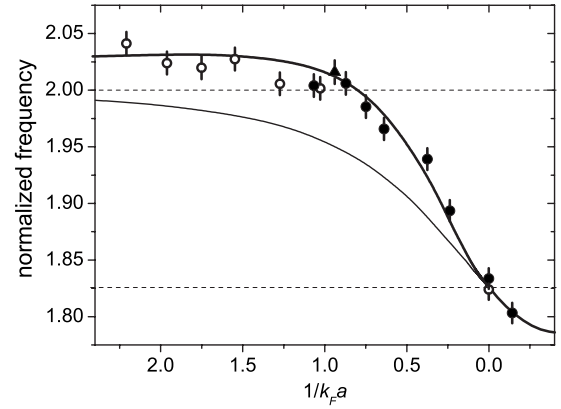

FIG. 34. Normalized frequency $\omega_r/\omega_\perp$ of the radial compression mode as a function of dimensionless interaction parameter $1/k_F a$ on the BEC side of the crossover. The experimental data agree well with Monte Carlo calculations of the equation of state (thick solid line) and the exact value $\sqrt{10/3} = 1.826$ at unitarity. The BEC limit $\omega_r/\omega_\perp = 2$ is approached from above due to the positive correction of the ground-state chemical potential beyond the mean field, predicted by Lee, Huang, and Yang. The thin monotonic line is the result of an extended BCS mean-field theory. From Altmeyer *et al.*, 2007.

In particular, the radial compression mode frequency ω_r is $\omega_r = \sqrt{10/3}\omega_\perp$ in the BCS limit and at unitarity, while it approaches $\omega_r = 2\omega_\perp$ in the BEC limit, where $\gamma = 1$. These predictions were confirmed experimentally by Bartenstein *et al.* (2004b) and by Kinast *et al.* (2004), providing direct evidence for superfluid hydrodynamics. The fact that the chemical potential Eq. (9) of a dilute repulsive Bose gas is larger than its mean-field limit $\mu_{Bose} \sim n$ implies $\gamma > 1$, i.e., the BEC limit is reached from above. The expected nonmonotonic behavior of ω_r as a function of $1/k_F a$ has been observed by Altmeyer *et al.* (2007). It provides the first quantitative test of the Lee-Huang-Yang correction to the chemical potential Eq. (9) of a dilute repulsive Bose gas (of dimers) (see Fig. 34).

The issue of damping of the collective modes in the BCS-BEC crossover has raised a number of questions, which are connected with recent developments in QCD and field theory. As pointed out by Gelman *et al.* (2004), not only the thermodynamics but also dynamical properties like the kinetic coefficients are described by universal scaling functions at the unitarity point. An example is the shear viscosity η, which determines the damping of sound and collective oscillations in trapped gases. At unitarity, its dependence on density n and temperature T is fixed by dimensional arguments to $\eta = \hbar n \alpha(T/\mu)$, where μ is the chemical potential and $\alpha(x)$ is a dimensionless universal function. At zero temperature, in particular, $\eta(T=0) = \alpha_\eta \hbar n$ is linear in the density, which defines a quantum viscosity coefficient α_η. From a simple fluctuation-dissipation-type argument in the *normal* phase, a lower bound $\alpha_\eta \geq 1/6\pi$ was derived by Gelman *et al.* (2004). Assuming that a hydrodynamic description applies, the effective shear viscosity can be inferred from the damping rate of the collective modes.

In particular, the damping of the axial mode near the unitarity limit in the experiments by Bartenstein *et al.* (2004b) gives $\alpha_\eta \approx 0.3$ at the lowest attainable temperatures. Based on these results, it has been speculated that ultracold atoms near a Feshbach resonance are a nearly perfect liquid (Gelman *et al.*, 2004). A proper definition of viscosity coefficients like η, however, requires hydrodynamic damping. At zero temperature, this is usually not the case. It is valid at $T=0$ in one dimension, where exact results on α_η have been obtained for arbitrary coupling along the BCS-BEC crossover (Punk and Zwerger, 2006).

At finite temperature, damping is typically associated with the presence of thermally excited quasiparticles, which also give rise to a nonzero entropy density $s(T)$. It was shown by Kovtun *et al.* (2005) that in a rather special class of relativistic field theories, which are dual to some string theory, the ratio $\eta(T)/s(T)=\hbar/4\pi k_B$ has a universal value. For more general models, this value is conjectured to provide a lower bound on η/s. Since the ratio does not involve the velocity of light, the string theory bound on η/s may apply also to nonrelativistic systems like the unitary Fermi gas, which lack an intrinsic scale beyond temperature and density. Quantitative results for the viscosity of the unitary Fermi gas in its normal phase were obtained by Bruun and Smith (2007). Near the superfluid transition, the dimensionless coefficient α is of order 0.2. Using the results for the entropy discussed above, gives $\eta/s \approx 0.28\hbar/k_B$ near T_c, which is larger than the string theory bound by a factor ~ 3.5. In the superfluid regime, the η/s ratio is expected to diverge (Rupak and Schäfer, 2007), implying a minimum of η/s near the transition temperature. Recent measurements of this ratio, using the damping of the radial breathing mode in a strongly anisotropic trap have been performed by Turlapov *et al.* (2007). The results show indeed a very low viscosity of the unitary gas with a ratio η/s which is not far from the string theory bound. Exact results on *bulk* rather than shear viscosities were obtained by Son (2007). He noted that the unitary Fermi gas exhibits a conformal symmetry that constrains the phenomenological coefficients in the dissipative part of the stress tensor. In particular, the bulk viscosity vanishes identically in the normal state and thus no entropy is generated in a uniform expansion. In the superfluid phase, which is generally characterized by the shear plus three different bulk viscosities (Forster, 1975), this result implies that two of the bulk viscosity coefficients vanish at unitarity, while one of them may still be finite.

rf spectroscopy. A microscopic signature of pairing between fermions is provided by rf spectroscopy. This was first suggested by Törmä and Zoller (2000). Following earlier work by Gupta *et al.* (2003) and Regal and Jin (2003) in the nonsuperfluid regime, such an experiment was performed by Chin *et al.* (2004). A rf field with frequency ω_L is used to drive transitions between one of the hyperfine states $|2\rangle=|\downarrow\rangle$ that is involved in the pairing and an empty hyperfine state $|3\rangle$, which lies above it by an energy $\hbar\omega_{23}$ due to the magnetic field splitting of
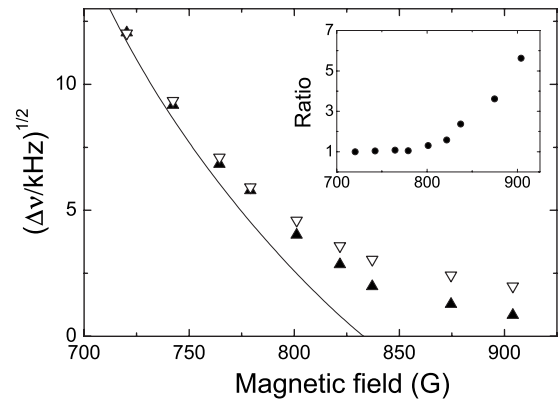

FIG. 35. Effective pairing gap in ^{6}Li from rf spectroscopy as a function of magnetic field. The solid line is the two-particle binding energy, which vanishes at the Feshbach resonance at $B_0=834$ G coming from the BEC side. Open and closed symbols are for Fermi temperatures $T_F=3.6$ and 1.2 μK, respectively. The ratio of the effective pairing gaps strongly depends on T_F on the BCS side (inset). From Chin *et al.*, 2004.

bare atom hyperfine levels. In the absence of any interactions, the spectrum exhibits a sharp peak at $\omega_L=\omega_{23}$. The presence of attractive interactions between the two lowest hyperfine states $|1\rangle$ and $|2\rangle$ will lead to an upward shift of this resonance. In a molecular picture, which is valid far on the BEC side of the crossover, this shift is expected to coincide with the two-particle binding energy ε_b. Indeed, it was shown by Chin and Julienne (2005) that both scattering lengths and molecular binding energies may be extracted from rf spectra of weakly bound molecules. For a quantitative analysis, however, it is important even at the level of single molecules to properly account for the nonvanishing interaction $a_{13,23} \neq 0$ of atoms in state $|3\rangle$ with those in the initial states $|1\rangle$ and $|2\rangle$ forming the molecule (Gupta *et al.*, 2003). In the experiments of Chin *et al.* (2004), the rf spectrum exhibited a dominant free-atom peak centered at $\omega_L=\omega_{23}$ for temperatures $T \approx T_F$. At low temperatures $T \lesssim 0.2T_F$, where the gas is superfluid, an additional peak is observed, which is shifted with respect to the free transition. As shown in Fig. 35, the shift essentially follows the two-particle binding energy on the BEC side of the crossover but stays finite on the BCS side, $a<0$. In particular, the size of the shift near unitarity increases with the Fermi energy because the formation of bound pairs is a many-body effect. A theoretical analysis of these observations, which is based on an extended BCS description of pairing generalized to finite temperature within a T-matrix formalism, was given by Kinnunen *et al.* (2004), He *et al.* (2005), and Ohashi and Griffin (2005). By including the necessary average over the inhomogeneous gap parameter $\Delta(\mathbf{x})$ in a harmonic trap, reasonable agreement with the experimentally observed spectra has been obtained. An important point to realize is that strong attractive interactions near unitarity lead to an effective "pairing gap" already in the normal state above T_c. The rf shift is therefore not a direct measure

of the superfluid order parameter (Kinnunen *et al.*, 2004; He *et al.*, 2005) or the gap Δ.

The models discussed above rely on the assumption that interactions with the final state $|3\rangle$ are negligible. When this is not the case, the results can change significantly. For instance, when the interaction constants $g_{\sigma\sigma'}$ between the states $|\sigma=1,2,3\rangle$ which are involved are identical, neither mean-field ("clock") shifts nor the effects of pairing show up in the long-wavelength rf spectrum (Yu and Baym, 2006). A theory for the average frequency shift of the rf spectra of homogeneous gases at zero temperature, which takes into account both many-body correlations and the interactions with the final state $|3\rangle$, was given by Baym *et al.* (2007) and Punk and Zwerger (2007). Near $T=0$, where only a single peak is observed in the rf spectrum, its position can be determined from a sum-rule approach. Introducing the detuning $\omega=\omega_L-\omega_{23}$ of the rf field from the bare $|2\rangle$-$|3\rangle$ transition, the average clock shift

$$\hbar\bar{\omega} = \left(\frac{1}{g_{12}} - \frac{1}{g_{13}}\right) \frac{1}{n_2} \frac{\partial(-u)}{\partial g_{12}^{-1}} \tag{149}$$

can be expressed in terms of the derivative of the ground-state energy density u with respect to the inverse of the renormalized coupling constant $g_{12}=4\pi\hbar^2 a_{12}/M$ (Baym *et al.*, 2007). The expression is finite for all coupling strengths g_{12} and evolves smoothly from the BCS to the BEC limit. In particular, the average clock shift vanishes if $g_{12}=g_{13}$ (Zwierlein *et al.*, 2003a). This is directly connected with the result mentioned above, because the interaction between states $|2\rangle$ and $|3\rangle$ drops out for the average shift $\bar{\omega}$. For negligible populations of the state $|3\rangle$, $\partial(-u)/\partial g_{12}^{-1}=\hbar^4 C/M^2$ can be expressed in terms of the constant C, which characterizes the asymptotic behavior $\lim n_{\mathbf{k}}=C/k^4$ of the momentum distribution at large momenta of the crossover problem in the $|1\rangle$-$|2\rangle$ channel (Punk and Zwerger, 2007). Within an extended BCS description of the ground-state wave function, the constant $\hbar^4 C_{\text{BCS}}/M^2 \equiv \Delta^2$ is precisely the square of the gap parameter. In the BCS limit, Eq. (149) thus reproduces the weak-coupling result obtained by Yu and Baym (2006). In the BEC limit, where the BCS ground state becomes exact again, the asymptotic behavior $\Delta_{\text{BEC}}=4\varepsilon_F/\sqrt{3\pi k_F a_{12}}$ gives $\hbar\bar{\omega}=2\varepsilon_b(1-a_{12}/a_{13})$, with $\varepsilon_b=\hbar^2/Ma_{12}^2$ the two-particle binding energy. This agrees with the first moment of the spectrum of a bound-free transition in the molecular limit (Chin and Julienne, 2005). The dependence on k_F drops out, as it must. The most interesting regime is that around the unitarity point $1/g_{12}=0$, where the average rf shift is $\bar{\omega}=-0.46 v_F/a_{13}$. The prefactor is obtained from a numerical evaluation of the derivative in Eq. (149) (Baym *et al.*, 2007) or, equivalently, the constant C in the momentum distribution at the unitarity point (Punk and Zwerger, 2007) (note that the dependence $\bar{\omega}\sim -v_F/a_{13}$ at unitarity also holds in an extended BCS description; however, the numerical factor 0.56 differs from the exact value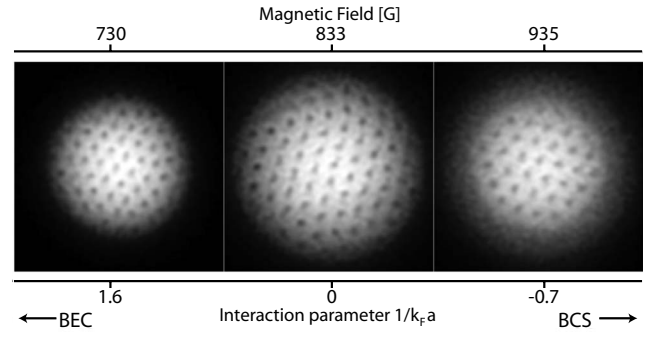). Compared with locally resolved rf spectra, which were measured by Shin *et al.* (2007), the predicted average shift in the case of ^{6}Li is almost twice the observed peak position. This is probably due to the fact that $\bar{\omega}$ has a considerable contribution from the higher-frequency part of the spectrum. An unexpected prediction of Eq. (149) is the *linear* dependence of the shift on the Fermi wave vector k_F at unitarity. Experimentally, this might be distinguished from the naive scaling proportional to ε_F by spatially resolved rf spectra (Shin *et al.*, 2007).

FIG. 36. Vortex lattice in a rotating gas of ^{6}Li precisely at the Feshbach resonance and on the BEC and BCS side. From Zwierlein *et al.*, 2005.

Vortices. As noted above, the appearance of shifts in the rf spectrum is not a proof of superfluidity. Indeed, pairing effects appear in the normal state above T_c as a precursor to superfluidity, or may be present even at zero temperature in unbalanced Fermi gases above the Clogston-Chandrasekhar limit, as observed by Schunck *et al.* (2007). Beyond the evidence for superfluidity from the collective mode frequencies (Bartenstein *et al.*, 2004b; Kinast *et al.*, 2004) a crucial step which verifies the existence of a fermionic superfluid, was the observation of triangular vortex lattices in rotating Fermi gases near unitarity by Zwierlein *et al.* (2005) (see Fig. 36). Vortex lattices require conservation of vorticity, which is a consequence of superfluid hydrodynamics. The regularity of the lattice shows that all vortices have the same vorticity. Since it is a superfluid of fermionic *pairs*, the expected circulation per vortex is $h/2M$. This is indeed the value found from equating the total circulation at a given stirring frequency with the number of vortices and the transverse area of the cloud.

IX. PERSPECTIVES

Cold atoms provide a novel tool for studying the physics of strong correlations in a widely tunable range and in unprecedentedly clean sytems. Basic models in many-body physics, such as the Hubbard model with on-site interaction or the Haldane pseudopotentials for physics in the lowest Landau level, which were originally introduced in a condensed-matter context as idealized descriptions of strong-correlation effects in real materials, can now be applied on a quantitative level. In the following, an outline of possible future directions is given.

A. Quantum magnetism

One of the major challenges with ultracold atoms in optical lattices in the near future lies in the realization and study of configurations that can serve as tunable model systems for basic problems in quantum magnetism. For two-component mixtures of bosonic or fermionic atoms in an optical lattice that are labeled by a pseudospin variable $|\uparrow\rangle, |\downarrow\rangle$ and dominating interactions $U \gg J$ between them, second-order perturbation theory in the kinetic energy term allows one to map the corresponding (Bose-)Hubbard Hamiltonian to an anisotropic Heisenberg model (XXZ model) with effective spin-spin interactions between atoms on neighboring lattice sites,

$$\sum_{\mathbf{R},\mathbf{R}'} [J_{\mathrm{ex}}^z S_{\mathbf{R}}^z S_{\mathbf{R}'}^z \pm J_{\mathrm{ex}}^\perp (S_{\mathbf{R}}^x S_{\mathbf{R}'}^x + S_{\mathbf{R}}^y S_{\mathbf{R}'}^y)], \qquad (150)$$

where the $+$ $(-)$ sign holds for the case of fermions or bosons, respectively (Duan *et al.*, 2003; Kuklov and Svistunov, 2003). By tuning the exchange terms $J_{\mathrm{ex}}^z = 2(J_\uparrow^2 + J_\downarrow^2)/U_{\uparrow\downarrow} - 4J_\uparrow^2/U_{\uparrow\uparrow} - 4J_\downarrow^2/U_{\downarrow\downarrow}$ and $J_{\mathrm{ex}}^\perp = 4J_\uparrow J_\downarrow/U_{\uparrow\downarrow}$ via spin-dependent tunneling amplitudes or spin-dependent interactions, one can change between various quantum phases. One possibility, pointed out by Kuklov and Svistunov (2003), is the realization of supercounterflow, i.e., superfluidity in the relative motion of the two components, while the system is a Mott insulator as far as the total density is concerned. Another possibility is the formation of topological quantum phases, arising for different exchange couplings along different lattice directions (Kitaev, 2006), which can be realized with optical lattices (Duan *et al.*, 2003). The most natural case occurs, however, for equal tunneling amplitudes and on-site interactions. It yields an isotropic Heisenberg-type spin Hamiltonian

$$H = J_{\mathrm{ex}} \sum_{\mathbf{R},\mathbf{R}'} \mathbf{S}_{\mathbf{R}} \cdot \mathbf{S}_{\mathbf{R}'}. \qquad (151)$$

Here the superexchange coupling $J_{\mathrm{ex}} = \pm 4J^2/U_{\uparrow\downarrow}$ has a positive (negative) sign for the case of fermions (bosons) and thus favors antiferromagnetically (ferromagnetically) ordered phases. In the case of fermions, it can easily be understood why the antiferromagnetically ordered phase is preferred: an initial spin-triplet state cannot lower its energy via second-order hopping processes, as the two spins pointing in the same direction can never be placed on a single lattice site. The spin-singlet term, however, is not subject to this restriction and can lower its energy via a second-order exchange hopping process (Auerbach, 2006). Recently, the tunneling dynamics based on second-order hopping events was observed in an array of tightly confining double wells (Fölling *et al.*, 2007). Remarkably, the observed second-order coupling strengths $\sim J^2/hU$ can be almost on the order of 1 kHz and thus three to four orders of magnitude larger than the direct magnetic dipole interaction between two alkali-metal atoms on neighboring lattice sites.

Observation of such magnetically ordered quantum phases requires reaching very low temperatures $k_B T$ $< 4J^2/U$ (for $J/U \ll 1$) in the experiment. Werner *et al.* (2005) have shown that such temperatures could be within reach experimentally, as a Pomeranchuk-type cooling effect during the loading of atoms in the lattice assists in a cooling of atoms. In particular, it turns out that, for an initial temperature of a homogeneous two-component Fermi gas below $T/T_F \simeq 0.08$, an antiferromagnetically ordered phase could be reached at unit filling, when the optical lattice potential is ramped up adiabatically. A more robust implementation of spin Hamiltonians might be reached via ground-state polar molecules, which have much larger spin-spin coupling strengths (Micheli *et al.*, 2006). Such nearest-neighbor spin interactions are mediated via a long-range electric dipole-dipole interaction between the molecules. Several experimental groups are currently pursuing the goal of creating such ground-state polar molecules out of ultracold atoms via Feshbach sweeps (Ospelkaus *et al.*, 2006, 2008) and subsequent photoassociation, or by directly slowing and sympathetically cooling stable polar molecules. Noise correlation or Bragg spectroscopy might allow one to uniquely identify such antiferromagnetically ordered phases.

From a condensed-matter point of view, one of the most challenging problems is the realization and study of the fermionic repulsive Hubbard model in an optical lattice with adjustable interactions and filling fraction, in particular in 2D. As discussed by Hofstetter *et al.* (2002), such a system would constitute a cold atom version of one of the most intensely studied models in condensed-matter physics. It allows one to access unconventional normal and d-wave superconducting phases as found in high-temperature superconductors (Lee *et al.*, 2006). Of course, realization of these models with cold atoms would not solve the latter problem; however, it would be an extremely valuable tool to test some of the still open issues in this field. In this context, specific proposals have been made for realizing so-called resonating valence bond states by adiabatically transforming spin patterns in optical superlattices (Trebst *et al.*, 2006). More complex spin-liquid states might be created by enforcing "frustration" in antiferromagnetically ordered phases through triangular or Kagome-type lattices (Santos *et al.*, 2004). For a review of these models, see Lewenstein *et al.* (2007).

Quantum impurity problems, which have played an important role in the study of magnetism, may be realized in the cold atom context by confining single atoms in a tight optical trap or in a deep optical lattice. For hard-core bosons or fermions, the effective pseudospin one-half associated with the possible local occupation numbers $n = 0, 1$ can be coupled to a reservoir of either a BEC or a degenerate Fermi gas, using Raman transitions (Recati *et al.*, 2005).

B. Disorder

It was noted by Anderson (1958a) that waves in a medium with a static ("quenched") randomness may become localized due to constructive interference between

multiply reflected waves. Qualitatively, this happens below a "mobility edge," where the mean free path ℓ (calculated, e.g., in a Born approximation treatment of the scattering by the disorder potential) becomes smaller than the wavelength λ. This so-called Ioffe-Regel criterion applies in a 3D situation with short-range disorder and in the absence of interactions.[26] In the interacting case, in which localization due to both disorder (Anderson) and interactions (Mott) is possible, the problem is still not well understood [see, e.g., Belitz and Kirkpatrick (1994) and Basko *et al.* (2006)]. Cold atoms thus provide a novel tool to investigate the localization problem, in particular since interactions are tunable over a wide range.

For noninteracting bosons, the ground state in the presence of disorder is obtained by putting all particles in the lowest single-particle level of the random potential. On adding weak repulsive interactions, a finite number of localized states in the so-called Lifschitz tails of the single-particle spectrum (Lifschitz *et al.*, 1988) will be occupied. As long as the chemical potential is in this low-energy range, these states have negligible spatial overlap. For very low densities, repulsive bosons are therefore expected to form a "Lifshitz glass" of fragmented, local condensates (Lugan *et al.*, 2007). With increasing densities, these local condensates will be coupled by Josephson tunneling and eventually form a superfluid, where coherence is established over the whole sample. A quantitative analysis of this transition was first given by Giamarchi and Schulz (1988) in the particular case of one dimension. Using a quantum hydrodynamic Luttinger-liquid description, they found that weak interaction tends to suppress the effect of Anderson localization. This effect also appears for a commensurate filling in an optical lattice; see Rapsch *et al.* (1999). Specifically, weak disorder does not destroy the superfluid, provided the Luttinger exponent K introduced in Sec. V.B is larger than $3/2$. Within the Lieb-Liniger model with an effective coupling constant γ defined in Eq. (88), this requires $\gamma \lesssim 8$. In the opposite regime $K < 3/2$ of low densities or strong interactions near the Tonks-Girardeau limit, even weak disorder destroys the superfluid. The ground state then lacks long-range phase coherence, consistent with the Lifshitz glass discussed above. Exact results for the momentum distribution and the local density of states have been obtained by DeMartino *et al.* (2005) in the special limit of the Tonks-Girardeau gas, where the problem is equivalent to noninteracting fermions (see Sec. V.B). Interacting bosons in higher dimensions were studied by Fisher *et al.* (1989) using the Bose-Hubbard model Eq. (65). To account for disorder, the on-site energies $\epsilon_{\mathbf{R}}$ are assumed to have a random component, with zero average and finite variance

$$\langle(\epsilon_{\mathbf{R}} - \langle\epsilon_{\mathbf{R}}\rangle)(\epsilon_{\mathbf{R}'} - \langle\epsilon_{\mathbf{R}'}\rangle)\rangle = \Delta\delta_{\mathbf{R},\mathbf{R}'}, \qquad (152)$$

where Δ is a measure of the strength of the disorder. It has been shown by Fisher *et al.* (1989) that, even at weak disorder $\Delta < U/2$, a novel so-called Bose glass phase appears, which separates the SF and MI states.[27] At strong disorder $\Delta > U/2$, the MI states are destroyed completely. The Bose glass is characterized by a vanishing superfluid and condensate density. It will thus show no sharp interference peaks in a time-of-flight experiment after release from an optical lattice (see Sec. IV.B). In contrast to the MI phase, the Bose glass has both a finite compressibility (i.e., there is no shell structure in a trap) and a continuous excitation spectrum.

A concrete proposal for studying localization effects with cold atoms was made by Damski *et al.* (2003), who suggested using laser speckle patterns as a means to realize frozen disorder. Such patterns have been employed by groups in Florence (Lye *et al.*, 2005) and Orsay (Clément *et al.*, 2005). They are produced by a laser beam that is scattered from a ground glass diffuser (Clément *et al.*, 2006). The speckle pattern has a random intensity I, which is exponentially distributed $P(I) \sim \exp(-I/\langle I\rangle)$. The rms intensity fluctuation σ_I is thus equal to the average intensity $\langle I\rangle$. Fluctuations in the intensity give rise to a random value of the optical dipole potential in Eq. (31), which is experienced by the atoms. An important parameter characterizing the speckle pattern is the spatial correlation length σ_R, which is the scale over which $\langle I(\mathbf{x})I(0)\rangle$ decays to $\langle I\rangle^2$. When the optical setup is diffraction limited, the smallest achievable σ_R's can take values down to 1 μm (Clément *et al.*, 2006), which is comparable to typical healing lengths ξ in dilute gases. Reaching this limit is important, since smooth disorder potentials with $\sigma_R \gg \xi$ are not suitable to study Anderson localization in expanding BEC's. Indeed, the typical range of momenta after expansion reaches up to $k_{\max} \approx 1/\xi$. For $\sigma_R \gg \xi$, therefore, the spectral range of the disorder is much smaller than the momenta of matter waves. Even speckle patterns with long correlation lengths, however, can lead to a strong suppression of the axial expansion of an elongated BEC. This was observed experimentally by Clément *et al.* (2005), Fort *et al.* (2005), and Schulte *et al.* (2005). The effect is not due to Anderson localization, however. Instead, it is caused by classical total reflection, because during expansion the density and chemical potential of the gas decrease. Eventually, therefore, matter waves have energies below the typical disorder potentials and the gas undergoes fragmentation. A suggestion for realizing Anderson localization of noninteracting particles in 1D has recently been made by Sanchez-Palencia *et al.* (2007). It is based on a 1D BEC, which after expansion is transformed into a distribution of free matter waves with momenta up to $1/\xi$. For short-range disorder with $\sigma_R < \xi$, these waves will all be localized, even for quite weak disorder.

---

[26]In 1D and 2D, arbitrary weak disorder leads to localization, i.e., even waves with $\lambda \ll \ell$ are localized.

[27]The Lifshitz glass may be thought of as the low-density or strong-disorder limit of the Bose glass.

A rather direct approach to study the interplay between disorder and strong interactions makes use of bichromatic optical lattices (Fallani *et al.*, 2007). Such lattices provide a pseudorandom potential if the lattice periods are incommensurate. On adding the incommensurate lattice in the superfluid state, strong suppression of the interference pattern is found. Starting from a MI phase, the sharp excitation spectrum is smeared out with increasing amplitude of the incommensurate lattice. Both observations are consistent with the presence of a Bose glass phase for a strong incommensurate lattice potential (Fallani *et al.*, 2007). A different method for realizing short-range disorder in cold gases was suggested by Gavish and Castin (2005). It employs a two-species mixture of atoms in an optical lattice. Because of a finite interspecies scattering length, the component that is free to move around in the lattice experiences an on-site random potential of the type (152), provided atoms of the different species or spin state are frozen at random sites. The interplay between disorder and interactions is, of course, also an intriguing problem for fermions. A quantitative phase diagram for short-range disorder plus repulsive interactions has been determined by Byczuk *et al.* (2005). So far, however, no experiments have been done in this direction.

C. Nonequilibrium dynamics

A unique feature of many-body physics with cold atoms is the possibility to modify both the interactions and external potentials dynamically. In the context of the SF-MI transition, this has been discussed in Sec. IV.C. Below, we give an outline of recent developments in this area.

The basic question about the efficiency of collisions in establishing a new equilibrium from an initial out-of-equilibrium state was adressed by Kinoshita *et al.* (2006) for Bose gases in one dimension. An array of several thousand 1D tubes created by a strong 2D optical lattice (see Sec. V.B) was subject to a pulsed optical lattice along the axial direction. The zero-momentum state is depleted and essentially all atoms are transferred to momenta $\pm 2\hbar k$, where k is the wave vector of the pulsed axial optical lattice. The two wave packets in each tube separate and then recollide again after a time π/ω_0, which is half the oscillation period in the harmonic axial trap with frequency ω_0. The associated collision energy $(2\hbar k)^2/M$ was around $0.45\hbar\omega_\perp$, i.e., much smaller than the minimum energy $2\hbar\omega_\perp$ necessary to excite higher transverse modes. The system thus remains strictly 1D during its time evolution. It was found that, even after several hundred oscillation periods, the initial nonequilibrium momentum distribution was preserved.

This striking observation raises a number of questions. Specifically, is the absence of a broadening of the momentum distribution connected with the integrability of the 1D Bose gas? More generally, one can ask whether, and under what conditions, the unitary time evolution of a nonequilibrium initial state in a strongly interacting but nonintegrable quantum system will evolve into a state in which at least one- and two-particle correlations are stationary and the information about the precise initial conditions is hidden in some—in practice unobservable—high-order correlations. The nonequilibrium dynamics for the integrable case of bosons in 1D was addressed recently by Rigol *et al.* (2007). Taking as a model a Tonks-Girardeau gas on a lattice, they showed numerically that the momentum distribution at large times is well described by that of an equilibrium state with a density matrix of the form $\hat\rho \sim \exp(-\Sigma_m\lambda_m\hat A_m)$. Here $\hat A_m$ denote the full set of conserved quantities, which are known explicitly for the Tonks-Girardeau gas because it is equivalent to free fermions. The Lagrange multipliers λ_m are fixed by the initial conditions of given expectation values $\langle \hat A_m\rangle$ at $t=0$. This is the standard procedure in statistical physics, where equilibrium is described microscopically as a state of maximum entropy consistent with the given "macroscopic" data $\langle \hat A_m\rangle$ (Balian, 1991). In particular, an initially double-peaked momentum distribution is preserved in the stationary state described by the maximum entropy density operator $\hat\rho$ (Rigol *et al.*, 2007). The hypothesis that the absence of momentum relaxation is related to the integrability of the 1D Bose gas could be tested by going to higher momenta k, where the 1D scattering amplitude is no longer given by the low-energy form of Eq. (85). For such a case, the pseudopotential approximation breaks down and three-body collisions or longer-ranged interactions can become relevant. For the extreme case of two free 3D colliding BECs, equilibration has indeed been observed to set in after a few collisions (Kinoshita *et al.*, 2006).

In nonintegrable systems like the 1D Bose-Hubbard model, where no conserved quantities exist beyond the energy, the standard reasoning of statistical physics gives rise to a microcanonical density operator, whose equivalent "temperature" is set by the energy of the initial state.[28] Note that the microstate $\exp(-i\hat Ht/\hbar)|\psi(0)\rangle$, which evolves from the initial state by the unitary time evolution of a closed system, remains time dependent. Its statistical (von Neumann) entropy vanishes. By contrast, the microcanonical density operator describes a stationary situation, with a nonzero *thermodynamic* entropy. It is determined by the number of energy eigenstates near the exact initial energy that are accessible in an energy range much smaller than the microscopic scale set by the one-or two-body terms in the Hamiltonian but much larger that the inverse of the recurrence time. For 1D problems, the hypothesis that simple macroscopic observables are eventually well described by such a stationary density operator can be tested quantitatively using the adaptive time-dependent density-matrix renormalization group (Daley *et al.*, 2004; White and Feiguin, 2004). In the case of the 1D BHM, an

---

[28]In the semiclassical limit, this eigenstate thermalization hypothesis can be derived under relatively weak assumptions, see Srednicki (1994).

effectively "thermal" stationary state arises for long time dynamics after a quench from the SF to the MI (Kollath *et al.*, 2007) (see Sec. IV.C). Apparently, however, the description by a stationary thermal density operator is valid only for not too large values of the final repulsion U_f.

A different aspect of the nonequilibrium dynamics of 1D Bose gases was studied by Hofferberth *et al.* (2007). A single 1D condensate formed in a magnetic microtrap on an atom chip (Folman *et al.*, 2002) is split into two parts by applying rf potentials (Schumm *et al.*, 2005) The splitting process is done in a phase-coherent manner, such that at time $t=0$ the two condensates have a vanishing relative phase. They are kept in a double-well potential for a time t and then released from the trap. As discussed in Sec. III.C, the resulting interference pattern provides information about the statistics of the interference amplitude. In the nonequilibrium situation discussed here, the relevant observable analogous to Eq. (62) is the operator $\exp[i\hat{\theta}(z,t)]$ integrated along the axial z direction of the two condensates. Here $\hat{\theta}(z,t)$ is the time-dependent phase *difference* between the two independently fluctuating condensates. Using the quantum hydrodynamic Hamiltonian Eq. (91), it has been shown by Burkov *et al.* (2007) that the expectation value of this operator decays subexponentially for large times $t \gg \hbar/k_B T$ where phase fluctuations can be described classically. This behavior is in good agreement with experiments (Hofferberth *et al.*, 2007). In particular, it allows one to determine the temperature of the 1D gas precisely.

The dynamics of the superfluid gap parameter in attractive Fermi gases after a sudden change of the coupling constant was investigated by Barankov *et al.* (2004), Barankov and Levitov (2006), and Yuzbashyan *et al.* (2006) using the exactly integrable BCS Hamiltonian. Such changes in the coupling constant are experimentally feasible by simply changing the magnetic field in a Feshbach resonance. Depending on the initial conditions, different regimes have been found where the gap parameter may oscillate without damping, approaches an "equilibrium" value different from that associated with the coupling constant after the quench, or decays to zero monotonically if the coupling constant is reduced to very small values.

ACKNOWLEDGMENTS

APPENDIX: BEC AND SUPERFLUIDITY

Following the early suggestion of London that superfluidity (SF) in ^{4}He has its origin in Bose-Einstein condensation (BEC), the relation between both phenomena has been a subject of considerable debate. In the following, we outline their basic definitions and show that SF is the more general phenomenon, which is both necessary and sufficient for the existence of either standard BEC or of quasicondensates in low-dimensional systems. For a further discussion of the connections between BEC and superfluidity, see Leggett (2006).

The definition of BEC in an interacting system of bosons is based on the properties of the one-particle density matrix $\hat{\rho}_1$, which is defined by its matrix elements

$$G^{(1)}(\mathbf{x},\mathbf{x}') = \langle \mathbf{x}'|\hat{\rho}_1|\mathbf{x}\rangle = \langle \hat{\psi}^\dagger(\mathbf{x})\hat{\psi}(\mathbf{x}')\rangle \quad \text{(A1)}$$

in position space.[29] As a Hermitian operator with $\text{Tr}\,\hat{\rho}_1 = \int n(\mathbf{x}) = N$, $\hat{\rho}_1$ has a complete set $|n\rangle$ of eigenstates with positive eigenvalues $\lambda_n^{(1)}$ which sum up to N. As realized by Penrose and Onsager (1956), the criterion for BEC is that there is precisely one eigenvalue $\lambda_0^{(1)} = N_0$ of order N while all other eigenvalues are nonextensive.[30] The separation between extensive and nonextensive eigenvalues $\lambda_n^{(1)}$ is well defined only in the thermodynamic limit $N \to \infty$. In practice, however, the distinction between the BEC and the normal phase above T_c is rather sharp even for the typical particle numbers $N \approx 10^4 - 10^7$ of cold atoms in a trap. This is true in spite of the fact that the nonextensive eigenvalues are still rather large (see below). The macroscopic eigenvalue N_0 determines the number of particles in the condensate. In terms of the single-particle eigenfunctions $\varphi_n(\mathbf{x}) = \langle \mathbf{x}|n\rangle$ associated with the eigenstates $|n\rangle$ of $\hat{\rho}_1$, the existence of a condensate is equivalent to a macroscopic occupation of a single state created by the operator $\hat{b}_0^\dagger = \int \varphi_0(\mathbf{x})\hat{\psi}^\dagger(\mathbf{x})$. In a translation invariant situation, the eigenfunctions are plane waves. The eigenvalues $\lambda_k^{(1)}$ then coincide with the occupation numbers $\langle \hat{b}_k^\dagger \hat{b}_k\rangle$ in momentum space. In the thermodynamic limit $N, V \to \infty$ at constant density n, the one-particle density matrix

$$\langle \mathbf{x}'|\hat{\rho}_1|\mathbf{x}\rangle = n_0 + \int_k \tilde{n}(\mathbf{k})e^{-i\mathbf{k}\cdot(\mathbf{x}-\mathbf{x}')} \to n_0 \quad \text{(A2)}$$

approaches a finite value $n_0 = \lim N_0/V$ as $r = |\mathbf{x}-\mathbf{x}'| \to \infty$. This property is called off-diagonal long-range order (ODLRO). Physically, the existence of ODLRO implies that the states in which a boson is removed from an

---

[29]In an inhomogeneous situation, it is convenient to define a reduced one-particle density matrix $g^{(1)}$ by $G^{(1)}(\mathbf{x},\mathbf{x}') = \sqrt{n(\mathbf{x})n(\mathbf{x}')}g^{(1)}(\mathbf{x},\mathbf{x}')$.

[30]In principle, it is also possible that more than one eigenvalue is extensive. This leads to so-called fragmented BEC's which may appear, e.g., in multicomponent spinor condensates as shown by Ho (1998).

N-particle system at positions $\mathbf{x}$ and $\mathbf{x}'$ have a finite over-lap even in the limit when the separation between two points is taken to infinity.[31] For cold gases, the presence of ODLRO below T_c, at least over a scale of the order of micrometers, was observed experimentally by measuring the decay of the interference contrast between atomic beams outcoupled from two points at a distance r from a BEC in a trap (Bloch *et al.*, 2000). The momentum distribution $\tilde{n}(\mathbf{k})$ of noncondensate particles is singular at small momenta. In the limit $\mathbf{k} \rightarrow \mathbf{0}$, it behaves like $\tilde{n}(\mathbf{k}) \sim c/k$ at zero and $\tilde{n}(\mathbf{k}) \sim T/k^2$ at finite temperature, respectively (Lifshitz and Pitaevskii, 1980). Since $k_{\min} \sim N^{-1/3}$ in a finite system, the lowest nonextensive eigenvalues of the one-particle density matrix are still very large, scaling like $\lambda_n^{(1)} \sim N^{1/3}$ at zero and $\lambda_n^{(1)} \sim N^{2/3}$ at finite temperature.

The definition of BEC via the existence of ODLRO (A2) is closely related with Feynman's intuitive picture of Bose-Einstein condensation as a transition, below which bosons are involved in exchange cycles of infinite size (Feynman, 1953). In fact, a precise connection exists with the superfluid density defined in Eq. (A4) below, which can be expressed in terms of the square of the winding number in a Feynman path representation of the equilibrium density matrix (Pollock and Ceperley, 1987). As discussed by Ceperley (1995) and Holzmann and Krauth (1999), the connection between the *condensate* density and infinite cycles is also suggestive in terms of the path-integral representation of the one-particle density matrix. It is difficult, however, to put this on a rigorous footing beyond the simple case of an ideal Bose gas (Ueltschi, 2006; Chevallier and Krauth, 2007).

While a microscopic definition of BEC is straightforward, at least in principle, the notion of superfluidity is more subtle. On a phenomenological level, the basic properties of superfluids may be explained by introducing a complex order parameter $\psi(\mathbf{x}) = |\psi(\mathbf{x})| \exp i\phi(\mathbf{x})$, whose magnitude squared gives the superfluid density n_s, while the phase $\phi(\mathbf{x})$ determines the superfluid velocity via $\mathbf{v}_s = (\hbar/M) \nabla \phi(\mathbf{x})$ (Pitaevskii and Stringari, 2003). The latter equation immediately implies that superfluid flow is irrotational and that the circulation $\Gamma = \oint \mathbf{v}_s d\mathbf{s}$ is quantized in an integer number of circulation quanta h/M. Note that these conclusions require a finite value $n_s \neq 0$, yet are independent of its magnitude. In order to connect this phenomenological picture of SF with the microscopic definition of BEC, the most obvious assumption is to identify the order parameter $\psi(\mathbf{x})$ with the eigenfunction $\varphi_0(\mathbf{x})$ of $\hat{\rho}_1$ associated with the single extensive eigenvalue, usually choosing a normalization such that $\psi(\mathbf{x}) = \sqrt{N_0}\varphi_0(\mathbf{x})$. Within this assumption, BEC and SF appear as essentially identical phenomena. This simple identification is not valid, however, beyond a Gross-Pitaevskii description or for low-dimensional sys-

tems. The basic idea of how to define superfluidity in general terms goes back to Fisher *et al.* (1973) and Leggett (1973). It is based on considering the sensitivity of the many-body wave function with respect to a change in the boundary condition (bc). Specifically, consider N bosons in a volume $V = L^3$ and choose boundary conditions where the many-body wave function

$$\Psi_\Theta(\mathbf{x}_1, \mathbf{x}_2, \ldots, \mathbf{x}_i, \ldots, \mathbf{x}_N) \qquad (A3)$$

is multiplied by a pure phase factor $e^{i\Theta}$ if $\mathbf{x}_i \rightarrow \mathbf{x}_i + L\mathbf{e}$ for all $i = 1, \ldots, N$ and with $\mathbf{e}$ a unit vector in one of the directions.[32] The dependence of the many-body energy eigenvalues $E_n(\Theta)$ on Θ leads to a phase-dependent equilibrium free energy $F(\Theta)$. The difference $\Delta F(\Theta) = F(\Theta) - F(\Theta = 0)$ is thus a measure for the sensitivity of the many-body system in a thermal equilibrium state to a change in the bc's. Since the eigenstates of a time reversal invariant Hamiltonian can always be chosen real, the energies $E_n(\Theta)$ and the resulting $\Delta F(\Theta)$ must be even in Θ. For small deviations $\Theta \ll 1$ from periodic bc's, the expected leading behavior is therefore quadratic. The superfluid density $n_s(T)$ is then defined by the free-energy difference per volume,

$$\Delta F(\Theta)/V = (\hbar^2/2M)n_s(T)(\Theta/L)^2 + \cdots, \qquad (A4)$$

to leading order in Θ. In a superfluid, therefore, a small change in the bc's leads to a change in the free energy per volume, which scales like $\gamma/2(\Theta/L)^2$. The associated proportionality constant $\gamma = \hbar^2 n_s/M$ is the helicity modulus. The definition (A4) for superfluidity, which is based only on equilibrium properties and also applies to finite systems, is quite different from that for the existence of BEC. Yet it turns out that the two phenomena are intimately connected in the sense that a finite superfluid density is both necessary and sufficient for either standard BEC or the existence of quasicondensates in lower dimensions.

Following Leggett (1973), the physical meaning of the phase Θ and the associated definition of n_s can be understood by considering bosons (gas or liquid) in a superfluid state, which are enclosed between two concentric cylinders with almost equal radii R, corotating with an angular frequency $\Omega = \Omega \mathbf{e}_z$.[33] In the rotating frame, the problem is stationary, however it acquires an effective gauge potential $A = M\Omega \wedge \mathbf{x}$, as shown in Eq. (113). Formally, A can be eliminated by a gauge transformation at the expense of a many-body wave function, which is no longer single valued. It changes by a factor $e^{i\Theta}$ under changes $\theta_i \rightarrow \theta_i + 2\pi$ of the angular coordinate of each particle i, precisely as in Eq. (A3), where $\Theta = -2\pi MR^2\Omega/\hbar$ is linear in the angular frequency. The presence of a phase-dependent free-

---

[31]For a discussion on the topological properties of the many-body wave function that are required to give ODLRO, see Leggett (1973).

---

[32]For simplicity, we assume isotropy in space. More generally, the sensitivity with respect to changes in the bc's may depend on the direction, in which case the superfluid density becomes a tensor.

[33]The walls are assumed to violate perfect cylindrical symmetry to allow for the transfer of angular momentum to the fluid.

energy increase $\Delta F(\Theta)$ of the superfluid in the rotating frame implies that the equilibrium state in this frame carries a nonzero (kinematic) angular momentum L_z' $=-\partial\Delta F(\Theta)/\partial\Omega=-(n_s/n)L_z^{(0)}$, where $L_z^{(0)}=I_{cl}\Omega$ is the rigid-body angular momentum in the lab frame and I_{cl} $=NMR^2$ is the classical moment of inertia. A fraction n_s/n of the superfluid thus appears to stay at rest in the lab frame for small angular frequencies $\Omega\ll\hbar/MR^2$, where $\Theta\ll1$. As a result, the apparent moment of inertia is smaller than that of classical rigid-body-like rotation. Superfluidity, as defined by Eq. (A4), implies the appearance of nonclassical rotational inertia (NCRI) (Leggett, 1973). In the context of cold gases, this phenomenon has been observed experimentally by Madison *et al.* (2000). They have shown that a trapped gas in the presence of a small, nonsymmetric perturbation remains at zero angular momentum (i.e., no vortex enters) for sufficiently small angular frequencies.

The example of a rotating system shows that a finite value of Θ is associated with a nonvanishing current in the system. Indeed, a finite superfluid density in the sense of Eq. (A4) implies the existence of long-range current-current correlations, which is the original microscopic definition of n_s by Hohenberg and Martin (1965). To describe states of a superfluid with finite currents, it is useful to introduce a smoothly varying local phase $\phi(\mathbf{x})$ on scales much larger than the interparticle spacing, which is connected with the total phase difference between two arbitrary points by $\Theta=\int d\mathbf{s}\cdot\boldsymbol{\nabla}\phi(\mathbf{x})$. This local phase variable is now precisely the phase of the coarse-grained complex order parameter $\psi(\mathbf{x})$ introduced by Landau. This identification becomes evident by noting that a nonvanishing phase gradient gives rise to a finite superfluid velocity $\mathbf{v}_s=(\hbar/M)\boldsymbol{\nabla}\phi(\mathbf{x})$. The free-energy increase

$$\Delta F(\Theta) = \frac{\gamma(T)}{2}\int d^3x[\boldsymbol{\nabla}\phi(\mathbf{x})]^2 \quad (A5)$$

associated with a change in the boundary conditions is therefore the kinetic energy $(M/2)\int n_s(\mathbf{v}_s)^2$ of superfluid flow with velocity $\mathbf{v}_s$ and density n_s. An immediate consequence of Eq. (A5) is the quite general form of the excitation spectrum of superfluids at low energies. Indeed, considering the fact that phase and particle number are conjugate variables, the operator $\delta\hat{n}(\mathbf{x})$ for small fluctuations of the density obeys the canonical commutation relation $[\delta\hat{n}(\mathbf{x}),\hat{\phi}(\mathbf{x}')]=i\delta(\mathbf{x}-\mathbf{x}')$ with the quantized phase operator $\hat{\phi}(\mathbf{x})$. For any Bose gas (or liquid) with a finite compressibility $\kappa=\partial n/\partial\mu\neq0$ at zero temperature,[34] the energy of small density fluctuations is $\int[\delta n(\mathbf{x})]^2/2\kappa$. Combining this with Eq. (A5), the effective Hamiltonian for low-lying excitations of an arbitrary superfluid is of the quantum hydrodynamic form

$$\hat{H} = \int d^3x\left(\frac{\hbar^2 n_s}{2M}[\boldsymbol{\nabla}\hat{\phi}(\mathbf{x})]^2 + \frac{1}{2\kappa}[\delta\hat{n}(\mathbf{x})]^2\right). \quad (A6)$$

This Hamiltonian describes harmonic phonons with a linear spectrum $\omega=cq$ and a velocity that is determined by $Mc^2=n_s/\kappa$. In a translation invariant situation, where $n_s(T=0)\equiv n$, this velocity coincides with that of a standard (first sound) compression mode in a gas or liquid. This coincidence is misleading, however, since Eq. (A6) describes true elementary excitations and not a hydrodynamic, collision-dominated mode. States with a single phonon are thus exact low-lying eigenstates of the strongly interacting many-body system, whose ground state exhibits the property (A4). As the Lieb-Liniger solution of a 1D Bose gas shows, this mode exists even in the absence of BEC. It only requires a finite value of the superfluid density, as specified by Eq. (A4). A mode of this type will therefore be present in the SF phase of bosons in an optical lattice in any dimension and also in the presence of a finite disorder, as long as the superfluid density is nonvanishing.

The connection between SF and BEC now follows from the macroscopic representation (Popov, 1983)

$$\hat{\psi}(\mathbf{x}) = \exp[i\hat{\phi}(\mathbf{x})][n + \delta\hat{n}(\mathbf{x})]^{1/2} \approx \sqrt{\tilde{n}_0}\exp[i\hat{\phi}(\mathbf{x})] \quad (A7)$$

of the Bose field in terms of density and phase operators. The parameter $\tilde{n}_0$ is a quasicondensate density. Its existence relies on the assumption that there is a broad range $\xi\ll|\mathbf{x}|\ll\ell_\phi$ of intermediate distances, where the one-particle density matrix is equal to a finite value $\tilde{n}_0$ $<n$,[35] beyond which only phase fluctuations contribute. Using the harmonic Hamiltonian Eq. (A6), the asymptotic decay of $G^{(1)}(\mathbf{x})=\tilde{n}_0\exp[-\delta\phi^2(\mathbf{x})/2]$ at large separations is determined by the mean-square fluctuations

$$\delta\phi^2(\mathbf{x}) = \frac{1}{\hbar\kappa}\int\frac{d^dq}{(2\pi)^d}\frac{1-\cos\mathbf{q}\cdot\mathbf{x}}{cq}\coth\left(\frac{\hbar cq}{2k_BT}\right) \quad (A8)$$

of the phase difference between points separated by $\mathbf{x}$. Equation (A7) and the notion of a quasicondensate require the existence of a finite superfluid density at least at $T=0$, but not that of BEC. From Eq. (A8), it is straightforward to see that plain BEC in the sense of a nonvanishing condensate density $n_0=\tilde{n}_0$ $\times\exp-[\delta\phi^2(\infty)/2]$ at nonzero temperatures only exists in 3D. In two dimensions, the logarithmic divergence of $\delta\phi^2(\mathbf{x})\to2\eta\ln|\mathbf{x}|$ at large distances leads to an algebraic decay $g^{(1)}(\mathbf{x})\sim|\mathbf{x}|^{-\eta}$, consistent with the Mermin-Wagner-Hohenberg theorem. Since $\kappa c^2=n_s(T)/M$, the exponent $\eta(T)=[n_s(T)\lambda_T^2]^{-1}$ is related to the exact value of the superfluid density as pointed out in Eq. (100). A similar behavior, due to quantum rather than thermal

---

[34]This condition rules out the singular case of an ideal Bose gas, where $\kappa=\infty$ and thus $c=0$. The ideal gas is therefore not a SF, even though it has a finite superfluid density that coincides with the condensate density (Fisher *et al.*, 1973).

[35]The short-range decay from $G^{(1)}(\mathbf{0})=n$ to $\tilde{n}_0$ is due fluctuations at scales smaller than ξ, which require a microscopic calculation. The integral (A8) is therefore cutoff at $q_{max}\approx1/\xi$.

phase fluctuations, applies in 1D at zero temperature; see Sec. V.B.

The arguments above show that SF in the sense of Eq. (A4) plus the assumption of a finite compressibility κ are sufficient conditions for either plain BEC in 3D or the existence of quasicondensates in 2D at finite and in 1D at zero temperature.[36] For the reverse question, whether SF is also *necessary* for the existence of BEC, the answer is again yes, in the general sense that BEC is replaced by quasicondensates in low dimensions. Indeed, for a translation invariant system, Leggett (1998) has shown that the existence of ODLRO in the ground state with an arbitrary small condensate fraction n_0/n implies perfect superfluidity $n_s(T=0) \equiv n$ at zero temperature. Note that this includes the case of 2D gases, where only a quasi-condensate survives at nonzero temperature. In 1D, the presence of quasi-long-range order in $g^{(1)} \sim |x|^{-1/2K}$ implies a finite value of n_s by $K = \pi\hbar\kappa c$ for bosonic Luttinger liquids. In more general terms, the fact that ODLRO in a BEC implies superfluidity follows from the Nambu-Goldstone theorem. It states that the appearance of (quasi-)long-range order in the phase implies the existence of an elementary excitation, whose energy vanishes in the limit of zero momentum. As emphasized, e.g., by Weinberg (1986), the order parameter phase $\phi(\mathbf{x})$ introduced above is the Nambu-Goldstone field associated with the broken $U(1)$ gauge symmetry [this notion has to be treated with care; see, e.g., Wen (2004)]. In the present context, a broken gauge symmetry is the statement of Eq. (A4), namely, that the free energy contains a term quadratic in a phase twist imposed at the boundaries of the system. For systems with a finite compressibility, the dynamics of the Nambu-Goldstone mode is described by the quantum hydrodynamic Hamiltonian Eq. (A6). The definition (A4) of superfluidity and the resulting generic quantum hydrodynamic Hamiltonian (A6), which are connected to long- (or quasi-long-)-range order via Eqs. (A7) and (A8), are thus completely general and are not tied, e.g., to translation-invariant systems. Despite their different definitions based on long-range current or long-range phase correlations, the two phenomena SF and BEC (in its generalized sense) are therefore indeed two sides of the same coin.

REFERENCES

Abo-Shaeer, J. R., C. Raman, J. M. Vogels, and W. Ketterle, 2001, Science **292**, 476.

Adhikari, S. K., 1986, Am. J. Phys. **54**, 362.

Aftalion, A., 2006, *Vortices in Bose-Einstein Condensates* (Birkhäuser, Boston).

Aftalion, A., X. Blanc, and J. Dalibard, 2005, Phys. Rev. A **71**, 023611.

Aftalion, A., X. Blanc, and F. Nier, 2006, Phys. Rev. A **73**, 011601.

Aftalion, A., and I. Danaila, 2004, Phys. Rev. A **69**, 033608.

Ahufinger, V., L. Sanchez-Palencia, A. Kantian, A. Sanpera, and M. Lewenstein, 2005, Phys. Rev. A **72**, 063616.

Aizenman, M., E. H. Lieb, R. Seiringer, J. P. Solovej, and J. Yngvason, 2004, Phys. Rev. A **70**, 023612.

Akkineni, V. K., D. M. Ceperley, and N. Trivedi, 2007, Phys. Rev. B **76**, 165116.

Alon, O. E., A. I. Streltsov, and L. S. Cederbaum, 2005, Phys. Rev. Lett. **95**, 030405.

Altman, E., and A. Auerbach, 2002, Phys. Rev. Lett. **89**, 250404.

Altman, E., E. Demler, and M. D. Lukin, 2004, Phys. Rev. A **70**, 013603.

Altman, E., and A. Vishwanath, 2005, Phys. Rev. Lett. **95**, 110404.

Altmeyer, A., S. Riedl, C. Kohstall, M. J. Wright, R. Geursen, M. Bartenstein, C. Chin, J. H. Denschlag, and R. Grimm, 2007, Phys. Rev. Lett. **98**, 040401.

Andersen, J., 2002, Eur. Phys. J. B **28**, 389.

Andersen, J. O., U. Al Khawaja, and H. T. C. Stoof, 2002, Phys. Rev. Lett. **88**, 070407.

Anderson, M. H., J. R. Ensher, M. R. Matthews, C. E. Wieman, and E. A. Cornell, 1995, Science **269**, 198.

Anderson, P. W., 1958a, Phys. Rev. **109**, 1492.

Anderson, P. W., 1958b, Phys. Rev. **112**, 1900.

Andrews, M. R., C. G. Townsend, H. J. Miesner, D. S. Durfee, D. M. Kurn, and W. Ketterle, 1997, Science **275**, 637.

Anglin, J. R., 2002, Phys. Rev. A **65**, 063611.

Anglin, J. R., and M. Crescimanno, 2002, e-print arXiv:cond-mat/0210063.

Arnold, P., J. E. Drut, and D. T. Son, 2007, Phys. Rev. A **75**, 043605.

Arnold, P., and G. Moore, 2001, Phys. Rev. Lett. **87**, 120401.

Ashcroft, N. W., and N. D. Mermin, 1976, *Solid State Physics* (Holt, Rinehardt and Winston, New York).

Astrakharchik, G. E., J. Boronat, J. Casulleras, and S. Giorgini, 2004, Phys. Rev. Lett. **93**, 200404.

Astrakharchik, G. E., J. Boronat, J. Casulleras, and S. Giorgini, 2005a, Phys. Rev. Lett. **95**, 190407.

Astrakharchik, G. E., J. Boronat, J. Casulleras, and S. Giorgini, 2005b, Phys. Rev. Lett. **95**, 230405.

Auerbach, A., 2006, *Interacting Electrons and Quantum Magnetism* (Springer, Berlin).

Auslaender, O. M., H. Steinberg, A. Yacoby, Y. Tserkovnyak, B. I. Halperin, K. W. Baldwin, L. N. Pfeiffer, and K. W. West, 2005, Science **308**, 88.

Bagnato, V., and D. Kleppner, 1991, Phys. Rev. A **44**, 7439.

Baker, G. A., 1999, Phys. Rev. C **60**, 054311.

Baksmaty, L. O., S. J. Woo, S. Choi, and N. P. Bigelow, 2004, Phys. Rev. Lett. **92**, 160405.

Balian, R., 1991, *From Microphysics to Macrophysics, Vol. I* (Springer, Berlin).

Barankov, R. A., and L. S. Levitov, 2006, Phys. Rev. Lett. **96**, 230403.

Barankov, R. A., L. S. Levitov, and B. Z. Spivak, 2004, Phys. Rev. Lett. **93**, 160401.

Baranov, M. A., Y. Kagan, and M. Y. Kagan, 1996, JETP Lett. **64**, 301.

Barberán, N., M. Lewenstein, K. Osterloh, and D. Dagnino, 2006, Phys. Rev. A **73**, 063623.

Bartenstein, M., A. Altmeyer, S. Riedl, S. Jochim, C. Chin, J. Hecker-Denschlag, and R. Grimm, 2004a, Phys. Rev. Lett. **92**,

---

[36]In a trap, a quasicondensate in 1D may exist even at finite temperature, provided the cloud size is smaller than the phase coherence length; see Sec. V.B.

120401.

Bartenstein, M., A. Altmeyer, S. Riedl, S. Jochim, C. Chin, J. Hecker-Denschlag, and R. Grimm, 2004b, Phys. Rev. Lett. **92**, 203201.

Basko, D., I. Aleiner, and B. Altshuler, 2006, Ann. Phys. (N.Y.) **321**, 1126.

Batrouni, G. G., V. Rousseau, R. T. Scalettar, M. Rigol, A. Muramatsu, P. J. H. Denteneer, and M. Troyer, 2002, Phys. Rev. Lett. **89**, 117203.

Baym, G., 1998, Acta Phys. Pol. B **29**, 1839.

Baym, G., 2003, Phys. Rev. Lett. **91**, 110402.

Baym, G., 2004, Phys. Rev. A **69**, 043618.

Baym, G., J. P. Blaizot, M. Holzman, F. Laloe, and D. Vautherin, 1999, Phys. Rev. Lett. **83**, 1703.

Baym, G., and C. J. Pethick, 2003, Phys. Rev. A **69**, 043619.

Baym, G., C. J. Pethick, Z. Yu, and M. W. Zwierlein, 2007, Phys. Rev. Lett. **99**, 190407.

Belitz, D., and T. R. Kirkpatrick, 1994, Rev. Mod. Phys. **66**, 261.

Berezinskii, V. L., 1971, Sov. Phys. JETP **34**, 601.

Bergeman, T., M. G. Moore, and M. Olshanii, 2003, Phys. Rev. Lett. **91**, 163201.

Berry, M. V., 1984, Proc. R. Soc. London, Ser. A **392**, 45.

Bhaduri, R. K., S. M. Reimann, S. Viefers, A. Ghose Choudhury, and M. K. Srivastava, 2000, J. Phys. B **33**, 3895.

Bishop, D. J., and J. D. Reppy, 1978, Phys. Rev. Lett. **40**, 1727.

Bishop, D. J., and J. D. Reppy, 1980, Phys. Rev. B **22**, 5171.

Blakie, P., and J. Porto, 2004, Phys. Rev. A **69**, 013603.

Bloch, I., T. W. Hänsch, and T. Esslinger, 2000, Nature **403**, 166.

Boesten, H. M. J. M., C. C. Tsai, J. R. Gardner, D. J. Heinzen, and B. J. Verhaar, 1997, Phys. Rev. A **55**, 636.

Bogoliubov, N. N., 1960, Physica (Amsterdam) **26**, S1.

Bohn, J. L., and P. S. Julienne, 1999, Phys. Rev. A **60**, 414.

Bourdel, T., J. Cubizolles, L. Khaykovich, K. Magalhaes, S. Kokkelmans, G. Shlyapnikov, and C. Salomon, 2003, Phys. Rev. Lett. **91**, 020402.

Bourdel, T., L. Khaykovich, J. Cubizolles, J. Zhang, F. Chevy, M. Teichmann, L. Tarruell, S. J. J. M. F. Kokkelmans, and C. Salomon, 2004, Phys. Rev. Lett. **93**, 050401.

Bourne, H. P., N. K. Wilkin, and J. M. F. Gunn, 2006, Phys. Rev. Lett. **96**, 240401.

Brack, M., and R. K. Bhaduri, 1997, *Semiclassical Physics* (Addison-Wesley, Reading, MA), Chap. 4.4.

Bradley, C. C., C. A. Sackett, J. J. Tollett, and R. G. Hulet, 1995, Phys. Rev. Lett. **75**, 1687.

Brennen, G., C. Caves, P. Jessen, and I. H. Deutsch, 1999, Phys. Rev. Lett. **82**, 1060.

Bretin, V., S. Stock, Y. Seurin, and J. Dalibard, 2004, Phys. Rev. Lett. **92**, 050403.

Brodsky, I. V., M. Y. Kagan, A. V. Klaptsov, R. Combescot, and X. Leyronas, 2006, Phys. Rev. A **73**, 032724.

Brune, M., F. Schmidt-Kaler, A. Maali, J. Dreyer, E. Hagley, J. M. Raimond, and S. Haroche, 1996, Phys. Rev. Lett. **76**, 1800.

Bruun, G. M., and C. J. Pethick, 2004, Phys. Rev. Lett. **92**, 140404.

Bruun, G. M., and H. Smith, 2007, Phys. Rev. A **75**, 043612.

Büchler, H. P., G. Blatter, and W. Zwerger, 2003, Phys. Rev. Lett. **90**, 130401.

Bulgac, A., J. Drut, and P. Magierski, 2006, Phys. Rev. Lett. **96**, 090404.

Bulgac, A., J. E. Drut, and P. Magierski, 2007, Phys. Rev. Lett. **99**, 120401.

Burger, S., F. S. Cataliotti, C. Fort, P. Maddaloni, F. Minardi, and M. Inguscio, 2002, Europhys. Lett. **57**, 1.

Burkov, A. A., M. D. Lukin, and E. Demler, 2007, Phys. Rev. Lett. **98**, 200404.

Burovski, E., N. Prokof'ev, B. Svistunov, and M. Troyer, 2006, Phys. Rev. Lett. **96**, 160402.

Busch, T., B. G. Englert, K. Rzazewski, and M. Wilkens, 1998, Found. Phys. **28**, 549.

Byczuk, K., W. Hofstetter, and D. Vollhardt, 2005, Phys. Rev. Lett. **94**, 056404.

Campbell, G., J. Mun, M. Boyd, P. Medley, A. E. Leanhardt, L. G. Marcassa, D. E. Pritchard, and W. Ketterle, 2006, Science **313**, 5787.

Capogrosso-Sansone, B., N. V. Prokof'ev, and B. V. Svistunov, 2007, Phys. Rev. B **75**, 134302.

Capuzzi, P., P. Vignolo, F. Federici, and M. P. Tosi, 2006, Phys. Rev. A **73**, 021603(R).

Carlson, J., C. S. Y. V. R. Pandharipande, and K. E. Schmidt, 2003, Phys. Rev. Lett. **91**, 050401.

Carr, L. D., G. V. Shlyapnikov, and Y. Castin, 2004, Phys. Rev. Lett. **92**, 150404.

Castin, Y., 2004, J. Phys. IV **116**, 87.

Castin, Y., and J. Dalibard, 1997, Phys. Rev. A **55**, 4330.

Castin, Y., and R. Dum, 1998, Phys. Rev. A **57**, 3008.

Castin, Y., Z. Hadzibabic, S. Stock, J. Dalibard, and S. Stringari, 2006, Phys. Rev. Lett. **96**, 040405.

Cataliotti, F. S., S. Burger, C. Fort, P. Maddaloni, F. Minardi, A. Trombettoni, A. Smerzi, and M. Inguscio, 2001, Science **293**, 843.

Cazalilla, M. A., 2003, Phys. Rev. A **67**, 063613.

Cazalilla, M. A., 2004a, J. Phys. B **37**, S1.

Cazalilla, M. A., 2004b, Phys. Rev. A **70**, 041604.

Cazalilla, M. A., N. Barberán, and N. R. Cooper, 2005, Phys. Rev. B **71**, 121303.

Cazalilla, M. A., A. F. Ho, and T. Giamarchi, 2006, New J. Phys. **8**, 158.

Ceperley, D. M., 1995, Rev. Mod. Phys. **67**, 279.

Chandrasekhar, B. S., 1962, Appl. Phys. Lett. **1**, 7.

Chang, C. C., N. Regnault, T. Jolicoeur, and J. K. Jain, 2004, Phys. Rev. A **72**, 013611.

Chen, Q., C. A. Regal, M. Greiner, D. S. Jin, and K. Levin, 2006a, Phys. Rev. A **73**, 041601.

Chen, Q., C. A. Regal, D. S. Jin, and K. Levin, 2006b, Phys. Rev. A **74**, 011601.

Chen, Q. J., J. Stajic, S. N. Tan, and K. Levin, 2005, Phys. Rep. **412**, 1.

Cherny, A. Y., and A. A. Shanenko, 2001, Phys. Rev. E **64**, 027105.

Chester, G. V., 1970, Phys. Rev. A **2**, 256.

Chevallier, M., and W. Krauth, 2007, Phys. Rev. E **76**, 051109.

Chevy, F., 2006, Phys. Rev. A **73**, 041604.

Chevy, F., V. Bretin, P. Rosenbusch, K. W. Madison, and J. Dalibard, 2001a, Phys. Rev. Lett. **88**, 250402.

Chevy, F., K. W. Madison, V. Bretin, and J. Dalibard, 2001b, Phys. Rev. A **64**, 031601(R).

Chin, C., M. Bartenstein, A. Altmeyer, S. Riedl, S. Jochim, J. Hecker-Denschlag, and R. Grimm, 2004, Science **305**, 1128.

Chin, C., and P. S. Julienne, 2005, Phys. Rev. A **71**, 012713.

Choi, S., L. O. Baksmaty, S. J. Woo, and N. P. Bigelow, 2003, Phys. Rev. A **68**, 031605.

Clark, B. K., and D. M. Ceperley, 2006, Phys. Rev. Lett. **96**, 105302.

Clark, S. R., and D. Jaksch, 2004, Phys. Rev. A **70**, 043612.

Clément, D., A. F. Varón, M. Hugbart, J. A. Retter, P. Bouyer, L. Sanchez-Palencia, D. M. Gangardt, G. V. Shlyapnikov, and A. Aspect, 2005, Phys. Rev. Lett. **95**, 170409.

Clément, D., A. Varon, J. Retter, L. Sanchez-Palencia, A. Aspect, and P. Bouyer, 2006, New J. Phys. **8**, 165.

Clogston, A. M., 1962, Phys. Rev. Lett. **9**, 266.

Coddington, I., P. Engels, V. Schweikhard, and E. A. Cornell, 2003, Phys. Rev. Lett. **91**, 100402.

Coddington, I., P. C. Haljan, P. Engels, V. Schweikhard, S. Tung, and E. A. Cornell, 2004, Phys. Rev. A **70**, 063607.

Colombe, Y., E. Knyazchyan, O. Morizot, B. Mercier, V. Lorent, and H. Perrin, 2004, Europhys. Lett. **67**, 593.

Combescot, R., M. Y. Kagan, and S. Stringari, 2006, Phys. Rev. A **74**, 042717.

Cooper, N. R., S. Komineas, and N. Read, 2004, Phys. Rev. A **70**, 033604.

Cooper, N. R., F. J. M. van Lankvelt, J. W. Reijnders, and K. Schoutens, 2005, Phys. Rev. A **72**, 063622.

Cooper, N. R., and N. K. Wilkin, 1999, Phys. Rev. B **60**, R16279.

Cooper, N. R., N. K. Wilkin, and J. M. F. Gunn, 2001, Phys. Rev. Lett. **87**, 120405.

Cornish, S. L., N. R. Claussen, J. L. Roberts, E. A. Cornell, and C. E. Wieman, 2000, Phys. Rev. Lett. **85**, 1795.

Courteille, P., R. Freeland, D. Heinzen, F. van Abeelen, and B. Verhaar, 1998, Phys. Rev. Lett. **81**, 69.

Cozzini, M., B. Jackson, and S. Stringari, 2006, Phys. Rev. A **73**, 013603.

Cozzini, M., L. P. Pitaevskii, and S. Stringari, 2004, Phys. Rev. Lett. **92**, 220401.

Cristiani, M., O. Morsch, N. Malossi, M. Jona-Lasinio, M. Anderlini, E. Courtade, and E. Arimondo, 2004, Opt. Express **12**, 4.

Cubizolles, J., T. Bourdel, S. J. J. M. F. Kokkelmans, G. V. Shlyapnikov, and C. Salomon, 2003, Phys. Rev. Lett. **91**, 240401.

Cummings, F. W., and J. R. Johnston, 1966, Phys. Rev. **151**, 105.

Daley, A., C. Kollath, U. Schollwöck, and G. Vidal, 2004, J. Stat. Mech.: Theory Exp. 2004, P04005.

Dalfovo, F. S., L. P. Pitaevkii, S. Stringari, and S. Giorgini, 1999, Rev. Mod. Phys. **71**, 463.

Damski, B., J. Zakrzewski, L. Santos, P. Zoller, and M. Lewenstein, 2003, Phys. Rev. Lett. **91**, 080403.

Davis, K. B., and P. B. Blakie, 2006, Phys. Rev. Lett. **96**, 060404.

Davis, K. B., M.-O. Mewes, M. R. Andrews, N. J. van Druten, D. S. Durfee, D. M. Kurn, and W. Ketterle, 1995, Phys. Rev. Lett. **75**, 3969.

De Dominicis, C., and P. C. Martin, 1964a, J. Math. Phys. **5**, 14.

De Dominicis, C., and P. C. Martin, 1964b, J. Math. Phys. **5**, 31.

DeMarco, B., J. L. Bohn, J. P. Burke, Jr., M. Holland, and D. S. Jin, 1999, Phys. Rev. Lett. **82**, 4208.

DeMarco, B., and D. D. Jin, 1999, Science **285**, 1703.

DeMarco, B., C. Lannert, S. Vishveshwara, and T.-C. Wei, 2005, Phys. Rev. A **71**, 063601.

DeMartino, A., M. Thorwart, R. Egger, and R. Graham, 2005, Phys. Rev. Lett. **94**, 060402.

DePalo, S., M. L. Chiofalo, M. J. Holland, and S. J. J. M. F. Kokkelmans, 2005, Laser Phys. **15**, 376.

Dettmer, S., D. Hellweg, P. Ryyty, J. J. Arlt, W. Ertmer, K. Sengstock, D. S. Petrov, G. V. Shlyapnikov, H. Kreutzmann, L. Santos, and M. Lewenstein, 2001, Phys. Rev. Lett. **87**, 160406.

Diener, R. B., and T. L. Ho, 2004, e-print arXiv:cond-mat/0405174.

Donnelly, R. J., 1991, *Quantized Vortices in Helium II* (Cambridge University Press, Cambridge).

Donner, T., S. Ritter, T. Bourdel, A. Ottl, M. Köhl, and T. Esslinger, 2007, Science **315**, 1556.

Drechsler, M., and W. Zwerger, 1992, Ann. Phys. **1**, 15.

Drummond, P., and K. Kheruntsyan, 2004, Phys. Rev. A **70**, 033609.

Duan, L. M., 2006, Phys. Rev. Lett. **96**, 103201.

Duan, L.-M., E. Demler, and M. D. Lukin, 2003, Phys. Rev. Lett. **91**, 090402.

Duine, R. A., and H. T. C. Stoof, 2004, Phys. Rep. **396**, 115.

Dukelsky, J., S. Pittel, and G. Sierra, 2004, Rev. Mod. Phys. **76**, 643.

Dum, R., and M. Olshanii, 1996, Phys. Rev. Lett. **76**, 1788.

Dunjko, V., V. Lorent, and M. Olshanii, 2001, Phys. Rev. Lett. **86**, 5413.

Dunningham, J. A., M. J. Collett, and D. F. Walls, 1998, Phys. Lett. A **245**, 49.

Dürr, S., T. Volz, A. Marte, and G. Rempe, 2004, Phys. Rev. Lett. **92**, 020406.

Dürr, S., T. Volz, N. Syassen, G. Rempe, E. van Kempen, S. Kokkelmans, B. Verhaar, and H. Friedrich, 2005, Phys. Rev. A **72**, 052707.

Dutta, S. K., B. K. Teo, and G. Raithel, 1999, Phys. Rev. Lett. **83**, 1934.

Eagles, B., 1969, Phys. Rev. **186**, 456.

Eckardt, A., C. Weiss, and M. Holthaus, 2005, Phys. Rev. Lett. **95**, 260404.

Einstein, A., 1925, Sitzungsber. Preuss. Akad. Wiss., Phys. Math. Kl. **1**, 3.

Engelbrecht, J. R., M. Randeria, and S. de Melo, 1997, Phys. Rev. B **55**, 15153.

Engels, P., I. Coddington, P. C. Haljan, and E. A. Cornell, 2002, Phys. Rev. Lett. **89**, 100403.

Esteve, J., J. B. Trebbia, T. Schumm, A. Aspect, C. I. Westbrook, and I. Bouchoule, 2006, Phys. Rev. Lett. **96**, 130403.

Fallani, L., J. E. Lye, V. Guarrera, C. Fort, and M. Inguscio, 2007, Phys. Rev. Lett. **98**, 130404.

Fallani, L., L. D. Sarlo, J. Lye, M. Modugno, R. Saers, C. Fort, and M. Inguscio, 2004, Phys. Rev. Lett. **93**, 140406.

Fano, U., 1961, Phys. Rev. **124**, 1866.

Fedichev, P., M. Bijlsma, and P. Zoller, 2004, Phys. Rev. Lett. **92**, 080401.

Fedichev, P. O., U. R. Fischer, and A. Recati, 2003, Phys. Rev. A **68**, 011602.

Fedichev, P. O., M. W. Kagan, G. V. Shlyapnikov, and J. T. M. Walraven, 1996, Phys. Rev. Lett. **77**, 2913.

Fedichev, P. O., M. W. Reynold, and G. V. Shlyapnikov, 1996, Phys. Rev. Lett. **77**, 2921.

Fernández, J. P., and W. J. Mullin, 2002, J. Low Temp. Phys. **128**, 233.

Fertig, C. D., K. M. O'Hara, J. H. Huckans, S. L. Rolston, W. D. Phillips, and J. V. Porto, 2005, Phys. Rev. Lett. **94**, 120403.

Feshbach, H., 1958, Ann. Phys. (N.Y.) **5**, 337.

Fetter, A. L., 2001, Phys. Rev. A **64**, 063608.

Fetter, A. L., 2007, Phys. Rev. A **75**, 013620.

Fetter, A. L., and A. A. Svidzinsky, 2001, J. Phys.: Condens. Matter **13**, R135.

Feynman, R. P., 1953, Phys. Rev. **91**, 1291.

Feynman, R. P., 1955, *Progress in Low Temperature Physics* (North-Holland, Amsterdam).

Fischer, U. R., and G. Baym, 2003, Phys. Rev. Lett. **90**, 140402.

Fisher, D. S., and P. C. Hohenberg, 1988, Phys. Rev. B **37**, 4936.

Fisher, M. E., M. N. Barber, and D. Jasnow, 1973, Phys. Rev. A **8**, 1111.

Fisher, M. P. A., P. B. Weichman, G. Grinstein, and D. S. Fisher, 1989, Phys. Rev. B **40**, 546.

Flambaum, V. V., G. F. Gribakin, and D. S. Harabati, 1999, Phys. Rev. A **59**, 1998.

Fölling, S., F. Gerbier, A. Widera, O. Mandel, T. Gericke, and I. Bloch, 2005, Nature **434**, 481.

Fölling, S., S. Trotzky, P. Cheinet, M. Feld, R. Saers, A. Widera, T. Müller, and I. Bloch, 2007, Nature **448**, 1029.

Fölling, S., A. Widera, T. Müller, F. Gerbier, and I. Bloch, 2006, Phys. Rev. Lett. **97**, 060403.

Folman, R., P. Krüger, J. Schmiedmayer, J. Denschlag, and C. Henkel, 2002, Adv. At., Mol., Opt. Phys. **48**, 263.

Forster, D., 1975, *Hydrodynamic Fluctuations, Broken Symmetry, and Correlation Functions*, Frontiers in Physics Vol. 47 (Benjamin, Reading, MA), pp. 241–251.

Fort, C., L. Fallani, V. Guarrera, J. E. Lye, M. Modugno, D. S. Wiersma, and M. Inguscio, 2005, Phys. Rev. Lett. **95**, 170410.

Fregoso, B. M., and G. Baym, 2006, Phys. Rev. A **73**, 043616.

Fröhlich, J., and U. M. Studer, 1993, Rev. Mod. Phys. **65**, 733.

Fuchs, J. N., A. Recati, and W. Zwerger, 2004, Phys. Rev. Lett. **93**, 090408.

Fulde, P., and R. A. Ferrell, 1964, Phys. Rev. **135**, A550.

Gangardt, D. M., and G. V. Shlyapnikov, 2003, Phys. Rev. Lett. **90**, 010401.

Gaudin, M., 1967, Phys. Lett. **24**, 55.

Gavish, U., and Y. Castin, 2005, Phys. Rev. Lett. **95**, 020401.

Gea-Banacloche, J., A. M. Rey, G. Pupillo, C. J. Williams, and C. W. Clark, 2006, Phys. Rev. A **73**, 013605.

Gelman, B. A., E. V. Shuryak, and I. Zahed, 2004, e-print arXiv:nucl-th/0410067.

Gerbier, F., 2007, Phys. Rev. Lett. **99**, 120405.

Gerbier, F., S. Fölling, A. Widera, and I. Bloch, 2007, e-print arXiv:cond-mat/0701420.

Gerbier, F., S. Fölling, A. Widera, O. Mandel, and I. Bloch, 2006, Phys. Rev. Lett. **96**, 090401.

Gerbier, F., J. H. Thywissen, S. Richard, M. Hugbart, P. Bouyer, and A. Aspect, 2004, Phys. Rev. Lett. **92**, 030405.

Gerbier, F., A. Widera, S. Fölling, O. Mandel, T. Gericke, and I. Bloch, 2005a, Phys. Rev. A **72**, 053606.

Gerbier, F., A. Widera, S. Fölling, O. Mandel, T. Gericke, and I. Bloch, 2005b, Phys. Rev. Lett. **95**, 050404.

Giamarchi, T., 2004, *Quantum Physics in One Dimension* (Oxford University Press, Oxford).

Giamarchi, T., and H. J. Schulz, 1988, Phys. Rev. B **37**, 325.

Gies, C., and D. A. W. Hutchinson, 2004, Phys. Rev. A **70**, 043606.

Gies, C., B. P. van Zyl, S. A. Morgan, and D. A. W. Hutchinson, 2004, Phys. Rev. A **69**, 023616.

Gifford, S. A., and G. Baym, 2004, Phys. Rev. A **70**, 033602.

Ginzburg, V. L., and L. D. Landau, 1950, Zh. Eksp. Teor. Fiz. **20**, 1064.

Giorgini, S., L. P. Pitaevskii, and S. Stringari, 1997, J. Low Temp. Phys. **109**, 309.

Girardeau, M., 1960, J. Math. Phys. **1**, 516.

Glauber, R. J., 1963, Phys. Rev. **131**, 2766.

Gor'kov, L. P., and T. K. Melik-Barkhudarov, 1961, Sov. Phys. JETP **13**, 1018.

Görlitz, A., J. M. Vogels, A. E. Leanhardt, C. Raman, T. L. Gustavson, J. R. Abo-Shaeer, A. P. Chikkatur, S. Gupta, S.

Inouye, T. Rosenband, and W. Ketterle, 2001, Phys. Rev. Lett. **87**, 130402.

Granger, B. E., and D. Blume, 2004, Phys. Rev. Lett. **92**, 133202.

Greiner, M., I. Bloch, M. O. Mandel, T. Hänsch, and T. Esslinger, 2001, Phys. Rev. Lett. **87**, 160405.

Greiner, M., M. O. Mandel, T. Esslinger, T. Hänsch, and I. Bloch, 2002a, Nature **415**, 39.

Greiner, M., M. O. Mandel, T. Hänsch, and I. Bloch, 2002b, Nature **419**, 51.

Greiner, M., C. A. Regal, J. Stewart, and D. S. Jin, 2005, Phys. Rev. Lett. **94**, 110401.

Greiner, M., C. A. Regal, and D. S. Jin, 2003, Nature **426**, 537.

Gribakin, G. F., and V. V. Flambaum, 1993, Phys. Rev. A **48**, 546.

Griesmaier, A., J. Werner, S. Hensler, J. Stuhler, and T. Pfau, 2005, Phys. Rev. Lett. **94**, 160401.

Grimm, R., M. Weidemüller, and Y. B. Ovchinnikov, 2000, Adv. At., Mol., Opt. Phys. **42**, 95.

Gritsev, V., E. Altman, E. Demler, and A. Polkovnikov, 2006, Nat. Phys. **2**, 705.

Gross, E. P., 1961, Nuovo Cimento, Suppl. **20**, 454.

Grynberg, G., B. Lounis, P. Verkerk, J.-Y. Courtois, and C. Salomon, 1993, Phys. Rev. Lett. **70**, 2249.

Grynberg, G., and C. Robillard, 2001, Phys. Rep. **355**, 335.

Guéry-Odelin, D., 2000, Phys. Rev. A **62**, 033607.

Guilleumas, M., and L. P. Pitaevskii, 2003, Phys. Rev. A **67**, 053607.

Günter, K., T. Stöferle, H. Moritz, M. Köhl, and T. Esslinger, 2005, Phys. Rev. Lett. **95**, 230401.

Gupta, S., Z. Hadzibabic, M. W. Zwierlein, C. A. Stan, K. Dieckmann, C. H. Schunck, E. G. M. van Kempen, B. J. Verhaar, and W. Ketterle, 2003, Science **300**, 1723.

Hadzibabic, Z., P. Krüger, M. Cheneau, B. Battelier, and J. Dalibard, 2006, Nature **441**, 1118.

Hadzibabic, Z., S. Stock, B. Battelier, V. Bretin, and J. Dalibard, 2004, Phys. Rev. Lett. **93**, 180403.

Haldane, F. D. M., 1981, Phys. Rev. Lett. **47**, 1840.

Haldane, F. D. M., 1983, Phys. Rev. Lett. **51**, 605.

Haljan, P. C., I. Coddington, P. Engels, and E. A. Cornell, 2001, Phys. Rev. Lett. **87**, 210403.

Hanbury Brown, R., and R. Q. Twiss, 1956a, Nature **177**, 27.

Hanbury Brown, R., and R. Q. Twiss, 1956b, Nature **178**, 1447.

Hamer, C. J., and J. B. Kogut, 1979, Phys. Rev. B **20**, 3859.

Haussmann, R., W. Rantner, S. Cerrito, and W. Zwerger, 2007, Phys. Rev. A **75**, 023610.

Haussmann, R., and W. Zwerger, e-print arXiv:0805.3226.

He, L., and D. Vanderbilt, 2001, Phys. Rev. Lett. **86**, 5341.

He, Y., Q. Chen, and K. Levin, 2005, Phys. Rev. A **72**, 011602.

Hechenblaikner, G., J. M. Krueger, and C. J. Foot, 2005, Phys. Rev. A **71**, 013604.

Heiselberg, H., 2001, Phys. Rev. A **63**, 043606.

Heiselberg, H., 2004, Phys. Rev. Lett. **93**, 040402.

Heiselberg, H., and B. Mottelson, 2002, Phys. Rev. Lett. **88**, 190401.

Heiselberg, H., C. J. Pethick, H. Smith, and L. Viverit, 2000, Phys. Rev. Lett. **85**, 2418.

Hellweg, D., L. Cacciapuoti, M. Kottke, T. Schulte, K. Sengstock, W. Ertmer, and J. J. Arlt, 2003, Phys. Rev. Lett. **91**, 010406.

Hemmerich, A., and T. W. Hänsch, 1993, Phys. Rev. Lett. **70**, 410.

Henny, M., S. Oberholzer, C. Strunk, T. Heinzel, K. Ensslin,

M. Holland, and C. Schönenberger, 1999, Science **284**, 296.

Herbig, J., T. Kraemer, M. Mark, T. Weber, C. Chin, H. C. Nägerl, and R. Grimm, 2003, Science **301**, 1510.

Hinds, E. A., M. G. Boshier, and I. G. Hughes, 1998, Phys. Rev. Lett. **80**, 645.

Ho, A. F., 2006, Phys. Rev. A **73**, 061601.

Ho, A. F., M. A. Cazalilla, and T. Giamarchi, 2004, Phys. Rev. Lett. **92**, 130405.

Ho, T. L., 1998, Phys. Rev. Lett. **81**, 742.

Ho, T. L., 2001, Phys. Rev. Lett. **87**, 060403.

Ho, T. L., 2004, Phys. Rev. Lett. **92**, 090402.

Ho, T. L., and M. Ma, 1999, J. Low Temp. Phys. **115**, 61.

Ho, T. L., and V. B. Shenoy, 1996, Phys. Rev. Lett. **77**, 2595.

Ho, T. L., and Q. Zhou, 2007, Phys. Rev. Lett. **99**, 120404.

Hodby, E., G. Hechenblaikner, S. A. Hopkins, O. M. Marago, and C. J. Foot, 2001, Phys. Rev. Lett. **88**, 010405.

Hofferberth, S., I. Lesanovsky, B. Fischer, T. Schumm, and J. Schmiedmayer, 2007, Nature **449**, 324.

Hofferberth, S., I. Lesanovsky, T. Schumm, A. Imambekov, V. Gritsev, E. Demler, and J. Schmiedmayer, 2008, Nat. Phys. **4**, 429.

Hofstetter, W., J. I. Cirac, P. Zoller, E. Demler, and M. D. Lukin, 2002, Phys. Rev. Lett. **89**, 220407.

Hohenberg, P. C., 1967, Phys. Rev. **158**, 383.

Hohenberg, P. C., and P. C. Martin, 1965, Ann. Phys. (N.Y.) **34**, 291.

Holland, M., S. J. J. M. F. Kokkelmans, M. L. Chiofalo, and R. Walser, 2001, Phys. Rev. Lett. **87**, 120406.

Holzmann, M., G. Baym, J. P. Blaizot, and F. Laloe, 2007, Proc. Natl. Acad. Sci. U.S.A. **104**, 1476.

Holzmann, M., J. N. Fuchs, G. Baym, J. P. Blaizot, and F. Laloe, 2004, C. R. Phys. **5**, 21.

Holzmann, M., and W. Krauth, 1999, Phys. Rev. Lett. **83**, 2687.

Hooley, C., and J. Quintanilla, 2004, Phys. Rev. Lett. **93**, 080404.

Hu, H., P. D. Drummond, and X. Liu, 2007, Nat. Phys. **3**, 469.

Hu, H., X.-J. Liu, and P. D. Drummond, 2007, Phys. Rev. Lett. **98**, 070403.

Huber, S. D., E. Altman, H. P. Büchler, and G. Blatter, 2007, Phys. Rev. B **75**, 085106.

Iannuzzi, M., A. Orecchini, F. Sacchetti, P. Facchi, and S. Pascazio, 2006, Phys. Rev. Lett. **96**, 080402.

Imamoglu, A., M. Lewenstein, and L. You, 1997, Phys. Rev. Lett. **78**, 2511.

Inouye, S., M. Andrews, J. Stenger, H. J. Miesner, S. Stamper-Kurn, and W. Ketterle, 1998, Nature **392**, 151.

Inouye, S., S. Gupta, T. Rosenband, A. P. Chikkatur, A. Görlitz, T. L. Gustavson, A. E. Leanhardt, D. E. Pritchard, and W. Ketter, 2001, Phys. Rev. Lett. **87**, 080402.

Ishikawa, M., and H. Takayama, 1980, J. Phys. Soc. Jpn. **49**, 1242.

Ismail-Beigi, S., and T. A. Arias, 1999, Phys. Rev. Lett. **82**, 2127.

Iucci, A., M. A. Cazalilla, A. F. Ho, and T. Giamarchi, 2006, Phys. Rev. A **73**, 041608.

Jackson, A. D., and G. M. Kavoulakis, 2000, Phys. Rev. Lett. **85**, 2854.

Jackson, A. D., and G. M. Kavoulakis, 2002, Phys. Rev. Lett. **89**, 070403.

Jackson, A. D., and E. Zaremba, 2002, Phys. Rev. Lett. **89**, 150402.

Jain, J. K., 1989, Phys. Rev. Lett. **63**, 199.

Jaksch, D., H. J. Briegel, J. I. Cirac, C. W. Gardiner, and P.

Zoller, 1999, Phys. Rev. Lett. **82**, 1975.

Jaksch, D., C. Bruder, J. I. Cirac, C. W. Gardiner, and P. Zoller, 1998, Phys. Rev. Lett. **81**, 3108.

Jaksch, D., and P. Zoller, 2003, New J. Phys. **5**, 56.1.

Jaksch, D., and P. Zoller, 2005, Ann. Phys. (N.Y.) **315**, 52.

Javanainen, J., and S. M. Yoo, 1996, Phys. Rev. Lett. **76**, 161.

Jeltes, T., J. McNamara, W. Hogervorst, W. Vassen, V. Krachmalnicoff, M. Schellekens, A. Perrin, H. Chang, D. Boiron, A. Aspect, and C. Westbrook, 2007, Nature **445**, 402.

Jessen, P., and I. H. Deutsch, 1996, Adv. At., Mol., Opt. Phys. **37**, 95.

Jo, G.-B., Y. Shin, S. Will, T. Pasquini, M. Saba, W. Ketterle, D. Pritchard, M. Vengalattore, and M. Prentiss, 2007, Phys. Rev. Lett. **98**, 030407.

Jochim, S., M. Bartenstein, A. Altmeyer, G. Hendl, C. Chin, J. Hecker-Denschlag, and R. Grimm, 2003a, Phys. Rev. Lett. **91**, 240402.

Jochim, S., M. Bartenstein, A. Altmeyer, G. Hendl, S. Riedl, C. Chin, J. Hecker-Denschlag, and R. Grimm, 2003b, Science **302**, 2101.

Joseph, J., B. Clancy, L. Luo, J. Kinast, A. Turlapov, and J. E. Thomas, 2007, Phys. Rev. Lett. **98**, 170401.

Julienne, P. S., E. Tiesinga, and T. Köhler, 2004, J. Mod. Opt. **51**, 1787.

Juzeliunas, G., and P. Öhberg, 2004, Phys. Rev. Lett. **93**, 033602.

Juzeliunas, G., P. Öhberg, J. Ruseckas, and A. Klein, 2005, Phys. Rev. A **71**, 053614.

Juzeliunas, G., J. Ruseckas, P. Öhberg, and M. Fleischhauer, 2006, Phys. Rev. A **73**, 025602.

Kagan, Y., V. A. Kashurnikov, A. V. Krasavin, N. V. Prokof'ev, and B. V. Svistunov, 2000, Phys. Rev. A **61**, 043608.

Kagan, Y., and L. A. Maksimov, 2003, JETP Lett. **78**, 734.

Kagan, Y., G. V. Shlyapnikov, and J. T. M. Walraven, 1996, Phys. Rev. Lett. **76**, 2670.

Kagan, Y., B. V. Svistunov, and G. V. Shlyapnikov, 1987, Phys. Rev. A **54**, R1753.

Kailasvuori, J. M., T. H. Hansson, and G. M. Kavoulakis, 2002, Phys. Rev. A **66**, 053603.

Kalos, M. H., D. Levesque, and L. Verlet, 1974, Phys. Rev. A **9**, 2178.

Kasamatsu, K., M. Tsubota, and M. Ueda, 2002, Phys. Rev. A **66**, 053606.

Kashurnikov, V. A., N. V. Prokof'ev, and B. V. Svistunov, 2001, Phys. Rev. Lett. **87**, 120402.

Kashurnikov, V. A., N. V. Prokof'ev, and B. V. Svistunov, 2002, Phys. Rev. A **66**, 031601.

Kastberg, A., W. D. Phillips, S. L. Rolston, R. J. C. Spreeuw, and P. S. Jessen, 1995, Phys. Rev. Lett. **74**, 1542.

Kestner, J. P., and L. M. Duan, 2006, Phys. Rev. A **74**, 053606.

Kiesel, H., A. Renz, and F. Hasselbach, 2002, Nature **418**, 392.

Kim, S.-H., C. Won, S. D. Oh, and W. Jhe, 2000, e-print arXiv:cond-mat/0003342.

Kinast, J., S. L. Hemmer, M. E. Gehm, A. Turlapov, and J. E. Thomas, 2004, Phys. Rev. Lett. **92**, 150402.

Kinast, J., A. Turlapov, J. E. Thomas, Q. Chen, J. Stajic, and K. Levin, 2005, Science **307**, 1296.

Kinnunen, J., M. Rodriguez, and P. Törmä, 2004, Science **305**, 1131.

Kinoshita, T., T. Wenger, and D. S. Weiss, 2004, Science **305**, 1125.

Kinoshita, T., T. Wenger, and D. S. Weiss, 2005, Phys. Rev. Lett. **95**, 190406.

Kinoshita, T., T. Wenger, and D. S. Weiss, 2006, Nature **440**, 900.

Kitaev, A., 2006, Ann. Phys. (N.Y.) **321**, 2.

Kleiner, W. H., L. M. Roth, and S. H. Autler, 1964, Phys. Rev. **133**, A1226.

Köhl, M., 2006, Phys. Rev. A **73**, 031601.

Köhl, M., H. Moritz, T. Stöferle, K. Günter, and T. Esslinger, 2005a, Phys. Rev. Lett. **94**, 080403.

Köhl, M., H. Moritz, T. Stöferle, C. Schori, and T. Esslinger, 2005b, J. Low Temp. Phys. **138**, 635.

Köhler, T., K. Góral, and P. S. Julienne, 2006, Rev. Mod. Phys. **78**, 1311.

Kohn, W., 1959, Phys. Rev. **115**, 809.

Kohn, W., 1996, Phys. Rev. Lett. **76**, 3168.

Kohn, W., 1999, Rev. Mod. Phys. **71**, 1253.

Kohn, W., and J. M. Luttinger, 1965, Phys. Rev. Lett. **15**, 524.

Kollath, C., A. Iucci, T. Giamarchi, W. Hofstetter, and U. Schollwöck, 2006, Phys. Rev. Lett. **97**, 050402.

Kollath, C., A. Läuchli, and E. Altman, 2007, Phys. Rev. Lett. **98**, 180601.

Kollath, C., U. Schollwöck, J. von Delft, and W. Zwerger, 2004, Phys. Rev. A **69**, 031601(R).

Kollath, C., U. Schollwöck, and W. Zwerger, 2005, Phys. Rev. Lett. **95**, 176401.

Kosterlitz, J. M., and D. J. Thouless, 1973, J. Phys. C **6**, 1181.

Kovtun, P. K., D. T. Son, and A. O. Starinets, 2005, Phys. Rev. Lett. **94**, 111601.

Krüger, P., Z. Hadzibabic, and J. Dalibard, 2007, Phys. Rev. Lett. **99**, 040402.

Kühner, T. D., S. R. White, and H. Monien, 2000, Phys. Rev. B **61**, 12474.

Kuklov, A. B., and B. V. Svistunov, 2003, Phys. Rev. Lett. **90**, 100401.

Lahaye, T., T. Koch, B. Frohlich, M. Fattori, J. Metz, A. Griesmaier, S. Giovanazzi, and T. Pfau, 2007, Nature **448**, 672.

Lamacraft, A., 2006, Phys. Rev. A **73**, 011602.

Landau, L. D., and E. M. Lifshitz, 1987, *Quantum Mechanics* (Pergamon, New York).

Langer, J., 1968, Phys. Rev. **167**, 183.

Larkin, A. I., and Y. N. Ovchinnikov, 1965, Sov. Phys. JETP **20**, 762.

Lee, M. D., S. A. Morgan, M. J. Davis, and K. Burnett, 2002, Phys. Rev. A **65**, 043617.

Lee, P., N. Nagaosa, and X.-G. Wen, 2006, Rev. Mod. Phys. **78**, 17.

Lee, P. J., M. Anderlini, B. L. Brown, J. Sebby-Strabley, W. D. Phillips, and J. V. Porto, 2007, Phys. Rev. Lett. **99**, 020402.

Leggett, A. J., 1973, Phys. Fenn. **8**, 125.

Leggett, A. J., 1980, J. Phys. Colloq. **41**, 7.

Leggett, A. J., 1998, J. Stat. Phys. **93**, 927.

Leggett, A. J., 2001, Rev. Mod. Phys. **73**, 307.

Leggett, A. J., 2006, *Quantum Liquids* (Oxford University Press, Oxford).

Levinsen, J., and V. Gurarie, 2006, Phys. Rev. A **73**, 053607.

Lewenstein, M., A. Sanpera, V. Ahufinger, B. Damski, A. S. De, and U. Sen, 2007, Adv. Phys. **56**, 243.

Li, J., Y. Yu, A. Dudarev, and Q. Niu, 2006, New J. Phys. **8**, 154.

Lieb, E., and R. Seiringer, 2006, Commun. Math. Phys. **264**, 505.

Lieb, E. H., 1963a, Phys. Rev. **130**, 1616.

Lieb, E. H., 1963b, Phys. Rev. **130**, 2518.

Lieb, E. H., and W. Liniger, 1963, Phys. Rev. **130**, 1605.

Lieb, E. H., R. Seiringer, and J. Yngvason, 2000, Phys. Rev. A **61**, 043602.

Lieb, E. H., R. Seiringer, and J. Yngvason, 2001, Commun. Math. Phys. **224**, 17.

Lifschitz, I., S. Gredeskul, and L. Pastur, 1988, *Introduction to the Theory of Disordered Systems* (Wiley, New York).

Lifshitz, E. M., and L. P. Pitaevskii, 1980, *Statistical Physics* (Pergamon, Oxford).

Lignier, H., C. Sias, D. Ciampini, Y. Singh, A. Zenesini, O. Morsch, and E. Arimondo, 2007, Phys. Rev. Lett. **99**, 220403.

Liu, W. V., 2006, Phys. Rev. Lett. **96**, 080401.

Lugan, P., D. Clement, P. Bouyer, A. Aspect, M. Lewenstein, and L. Sanchez-Palencia, 2007, Phys. Rev. Lett. **98**, 170403.

Lundh, E., 2002, Phys. Rev. A **65**, 043604.

Luo, L., B. Clancy, J. Joseph, J. Kinast, and J. E. Thomas, 2007, Phys. Rev. Lett. **98**, 080402.

Luttinger, J. M., and J. C. Ward, 1960, Phys. Rev. **118**, 1417.

Lye, J. E., L. Fallani, M. Modugno, D. S. Wiersma, C. Fort, and M. Inguscio, 2005, Phys. Rev. Lett. **95**, 070401.

MacDonald, A. H., 1994, e-print arXiv:cond-mat/9410047.

Madison, K. W., F. Chevy, W. Wohlleben, and J. Dalibard, 2000, Phys. Rev. Lett. **84**, 806.

Mandel, O., M. Greiner, A. Widera, T. Rom, T. W. Hänsch, and I. Bloch, 2003a, Phys. Rev. Lett. **91**, 010407.

Mandel, O., M. Greiner, A. Widera, T. Rom, T. W. Hänsch, and I. Bloch, 2003b, Nature **425**, 937.

Marcelis, B., E. G. M. van Kempen, B. J. Verhaar, and S. J. J. M. F. Kokkelmans, 2004, Phys. Rev. A **70**, 012701.

Martikainen, J.-P., and H. T. C. Stoof, 2003, Phys. Rev. Lett. **91**, 240403.

Matthews, M. R., B. P. Anderson, P. C. Haljan, D. S. Hall, C. E. Wieman, and E. A. Cornell, 1999, Phys. Rev. Lett. **83**, 2498.

Mermin, N. D., and H. Wagner, 1966, Phys. Rev. Lett. **17**, 1307.

Micheli, A., G. Brennen, and P. Zoller, 2006, Nat. Phys. **2**, 341.

Miller, D. E., J. K. Chin, C. A. Stan, Y. Liu, W. Setiawan, C. Sanner, and W. Ketterle, 2007, Phys. Rev. Lett. **99**, 070402.

Minnhagen, P., 1987, Rev. Mod. Phys. **59**, 1001.

Mizushima, T., Y. Kawaguchi, K. Machida, T. Ohmi, T. Isoshima, and M. M. Salomaa, 2004, Phys. Rev. Lett. **92**, 060407.

Mora, C., and Y. Castin, 2003, Phys. Rev. A **67**, 053615.

Mora, C., R. Egger, A. O. Gogolin, and A. Komnik, 2005, Phys. Rev. Lett. **93**, 170403.

Morgan, S. A., M. D. Lee, and K. Burnett, 2002, Phys. Rev. A **65**, 022706.

Moritz, H., T. Stöferle, K. Günter, M. Köhl, and T. Esslinger, 2005, Phys. Rev. Lett. **94**, 210401.

Moritz, H., T. Stöferle, M. Köhl, and T. Esslinger, 2003, Phys. Rev. Lett. **91**, 250402.

Morsch, O., and M. Oberthaler, 2006, Rev. Mod. Phys. **78**, 179.

Mueller, E. J., 2004, Phys. Rev. A **70**, 041603.

Mun, J., P. Medley, G. K. Campbell, L. G. Marcassa, D. E. Pritchard, and W. Ketterle, 2007, Phys. Rev. Lett. **99**, 150604.

Nakajima, T., and M. Ueda, 2003, Phys. Rev. Lett. **91**, 140401.

Nelson, D. R., and J. M. Kosterlitz, 1977, Phys. Rev. Lett. **39**, 1201.

Nikolic, P., and S. Sachdev, 2007, Phys. Rev. A **75**, 033608.

Nishida, Y., 2007, Phys. Rev. A **75**, 063618.

Nishida, Y., and D. T. Son, 2006, Phys. Rev. Lett. **97**, 050403.

Nishida, Y., and D. T. Son, 2007, Phys. Rev. A **75**, 063617.

Niu, Q., I. Carusotto, and A. B. Kuklov, 2006, Phys. Rev. A **73**, 053604.

Nozières, P., and S. Schmitt-Rink, 1985, J. Low Temp. Phys. **59**,

195.

Nussinov, Z., and S. Nussinov, 2006, Phys. Rev. A **74**, 053622.

Nygaard, N., B. I. Schneider, and P. Julienne, 2006, Phys. Rev. A **73**, 042705.

O'Hara, K. M., S. L. Hemmer, M. E. Gehm, S. R. Granade, and J. E. Thomas, 2002, Science **298**, 2179.

Ohashi, Y., and A. Griffin, 2002, Phys. Rev. Lett. **89**, 130402.

Ohashi, Y., and A. Griffin, 2005, Phys. Rev. A **72**, 063606.

Oliver, W. D., J. Kim, R. C. Liu, and Y. Yamamoto, 1999, Science **284**, 299.

Olshanii, M., 1998, Phys. Rev. Lett. **81**, 938.

Olshanii, M., and V. Dunjko, 2003, Phys. Rev. Lett. **91**, 090401.

Olshanii, M., and L. Pricoupenko, 2002, Phys. Rev. Lett. **88**, 010402.

Olshanii, M., and D. Weiss, 2002, Phys. Rev. Lett. **89**, 090404.

Orso, G., 2007, Phys. Rev. Lett. **98**, 070402.

Ortiz, G., and J. Dukelsky, 2005, Phys. Rev. A **72**, 043611.

Orzel, C., A. K. Tuchmann, K. Fenselau, M. Yasuda, and M. A. Kasevich, 2001, Science **291**, 2386.

Ospelkaus, C., S. Ospelkaus, L. Humbert, P. Ernst, K. Sengstock, and K. Bongs, 2006, Phys. Rev. Lett. **97**, 120402.

Ospelkaus, S., A. Pe'er, K.-K. Ni, J. J. Zirbel, B. Neyenhuis, S. Kotochigova, P. S. Julienne, J. Ye, and D. S. Jin, 2008, e-print arXiv:0802.1093.

Osterloh, K., M. Baig, L. Santos, P. Zoller, and M. Lewenstein, 2005, Phys. Rev. Lett. **95**, 010403.

Öttl, A., S. Ritter, M. Köhl, and T. Esslinger, 2005, Phys. Rev. Lett. **95**, 090404.

Paredes, B., P. Fedichev, J. I. Cirac, and P. Zoller, 2001, Phys. Rev. Lett. **87**, 010402.

Paredes, B., A. Widera, V. Murg, O. Mandel, S. Fölling, J. I. Cirac, G. V. Shlyapnikov, T. W. Hänsch, and I. Bloch, 2004, Nature **429**, 277.

Paredes, B., P. Zoller, and J. I. Cirac, 2002, Phys. Rev. A **66**, 033609.

Partridge, G. B., W. Li, L. Kumar, Y. Liao, and R. G. Hulet, 2006, Science **311**, 503.

Partridge, G. B., K. E. Strecker, R. I. Kamar, M. W. Jack, and R. G. Hulet, 2005, Phys. Rev. Lett. **95**, 020404.

Pedri, P., L. Pitaevskii, S. Stringari, C. Fort, S. Burger, F. S. Cataliotti, P. Maddaloni, F. Minardi, and M. Inguscio, 2001, Phys. Rev. Lett. **87**, 220401.

Peierls, R. E., 1935, Ann. Inst. Henri Poincare **5**, 177.

Peil, S., J. V. Porto, B. L. Tolra, J. M. Obrecht, B. E. King, M. Subbotin, S. L. Rolston, and W. D. Phillips, 2003, Phys. Rev. A **67**, 051603.

Penrose, O., and L. Onsager, 1956, Phys. Rev. **104**, 576.

Perali, A., P. Pieri, L. Pisani, and G. C. Strinati, 2004, Phys. Rev. Lett. **92**, 220404.

Perali, A., P. Pieri, and G. C. Strinati, 2005, Phys. Rev. Lett. **95**, 010407.

Pethick, C., and H. Smith, 2002, *Bose-Einstein Condensation in Dilute Gases* (Cambridge University Press, Cambridge, U.K.).

Petrov, D. S., 2004, Phys. Rev. Lett. **93**, 143201.

Petrov, D. S., M. A. Baranov, and G. V. Shlyapnikov, 2003, Phys. Rev. A **67**, 031601.

Petrov, D. S., D. M. Gangardt, and G. V. Shlyapnikov, 2004, J. Phys. IV **116**, 5.

Petrov, D. S., M. Holzmann, and G. V. Shlyapnikov, 2000, Phys. Rev. Lett. **84**, 2551.

Petrov, D. S., C. Salomon, and G. V. Shlyapnikov, 2004, Phys. Rev. Lett. **93**, 090404.

Petrov, D. S., S. Salomon, and G. V. Shlyapnikov, 2005, Phys.

Rev. A **71**, 012708.

Petrov, D. S., and G. V. Shlyapnikov, 2001, Phys. Rev. A **64**, 012706.

Petrov, D. S., G. V. Shlyapnikov, and J. T. M. Walraven, 2000, Phys. Rev. Lett. **85**, 3745.

Pilati, S., J. Boronat, J. Casuelleras, and S. Giorgini, 2005, Phys. Rev. A **71**, 023605.

Pistolesi, F., and G. C. Strinati, 1996, Phys. Rev. B **53**, 15168.

Pitaevskii, L., and S. Stringari, 2003, *Bose-Einstein Condensation* (Oxford University Press, Oxford).

Pitaevskii, L. P., 1961, Sov. Phys. JETP **13**, 451.

Pitaevskii, L. P., 1996, Phys. Lett. A **221**, 14.

Pitaevskii, L. P., and A. Rosch, 1997, Phys. Rev. A **55**, R853.

Polkovnikov, A., 2007, Europhys. Lett. **78**, 10006.

Polkovnikov, A., E. Altman, and E. Demler, 2006, Proc. Natl. Acad. Sci. U.S.A. **103**, 6125.

Polkovnikov, A., E. Altman, E. Demler, B. Halperin, and M. D. Lukin, 2005, Phys. Rev. A **71**, 063613.

Polkovnikov, A., S. Sachdev, and S. M. Girvin, 2002, Phys. Rev. A **66**, 053607.

Pollet, L., S. Rombouts, and P. Denteneer, 2004, Phys. Rev. Lett. **93**, 210401.

Pollock, E. L., and D. M. Ceperley, 1987, Phys. Rev. B **36**, 8343.

Popov, V. N., 1983, *Functional Integrals in Quantum Field Theory and Statistical Physics* (Reidel, Dordrecht).

Popov, V. N., 1987, *Functional Integrals and Collective Modes* (Cambridge University Press, Cambridge, U.K.).

Posazhennikova, A., 2006, Rev. Mod. Phys. **78**, 1111.

Pricoupenko, L., 2004, Phys. Rev. A **70**, 013601.

Prokof'ev, N. V., O. Ruebenacker, and B. V. Svistunov, 2001, Phys. Rev. Lett. **87**, 270402.

Prokof'ev, N. V., and B. V. Svistunov, 2005, Phys. Rev. A **66**, 043608.

Pu, H., L. O. Baksmaty, S. Yi, and N. P. Bigelow, 2005, Phys. Rev. Lett. **94**, 190401.

Punk, M., and W. Zwerger, 2006, New J. Phys. **8**, 168.

Punk, M., and W. Zwerger, 2007, Phys. Rev. Lett. **99**, 170404.

Pupillo, G., A. Rey, and G. Batrouni, 2006, Phys. Rev. A **74**, 013601.

Rajagopal, K. K., P. Vignolo, and M. P. Tosi, 2004, Physica B **353**, 59.

Randeria, M., 1998, *High Temperature Superconductors*, Proceedings of the International School of Physics: Enrico Fermi, Course CXXXVI, Varenna (IOS, Amsterdam), p. 53.

Randeria, M., J.-M. Duan, and L.-Y. Shieh, 1990, Phys. Rev. B **41**, 327.

Randeria, M., N. Trivedi, A. Moreo, and R. T. Scalletter, 1992, Phys. Rev. Lett. **69**, 2001.

Rapsch, S., U. Schollwöck, and W. Zwerger, 1999, Europhys. Lett. **46**, 559.

Read, N., and N. R. Cooper, 2003, Phys. Rev. A **68**, 035601.

Read, N., and E. Rezayi, 1999, Phys. Rev. B **59**, 8084.

Recati, A., I. Carusotto, C. Lobo, and S. Stringari, 2006, Phys. Rev. Lett. **97**, 190403.

Recati, A., P. O. Fedichev, W. Zwerger, J. van Delft, and P. Zoller, 2005, Phys. Rev. Lett. **94**, 040404.

Recati, A., P. O. Fedichev, W. Zwerger, and P. Zoller, 2003, Phys. Rev. Lett. **90**, 020401.

Regal, C. A., M. Greiner, S. Giorgini, M. Holland, and D. S. Jin, 2005, Phys. Rev. Lett. **95**, 250404.

Regal, C. A., M. Greiner, and D. S. Jin, 2004a, Phys. Rev. Lett. **92**, 040403.

Regal, C. A., M. Greiner, and D. S. Jin, 2004b, Phys. Rev. Lett. **92**, 083201.

Regal, C. A., and D. S. Jin, 2003, Phys. Rev. Lett. **90**, 230404.

Regal, C. A., C. Ticknor, J. L. Bohn, and D. S. Jin, 2003, Nature **424**, 47.

Regnault, N., and T. Jolicoeur, 2003, Phys. Rev. Lett. **91**, 030402.

Regnault, N., and T. Jolicoeur, 2004, Phys. Rev. B **69**, 235309.

Reijnders, J. W., and R. A. Duine, 2004, Phys. Rev. Lett. **93**, 060401.

Reijnders, J. W., and R. A. Duine, 2005, Phys. Rev. A **71**, 063607.

Rempe, G., H. Walther, and N. Klein, 1987, Phys. Rev. Lett. **58**, 353.

Rey, A. M., P. B. Blakie, G. Pupillo, C. J. Williams, and C. W. Clark, 2005, Phys. Rev. A **72**, 023407.

Rey, A. M., I. I. Satija, and C. W. Clark, 2006, Phys. Rev. A **73**, 063610.

Richard, S., F. Gerbier, J. H. Thywissen, M. Hugbart, P. Bouyer, and A. Aspect, 2003, Phys. Rev. Lett. **91**, 010405.

Rigol, M., V. Dunjko, V. Yurovsky, and M. Olshanii, 2007, Phys. Rev. Lett. **98**, 050405.

Rigol, M., and A. Muramatsu, 2004, Phys. Rev. A **70**, 043627.

Rigol, M., R. T. Scalettar, P. Sengupta, and G. G. Batrouni, 2006, Phys. Rev. B **73**, 121103.

Rokhsar, D. S., and B. G. Kotliar, 1991, Phys. Rev. B **44**, 10328.

Rom, T., T. Best, D. van Oosten, U. Schneider, S. Fölling, B. Paredes, and I. Bloch, 2006, Nature **444**, 733.

Roomany, H. H., and H. W. Wyld, 1980, Phys. Rev. D **21**, 3341.

Röpke, G., A. Schnell, P. Schuck, and P. Nozières, 1998, Phys. Rev. Lett. **80**, 3177.

Rosenbusch, P., D. Petrov, S. Sinha, F. Chevy, V. Bretin, Y. Castin, G. Shlyapnikov, and J. Dalibard, 2002, Phys. Rev. Lett. **88**, 250403.

Rupak, G., and T. Schäfer, 2007, Phys. Rev. A **76**, 053607.

Ruseckas, J., G. Juzeliunas, P. Öhberg, and M. Fleischhauer, 2005, Phys. Rev. Lett. **95**, 010404.

Rychtarik, D., B. Engeser, H.-C. Nägerl, and R. Grimm, 2004, Phys. Rev. Lett. **92**, 173003.

Sá de Melo, C. A. R. M. Randeria, and J. R. Engelbrecht, 1993, Phys. Rev. Lett. **71**, 3202.

Sachdev, S., 1999, *Quantum Phase Transitions* (Cambridge University Press, Cambridge, U.K.).

Safonov, A. I., S. A. Vasilyev, I. S. Yasnikov, I. I. Lukashevich, and T. V. Jaakkola, 1998, Phys. Rev. Lett. **81**, 4545.

Sanchez-Palencia, L., D. Clement, P. Lugan, P. Bouyer, G. V. Shlyapnikov, and A. Aspect, 2007, Phys. Rev. Lett. **98**, 210401.

Santos, L., M. A. Baranov, J. Cirac, H.-U. Everts, H. Fehrmann, and M. Lewenstein, 2004, Phys. Rev. Lett. **93**, 030601.

Scarola, V. W., E. Demler, and S. D. Sarma, 2006, Phys. Rev. A **73**, 051601(R).

Schellekens, M., R. Hoppeler, A. Perrin, J. V. Gomes, D. Boiron, A. Aspect, and C. I. Westbrook, 2005, Science **310**, 648.

Schick, M., 1971, Phys. Rev. A **3**, 1067.

Schollwöck, U., 2005, Rev. Mod. Phys. **77**, 259.

Schori, C., T. Stöferle, H. Moritz, H. Köhl, and T. Esslinger, 2004, Phys. Rev. Lett. **93**, 240402.

Schrader, D., I. Dotsenko, M. Khudaverdyan, Y. Miroshnychenko, A. Rauschenbeutel, and D. Meschede, 2004, Phys. Rev. Lett. **93**, 150501.

Schreck, F., L. Khaykovich, K. L. Corwin, G. Ferrari, T. Bourdel, J. Cubizolles, and C. Salomon, 2001, Phys. Rev. Lett. **87**, 080403.

Schulman, L. S., 1981, *Techniques and Applications of Path Integration* (Wiley, New York).

Schulte, T., S. Drenkelforth, J. Kruse, W. Ertmer, J. Arlt, K. Sacha, J. Zakrzewski, and M. Lewenstein, 2005, Phys. Rev. Lett. **95**, 170411.

Schumm, T., S. Hofferberth, L. M. Andersson, S. Wildermuth, S. Groth, I. Bar-Joseph, J. Schmiedmayer, and P. Krüger, 2005, Nat. Phys. **1**, 57.

Schunck, C. H., Y. Shin, A. Schirotzek, M. W. Zwierlein, and W. Ketterle, 2007, Science **316**, 867.

Schweikhard, V., I. Coddington, P. Engels, V. P. Mogendorff, and E. A. Cornell, 2004, Phys. Rev. Lett. **92**, 040404.

Schweikhard, V., S. Tung, and E. A. Cornell, 2007, Phys. Rev. Lett. **99**, 030401.

Sebby-Strabley, J., M. Anderlini, P. Jessen, and J. Porto, 2006, Phys. Rev. A **73**, 033605.

Sebby-Strabley, J., B. Brown, M. Anderlini, P. Lee, P. Johnson, W. Phillips, and J. Porto, 2007, Phys. Rev. Lett. **98**, 200405.

Sengupta, P., M. Rigol, G. G. Batrouni, P. J. H. Denteneer, and R. T. Scalettar, 2005, Phys. Rev. Lett. **95**, 220402.

Sensarma, R., M. Randeria, and T.-L. Ho, 2006, Phys. Rev. Lett. **96**, 090403.

Sheehy, D. E., and L. Radzihovsky, 2004a, Phys. Rev. A **70**, 051602.

Sheehy, D. E., and L. Radzihovsky, 2004b, Phys. Rev. A **70**, 063620.

Sheehy, D. E., and L. Radzihovsky, 2006, Phys. Rev. Lett. **96**, 060401.

Sheshadri, K., H. R. Krishnamurty, R. Pandit, and T. V. Ramakrishnan, 1993, Europhys. Lett. **22**, 257.

Shin, Y., C. H. Schunck, A. Schirotzek, and W. Ketterle, 2007, Phys. Rev. Lett. **99**, 090403.

Shin, Y., C. H. Schunck, A. Schirotzek, and W. Ketterle, 2008, Nature **451**, 689.

Simula, T. P., and P. B. Blakie, 2006, Phys. Rev. Lett. **96**, 020404.

Simula, T. P., M. D. Lee, and D. A. W. Hutchinson, 2005, Philos. Mag. Lett. **85**, 395.

Sinha, S., and G. V. Shlyapnikov, 2005, Phys. Rev. Lett. **94**, 150401.

Sinova, J., C. B. Hanna, and A. H. MacDonald, 2002, Phys. Rev. Lett. **89**, 030403.

Smith, N. L., W. H. Heathcote, G. Hechenblaikner, E. Nugent, and C. J. Foot, 2005, J. Phys. B **38**, 223.

Snoek, M., and H. T. C. Stoof, 2006a, Phys. Rev. A **74**, 033615.

Snoek, M., and H. T. C. Stoof, 2006b, Phys. Rev. Lett. **96**, 230402.

Sols, F., 1994, Physica B **194-196**, 1389.

Son, D. T., 2007, Phys. Rev. Lett. **98**, 020604.

Sonin, E. B., 1987, Rev. Mod. Phys. **59**, 87.

Sonin, E. B., 2005a, Phys. Rev. A **71**, 011603.

Sonin, E. B., 2005b, Phys. Rev. A **72**, 021606.

Sørensen, A. S., E. Demler, and M. D. Lukin, 2005, Phys. Rev. Lett. **94**, 086803.

Spielman, I. B., W. D. Phillips, and J. V. Porto, 2007, Phys. Rev. Lett. **98**, 080404.

Spielman, I. B., W. D. Phillips, and J. V. Porto, 2008, Phys. Rev. Lett. **100**, 120402.

Srednicki, M., 1994, Phys. Rev. E **50**, 888.

Stewart, J. T., J. P. Gaebler, C. A. Regal, and D. S. Jin, 2006, Phys. Rev. Lett. **97**, 220406.

Stock, S., V. Bretin, F. Chevy, and J. Dalibard, 2004, Europhys. Lett. **65**, 594.

Stock, S., Z. Hadzibabic, B. Battelier, M. Cheneau, and J. Dalibard, 2005, Phys. Rev. Lett. **95**, 190403.

Stöferle, T., H. Moritz, K. Günter, M. Köhl, and T. Esslinger, 2006, Phys. Rev. Lett. **96**, 030401.

Stöferle, T., H. Moritz, C. Schori, M. Köhl, and T. Esslinger, 2004, Phys. Rev. Lett. **92**, 130403.

Stoof, H. T. C., 1994, Phys. Rev. A **49**, 3824.

Stoof, H. T. C., M. Houbiers, C. A. Sackett, and R. G. Hulet, 1996, Phys. Rev. Lett. **76**, 10.

Strecker, K. E., G. B. Partridge, and R. G. Hulet, 2003, Phys. Rev. Lett. **91**, 080406.

Stringari, S., 2004, Europhys. Lett. **65**, 749.

Tanatar, B., A. M. P. Vignolo, and M. P. Tosi, 2002, Phys. Lett. A **302**, 131.

Theis, M., G. Thalhammer, K. Winkler, M. Hellwig, G. Ruff, R. Grimm, and J. Hecker-Denschlag, 2004, Phys. Rev. Lett. **93**, 123001.

Thomas, J. E., A. Turlapov, and J. Kinast, 2005, Phys. Rev. Lett. **95**, 120402.

Tiesinga, E., B. J. Verhaar, and H. T. C. Stoof, 1993, Phys. Rev. A **47**, 4114.

Timmermans, E., K. Furuya, P. W. Milonni, and A. K. Kerman, 2001, Phys. Lett. A **285**, 228.

Tinkham, M., 1996, *Introduction to Superconductivity* (McGraw-Hill, New York).

Tkachenko, V. K., 1966, Sov. Phys. JETP **23**, 1049.

Tokatly, I. V., 2004, Phys. Rev. Lett. **93**, 090405.

Tolra, B. L., K. M. O'Hara, J. H. Huckans, W. D. Phillips, S. L. Rolston, and J. V. Porto, 2004, Phys. Rev. Lett. **92**, 190401.

Törmä, P., and P. Zoller, 2000, Phys. Rev. Lett. **85**, 487.

Trebst, S., U. Schollwöck, M. Troyer, and P. Zoller, 2006, Phys. Rev. Lett. **96**, 250402.

Trivedi, N., and M. Randeria, 1995, Phys. Rev. Lett. **75**, 312.

Trugman, S. A., and S. Kivelson, 1985, Phys. Rev. B **31**, 5280.

Truscott, A., K. Strecker, W. McAlexander, G. Partridge, and R. G. Hulet, 2001, Science **291**, 2570.

Tuchman, A., C. Orzel, A. Polkovnikov, and M. A. Kasevich, 2006, Phys. Rev. A **74**, 051601.

Tung, S., V. Schweikhard, and E. A. Cornell, 2006, Phys. Rev. Lett. **97**, 240402.

Turlapov, A., J. Kinast, B. Clancy, L. Luo, J. Joseph, and J. Thomas, 2007, J. Low Temp. Phys. **150**, 567.

Ueltschi, D., 2006, J. Math. Phys. **47**, 123303.

van Oosten, D., D. B. M. Dickerscheid, B. Farid, P. van der Straten, and H. Stoof, 2005, Phys. Rev. A **71**, 021601.

van Oosten, D., P. van der Straten, and H. T. C. Stoof, 2001, Phys. Rev. A **63**, 053601.

Visser, P. M., and G. Nienhuis, 1998, Phys. Rev. A **57**, 4581.

Vogels, J. M., K. Xu, C. Raman, J. R. Abo-Shaeer, and W. Ketterle, 2002, Phys. Rev. Lett. **88**, 060402.

Wang, D.-W., M. D. Lukin, and E. Demler, 2005, Phys. Rev. A **72**, 051604.

Watanabe, G., G. Baym, and C. J. Pethick, 2004, Phys. Rev. Lett. **93**, 190401.

Weinberg, S., 1986, Prog. Theor. Phys. **86**, 43.

Wen, X. G., 2004, *Quantum Field Theory of Many-Body Systems*, Oxford Graduate Texts (Oxford University Press, Oxford, U.K.).

Werner, F., and Y. Castin, 2006, Phys. Rev. A **74**, 053604.

Werner, F., O. Parcollet, A. Georges, and S. R. Hassan, 2005, Phys. Rev. Lett. **95**, 056401.

Wessel, S., F. Alet, S. Trebst, D. Leumann, M. Troyer, and G. G. Batrouni, 2005, J. Phys. Soc. Jpn. **74**, 10.

Wessel, S., F. Alet, M. Troyer, and G. G. Batrouni, 2004, Phys. Rev. A **70**, 053615.

Westbrook, C. I., R. N. Watts, C. E. Tanner, S. L. Rolston, W. Phillips, and P. Lett, 1990, Phys. Rev. Lett. **65**, 33.

White, S. R., and A. E. Feiguin, 2004, Phys. Rev. Lett. **93**, 076401.

Wilczek, F., and A. Zee, 1984, Phys. Rev. Lett. **52**, 2111.

Wilkin, N. K., and J. M. F. Gunn, 2000, Phys. Rev. Lett. **84**, 6.

Winkler, K., G. Thalhammer, F. Lang, R. Grimm, J. Hecker-Denschlag, A. J. Daley, A. Kantian, H. P. Büchler, and P. Zoller, 2006, Nature **441**, 853.

Woo, S. J., L. O. Baksmaty, S. Choi, and N. P. Bigelow, 2004, Phys. Rev. Lett. **92**, 170402.

Wouters, M., J. Tempere, and J. T. Devreese, 2003, Phys. Rev. A **68**, 053603.

Wright, E. M., D. F. Walls, and J. C. Garrison, 1996, Phys. Rev. Lett. **77**, 2158.

Xu, K., Y. Liu, D. Miller, J. Chin, W. Setiawan, and W. Ketterle, 2006, Phys. Rev. Lett. **96**, 180405.

Yang, C. N., 1967, Phys. Rev. Lett. **19**, 1312.

Yang, K., F. D. M. Haldane, and E. H. Rezayi, 2001, Phys. Rev. B **64**, 081301.

Yu, Z., and G. Baym, 2006, Phys. Rev. A **73**, 063601.

Yurke, B., and D. Stoler, 1986, Phys. Rev. Lett. **57**, 13.

Yuzbashyan, E. A., O. Tsyplyatyev, and B. L. Altshuler, 2006, Phys. Rev. Lett. **96**, 097005.

Zhang, C., V. W. Scarola, and S. D. Sarma, 2007, Phys. Rev. A **76**, 023605.

Zhang, P., Y. Li, and C. P. Sun, 2005, Eur. Phys. J. D **36**, 229.

Zobay, O., and B. M. Garraway, 2001, Phys. Rev. Lett. **86**, 1195.

Zwierlein, M. W., J. R. Abo-Shaeer, A. Schirotzek, C. H. Schunck, and W. Ketterle, 2005, Nature **435**, 1047.

Zwierlein, M. W., Z. Hadzibabic, S. Gupta, and W. Ketterle, 2003a, Phys. Rev. Lett. **91**, 250404.

Zwierlein, M. W., A. Schirotzek, C. H. Schunk, and W. Ketterle, 2006, Science **311**, 492.

Zwierlein, M. W., C. A. Stan, C. H. Schunck, S. M. F. Raupach, A. J. Kerman, and W. Ketterle, 2004, Phys. Rev. Lett. **92**, 120403.

Zwierlein, M. W., C. A. Stan, C. H. Schunk, S. M. F. Raupach, S. Gupta, Z. Hadzibabic, and W. Ketterle, 2003b, Phys. Rev. Lett. **91**, 250401.